

FORMATION AND CONTROL OF ATMOSPHERIC
AEROSOL NITRATE AND NITRIC ACID

Thesis by
Armistead Goode Russell

In Partial Fulfillment of the Requirements
for the Degree of
Doctor of Philosophy

California Institute of Technology
Pasadena, California

1985

(Submitted January 8, 1985)

© 1985

Armistead Goode Russell

All Rights Reserved

iii

to Jerri

ACKNOWLEDGMENTS

A great number of people have contributed to the completion of this thesis, to all of whom I am thankful. There are, however, a few to whom I am especially grateful. Foremost of these is my principal advisor, Dr. Glen Cass, without whom I would never have undertaken, much less completed this project. My discussions with Dr. Cass have been very helpful, thought provoking, and motivating. It has also been easy and instructive to work for him.

This work was conducted at the Environmental Quality Laboratory (EQL) of Caltech, and the support of its director, Dr. Norman H. Brooks is appreciated greatly. Dr. Greg McRae was instrumental to the outcome of this project. Much of this work is an outgrowth of techniques developed as part of his thesis, and it was with his guidance that much of the modeling was accomplished. Discussions with him led to a greater understanding of the problem. The ammonia emissions inventory used in parts of this thesis was assembled by Shohreh Gharib, Mari Peterson and Jim Tilden. I also derived a good deal of knowledge about the causes and dynamics of air pollution in discussions with Drs. John Seinfeld and Richard Flagan. I thank them for spending their time with me.

A number of people helped in the preparation of this manuscript to whom I wish to express my thanks. First, almost all of the superb typing or, in this modern age, processing of this thesis was done by Pat Houseworth and Christina Conti. I also thank them for the time that we spent talking on less technical subjects than air

pollution. Theresa Fall, Phil Dube', and Nancy Tomer helped in preparing many of the illustrations that are to follow.

The list of people crucial to the project does not end there. Over twenty Caltech students and staff, all to whom I am very thankful, gave up two or more days of their time to help conduct an experiment in the Los Angeles Basin. The South Coast Air Quality Management District (SCAQMD) provided much of the required air quality, meteorological and emissions data, and allowed me to use their sites for my experiments. I am grateful to the SCAQMD's staff members who helped in these matters, especially Bill Bope, Julian Foon, John Grissinger, Eric Lemke, and Chung Liu.

The California Air Resources Board provided not only emissions data, and use of one of their monitoring sites, but, under Agreement A2-150-32, also provided most of the monetary support required to conduct this project. I am thankful they have had the wisdom and foresight to understand that without this type of long-term support little progress will be made toward fixing the air pollution problems that now afflict many areas. Paul Allen, Andrew Ranzieri, Charles Unger and Kit Wagner helped provide emissions data and had helpful comments on the development of the modeling work. Doug Lawson and Jack Suder were the contract monitors.

This work has not been reviewed by the California Air Resources Board prior to publication, and all findings and conclusions are solely the responsibility of the author.

ABSTRACT

This work focuses on the formation, transport and control of atmospheric nitric acid and nitrate aerosol using both theoretical modeling and experimental techniques. A mathematical model was developed that describes the formation and transport of photochemically produced atmospheric gases and nitrate aerosol, using fundamental thermodynamic data to determine the quantity and state of the aerosol nitrate produced. Model predictions compared favorably with the field data available. A sensitivity study of the model indicated that the predicted aerosol nitrate concentrations are highly dependent on temperature. The trajectory model was used to study the fate of nitrogen oxides emissions and the chemical reactions responsible for the formation of atmospheric nitric acid. A majority of the NO_x emissions deposit out within 24 hours, primarily as HNO_3 . Previously it was believed that almost all of the atmospheric nitric acid was produced during daylight hours, however model results indicate that nighttime reactions can produce comparable quantities, especially in the upper portions of the boundary layer more than a hundred meters above ground.

An experimental program was designed and executed to collect a set of data for use in studying nitrate formation, and for use in evaluating the accuracy of air quality models. A large quantity of aerosol nitrate was observed to accumulate overnight near the coast, presumably due to the reaction between HNO_3 and sea salt aerosol or soil dust-like material. This aerosol is then transported inland the

following afternoon, and can contribute to the high particulate nitrate levels found inland. Data from the experiment were used to test the hypothesis that atmospheric HNO_3 and NH_3 are in equilibrium with the aerosol phase. Most of the data are consistent with the assumption that an external mixture containing some pure NH_4NO_3 is present. Additional improvement is obtained if an internally mixed $\text{NH}_4^+-\text{NO}_3^- - \text{SO}_4^{=}$ aerosol is assumed to be present.

Further evaluation of the air quality model against the data described above showed that the model accurately predicts the measured concentrations of O_3 , NO_2 , total nitrate, HNO_3 , and NH_3 . Representative emission control programs were tested using the model, and results indicated that NO_x emission control will reduce $\text{HNO}_3(\text{g})$, aerosol nitrate and PAN concentrations. For the particular trajectories studied, NO_x control would also have reduced the peak O_3 concentrations. Reducing NH_3 emissions will reduce aerosol nitrate formation at the expense of increasing HNO_3 concentrations. Controlling organic gas emissions will reduce O_3 and PAN. Further research areas suggested by this work also are presented.

TABLE OF CONTENTS

	<u>Page</u>
ACKNOWLEDGEMENTS	iv
ABSTRACT	vi
LIST OF FIGURES	x
LIST OF TABLES	xvi
CHAPTER 1 INTRODUCTION	1
1.1 Objective	1
1.2 The Importance of Nitrate Aerosol and Nitric Acid in the Atmosphere	2
1.3 Methodology of this Research	4
1.4 References	7
CHAPTER 2 MATHEMATICAL MODELING OF THE FORMATION AND TRANSPORT OF AMMONIUM NITRATE AEROSOL	9
CHAPTER 3 THE DYNAMICS OF NITRIC ACID PRODUCTION AND THE FATE OF NITROGEN OXIDES	26
CHAPTER 4 ACQUISITION OF REGIONAL AIR QUALITY MODEL VALIDATION DATA FOR NITRATE, SULFATE, AMMONIUM ION AND THEIR PRECURSORS	67
CHAPTER 5 AMMONIA AND NITRIC ACID CONCENTRATIONS IN EQUILIBRIUM WITH ATMOSPHERIC AEROSOLS: EXPERIMENT VS. THEORY	81

TABLE OF CONTENTS (Continued)

	<u>Page</u>
CHAPTER 6 VERIFICATION OF A PHOTOCHEMICAL MODEL TO PREDICT AEROSOL NITRATE AND NITRIC ACID CONCENTRATIONS, AND ITS USE FOR CONTROL MEASURE EVALUATION	96
6.1 Introduction	96
6.2 Model Description	98
6.3 Model Evaluation Data Base	101
6.4 Model Evaluation for 30-31 August 1982	108
6.5 Evaluation of Control Strategies for HNO ₃ and Aerosol Nitrate Abatement	140
6.6 Conclusions	150
6.7 References	152
CHAPTER 7 FUTURE RESEARCH	155
CHAPTER 8 SUMMARY AND CONCLUSIONS	164

LIST OF FIGURES

<u>Figure</u>	<u>Page</u>
2.1 Schematic representation of (a) vertically resolved Lagrangian trajectory model and (b) the computational grid cell convention	11
2.2 (a) NH_4NO_3 equilibrium dissociation constant as a function of temperature (r.h. 50%) and (b) NH_4NO_3 equilibrium dissociation constant as a function of r.h. (temperature, 25 C)	12
2.3 Flow diagram of NH_4NO_3 formation mechanism illustrating three basic steps in calculation procedure	13
2.4 Predicted NH_4NO_3 concentration surfaces at 15, 25 and 35 C and 45, 65 and 85% r.h. for total NH_3 and total HNO_3 concentrations up to 20 and 40 ppb, respectively	15
2.5 Gridded map of the South Coast Air Basin used for constructing NH_3 emissions inventory. Superimposed on the map is the trajectory path that reaches El Monte at 3 p.m. (PDT) on 28 June 1974	15
2.6 Spatial representation of daily emissions of NH_3 , NO_x reactive hydrocarbons (RHC) and CO in the South Coast Air Basin (Inventory period June 1974.)	18
2.7 Concentration profiles at El Monte on 28 June 1974. (a) Predicted NH_4NO_3 , measured NH_4^+ and measured NO_3^- , (b) Predicted total ammonia ($\text{NH}_3 + \text{NH}_4^+$) and measured total ammonia, (c) Predicted and measured O_3 concentrations and (d) Sensitivity of NH_4NO_3 formation to a $\pm 2^\circ\text{C}$ change in the temperature field	19,20
2.8 Predicted concentrations and observed meteorological variables for the air parcel reaching El Monte at 2 p.m. (PDT) 28 June 1974. (a) NH_4NO_3 , NH_3 , HNO_3 and PAN profiles, (b) Total ammonia and total nitrate profiles, (c) NO , NO_2 and O_3 profiles and (d) Meteorological parameters: mixing depth, temperature and relative humidity	22,23
2.9 Evolution of vertical concentration profiles of NH_3 (—), HNO_3 (---) and NH_4NO_3 (—) in the air parcel that reaches El Monte at 2 p.m. (PDT) 2 June 1974. Results shown are for 4 a.m., 8 a.m., and 12 noon and the location is given for the air parcel at those times	23

LIST OF FIGURES (Continued)

<u>Figure</u>	<u>Page</u>
3.1 Trajectory path used in analyzing the nitrogen oxides in the Los Angeles basin, June 28, 1974	32
3.2 Schematic representation of the net flux between nitrogen oxides species, including reaction paths for aerosol nitrate (NIT) formation. The width of these arrows indicates the magnitude of the net flux during the base case 24-hour trajectory simulation	34
3.3 Nitrogen balance on the air column illustrating the relative contributions, $F(n)$, from initial conditions, emissions and removal by dry deposition	36
3.4 Cumulative dry deposition of oxidized nitrogen air pollutants along a 24-hour trajectory in the Los Angeles area, in mg N per m^2 of surface area at the bottom of the moving air column	38
3.5 Diurnal variation in the contribution of different reaction pathways to the formation of gas phase nitric acid. The two reactions (53 and 54) between NO_3 and organics have been added together for display purposes	39
3.6 Predicted and measured NO_3 concentrations at Riverside, September 12, 1979. (—) Predicted and (+) Measured (Platt et al. 1980)	52
3.7 Predicted and measured O_3 and NO_2 concentrations at Riverside, September 12, 1979: (—) Predicted, (x) Measured NO_2 (Platt et al. 1980) and (o) Measured O_3 (Platt et al. 1980)	53
3.8 Predicted vertical NO_3 concentration profile at 1900 (PDT) on September 12, 1979. Air parcel is located at Riverside.	55
3.9 Predicted NO_3 concentrations at Riverside, September 12, 1979 for the base case and for several perturbations from the base case.	56
4.1 Locations of nitrate monitoring sites in the South Coast Air Basin	69

LIST OF FIGURES (Continued)

<u>Figure</u>	<u>Page</u>
4.2 Schematic of the sampling apparatus used at nine of the ten sites. The tenth station used only the two 10 lpm lines with dual filters.	69
4.3 (a) Nitrate concentrations observed at Rubidoux, August 30-31, 1982. (b) Trajectory of the air mass passing over the Long Beach area at 1100 hours on August 31 and over the Rubidoux Area at 1800 hours on August 31, 1982. (c) Nitrate concentrations at Long Beach, August 30-31, 1982.	71
4.4 Ionic species concentration at Long Beach (a) Cations and (a) Anions	72
4.5 Ionic species concentration at Rubidoux (a) Cations and (a) Anions	73
4.6 Particulate nitrate and gaseous nitric acid concentrations ($\mu\text{g m}^{-3}$ as NO_3^-) (a) Long Beach and (b) Lennox	74
4.7 Particulate ammonium and gaseous ammonia concentrations ($\mu\text{g m}^{-3}$ as NH_4^+) (a) Long Beach and (b) Lennox	75
4.8 (a) Particulate nitrate and gaseous nitric acid concentrations at Anaheim ($\mu\text{g m}^{-3}$ as NO_3^-) (b) Particulate ammonium and gaseous ammonia concentrations at Anaheim ($\mu\text{g m}^{-3}$ as NH_4^+)	76
4.9 (a) Particulate nitrate and gaseous nitric acid at Rubidoux ($\mu\text{g m}^{-3}$ as NO_3^-) (b) Particulate ammonium and gaseous ammonia concentrations at Rubidoux ($\mu\text{g m}^{-3}$ as NH_4^+)	77
4.10 Partial pressure concentration product of ammonia and nitric acid at Rubidoux.	78
4.11 Measured NO , NO_2 , HNO_3 , PAN and Nitrate (in $\mu\text{g m}^{-3}$ stated as equivalent NO_3^-) (a) Pasadena and (b) Rubidoux	79
5.1 Air monitoring sites in the South Coast Air Basin that surrounds Los Angeles	83

LIST OF FIGURES (Continued)

<u>Figure</u>	<u>Page</u>
5.2 Partial pressure product of ammonia and nitric acid in equilibrium with a sulfate, nitrate and ammonium containing aerosol as a function of relative humidity and ammonium nitrate ionic strength fraction at 25 C	84
5.3 Observed $[\text{HNO}_3][\text{NH}_3]$ concentration product and calculated dissociation constant of pure ammonium nitrate at Anaheim, California	86
5.4 Observed and calculated pollutant concentrations at Anaheim-external mixture with all aerosol nitrate available to form ammonium nitrate. (a) Nitric acid gas, (b) ammonia gas, (c) nitrate aerosol and (d) ammonium aerosol	87
5.5 Observed $[\text{HNO}_3][\text{NH}_3]$ concentration product and calculated dissociation constant of pure ammonium nitrate at Rubidoux, California	88
5.6 Observed and calculated pollutant concentrations at Rubidoux-external mixture with all aerosol nitrate available to form ammonium nitrate. (a) Nitric acid gas, (b) ammonia gas, (c) nitrate aerosol and (d) ammonium aerosol	88
5.7 Observed $[\text{HNO}_3][\text{NH}_3]$ concentration product and calculated dissociation constant of pure ammonium nitrate at Long Beach, California	89
5.8 Observed and calculated pollutant concentrations at Long Beach-external mixture with all aerosol nitrate available to form ammonium nitrate. (a) Nitric Acid Gas, (b) Ammonia Gas, (c) Nitrate Aerosol and (d) Ammonium Aerosol	90
5.9 Observed and calculated pollutant concentrations at Long Beach-external mixture with only FREE NITRATE available to form NH_4NO_3 , (a) HNO_3 , (b) NH_3 and (c) FREE NITRATE	91

LIST OF FIGURES (Continued)

<u>Figure</u>	<u>Page</u>
5.10 Comparison of observed and calculated gas phase concentrations at all monitoring stations under two alternative external mixture hypothesis (180 observations). Case (1), all aerosol nitrate available to form NH_4NO_3 . Case (2), only the FREE NITRATE available to form NH_4NO_3 . (a) ammonia (Case 1), (b) nitric acid (Case 1), (c) ammonia (Case 2) and (d) nitric (Case 2)	92
5.11 Observed and calculated $[\text{HNO}_3][\text{NH}_3]$ concentration product at Upland—comparison of external mixture and size segregated internal mixture hypothesis. (a) external mixture and (b) size segregated internal mixture	93
6.1 Gridded map of California's South Coast Air Basin (SoCAB) used for constructing concentration fields, meteorological fields, and emissions inventories. Symbols (•) indicate the locations of aerosol measurement stations used in this work. The solid line marks the boundary of the SoCAB	102
6.2 Spatial distribution of the 1982 estimated daily emissions of NH_3 , NO_x , THC and CO in the South Coast Air Basin	105
6.3 Observed and predicted O_3 at Rubidoux, CA, 31 August 1982	120
6.4 Observed and predicted NO_2 at Rubidoux, CA, 31 August 1982	121
6.5 Observed and predicted Total Nitrate ($\text{TN} = \text{AN} + \text{HNO}_3$) at Rubidoux, CA, 31 August 1982	122
6.6 Observed and predicted $\text{HNO}_3(\text{g})$ at Rubidoux, CA, 31 August 1982	123
6.7 Observed and predicted NO_3^- at Rubidoux, CA, 31 August 1982	124
6.8 Observed and predicted NH_3 at Rubidoux, CA, 31 August 1982	125
6.9 Observed and predicted NO_3^- at Rubidoux, CA, 31 August 1982 when the partition of computed TN between $\text{HNO}_3(\text{g})$ and aerosol nitrate is based on ambient temperatures and ammonia concentrations measured at the Rubidoux monitoring site	129

LIST OF FIGURES (Continued)

<u>Figure</u>	<u>Page</u>
6.10 Predicted Total Nitrate ($TN = HNO_3(g) + NH_4NO_3 + BAN$), Aerosol Nitrate ($AN = NH_4NO_3 + BAN$) and aerosol nitrate formed by reaction 58 (BAN , see text) at Rubidoux, CA, 31 August 1982	131
6.11 Observed and predicted O_3 at Upland, CA, 31 August 1982	133
6.12 Observed and predicted Total Nitrate at Upland, CA, 31 August 1982	134
6.13 Observed and predicted aerosol nitrate at Upland, CA, 31 August 1982	135
6.14 Observed and predicted Total Ammonia at Upland, CA, 31 August 1982	136
6.15 Predicted O_3 plotted against observed O_3 for both Rubidoux and Upland, CA, 31 August 1982	138

LIST OF TABLES

<u>Table</u>		<u>Page</u>
2.1	Sensitivity of ammonium nitrate formation model to input parameters	14
2.2	Summary of ammonia emissions by source category in the South Coast Air Basin 1974	16,17
3.1	Major reactions in the $\text{NO}_3\text{-N}_2\text{O}_5$ System at night	40
3.2	Species concentrations used in analysis	44
3.3	Percent of total nitric acid produced by each reaction along a 24-hour trajectory	48
4.1	Measurement uncertainties	70
5.1	Comparison of measurements at Long Beach to predictions given by the pure external mixture hypothesis based on FREE NITRATE (case 1) and by the size segregated internal mixture hypothesis (case 2)	94
6.1	1982 Estimated emissions in the South Coast Air Basin	104
6.2	Summary of ammonia emissions by source category in the South Coast Air Basin 1982	106
6.3	Splitting factors for converting total measured hydrocarbons (ppmC) into hydrocarbon classes for use as initial conditions	109
6.4	Predicted and measured concentrations along the trajectory beginning at Long Beach, California, at 1100 (PDT) 31 August 1982	113
6.5	Predicted inorganic nitrate concentrations at Rubidoux, California, resulting from decreases in emissions	142
6.6	Predicted peak one-hour ozone concentrations (ppb) at Rubidoux, California, as a function of emissions reductions	144
6.7	Predicted pollutant concentrations at Rubidoux, California, when emissions of SINK aerosol are included	147

CHAPTER 1

INTRODUCTION

1.1 Objective

Billions of dollars are spent annually to try to control, or reduce, the air pollution now affecting industrialized societies. Naturally the question arises, "Can the methods used by engineers to design solutions to these air pollution problems be improved?". If so, then more efficient and effective control programs may result that will achieve air quality objectives at the least possible cost. Mathematical models that relate alterations in pollutant emissions to the resulting changes in air quality are one of the most powerful tools used by engineers to test proposed pollutant abatement plans in advance of their adoption. Air quality models of this sort have yet to be developed for a number of important, but poorly understood, classes of air pollution problems. Before they can be constructed one must first understand the problem, and in particular how the different chemical constituents in the atmosphere interact to cause the formation of irritating substances (e.g. strong acids) and visibility-reducing secondary aerosols.

The objective of this research has been to create a better understanding of the atmospheric processes that govern the formation and transport of nitric acid (HNO_3) and nitrate aerosol. The knowledge gained then is used to formulate mathematical models that can be employed by engineers to devise more effective strategies for the control of aerosol nitrate and nitric acid. While exploring

rational emission control strategies that will reduce the formation of nitric acid and ammonium nitrate, the synergisms between coexisting pollutants, such as peroxyacetyl nitrate (PAN), ammonia (NH_3), nitrogen dioxide (NO_2), and ozone (O_3), also are investigated. The concepts developed are tested against experimental data obtained in the Los Angeles Basin, but the methods developed are generally applicable to other urban areas.

1.2 The Importance of Nitrate Aerosol and Nitric Acid in the Atmosphere

A substantial portion of the aerosol nitrate in the atmosphere is found to reside in a fine particle size fraction with particle diameter less than about 2 μm (Appel et al., 1978; Hobbs and Hegg, 1982; Grosjean, 1983). These fine particles, especially those with diameters of the same order as the wavelength of visible light scatter light very effectively and can lead to pronounced visibility degradation (Friedlander, 1977; van de Hulst, 1957). Aerosol nitrate is estimated to account for up to 40% of the severe visibility problem experienced in the eastern portion of the Los Angeles Basin (White and Roberts, 1977). Groblicki et al. (1981) estimate that about 17% of the decreased visibility in Denver is due to fine particulate nitrates. These small particles also are easily respirable (National Research Council, 1979), with possible accompanying health implications.

Nitric acid is of concern for a variety of reasons, not the least of which is that it is a precursor to the formation of aerosol

nitrate (Duce, 1969; Stelson and Seinfeld, 1982; Russell and Cass, 1984). The presence of nitric acid in the atmosphere leads to the acidification of rain and fog and to acidic dry deposition (Liljestrand and Morgan, 1978; Waldman et al., 1982; Huebert, 1983). Nitric acid also has been cited as a contributor to the formation of mutagenic, nitrated organic compounds in the atmosphere (Grosjean et al. 1983) and itself is probably not healthful if inhaled at high concentrations. Aerosol nitrates and nitric acid are also two of the major end products of nitrogen oxides (NO_x) emissions. Thus an understanding of how HNO_3 and aerosol nitrate are produced in the atmosphere forms an integral part of an improved understanding of the ultimate fate of NO_x emissions and the production of other photochemical pollutants (Seinfeld, 1975; Russell et al., 1985; Grosjean, 1983).

Problems associated with aerosol nitrate and nitric acid are not restricted to urban areas with large emissions of nitrogen oxides. Rural areas of the eastern United States and Canada experience acidification of the rain and lakes due to sulfates and nitrates that are being advected from more the populated areas (Galloway and Likens, 1981). Henderson, Nevada, near Las Vegas, experiences markedly decreased visibility from nitrate-containing aerosols (Clark County Health District, 1982), and it is the semi-rural areas near Riverside, Ca., 60 KM's downwind of Los Angeles, that experience the greatest decrease in visibility due to aerosol nitrates produced in the atmosphere of California's South Coast Air Basin.

1.3 Methodology of this Research

One major route for fine particle nitrate production is suspected to proceed by the reaction between gaseous ammonia and nitric acid to form ammonium nitrate (NH_4NO_3) particles. Nitric acid, in turn, is produced by a series of photochemical and thermal reactions involving primary NO_x , reactive hydrocarbon (RHC) emissions, and their products. Thus, to describe correctly the dynamics of atmospheric ammonium nitrate aerosol and nitric acid, one must describe the complete system which has become known as photochemical air pollution, or smog. Chapter 2 reports on the development and testing of the trajectory formulation of a photochemical air pollution model that describes the emissions of NO_x , RHC, and NH_3 from their sources, and the subsequent transport and reaction of these emissions to form O_3 , NO_2 , HNO_3 and ammonium nitrate aerosol in equilibrium with atmospheric ammonia and nitric acid.

Chapter 3 uses the trajectory model to investigate the relative importance of the competing chemical reactions that determine nitric acid concentrations in the atmosphere, as well as the fate of NO_x emissions and the deposition of nitrogenous pollutants. The research reveals that a significant amount of nitric acid can be formed at night as a product of nitrate radical (NO_3) and dinitrogen pentoxide (N_2O_5) reactions. This study confirms that the chemical mechanism, and the description of the transport, deposition, and emissions used can accurately reproduce the observed behavior of NO_3 concentrations in the atmosphere. Also in Chapter 3 the role that

scavenging of NO_3 and N_2O_5 by aerosols may play in the production of nitric acid and aerosol nitrates is discussed.

A major barrier encountered when studying the dynamics of atmospheric nitric acid and aerosol nitrate is the lack of high quality observations on the concentrations of these pollutants and their co-pollutants collected in a form that can be used to verify theoretical air quality modeling calculations. To advance this research project it was necessary to acquire a set of atmospheric pollutant concentration data that could be used to elucidate the important processes affecting basinwide nitrate concentrations, to further test an advanced trajectory model, and, eventually, to evaluate a full, grid-based, airshed model describing the dynamics of the pollutants. A major experiment was conducted in the Los Angeles Basin on 30-31 August, 1982, during which ionic aerosol constituents, nitric acid, ammonia and other gaseous precursor concentrations were measured for 48 consecutive hours at ten sites. Results and conclusions derived from the field experiment are described in Chapter 4. The results of this experiment are incorporated into the model evaluation effort described in Chapter 6.

The field experiment provided a very large set of data that can be used to test a key hypothesis in the air quality model: that nitric acid and ammonia are in equilibrium with the aerosol phase. A number of calculation procedures have been proposed to predict the equilibrium distribution of the species. Chapter 5 compares the field experimental findings to results obtained using alternative

theoretical hypotheses about the chemical composition of the aerosol species present in the atmosphere. The likely importance of aerosol nitrates formed by routes other than the reaction of HNO_3 with NH_3 , such as chloride displacement from sea salt by HNO_3 to form NaNO_3 , is investigated.

Chapter 6 describes an evaluation of the accuracy of an advanced photochemical, trajectory air quality model that describes aerosol nitrate and nitric acid formation. Model calculations are compared to results of the 30-31 August, 1982, field experiment. Within this chapter the effects of alternative control programs directed at reducing NO_x , NH_3 , and RHC emissions are depicted, and the implications of alternative control strategies are discussed further. Perturbing the emissions pattern in the air basin also illustrates the complex synergisms between photochemically generated air pollutants, and shows that a given reduction in precursor emissions need not result in a proportional reduction in the resulting pollutant concentrations. Future research needs are discussed in Chapter 7, and a summary of this work is contained in Chapter 8.

1.4 References

- Appel, B.R., Kothny, E.L., Hoffer, E.M., Hidy, G.M., and Wesolowski, J.J. (1978) "Sulfate and Nitrate Data from the California Aerosol Characterization Experiment (ACHEX)," Envir. Sci. Technol., 12 418-425.
- Clark County Health District (1982) "Air Quality in the Las Vegas Valley, Annual Report," Las Vegas, Nevada.
- Duce, R.A. (1969) "On the Source of Gaseous Chlorine in the Marine Atmosphere," J. Geophys. Res., 70, 1775-1779.
- Friedlander S.K. (1977) Smoke Dust and Haze, Wiley, New York.
- Galloway, J.N. and Likens, G.E. (1981) "Acid Precipitation: The Importance of Nitric Acid," Atmospheric Environment, 15, 1081-1085.
- Groblicki, P.J., Wolff, G.T. and Countess, R.J. (1981) "Visibility Reducing Species in the Denver "Brown Cloud", Part I. Relationships Between Extinction and Chemical Composition," Atmospheric Environment, 15, 2473-2484.
- Grosjean, D. (1983) "Distribution of Atmospheric Nitrogenous Pollutants at a Los Angeles Area Smog Receptor Site," Envir. Sci. Technol., 17 13-19.
- Grosjean, D., Fung, K. and Harrison, J. (1983) "Interactions of Polycyclic Aromatic Hydrocarbons With Atmospheric Pollutants," Envir. Sci. Technol., 17, 673-679.
- Hobbs, P.V. and Hegg, D.A. (1982) "Sulfate and Nitrate Size Distributions in the Near Field of Some Coal Fired Power Plants," Atmospheric Environment, 16, 2657-2662.
- Huebert, B.J. (1983) "Measurements of the Dry Deposition Flux of Nitric Acid Vapor to Grasslands and Forest," in Precipitation Scavenging, Dry Deposition, and Resuspension. Pruppacher, H.R., Semonin, R.G. and Slinn, W.G.N., coordinators, Elsevier, New York.
- Liljestrand, H.M. and Morgan, J.J. (1978) "Chemical Composition of Acid Precipitation in Pasadena, California," Envir. Sci. Technol., 12 1271-1273.
- National Research Council (1979) Airborne Particles University Park Press, Baltimore.

- Russell, A.G. and Cass, G.R. (1984) "Acquisition of Regional Air Quality Model Validation Data for Nitrate, Sulfate, Ammonium Ion and Their Precursors," Atmospheric Environment, 18, 1815-1827.
- Russell, A.G., McRae, G.J. and Cass, G.R. (1983) "Mathematical Modeling of the Formation and Transport of Ammonium Nitrate Aerosol," Atmospheric Environment, 17, 949-964.
- Russell, A.G., McRae, G.J. and Cass, G.R. (1985) "The Dynamics of Nitric Acid Production and the Fate of Nitrogen Oxides," Atmospheric Environment (in press).
- Seinfeld, J.H. (1975) Air Pollution, Physical and Chemical Fundamentals, McGraw Hill, New York.
- Stelson, A.W. and Seinfeld, J.H. (1982) "Relative Humidity and Temperature Dependence of the Ammonium Nitrate Dissociation Constant," Atmospheric Environment, 16, 983-992.
- van de Hulst, H.C. (1957) Light Scattering by Small Particles, Wiley, New York.
- Waldman, J.M., Munger, J.W., Jacob, D.J., Flagan, R.C., Morgan, J.J. and Hoffmann, M.R. (1982) "Chemical Composition of Acid Fog," Science, 218, 677-680.
- White, W. H. and Roberts, P.T. (1977) "On the Nature and Origins of Visibility Reducing Species in the Los Angeles Basin," Atmospheric Environment, 11, 803-812.

CHAPTER 2

MATHEMATICAL MODELING OF THE FORMATION AND
TRANSPORT OF AMMONIUM NITRATE AEROSOL

(Reprinted from Atmospheric Environment, 17, 949-964)

MATHEMATICAL MODELING OF THE FORMATION AND TRANSPORT OF AMMONIUM NITRATE AEROSOL

ARMISTEAD G. RUSSELL,* GREGORY J. McRAE† and GLEN R. CASS‡

*Department of Mechanical Engineering, †Environmental Quality Laboratory, ‡Environmental Engineering Science Department, California Institute of Technology, Pasadena, CA 91125, U.S.A.

(First received 19 April 1982; and in revised form 11 August 1982)

Abstract—A mathematical model describing the transport and formation of aerosol NH_4NO_3 is presented. Based on a vertically resolved Lagrangian trajectory formulation incorporating gas phase kinetics, NH_4NO_3 concentrations are computed at thermodynamic equilibrium with precursor HNO_3 vapor and NH_3 concentrations. Sensitivity analysis shows that NH_4NO_3 concentration predictions are strongly influenced by ambient temperature and NH_3 levels. A brief description of the NH_3 emissions inventory used in this study is included to indicate the important sources. The model was tested by comparison to ambient NH_3 , NH_4^+ and NO_3^- concentrations measured at El Monte, California during June 1974. Model results compare favorably with the ambient measurements and are used to explain trends in those measurements. An early morning nitrate peak develops as HNO_3 produced soon after sunrise reacts with NH_3 accumulated overnight. A second peak in nitrate concentration is predicted and observed at El Monte later in the day. Potential applications of this model to control strategy decisions and to study the fate of NO_x are discussed.

INTRODUCTION

Aerosol nitrates are important contributors to visibility reduction in cities with photochemical air pollution problems. White and Roberts (1977) estimate that during the ACHEX study, aerosol nitrates were responsible for about 40% of the light scattering observed at Riverside in the eastern Los Angeles Basin. Groblicki *et al.* (1981) report that 17% of the visibility problem in Denver is attributable to aerosol nitrates. Control strategies for urban visibility improvement in such cities will need to address aerosol nitrate abatement alternatives. Before this can be done, a reliable means is needed for predicting the relationship between pollutant emission sources and resulting nitrate concentrations.

Ammonium nitrate is a secondary pollutant formed from reactions between NH_3 and HNO_3 vapor. From thermodynamic considerations Stelson *et al.* (1979) and Stelson and Seinfeld (1982a, b) have shown that atmospheric NH_4NO_3 should be in equilibrium with precursor HNO_3 and NH_3 concentrations. The validity of this assumption has been tested in field experiments by Doyle *et al.* (1979), where it was found that the NH_4NO_3 equilibrium constant derived from published thermochemical data is consistent with atmospheric observations.

In this paper a mathematical model relating pollutant emissions to NH_4NO_3 concentrations is proposed and tested. Based on a Lagrangian trajectory formulation, the model includes transport, gas phase kinetics and aerosol production. A sensitivity analysis is performed on the NH_4NO_3 formation mechanism used in the trajectory model to indicate which parameters are most important to formation of atmospheric NH_4NO_3 . A summary of the emissions inventory used in this modeling study details the import-

ant sources of NH_3 and their spatial distribution (Cass *et al.*, 1982). Model results will be evaluated against NH_3 , NH_4^+ and NO_3^- concentrations observed at El Monte, California on 28 June 1974. Potential use of this model for studying acid deposition and the fate of nitrogen containing pollutants is discussed.

MODEL DESCRIPTION

Ammonium nitrate aerosol is classified as a secondary pollutant because it is formed in the atmosphere from reactions involving gas phase precursors. To predict NH_4NO_3 formation, this paper utilizes a photochemical trajectory model coupled with an equilibrium treatment of aerosol production. Concentrations of the gas phase precursors of NH_4NO_3 as well as other pollutant concentrations are calculated using a vertically resolved, Lagrangian trajectory form of the atmospheric diffusion equation presented in McRae *et al.* (1982a). The equation governing the concentration of species i , $c_i(z, t)$, is

$$\frac{\partial c_i}{\partial t} = \frac{\partial}{\partial z} \left(K_{zz} \frac{\partial c_i}{\partial z} \right) + R_i(c_1, c_2, \dots, c_n, T) - \frac{\partial v_s c_i}{\partial z}; \quad i = 1, 2, \dots, n \quad (1)$$

with initial conditions

$$c_i(z, 0) = c_i^0(z) \quad t = 0 \quad (2)$$

and boundary conditions

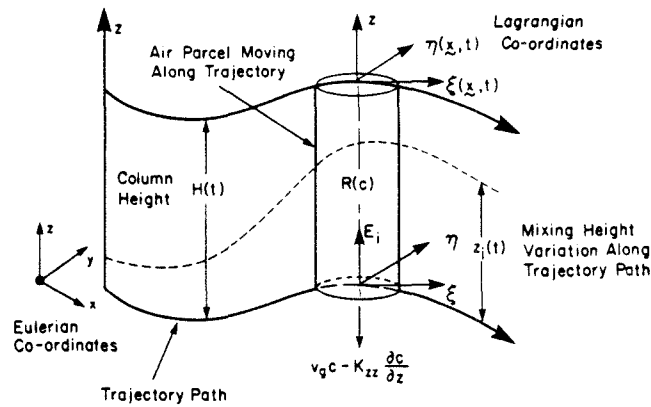
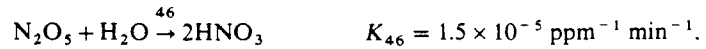
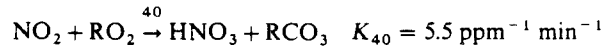
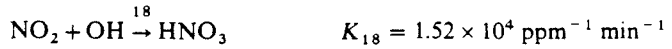
$$\left(K_{zz} \frac{\partial c_i}{\partial z} \right) = 0 \quad z = H \quad (3a)$$

$$\left[v_g^i c_i - K_{zz} \frac{\partial c_i}{\partial z} \right] = E_i \quad z = 0, \quad (3b)$$

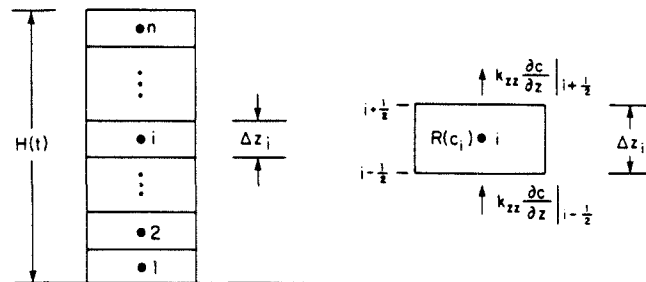
where $K_{zz}(z)$ is the vertical turbulent eddy diffusivity, $R_i(c_1, \dots, c_n, T)$ is the rate of chemical production of species i at temperature T , H is the height of the air column and v_s is the settling velocity. As used in (1), v_s is used to describe gravitational settling, but its effect on (1) is negligible for aerosol particles smaller than about $1 \mu\text{m}$. Aerosol NH_4NO_3 is generally associated with μm -sized particles, so gravitational settling can be neglected in the following calculations. Parameters associated with the boundary conditions are v_g^i , the deposition velocity, and E_i , the species mass flux per unit area. Treatment of surface deposition and the relationship of K_{zz} to atmospheric stability is described in McRae *et al.* (1982a) and will not be repeated here. Vertical transport of both gases and aerosols is dominated by turbulent eddies. It is important to note that models described by (1) are based on the assumptions that horizontal diffusion and vertical advection are small, and that the effects of wind shear are negligible. The effects of these simplifications are discussed in Liu and Seinfeld (1975).

Ground level ($z = 0$) boundary conditions are a statement of mass continuity, accounting for surface deposition, diffusive transport and emissions. Since the top of the region ($z = H$) is well above the mixing depth, turbulent transport through the top of the air column is negligible. Deposition velocities are used to describe the interaction and reaction of gases and aerosols with surfaces. In general, v_g^i is dependent on meteorological conditions and on the reactivity of species i with the underlying surface. Limits on the aerosol deposition rates can be found using the same modeling techniques as those for gaseous pollutants. The vertically resolved trajectory model and computational cells are shown schematically in Fig. 1.

The chemical kinetics associated with the term $R_i(c_1, \dots, c_n, T)$ in (1) are described using the photochemical reaction mechanism of Falls and Seinfeld (1978), Falls *et al.* (1979), McRae *et al.* (1982a) and McRae and Seinfeld (1983). Only those homogeneous gas phase pathways producing HNO_3 and their corresponding rate constants, at 25°C , will be given here. These pathways are:



(a)



(b)

Fig. 1. Schematic representation of (a) vertically resolved Lagrangian trajectory model and (b) the computational grid cell convention.

Other than direct emissions, the only source of HNO_3 is assumed to be the photochemical production through the above reactions. Reaction 18 is the dominant route producing HNO_3 for typical daytime atmospheric conditions. Photolytic loss of HNO_3 is ignored since it is small.

Equilibrium concentrations of gaseous NH_3 and HNO_3 , and the resulting concentration of solid or aqueous NH_4NO_3 can be calculated from fundamental thermodynamic principles using the method presented by Stelson and Seinfeld (1982a). The procedure is composed of several steps, requiring as input the ambient temperature and relative humidity (r.h.). First, the equilibrium state of NH_4NO_3 is defined. If the ambient relative humidity is less than the relative humidity of deliquescence, (r.h.d.), given by

$$\ln(\text{r.h.d.}) = 723.7/T + 1.7037, \quad (4)$$

then the equilibrium state of NH_4NO_3 is modeled as a solid. Supersaturated solutions also are possible. Formation of solid NH_4NO_3 , from the gas phase precursors, is described by the equilibrium system

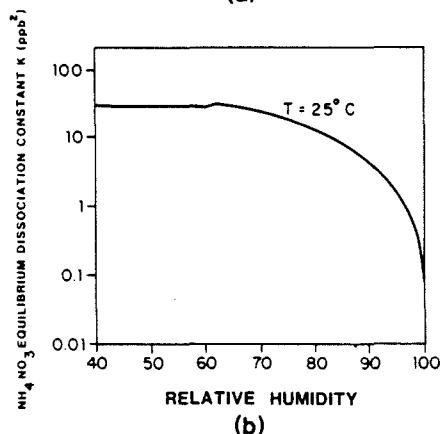
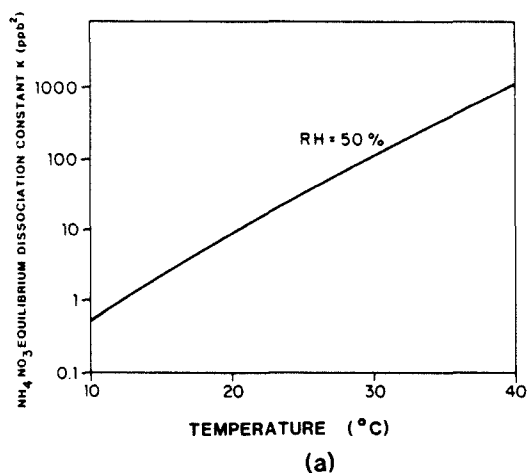
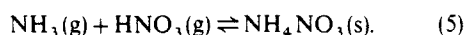


Fig. 2. (a) NH_4NO_3 equilibrium dissociation constant as a function of temperature (r.h. 50%). (b) NH_4NO_3 equilibrium dissociation constant as a function of r.h. (temperature, 25°C).

The dissociation constant is given by $K = P_{\text{NH}_3} P_{\text{HNO}_3}$, where P_{NH_3} and P_{HNO_3} are the partial pressures of NH_3 and HNO_3 , respectively. K can be estimated by integrating the van't Hoff equation. The resulting equation for K , in units of ppb^2 (assuming 1 atm of total pressure) is

$$\ln K = 84.6 - 24220/T - 6.1 \ln(T/298). \quad (6)$$

At relative humidities above that of deliquescence, NH_4NO_3 will be found in the aqueous state. A dissociation constant for the comparable reaction involving aqueous NH_4NO_3 can be found and is a function of both temperature and relative humidity. Temperature dependent equilibrium relative humidities above ionic solutions (r.h.t.) can be calculated from

$$\text{r.h.t.} = 100 \exp\left(\frac{-v m M \phi_T}{1000}\right), \quad (7)$$

where v is the number of moles of ions formed by ionization of one mole of solute, M the molecular weight of water, m the molality of the solution and ϕ_T is the osmotic coefficient given by

$$\phi_T = 1 + \frac{1}{m} \int_0^m m d(\ln \gamma^\pm)_T, \quad (8)$$

where γ^\pm is the mean molal activity of NH_4NO_3 in the solution at temperature T . The activity coefficient depends on temperature and molality. An iterative scheme is used to match the relative humidity calculated from (7) to the ambient relative humidity. This calculation gives the equilibrium solution molality and activity that are needed to evaluate K , the equilibrium dissociation constant, from the expression

$$\ln(K/(\gamma^\pm m)^2) = 54.18 - 15860/T + 11.206 \ln(T/298). \quad (9)$$

If the ambient relative humidity is between that of deliquescence and the value given by (7) for a saturated solution at $m = 25.954$, linear interpolation is used between the corresponding dissociation constants.

Figures 2(a) and (b) depict the dependence of K on T and r.h. For typical atmospheric conditions, the mechanism predicts an equilibrium dissociation constant between $0.04 (\text{ppb})^2$ at 5°C and 90% r.h. and $1400 (\text{ppb})^2$ at 40°C and a r.h. of 30%. Figure 2(b) indicates that extrapolation of the calculation scheme used for aqueous solutions to that for supersaturated solutions would give results slightly different than those found using (6) for solid NH_4NO_3 . In the case of a saturated solution surrounding solid NH_4NO_3 , equating the chemical potentials across interfaces shows that the appropriate dissociation constant is the same as that for the solid. This model assumes that the time required for the gaseous precursors, and water, to come to equilibrium is short compared to the characteristic time for the production of HNO_3 . This may not be true if the concentrations of the precursors differ by orders of magnitude, though this is seldom the case in

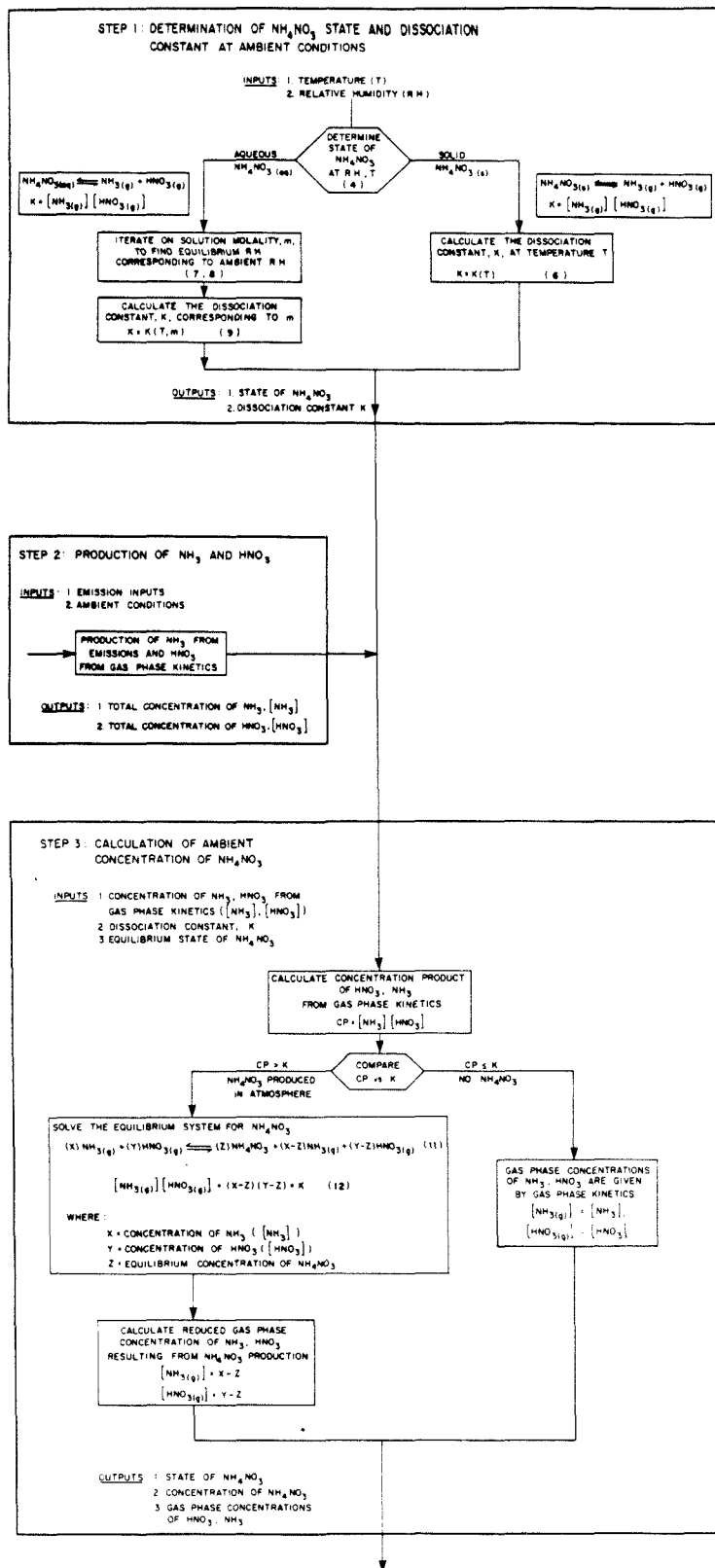


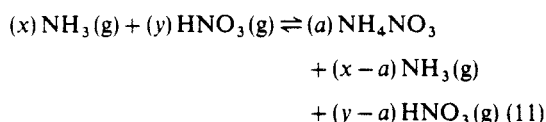
Fig. 3. Flow diagram of NH₄NO₃ formation mechanism illustrating three basic steps in calculation procedure.

urban basins. Nitric acid and NH_3 losses to other aerosol species are neglected at this point, and thus mixed aerosols are not considered. These effects can be incorporated once sufficient, appropriate field data become available to verify a more complex model.

Gas phase concentrations of NH_3 and HNO_3 and the concentration of NH_4NO_3 are then calculated from precursor concentrations and the equilibrium system



Concentrations of the different species can be determined mathematically by solving the following system of equations.



and

$$[\text{NH}_3(\text{g})][\text{HNO}_3(\text{g})] = (x-a)(y-a) = K, \quad (12)$$

where x is the total concentration of NH_3 plus NH_4^+ , y is the total concentration of HNO_3 plus nitrate, a is the resulting concentration of NH_4NO_3 aerosol, and $(x-a)$, $(y-a)$ are the equilibrium gas phase concentrations of NH_3 and HNO_3 , respectively.

If the product of the concentrations of NH_3 and HNO_3 is smaller than the dissociation constant,

$$[\text{NH}_3(\text{g})][\text{HNO}_3(\text{g})] = (x)(y) < K \quad (13)$$

no NH_4NO_3 should be present. In this case the gas phase concentrations are as given by the gas phase kinetics. The steps involved in predicting the nitrate concentrations are shown schematically in Fig. 3.

SENSITIVITY STUDY

A Fourier amplitude sensitivity test (FAST) (Koda *et al.*, 1979; McRae *et al.*, 1982b) was performed on the NH_4NO_3 calculation scheme to assess which parameters contribute most to the formation of NH_4NO_3 in the atmosphere. The ranges of species concentrations used in the analysis are representative of those observed by Tuazon *et al.* (1981) for Claremont, California and were measured by Fourier transform infrared (FTIR) spectroscopy. In these experiments the FTIR sampling cell temperature was often considerably higher than ambient, which could volatilize some of the NH_4NO_3 , so the measurements may give $\text{NH}_3(\text{g})$ and $\text{HNO}_3(\text{g})$ levels higher than ambient. The results of the FAST analysis are shown in Table 1, where it can be seen that NH_4NO_3 formation is most sensitive to variations in temperature. The reason for this is the strong dependence of the dissociation constant on T . Two insights can be gained from FAST analysis, the first being that it is critically important to specify the temperature field accurately. Secondly, since nitrate formation is sensitive to NH_3 over the range encountered, control of upwind NH_3 emissions

Table 1. Sensitivity of ammonium nitrate formation model to input parameters

Parameter	Range	Sensitivity* (%)
Temperature	10–40°C	41
Ammonia	4–23 ppb†	39
Nitric acid	6–49 ppb†	17
Relative humidity	20–90%	3

* Partial variance, normalized to 100%, indicates the relative importance of variation of model inputs on NH_4NO_3 formation.

† Values representative of those found in Tuazon *et al.* (1981) for Claremont, California.

should prove to be beneficial in limiting NH_4NO_3 concentrations at Claremont and that an accurate description of the NH_3 emissions is required for modeling purposes.

To show how the concentrations of NH_4NO_3 change with ambient meteorological conditions, representative levels of total NH_3 (i.e. $\text{NH}_3(\text{g}) + \text{NH}_4^+$) and total HNO_3 (i.e. $\text{HNO}_3(\text{g}) + \text{NO}_3^-$) were used to calculate NH_4NO_3 concentrations over a range of atmospheric conditions. Predicted concentrations of NH_4NO_3 ranged from 0 to $67.6 \mu\text{g m}^{-3}$, with typical values of about $10 \mu\text{g m}^{-3}$ corresponding to 25°C, 65% r.h., 8 ppb of total NH_3 and 16 ppb of total HNO_3 . Concentration plots in Fig. 4 again show that NH_4NO_3 formation is sensitive to temperature, decreasing rapidly as temperature increases. An interesting aspect of the temperature dependence is the flat area indicating that no NH_4NO_3 is present. Above 35°C little NH_4NO_3 would be present except at high ambient levels of the gas phase precursors, while at 15°C some NH_4NO_3 would be present at most precursor concentrations. Figure 4 also shows that there is little change in NH_4NO_3 formation as the r.h. changes, although the effect is to create slightly more NH_4NO_3 as r.h. increases.

EMISSIONS DATA REQUIRED FOR MODEL EVALUATION

Once the model has been formulated the next step is to evaluate its ability to predict ambient levels of NH_4NO_3 . The data required for such tests include; pollutant emissions, observed air quality and the prevailing meteorology. In the Los Angeles Basin accurate emission inventories exist only for the period between 26 and 28 June 1974, limiting model evaluation to those three days. Descriptions of the emission inventories for NO_x and reactive hydrocarbons together with the local meteorological conditions for this period are available in McRae and Seinfeld (1983). As indicated by the sensitivity analysis, there is a need for an accurate description of the NH_3 emissions. Cass *et al.* (1982) have recently completed such a study for the year 1974, and the principal results are summarized here. A grid system composed of 5×5 km cells was

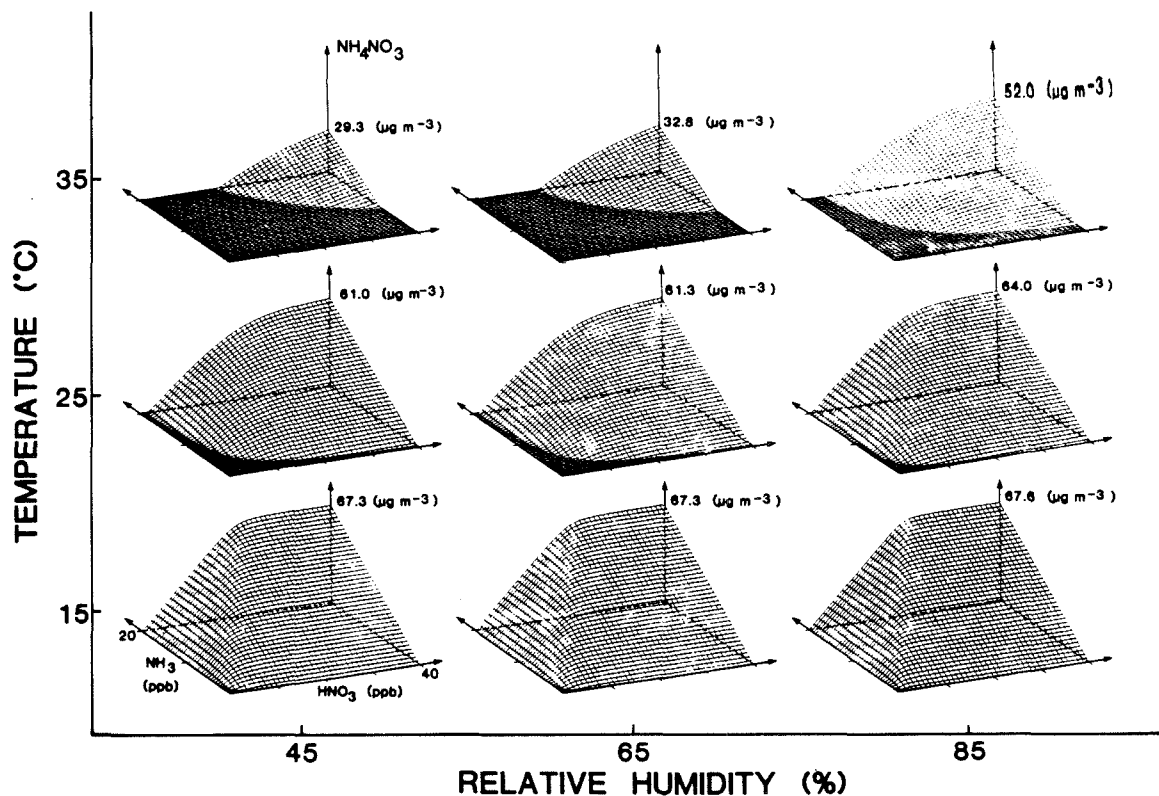


Fig. 4. Predicted NH_4NO_3 concentration surfaces at 15, 25 and 35°C and 45, 65 and 85% r.h. for total NH_3 and total HNO_3 concentrations up to 20 and 40 ppb, respectively.

superimposed on the South Coast Air Basin map (Fig. 5). Ammonia emissions were estimated within each grid cell for the 53 classes of mobile and stationary source types listed in Table 2.

Source tests show that trace amounts of NH_3 are present in the exhaust of both mobile and stationary

combustion sources (Cadle and Mulawa, 1980; Gentel *et al.*, 1973; Harkins and Nicksic, 1967; Henein, 1975; Hovey *et al.*, 1966; Hunter, 1971; Muzio and Arand, 1976; Wohlers and Bell, 1956). Emission factors for NH_3 release obtained from these and other references were combined with fuel use data reported by Cass

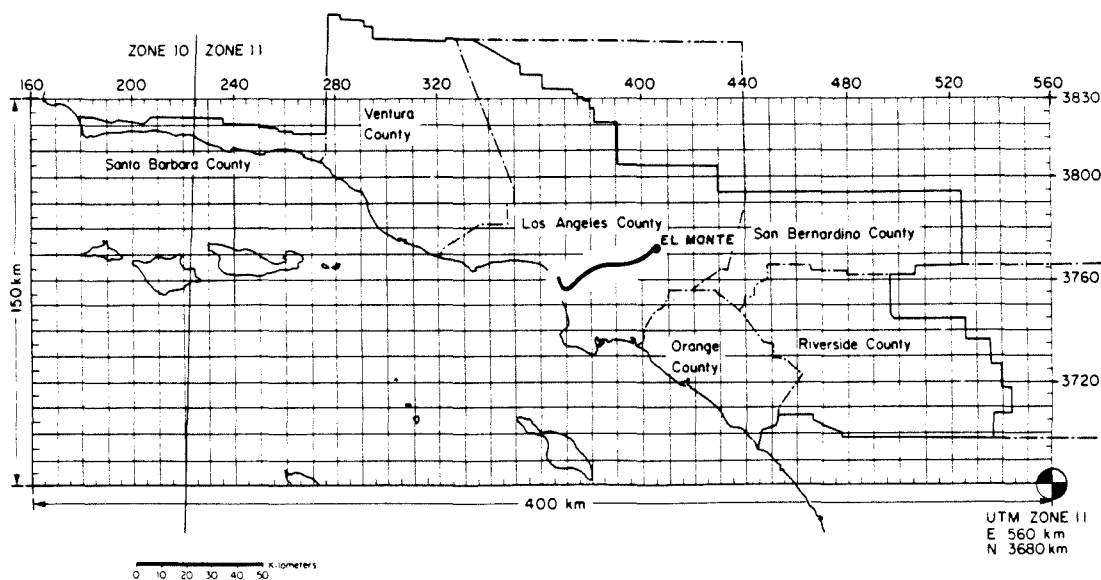


Fig. 5. Gridded map of the South Coast Air Basin used for constructing NH_3 emissions inventory. Superimposed on the map is the trajectory path that reaches El Monte at 3 p.m. (PDT) on 28 June 1974.

Table 2. Summary of ammonia emissions by source category in the South Coast Air Basin 1974

Source category	Total emissions (kg day ⁻¹)
Stationary fuel combustion	
Electric utility	
Natural gas	590.0
Residual oil	2000.0
Digester gas	0.5
Refinery fuel burning	
Natural gas	160.0
Residual oil	99.0
Refinery gas	420.0
Industrial fuel burning	
Natural gas	610.0
Liquified petroleum gas (LPG)	4.0
Residual oil	150.0
Distillate oil	140.0
Digester gas	9.0
Coke oven gas	15.0
Residential/commercial fuel burning	
Natural gas	270.0
Liquified petroleum gas (LPG)	4.0
Residual oil	62.0
Distillate oil	73.0
Coal	20.0
Sub totals	4626.5 (3.09%)
Mobile source fuel combustion	
Automotive	
Non-catalyst autos and light trucks	3309.0
Medium and heavy duty trucks	449.9
Diesel vehicles	370.0
LPG for carburetion	10.0
Civilian aircraft	
Jet	150.0
Piston	2.9
Shipping	
Residual oil boilers	70.0
Diesel ships	50.0
Railroad-diesel oil	90.0
Military	
Gasoline	10.0
Diesel	60.0
Jet fuel	50.0
Residual oil	0.8
Off highway vehicles	120.0
Sub totals	4742.6 (3.17%)
Industrial point sources	2070.0 (1.38%)
Soil surface	23790.0 (15.9%)
Fertilizer	
Farm crop	2870.0
Orchards	2390.0
Handling	380.0
Non-farm	7420.0
Sub totals	13060.0 (8.72%)
Livestock	
Cattle	
Dairy	24390.0
Feedlot	6880.0
Range	12160.0
Horses	16220.0
Sheep	990.0
Hogs	250.0
Chickens	18200.0
Turkeys	1120.0
Sub totals	80210.0 (53.6%)

Table 2. (contd).

Source category	Total emissions (kg day ⁻¹)
Domestic	
Dogs	10350.0
Cats	3230.0
Human respiration	46.0
Human perspiration	7000.0
Household ammonia use	600.0
Sub totals	21226.0 (14.2%)
Total	149725.1 (100.0%)

(1978) to give total NH₃ emissions from autos, trucks, railroads, shipping, plus industrial, residential and commercial fuel use. Within each fuel use category, the NH₃ emissions shown in Table 2 were distributed spatially in the same manner as NO_x emissions. A number of industrial processes are known to emit NH₃ (National Research Council, 1979; Miner, 1969), including refinery operations, NH₃-based fertilizer manufacturing, NH₃ storage facilities, refrigeration plants, chemical plants and steel mill coke ovens. Estimates of NH₃ emissions from industrial facilities were derived from source test information and questionnaires sent to individual companies.

Biological decay processes also produce NH₃ and the release rates from a variety of soil surface types are available (Porter *et al.*, 1975; Elliot *et al.*, 1971; Denmead *et al.*, 1978; Denmead *et al.*, 1976; Miner, 1976). Using aerial photographs and maps available from the U.S. Geological Survey (1976) the land use within each grid square was summarized by type. Emissions from exposed land surfaces were estimated within each square by matching emission rate data to soil surface types.

Chemical fertilizers used in the air basin include NH₃, urea, NH₄NO₃ and (NH₄)₂SO₄. Depending on fertilizer type and method of application, anywhere from a few percent to several tenths of the nitrogen content may be lost to the atmosphere as NH₃ (Baker *et al.*, 1959; Ernst and Massey, 1960; Gasser, 1964; McDowell and Smith, 1958; Stanley and Smith, 1955; Trickey and Smith, 1955; Wahhab *et al.*, 1957; Walkup and Nevins, 1966). The NH₃ loss characteristics of fertilizers were estimated by consultation with a local agricultural expert (Meyer, personal communication). Fertilizer use statistics were obtained from the California Department of Food and Agriculture (1974) and from the U.S. Bureau of the Census (1977). Chemical fertilizer consumption, subdivided into cropland, orchard and non-farm use, was combined with the NH₃ loss data to compute total NH₃ emissions.

Decomposition of livestock wastes is a major source of NH₃ emissions. Animal inventories by county were obtained from the U.S. Bureau of the Census (1977) and from state and county agricultural agents. Waste production rates, nitrogen content and NH₃ volatilization

rates were estimated for each major commercial animal type from previous studies (Adriano *et al.*, 1974; Fogg, 1971; Giddens and Rao, 1975; Lauer *et al.*, 1976; Luebs *et al.*, 1973a,b; Stewart, 1970; Taiganides and Hazen, 1966; Viets, 1971). Emissions from range animals were distributed spatially in proportion to pasture and herbaceous range land areas. U.S. Geological Survey (1976) maps were used to locate emissions from animals raised in confinement (e.g. dairy cattle, feedlot cattle). Ammonia losses from domestic animals (cats and dogs only) plus human respiration, perspiration and household cleaning chemicals were distributed in proportion to residential land use.

The overall spatial distribution of NH₃, NO_x, reactive hydrocarbon and CO emissions in the South Coast Air Basin is shown in Fig. 6. The largest spike in the NH₃ diagram is centered over the town of Chino on the prevailing upwind side of the city of Riverside, and results from the intensity of livestock operations in that area.

AIR QUALITY DATA FOR MODEL EVALUATION

Within the three day time period for which emission data are available, aerosol nitrate measurements were sought that were taken over short sampling intervals (1–2 h) using methods that would minimize the possible interferences. Simultaneous concentration measurements of related aerosol species such as sulfate and ammonium were desired, as well as the concentration of relevant gas phase species, such as NH₃, HNO₃, NO_x and O₃. The data set most nearly fulfilling the requirements was found for El Monte, California. The measurements were taken on 28 June 1974, and consist of 2-h averaged concentrations of aerosol nitrate and NH₄⁺, and gas phase NH₃ (Reynolds *et al.*, 1975). Aerosol nitrate and ammonium concentrations were obtained by using a low volume sampler with Gelman A glass fiber filters for collection followed by wet chemical analysis. Gaseous NH₃ concentrations were found using oxalic acid impregnated backup filters.

Ammonium nitrate data for other time periods in the Los Angeles area are available and are consistent with the results presented in Reynolds *et al.* (1975). These studies have found measured ambient nitrate

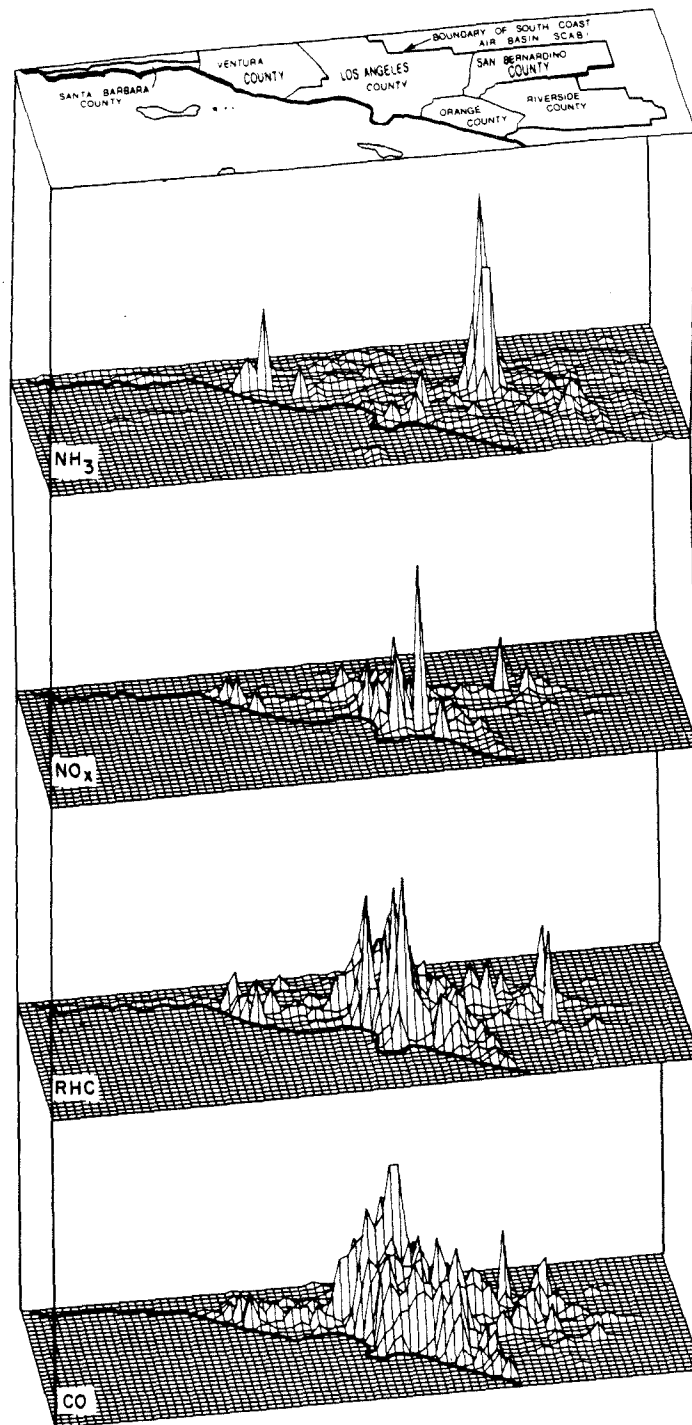


Fig. 6. Spatial representation of daily emissions of NH_3 , NO_x , reactive hydrocarbons (RHC) and CO in the South Coast Air Basin. (Inventory period June 1974.)

concentrations ranging up to $149 \mu\text{g m}^{-3}$, though values are generally lower (Lundgren, 1970; Hidy *et al.*, 1980; Appel *et al.*, 1978; Spicer, 1974; Appel *et al.*, 1981; Tuazon *et al.*, 1981). In Claremont, California, ambient levels of gaseous HNO_3 and NH_3 have been observed up to 49 and 23 ppb, respectively (Tuazon *et al.*, 1981). Concentrations of up to $86.4 \mu\text{g m}^{-3}$ of particulate

nitrate were also found at Claremont (Appel *et al.*, 1980). Nitrate levels were found to vary diurnally, peaking in the midmorning. Ozone and HNO_3 peaked later in the afternoon. Partial pressure products of NH_3 (g) and HNO_3 (g) from data taken at Claremont were compared against relative humidity and temperature. The product decreased with relative humidity and

increased with temperature, the same trend predicted from thermodynamic considerations.

When interpreting ambient measurements, it is important to be aware of the potential for artifact nitrate formation on filter substrates (Pierson *et al.*, 1980; Spicer and Schumacher, 1979; Appel *et al.*, 1979; Witz and McPhee, 1977). The physical nature of the nitrate artifact problem is that the gaseous HNO_3 may react with the filter substrate forming nitrate on the filter. This results in a positive error as more nitrate is measured on the filter than was deposited as an aerosol. A negative error can result from revolatilization of the NH_4NO_3 prior to sample analysis, or by reaction with other gaseous or particulate acids displacing the HNO_3 (Appel *et al.*, 1980). The observed revolatilization is in agreement with the equilibrium hypothesis employed in this paper. If the filter, after being loaded and before being analyzed, is exposed to a change in environment it would set up a new equilibrium between the aerosol and its environment, possibly altering the aerosol's measured composition. The new equilibrium could be due either to a change in temperature or to a change in the gaseous environment during or after sampling. To prevent this problem the NH_4NO_3 would have to be collected, stored and analyzed in a manner that prevents volatilization of the aerosol from the filter.

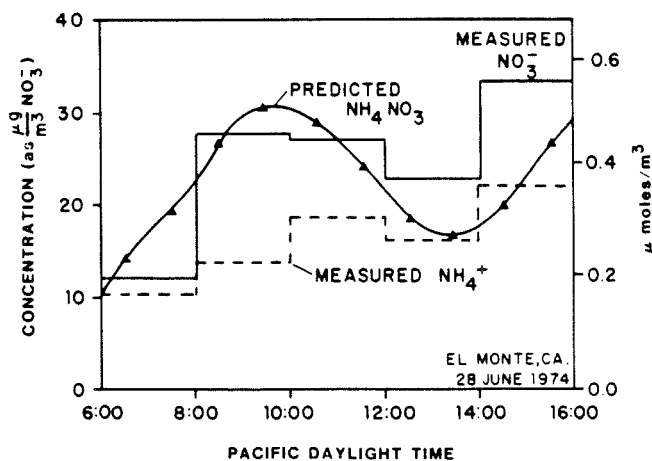
Steps have been taken to correct the filter artifact problem, the most direct being the use of a substrate that does not react with gaseous HNO_3 to form nitrate. Substrates that have been tested and show little reactivity with HNO_3 include polycarbonate, Teflon and quartz fiber (Spicer and Shumacher, 1979). Most glass fiber and nylon filters prove to be quite susceptible to artifact nitrate formation, although Gelman A filters are not as susceptible as many others (Appel *et al.*, 1979). Another method involves stripping the HNO_3 (g) from the sampling stream prior to filtration by passing the gas through a denuder, then measuring total nitrate downstream (Appel *et al.*, 1981).

MODEL EVALUATION AGAINST AMBIENT MEASUREMENTS

Usually ambient measurements are made at a fixed location. A Lagrangian model, however, predicts concentrations along a trajectory in a single air mass as it flows through the air basin. The path of a sample trajectory, the one starting at 1 a.m. and reaching E1 Monte at 3 p.m. Pacific Daylight Time (PDT) on 28 June 1974, is shown on a map of the Los Angeles basin (Fig. 5). Use of a trajectory model to predict concentrations at different times for a fixed geographical location then requires finding the path that each air mass takes to reach that location at the appropriate time. This is done for trajectories reaching E1 Monte throughout the day of 28 June 1974 using the method prescribed in Goodin *et al.* (1979).

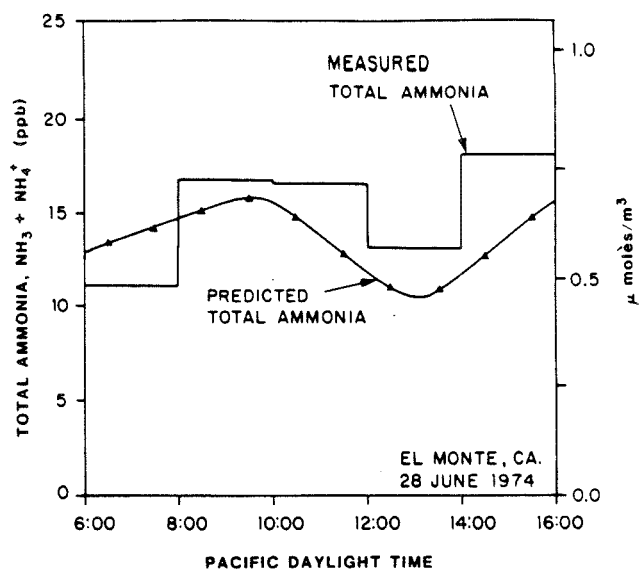
By taking a series of trajectories reaching E1 Monte during the day, a time history of species concentrations can be constructed (Fig. 7). Each concentration prediction shown represents a weighted average of three trajectories arriving at E1 Monte at 1 h intervals, and are plotted on the half hour. In Fig. 7(a), the predicted ground level NH_4NO_3 concentration is plotted along with the measured nitrate and NH_4^+ concentration. Concentrations are given in $\mu\text{mol m}^{-3}$ for all species and NO_3^- concentrations are restated in $\mu\text{g m}^{-3}$. Gas phase concentrations are also shown in ppm or ppb. Use of a system based on molar concentrations is more convenient in the presence of chemical reactions, and clarifies the relationship between aerosols and their gas phase precursors. Considering the difficulty in obtaining ambient nitrate measurements, comparison between observed and predicted nitrate concentrations is quite good.

From Fig. 7(a), it can be seen that the measured molar concentrations of aerosol nitrate exceed that of NH_4^+ . The difference could arise if species other than NH_4NO_3 were present in the aerosol (e.g. NaNO_3), or as a result of the filter artifact problem. Filter artifact problems can lead to either a positive error due to

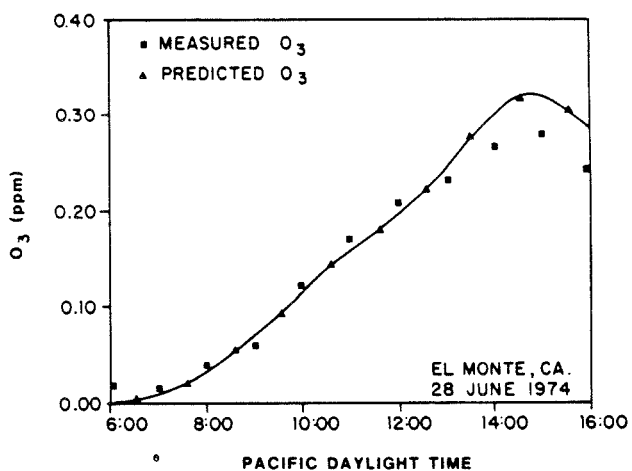


(a)

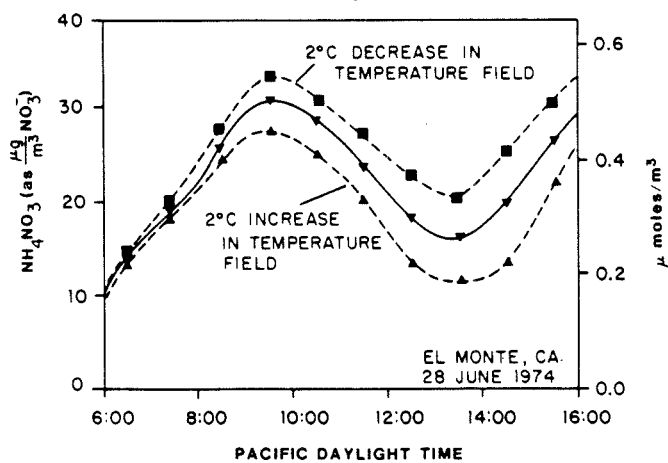
Fig. 7(a).



(b)



(c)



(d)

Fig. 7. Concentration profiles at El Monte on 28 June 1974. (a) Predicted NH_4NO_3 , measured NH_4^+ and measured NO_3^- . (b) Predicted total ammonia ($\text{NH}_3 + \text{NH}_4^+$) and measured total ammonia. (c) Predicted and measured O_3 concentrations. (d) Sensitivity of NH_4NO_3 formation to a $\pm 2^\circ\text{C}$ change in the temperature field.

HNO₃ reacting with the filter or a negative error from the volatilization of either ammonium or nitrate containing species. Twenty four hour averaged measurements for the day modeled showed only 5.1 μg m⁻³ of sulfate. Previous studies (e.g. Appel *et al.*, 1978) showed that most of the sulfate aerosol appears in the late afternoon. Thus, the interference from sulfate should be small for the period modeled. It is impossible to say how the predicted nitrate should compare to the measured nitrate concentrations without knowing the magnitude of the two types of possible sampling error.

Relatively little NH₄NO₃ is measured or predicted in the early morning. The concentration rises until about 10 a.m. (PDT) at which time it starts to decrease as the temperature increases. The same trend is found by other investigators (Appel *et al.*, 1980). Both the measurements and predictions for 28 June 1974, show an afternoon rise that is uncharacteristic of the usual decrease in NH₄NO₃ as the temperature increases. Figure 7(b), the plot of the predicted and measured total (gas plus aerosol phase) NH₃ concentrations, shows that the reason for the unexpected afternoon peak is that the air mass contains more NH₃. Figure 7(b) also serves as a check on the NH₃ emissions inventory. Even in the presence of possible transfer of revolatilized NH₃ to the oxalic acid impregnated backup filter used to measure NH₃, the sum of measured NH₃ and NH₄⁺ should give total NH₃. Predicted total NH₃ is about 10–20% low through most of the day, except in the early morning. Predictions follow the same diurnal trends as the measurements, indicating the spatial accuracy of the inventory over which the trajectory passed.

In view of the possible effects occurring from nitrate artifact formation, it is interesting to note that the predicted nitrate levels are high in the morning when the potential to form artifact nitrate is small. In the afternoon the increasing HNO₃ concentration raises the potential formation of artifact nitrate, and it is seen that the predicted nitrate concentrations begin to fall below the measured levels.

As an additional check on model performance, predicted O₃ concentrations at El Monte are compared to measurements in Fig. 7(c), and the two profiles compare well. Ozone measurements were not taken at El Monte, so the measured values being used are interpolated from surrounding monitoring sites.

A good measure of the sensitivity of nitrate formation to temperature variations is obtained from Fig. 7(d). Increase in the separation between the curves is due almost totally to the change in *K* from the temperature change, not from a change in the amount of total inorganic nitrate produced. This figure also illustrates the potential problems arising from either upsetting the equilibrium, or from errors in the temperature field specification.

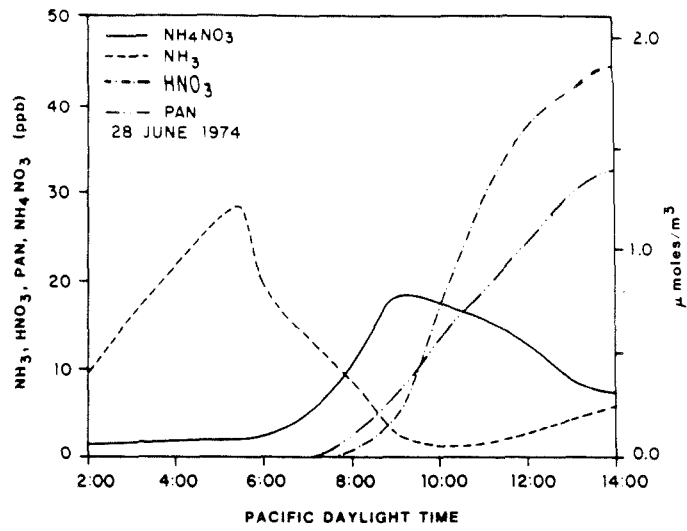
For model evaluation purposes it was necessary to compare predictions and observations at a fixed point; however, it is more illuminating to investigate dynamics of the nitrate aerosol production along a single

trajectory. In this manner the effects of the physical processes are more easily isolated. In the series of plots shown in Fig. 8, the evolution of pollutant concentrations is shown as the air mass traverses the basin. Early morning NH₃ emissions into the air parcel increase the NH₃ concentrations but have only a small effect on the aerosol levels because little HNO₃ has been produced by photochemical reactions (Fig. 8a). After sunrise, photochemical reactions start forming inorganic nitrate from the oxidation of NO_x emissions. Initially most of the nitrate formed is tied up in the aerosol phase increasing the NH₄NO₃ concentration and decreasing that of NH₃. Nitric acid continues to be the limiting species for aerosol formation until 8 a.m. when the HNO₃ concentration begins to rise rapidly. Both NH₄NO₃ and HNO₃ levels continue to increase, and NH₃ to drop, until about 9 a.m. when a midmorning NH₄NO₃ peak occurs. After this time the NH₄NO₃ concentration decreases due to two effects, aerosol volatilization by the increasing temperature and dilution by the growing mixed layer. The profile for PAN, an organic nitrate, is shown in Fig. 8(a). PAN follows the same diurnal trend as HNO₃, peaking at 33 ppb compared to 44 ppb for HNO₃. The peak HNO₃ concentration was 13% that of O₃. Tuazon *et al.* (1981) found a similar PAN to HNO₃ ratio and approximately the same maximum values. For example, the peak HNO₃ levels were 11% of the observed O₃ concentrations at Claremont, California in 1978.

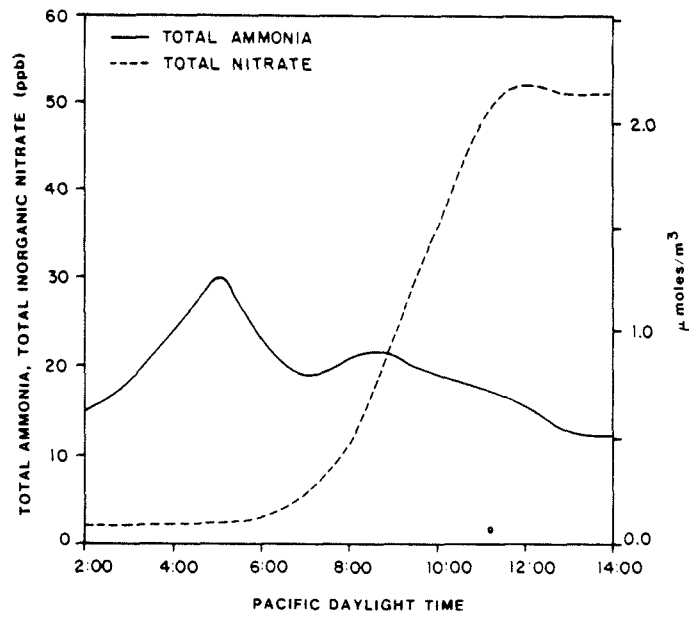
Figure 8(b) graphically illustrates the initial rise in NH₃ from emissions. Photochemical reaction of NO_x causes a rapid increase in the concentration of total inorganic nitrate shortly after sunrise at 5:45 a.m. Total nitrate increases until about noon when dilution and deposition of HNO₃ and NH₄NO₃ cause the total nitrate concentrations to stabilize. Profiles of three pollutants related to HNO₃ formation, O₃, NO and NO₂, are shown in Fig. 8(c) for comparison.

Vertically-resolved profiles of NH₄NO₃ and its precursors are plotted in Fig. 9 at three different times during the day. Early in the morning, the most marked profile is that of NH₃ showing that the emissions are being trapped within the mixed layer. Four hours later, at 8 a.m., the mixing depth has increased and so has the NH₄NO₃, but the availability of HNO₃ is still limiting the formation. By noon, HNO₃ is the most abundant species below the temperature inversion and NH₃ availability now limits aerosol formation. Directly above the inversion base the change in the NH₃ profile is created by the decrease in HNO₃ allowing a higher equilibrium NH₃ concentration.

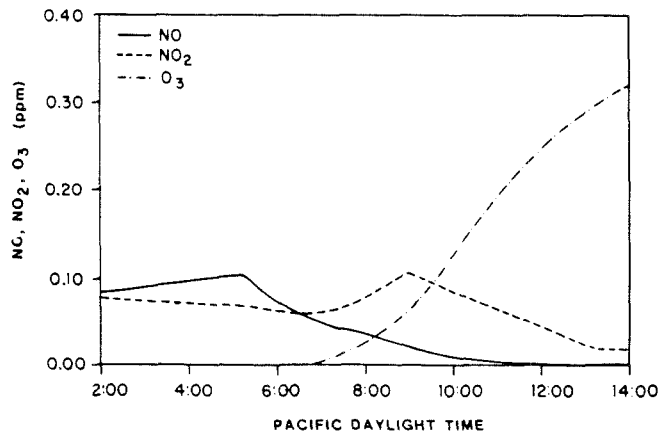
In this study, the currently available collection of simultaneous observations on emissions and air quality has been pursued as far as it can be taken, and it is apparent that additional model applications should be supported by a data set explicitly designed for nitrate air quality model verification. Such a data set should include simultaneous measurements on all species of interest including NH₃ and HNO₃ vapor, plus NH₄⁺ and NO₃⁻ concentrations. Measurement



(a)

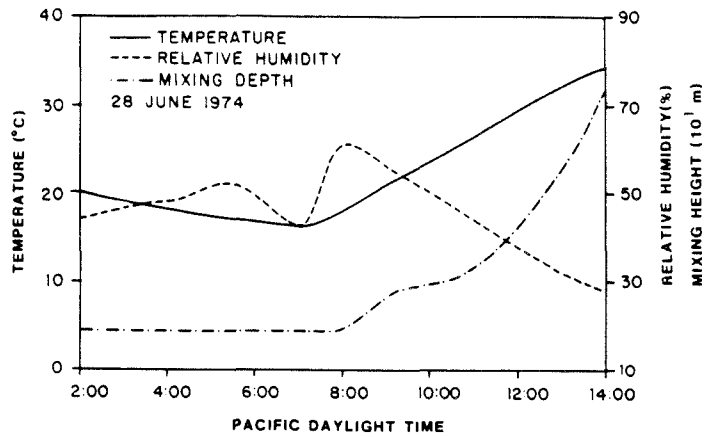


(b)



(c)

Figs 8(a)-(c).



(d)

Fig. 8. Predicted concentrations and observed meteorological variables for the air parcel reaching El Monte at 2 p.m. (PDT) 28 June 1974. (a) NH_4NO_3 , NH_3 , HNO_3 and PAN profiles. (b) Total ammonia and total nitrate profiles (c) NO , NO_2 and O_3 profiles. (d) Meteorological parameters: mixing depth, temperature and relative humidity.

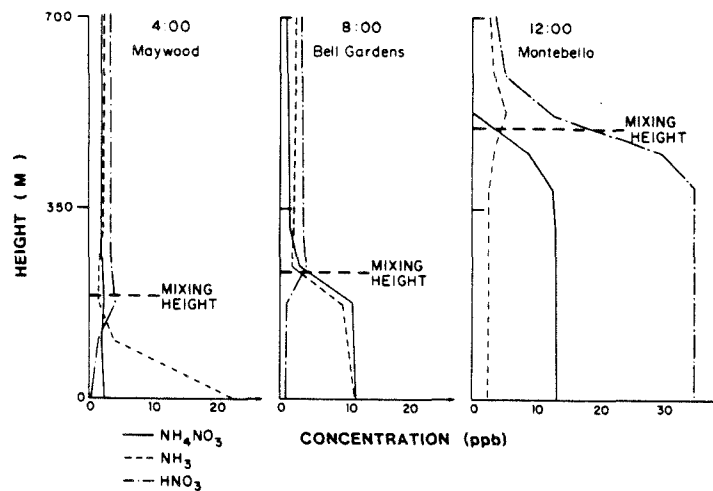


Fig. 9. Evolution of vertical concentration profiles of NH_3 (---), HNO_3 (-.-) and NH_4NO_3 (—) in the air parcel that reaches El Monte at 2 p.m. (PDT) 28 June 1974. Results shown are for 4 a.m., 8 a.m. and 12 noon and the location is given for the air parcel at those times.

methods should be selected that will minimize sampling artifact problems. The sensitivity analysis presented in this paper points to the need for highly accurate temperature data. Model structure dictates that temperature measurements must be available along the trajectory considered, not just at the end point of the trajectory.

FUTURE MODEL APPLICATIONS

Potential uses of this model include control strategy determination for visibility improvement and the

study of aerosol processes, acid deposition and the fate of nitrogen containing species. Results from this model as well as field measurements (Tuazon *et al.*, 1981) indicate that along most of the trajectories in the western portion of the Los Angeles Basin there is more HNO_3 than NH_3 , and that the main factors limiting the formation of aerosol are warm temperatures and lack of NH_3 . This result was also indicated by the sensitivity analysis performed on the formation mechanism alone. In the eastern part of the basin, downwind of the dairies, the situation may well be reversed, resulting in a HNO_3 deficiency.

Since both HNO_3 and NH_4NO_3 are products of NO_x reactions, the ability to model these two species can be valuable in studying the final fate of pollutant nitrogen. The model can give bounds on the amount of HNO_3 and aerosol nitrate deposition. Also by using the vertically resolved species concentrations, the mass of nitrogen containing species advected out of the basin can be approximated. Possible future uses of this work include studying acid deposition. An important part of that investigation would include the transport and production of NH_3 which would act to neutralize acid deposition of both the solid and aqueous phases.

CONCLUSIONS

The mathematical model for urban air pollution presented here solves the basic equations describing the transport and production of gaseous species, and the generation of NH_4NO_3 aerosol. This model is able to quantitatively predict an aerosol species concentration produced by gas phase reactions and condensation in an urban atmosphere directly from species emissions using a mechanistic description of atmospheric processes. Predictions of this model include vertically resolved species concentration profiles of gaseous pollutants and aerosol NH_4NO_3 .

Predictions from the proposed model agree well with the 1974 ambient measurements at El Monte, California, and show qualitatively the trends and concentrations found by more recent studies where measurement methods were used that suppress artifact nitrate problems. Future uses of the model include control strategy design for visibility improvement, the study of aerosol processes and the fate of NO_x emissions.

Acknowledgements—This work was supported by the California Air Resources Board under contract No. A7-169-30. The authors wish to acknowledge the assistance of Arthur Stelson and John Seinfeld in formulating the equilibrium model and William Goodin with help in supplying the necessary computational resources.

REFERENCES

- Adriano D. C., Chang A. C. and Sharpless R. (1974) Nitrogen loss from manure as influenced by moisture and temperature. *J. envir. Quality* **3**, 258–261.
- Appel B. R., Kothny E. L., Hoffer E. M., Hidy G. M. and Wesolowski J. J. (1978) Sulfate and nitrate data from the California aerosol characterization experiment (ACHEX). *Envir. Sci. Technol.* **12**, 418–425.
- Appel B. R., Wall S. M., Tokiwa Y. and Haik M. (1979) Interference effects in sampling particulate nitrate in ambient air. *Atmospheric Environment* **13**, 319–325.
- Appel B. R., Wall S. M., Tokiwa Y. and Haik M. (1980) Simultaneous nitric acid, particulate nitrate and acidity measurements in ambient air. *Atmospheric Environment* **14**, 549–554.
- Appel B. R., Tokiwa Y. and Haik M. (1981) Sampling of nitrates in ambient air. *Atmospheric Environment* **15**, 283–289.
- Baker J. H., Peech M. and Musgrave R. B. (1959) Determination of application losses of anhydrous ammonia. *Agron. J.* **51**, 361–362.
- Cadle S. H. and Mulawa P. A. (1980) Low molecular weight aliphatic amines in exhaust from catalyst-equipped cars. *Envir. Sci. Technol.* **14**, 718–723.
- California Department of Food and Agriculture (1974) Fertilizing materials—tonnage report, Oct–Nov–Dec 1974. California Department of Food and Agriculture, Sacramento, CA.
- Cass G. R. (1978) Methods for sulfate air quality management with applications to Los Angeles. Ph.D. thesis, California Institute of Technology, Pasadena, CA.
- Cass G. R., Gharib S., Peterson M. and Tilden J. W. (1982) The origin of ammonia emissions to the atmosphere in an urban area. Open File Report 82–6, Environmental Quality Laboratory, California Institute of Technology, Pasadena, CA.
- Denmead O. T., Freney J. R. and Simpson J. R. (1976) A closed ammonia cycle within a plant canopy. *Soil Biol. Biochem.* **8**, 161–164.
- Denmead O. T., Nulsen R. and Thurtell G. W. (1978) Ammonia exchange over a corn crop. *Soil Sci. Soc. Am. J.* **42**, 840–842.
- Doyle G. J., Tuazon E. C., Graham R. A., Mischke T. M., Winer A. M. and Pitts J. N., Jr. (1979) Simultaneous concentrations of ammonia and nitric acid in a polluted atmosphere and their equilibrium relationship to particulate ammonium nitrate. *Envir. Sci. Technol.* **13**, 1416–1419.
- Elliot L. F., Schuman G. E. and Viets F. G., Jr. (1971) Volatilization of nitrogen-containing compounds from beef cattle areas. *Soil Sci. Soc. Am. Proc.* **35**, 752–755.
- Ernst J. W. and Massey H. F. (1960) The effects of several factors on volatilization of ammonia formed from urea in the soil. *Soil Sci. Soc. Am. Proc.* **24**, 87–90.
- Falls A. H. and Seinfeld J. H. (1978) Continued development of a kinetic mechanism for photochemical smog. *Envir. Sci. Technol.* **12**, 1398–1406.
- Falls A. H., McRae G. J. and Seinfeld J. H. (1979) Sensitivity and uncertainty of reaction mechanisms for photochemical air pollution. *Int. J. chem. Kinetics* **11**, 1137–1162.
- Fogg C. E. (1971) Livestock waste management and the conservation plan. *Livestock Waste Management and Pollution Abatement—Proc. Int. Symp. Livestock Wastes*, American Society of Agricultural Engineers, St. Joseph, MI, pp. 34–35.
- Gasser J. K. R. (1964) Some factors affecting losses of ammonia from urea and ammonium sulphate applied to soils. *J. Soil Sci.* **15**, 258–272.
- Gentel J. E., Manary O. J. and Valenta J. C. (1973) Characterization of particulates and other non-regulated emissions from mobile sources and the effects of exhaust emissions control devices on these emissions. Dow Chemical Company, U.S. Environmental Protection Agency Document APTD-1567, Midland, MI.
- Giddens J. and Rao A. M. (1975) Effect of incubation and contact with soil on microbial and nitrogen changes in poultry manure. *J. envir. Quality* **4**, 275–278.
- Goodin W. R., McRae G. J. and Seinfeld J. H. (1979) An objective analysis technique for constructing three-dimensional, urban-scale wind fields. *J. appl. Met.* **19**, 98–108.
- Groblicki P. J., Wolff G. T. and Countess R. J. (1981) Visibility-reducing species in the Denver "brown cloud." Part I. Relationships between extinction and chemical composition. *Atmospheric Environment* **15**, 2473–2484.
- Harkins J. H. and Nicksic S. W. (1967) Ammonia in auto exhaust. *Envir. Sci. Technol.* **1**, 751–752.
- Henein N. (1975) The diesel as an alternative automobile engine. Wayne State University, SAE Paper 750931.
- Hidy G. M., Mueller P. K., Grosjean D., Appel B. R. and Wesolowski J. J., editors (1980) *The Character and Origins of Smog Aerosols*. John Wiley, New York, 776 pp.
- Hovey H. H., Risman A. and Cunnan J. F. (1966) The

- development of air contaminant emission tables for non-process emissions. *J. Air Pollut. Control Ass.* **16**, 362-366.
- Hunter J. E., Jr. (1971) Effect of catalytic converters on automotive ammonia emissions. General Motors Research Laboratories, Research Publication GMR-1061, Warren, MI.
- Koda M., McRae G. J. and Seinfeld J. H. (1979) Automatic sensitivity analysis of kinetic mechanisms. *Int. J. chem. Kinetics* **11**, 427-444.
- Lauer D. A., Bouldin D. R. and Klausner S. D. (1976) Ammonia volatilization from dairy manure spread on the soil surface. *J. envir. Quality* **5**, 134-141.
- Liu M.-K. and Seinfeld J. H. (1975) On the validity of grid and trajectory models of urban air pollution. *Atmospheric Environment* **9**, 555-574.
- Luebs R. E., Davis K. R. and Laag A. E. (1973a) Enrichment of the atmosphere with nitrogen compounds volatilized from a large dairy area. *J. envir. Quality* **2**, 137-141.
- Luebs R. E., Laag A. E. and Davis K. R. (1973b) Ammonia and related gases emanating from a large dairy area. *Calif. Agric.* February pp. 10-12.
- Lundgren D. A. (1970) Atmospheric aerosol composition and concentration as a function of particle size and of time. *J. Air Pollut Control Ass.* **20**, 603-608.
- McDowell L. L. and Smith G. E. (1958) The retention and reactions of anhydrous ammonia on different soil types. *Soil Sci. Soc. Am. Proc.* **22**, 38-42.
- McRae G. J. and Seinfeld J. H. (1983) Development of a second generation mathematical model for urban air pollution, II. Performance evaluation. *Atmospheric Environment* **17**, 501-523.
- McRae G. J., Goodin W. R. and Seinfeld J. H. (1982a) Development of a second generation mathematical model for urban air pollution, I. Model formulation. *Atmospheric Environment* **16**, 679-696.
- McRae G. J., Tilden J. W. and Seinfeld J. H. (1982b) Global sensitivity analysis—A computational implementation of the fourier amplitude sensitivity test (FAST). *Computers chem. Engng* **6**, 15-25.
- Miner J. R. (1976) Production and Transport of Gaseous NH₃ and H₂S Associated With Livestock Production. U.S. Environmental Protection Agency Document EPA-600/2-76-239, Ada, OK.
- Miner S. (1969) Air pollution aspects of ammonia, Litton Systems Inc., National Air Pollution Control Administration Document APTD 69-25, Bethesda, MD.
- Muzio L. J. and Arand J. K. (1976) Homogeneous gas phase decomposition of oxides of nitrogen, KVB Incorporated, Electric Power Research Institute Report FP-253, Project 461-1, Tustin, CA.
- National Research Council (1979) Ammonia. A report by the Subcommittee on Ammonia, Committee on Medical and Biologic Effects of Environmental Pollutants, National Research Council, University Park Press, Baltimore, MD.
- Pierson W. R., Brachaczek W. W., Korniski T. J., Truex T. J. and Butler J. W. (1980) Artifact formation of sulfate, nitrate and hydrogen ion on backup filters: Allegheny Mountain experiment. *J. Air Pollut. Control Ass.* **30**, 30-34.
- Porter L. K., Viets F. G., Jr., McCalla T. M. *et al.* (1975) Pollution Abatement from Cattle Feedlots in Northeastern Colorado and Nebraska, U.S. Environmental Protection Agency Report No. EPA-660/2-75-015, Corvallis, OR.
- Reynolds R., Tsou G. and Holmes J. (1975) The influence of gas phase ammonia on formation of aerosol. California Air Resources Board report, El Monte, CA.
- Spicer C. W. (1974) The fate of nitrogen oxides in the atmosphere. In *Advances in Environmental Science and Technology*, Vol. 7 (Edited by Pitts J. N. and Metcalf R. L.), Wiley, New York, pp. 163-261.
- Spicer C. W. and Schumacher P. M. (1979) Particulate nitrate: laboratory and field studies of major sampling interferences. *Atmospheric Environment* **13**, 543-552.
- Stanley F. A. and Smith G. E. (1955) Proper application improves value of NH₃. *Agricultural Ammonia News*, April-June.
- Stelson A. W., Friedlander S. K. and Seinfeld J. H. (1979) A note on the equilibrium relationship between ammonia and nitric acid and particulate ammonium nitrate. *Atmospheric Environment* **13**, 369-371.
- Stelson A. W. and Seinfeld J. H. (1982a) Relative humidity and temperature dependence of the ammonium nitrate dissociation constant. *Atmospheric Environment* **16**, 983-992.
- Stelson A. W. and Seinfeld J. H. (1982b) Relative humidity and pH dependence of the vapor pressure of ammonium nitrate-nitric acid solutions at 25°C. *Atmospheric Environment* **16**, 993-1000.
- Stewart B. A. (1970) Volatilization and nitrification of nitrogen from urine under simulated cattle feedlot conditions. *Envir. Sci. Technol.* **4**, 579-582.
- Taiganides E. P. and Hazen T. E. (1966) Properties of farm animal excreta. *Trans. Am. Soc. agric. Engrs* **9**, 374-376.
- Trickey N. G. and Smith G. E. (1955) Losses of nitrogen from solution materials. *Soil Sci. Soc. Am. Proc.* **19**, 222-224.
- Tuazon E. C., Winer A. M. and Pitts J. N. (1981) Trace pollutant concentrations in a multiday smog episode in the California South Coast Air Basin by long pathlength FT-IR spectroscopy. *Envir. Sci. Technol.* **15**, 1232-1237.
- U.S. Bureau of the Census (1977) 1974 Census of Agriculture, Vol. 1, Part 5, California State and County Data, U.S. Department of Commerce, Washington, DC.
- U.S. Geological Survey (1976) Land Use and Land Cover 1972-1975, Santa Ana, CA (1971-1974, San Bernardino, CA; 1971-1974, Santa Maria, CA; 1972-1975, Long Beach, CA; 1973-1975, Los Angeles, CA) U.S. Department of the Interior, Geological Survey, Open File Maps No. 76-114-1 (76-115-1; 76-117-1; 76-118-1; 76-119-1), Land Use Series.
- Viets F. G., Jr. (1971) Cattle feedlot pollution. *Animal Waste Management. Proc. Nat. Symp. Animal Waste Management*, Washington, DC, Council of State Governments, pp. 97-106. Also published in *Agric. Sci. Rev.* **9**, 1-8.
- Wahhab A., Randhawa M. S. and Alam S. Q. (1957) Loss of ammonia from ammonium sulphate under different conditions when applied to soils. *Soil Sci.* **84**, 249-255.
- Walkup H. G. and Nevins J. L. (1966) The cost of doing business in agricultural ammonia for direct application. *Agric. Ammonia News* **16**, 96-100.
- White W. H. and Roberts P. T. (1977) On the nature and origins of visibility reducing species in the Los Angeles Basin. *Atmospheric Environment* **11**, 803-812.
- Witz S. and McPhee R. D. (1977) Effect of different types of glass filters on total suspended particulates and their chemical composition. *J. Air Pollut. Control Ass.* **27**, 239-241.
- Wohlens H. C. and Bell G. B. (1956) Literature Review of Metropolitan Air Pollutant Concentrations—Preparation, Sampling, and Assay of Synthetic Atmospheres, Stanford Research Institute, final report on Project No. SU1816, Menlo Park, CA.

CHAPTER 3

THE DYNAMICS OF NITRIC ACID PRODUCTION AND

THE FATE OF NITROGEN OXIDES

(To appear in Atmospheric Environment)

THE DYNAMICS OF NITRIC ACID PRODUCTION AND
THE FATE OF NITROGEN OXIDES

Armistead G. Russell⁺, Gregory J. McRae^{*} and Glen R. Cass^x

Environmental Quality Laboratory 206-40
California Institute of Technology
Pasadena, California 91125

ABSTRACT

A mathematical model is used to study the fate of nitrogen oxides (NO_x) emissions and the reactions responsible for the formation of nitric acid (HNO_3). Model results indicate that the majority of the NO_x inserted into an air parcel in the Los Angeles basin is removed by dry deposition at the ground during the first 24 hours of travel, and that HNO_3 is the largest single contributor to this deposition flux. A significant amount of the nitric acid is produced at night by N_2O_5 hydrolysis. Perturbation of the N_2O_5 hydrolysis rate constant within the chemical mechanism results in redistribution of the pathway by which HNO_3 is formed, but does not greatly affect the total amount of HNO_3 produced. Inclusion of NO_3 -aerosol and N_2O_5 -aerosol reactions does not affect the system greatly at collision efficiencies, α , of 0.001, but at $\alpha = 0.1$ or $\alpha = 1.0$, a great deal of nitric acid could be produced by heterogeneous chemical processes.

Ability to account for the observed nitrate radical (NO_3) concentrations in the atmosphere provides a key test of the air quality modeling procedure. Predicted NO_3 concentrations compare well with those measured by Platt et al. (1980). Analysis shows that transport, deposition and emissions, as well as chemistry, are important in explaining the behavior of NO_3 in the atmosphere.

⁺ Department of Mechanical Engineering

^{*} Department of Chemical Engineering, Carnegie-Mellon University,
Pittsburgh, Pennsylvania 15213

^x Environmental Engineering Science Department

1. Introduction

Nitric acid is a major end product of nitrogen oxides emissions. Its presence in the atmosphere can lead to the acidification of rain and fog (Galloway and Likens, 1981; Waldman et al., 1982; Levine and Schwartz, 1982; Liljestr nd and Morgan, 1978; Adewuyi and Carmichael, 1982) and to dry deposition (Russell et al., 1984; Liljestr nd, 1980; Huebert, 1983). Aerosol nitrates, formed by reaction between nitric acid and either ammonia or preexisting aerosol, are key contributors to the visibility problems observed in cities like Los Angeles and Denver (White and Roberts, 1977; Groblicki et al., 1981). As a result, there is considerable interest in better understanding the mechanisms by which nitric acid is formed in and removed from the atmosphere.

Recent studies of the deposition of nitrogen-containing species and the formation of aerosol nitrates (McRae and Russell, 1984; Russell et al., 1983, 1984; Russell and Cass, 1984) show that an understanding of the fate of nitrogen oxides (NO_x) emissions depends on several poorly understood steps in the nitric acid production cycle. Calculations are sensitive to the treatment of dinitrogen pentoxide (N_2O_5) hydrolysis, dry deposition rates, aerosol scavenging processes, and temporary storage of NO_x in the form of aerosol nitrates and peroxyacetyl nitrate (PAN). The purpose of the present paper is to estimate the relative importance of these key processes to the formation and fate of nitric acid and other major nitrogen-containing pollutants.

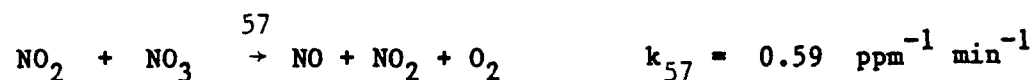
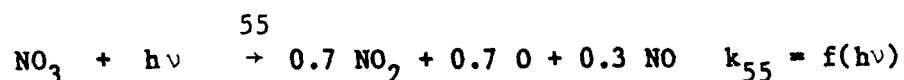
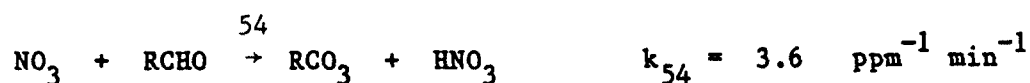
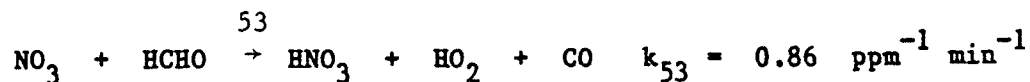
A number of different methods may be employed to investigate nitric acid production, notably: smog chamber studies, mathematical models, and atmospheric measurements. Each of these approaches has its individual strengths and weaknesses. Smog chamber studies do not take into account fresh emissions, diffusion, transport and deposition to natural surfaces, although they do allow accurate characterization of the pollutant evolution within a confined air mass. Studies based on atmospheric measurements have the advantage that the air being sampled has been exposed to all of the actual processes affecting pollutant formation. In practice, however, it is hard to follow individual air parcels in the field. In addition, field data usually are taken at ground level, with little or no attention being given to the chemistry and transport processes taking place aloft. Likewise, it is very difficult to separate the effects of transport, chemistry, and emissions from one another given most sets of field experimental data.

Mathematical models, in their many forms, can retain most of the strengths of the two previous methods. All theoretical formulations embody some degree of approximation, and a variety of assumptions must be used. However, if a model can be formulated that performs well when compared to smog chamber and field observations, its use has many advantages as a diagnostic tool for exploring atmospheric processes. These models incorporate descriptions of vertical diffusion, deposition, pollutant emissions and advective transport. By suppressing each of these processes in turn, one can investigate the extent to which particular physical or chemical mechanisms are

responsible for the time rate of change of pollutant concentrations observed at ground-based air monitoring sites. In the present study, a photochemical trajectory model will be used to explore the mechanisms that determine nitric acid concentrations in the atmosphere.

2. Trajectory Model Description

The trajectory model adopted for use in this study is described by Russell et al. (1983), and includes the effects of gas phase chemistry, the formation of nitrate aerosol, emissions, deposition and vertical diffusion. The photochemical mechanism based on McRae et al. (1982) has been augmented with the aerosol nitrate chemistry of Russell et al. (1983). Five additional reactions involving NO_3 have been added:



Rate constants for the nitrate radical attack on aldehydes and olefins, (OLE), are from Atkinson et al. (1984). The NO_3 photolysis rate used is from Graham and Johnston (1978). The ultimate products of reaction 56 are reported to be nitroxypoxyalkyl nitrates and dinitrates, abbreviated RPN (Bandow et al., 1980). Tests performed on the model

show that inclusion of reactions 53-57 has little effect on the predictions of ozone, NO or NO₂, but is important to the dynamics of NO₃ and the production of nitric acid. Two other nitric acid-producing reactions are:



The reaction numbers correspond to McRae et al. (1982). Rate constants have been updated to reflect the recommendations of Atkinson and Lloyd (1984) and Baulch et al. (1982).

An evaluation of the chemical mechanism's ability to describe the atmospheric chemistry was accomplished by comparing predictions against a set of smog chamber experiments (Falls and Seinfeld, 1978; McRae, 1981). That comparison showed good agreement between measurements and predictions for both ozone and the measured nitrogen-containing species. Evaluation of the complete trajectory model indicated that it adequately predicts the concentrations of gas phase pollutants, like ozone, and also the production of ammonium nitrate aerosol (see Russell et al., 1983).

3. Nitrogen Fluxes and the Fate of Nitrogen Oxides Emissions

The air quality model was applied to follow the fate of NO_x emissions along a 24-hour trajectory across the Los Angeles basin. The air parcel trajectory used in this analysis is shown in Figure 1, and

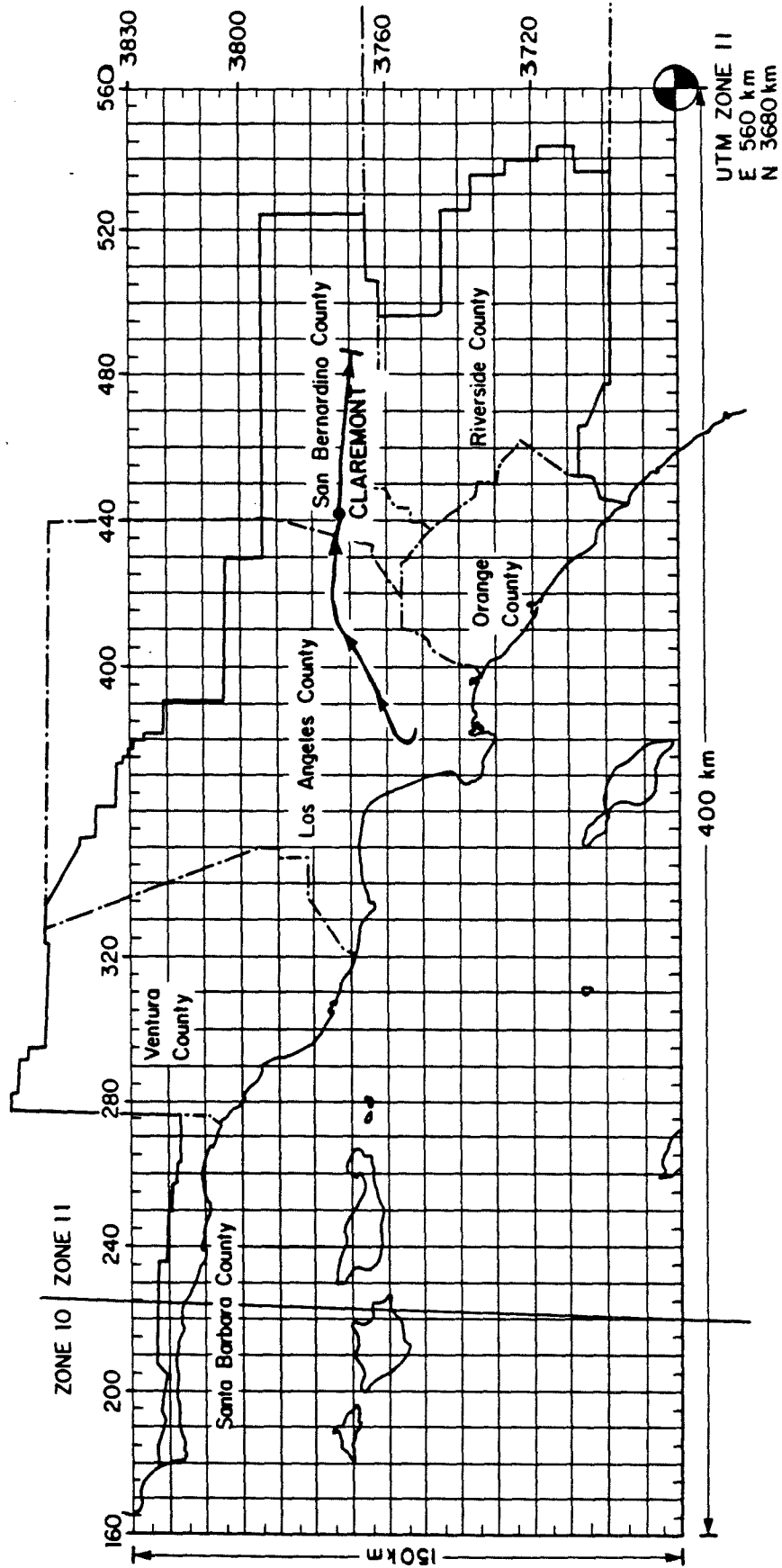


Figure 3.1

Trajectory path used in analyzing the nitrogen oxides in the Los Angeles basin, June 28, 1974.

passed over the Claremont, California, area at 1600 (PST) on 28 June 1974, the same day for which the initial model verification was accomplished. The air parcel was modeled as a column 1000m high, divided into 10 cells. The cell thicknesses, starting with the ground level cell, were 30m, 50m, 70m, five 100m thick, 150m and 200m. The day was marked by warm temperatures with an elevated inversion and high photochemical activity. Emissions into the air parcel were derived from a spatially resolved emissions inventory of the Los Angeles area. This trajectory was chosen because the Claremont area experiences high ozone levels, and because comparison will be made to NO_3 measurements taken in the same location by Platt et al. (1980).

Results of that model application are shown in Figure 2. The widths of the arrows in Figure 2 represent the magnitude of the integrated net fluxes of nitrogen species between the start of the trajectory and the end of that 24-hour period. These calculations represent net fluxes in the following manner:

$$F_{i \rightarrow j}(t) = \sum_m \int_0^t R_m^{i \rightarrow j} dt - \sum_n \int_0^t R_n^{j \rightarrow i} dt \quad (1)$$

where $F_{i \rightarrow j}(t)$ is the net flux of nitrogen from species i directly to species j from the beginning of the trajectory to time t , $R_m^{i \rightarrow j}$ is the instantaneous flux of nitrogen from species i to j by reaction m and $R_n^{j \rightarrow i}$ is similarly the flux from species j to i by reaction n . The summation is taken over all pertinent reactions. These results, of course, depend on the trajectory chosen and on the meteorology of the particular day studied, but they do indicate the general magnitude of

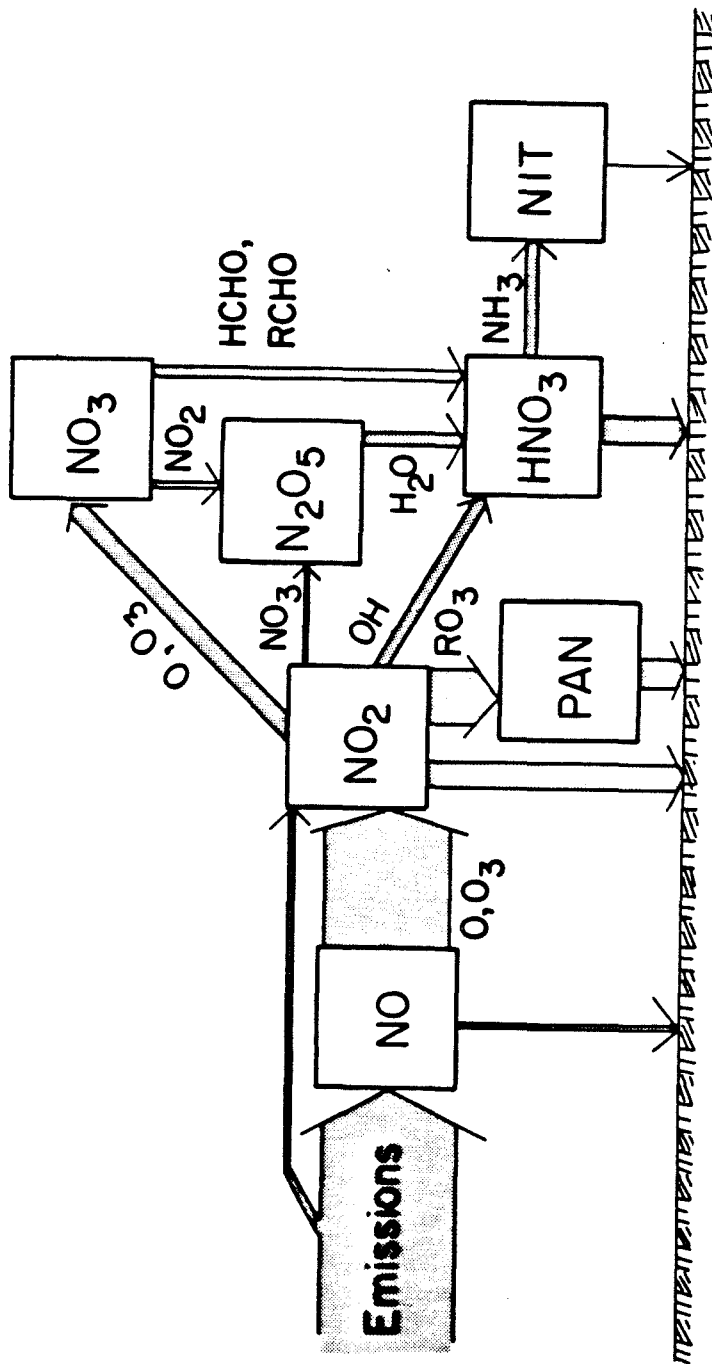


Figure 3.2

Schematic representation of the net flux between nitrogen oxides species, including reaction paths for aerosol nitrate (NIT) formation. The width of these arrows indicates the magnitude of the net flux during the base case 24-hour trajectory simulation.

each pathway. From Figure 2 it is seen that emissions of NO comprise about 97% of the flux of NO_x into the system, the remaining 3% being NO_2 . The NO is quickly oxidized to NO_2 (the net flux between species is shown), with very little nitrogen deposited out as NO. NO_2 then reacts to form a variety of products: 13% is converted directly to HNO_3 , 47% forms PAN, 13% NO_3 , 4% N_2O_5 , and 20% is removed by dry deposition at the earth's surface. Three percent of the NO_2 remains in the air parcel at the end of 24 hours. About 25% of the net NO_3 formed combines with NO_2 to form N_2O_5 , which hydrolyzes to form HNO_3 . Most of the NO_3 reacts with the organics to form HNO_3 . Dry deposition removes 43% of the PAN in the first 24 hours, leaving the rest to deposit out in subsequent days or to thermally decompose into NO_2 and the peroxyacetyl radical. Thus PAN can act as a reservoir for NO_2 . Since nitric acid is very reactive with most surfaces, it deposits out quickly. Almost 73% of the nitric acid formed is lost by dry deposition. Nitric acid and PAN are found to be the major end products of nitrogen oxides emissions at the end of 24 hours. Additional HNO_3 will be produced the next day from the remaining NO_2 and PAN.

A balance on the nitrogen in the air column, Figure 3, indicates the importance of dry deposition. Fifty-eight percent of the NO_x initially present in the air parcel or emitted along the trajectory has deposited out before reaching the end of the 24-hour trajectory. The high HNO_3 formation rates present in photochemical smog promote rapid nitrogen oxides removal at the ground because the deposition velocity of HNO_3 is higher than for many other NO_x species (Huebert, 1983). In

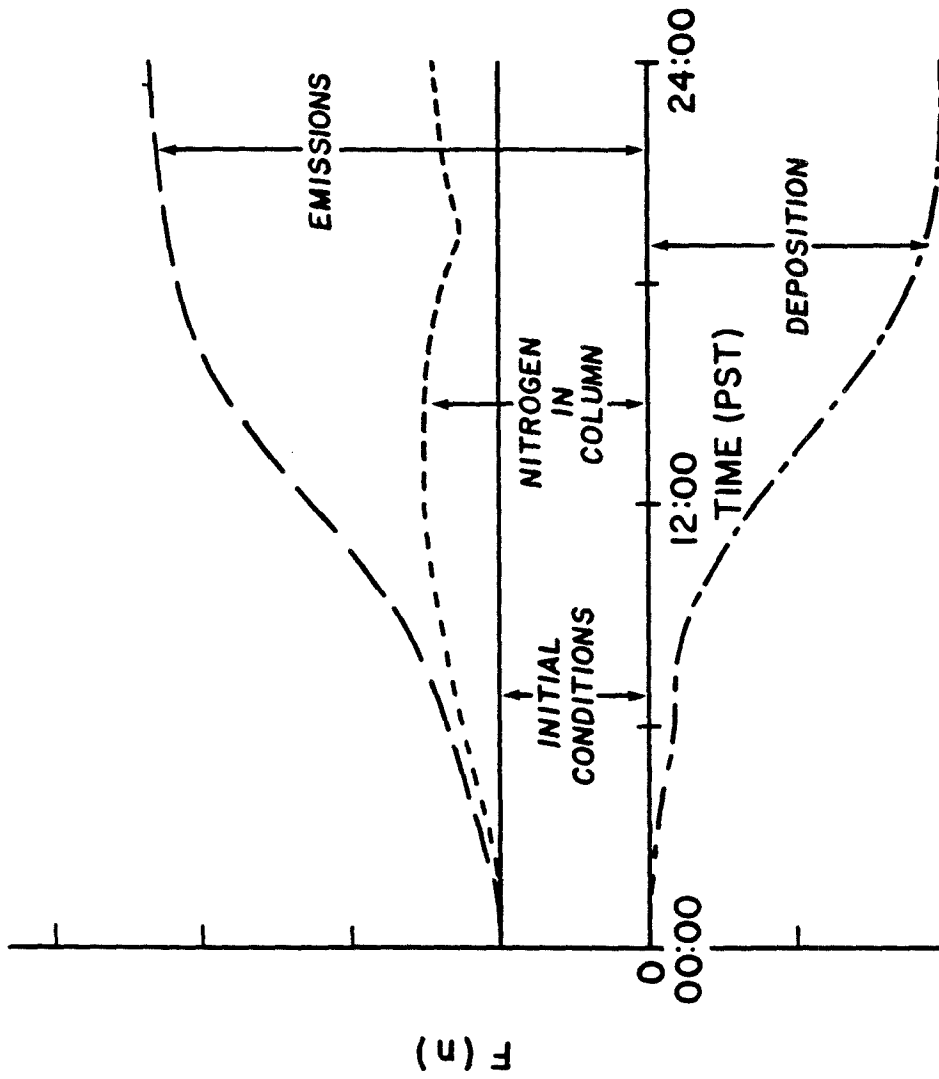


Figure 3.3

Nitrogen balance on the air column illustrating the relative contributions, $F(n)$, from initial conditions, emissions and removal by dry deposition.

addition, the smog condition studied here is caused in part by low mixing depths that increase pollutant concentrations adjacent to the ground, accelerating dry deposition processes. A plot of the cumulative deposition along the trajectory shows that 39% of the oxides of nitrogen deposited as HNO_3 (Figure 4). PAN and NO_2 contribute 33% and 24%, respectively, to the dry deposition flux, while particulate ammonium nitrate accounts for only 1%.

4. Nitric Acid Production at Night

A comparison of the rates of the four reactions (18, 46, 53, 54) leading to HNO_3 formation is shown in Figure 5. As expected, most of the daytime production of nitric acid occurs due to the reaction of NO_2 with OH. During daylight hours the NO_3 and N_2O_5 levels are very low because of NO_3 photolysis and NO_3 scavenging by NO (Stockwell and Calvert, 1983). At night a considerable amount of nitric acid may be produced by N_2O_5 hydrolysis and NO_3 reactions with organics. During the 24-hour period studied, OH attack on NO_2 and N_2O_5 hydrolysis, respectively, account for 44% and 24% of the total nitric acid produced. The two NO_3 reactions (53,54), in total, account for 32% of the nitric acid generated, mostly by reaction 54.

Clearly the relative importance of various nitric acid formation pathways is dependant on the accuracy of measured rate data. The rate constant for N_2O_5 hydrolysis, k_{46} , adopted in Table 1 is the value recently measured by Tuazon et al. (1983). Earlier research by Morris and Niki (1973) placed an upper limit on k_{46} that is a factor of 8

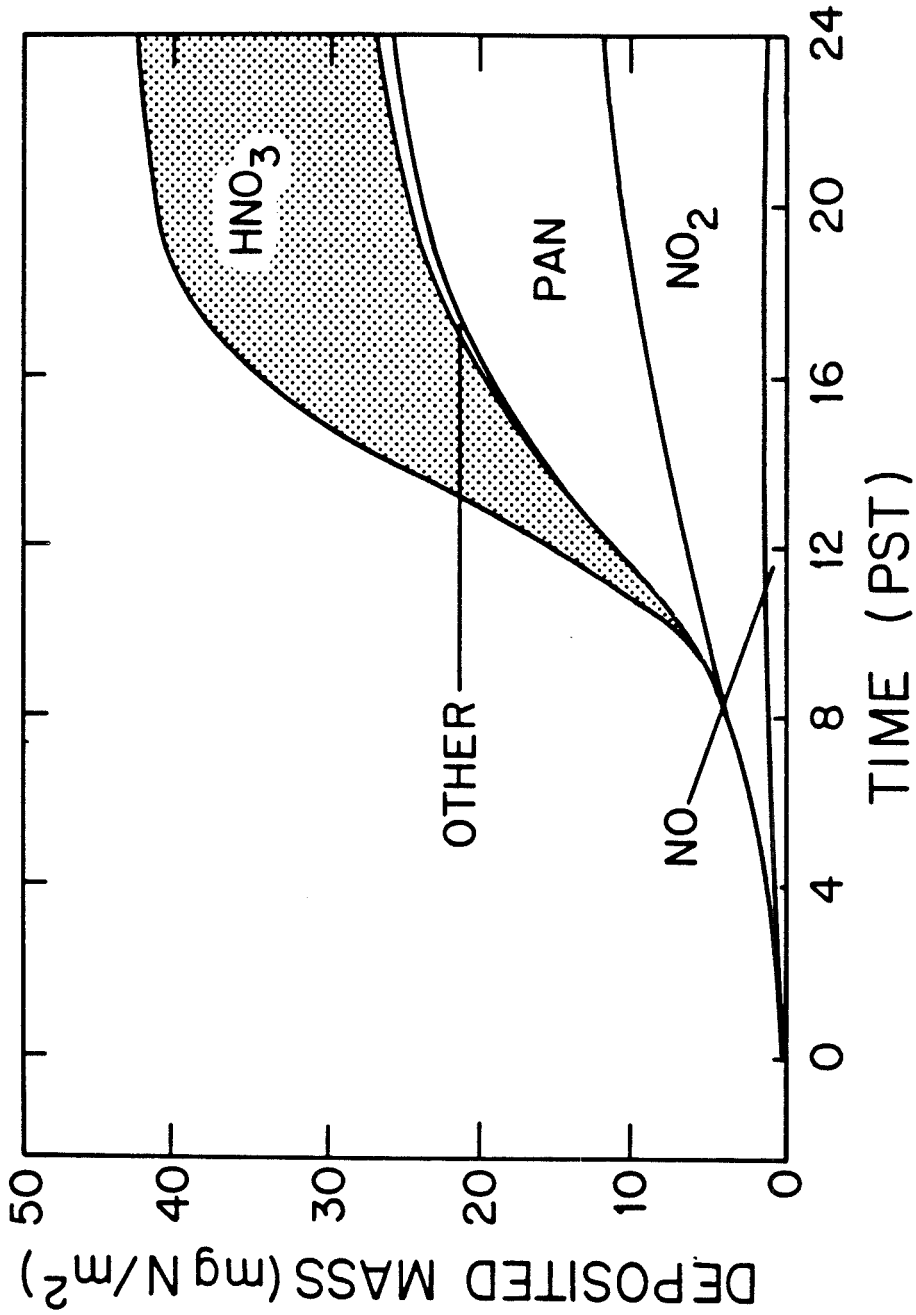


Figure 3.4

Cumulative dry deposition of oxidized nitrogen air pollutants along a 24-hour trajectory in the Los Angeles area, in mg N per m² of surface area at the bottom of the moving air column.

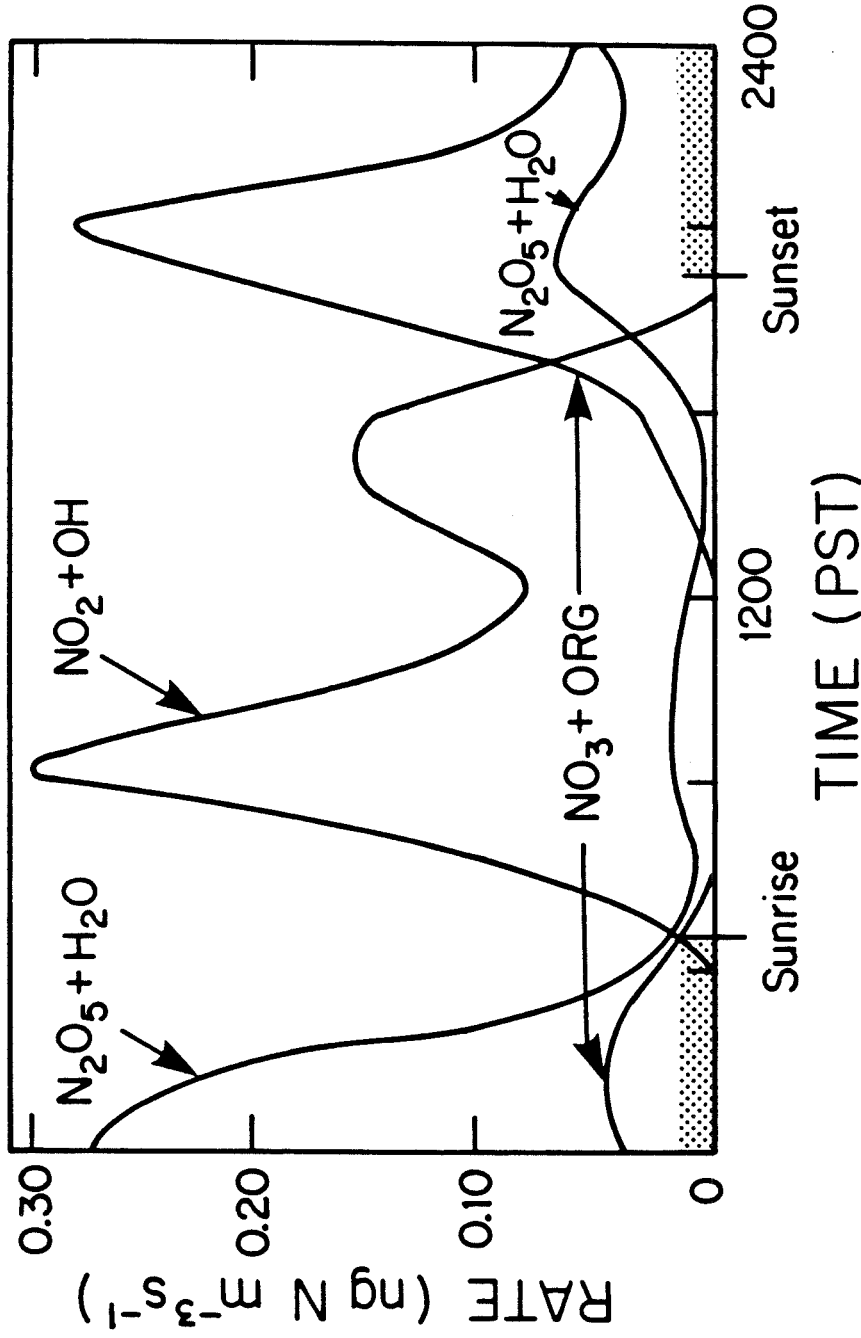


Figure 3.5

Diurnal variation in the contribution of different reaction pathways to the formation of gas phase nitric acid. The two reactions (53 and 54) between NO_3 and organics have been added together for display purposes.

TABLE 1

Major Reactions in the $\text{NO}_3\text{-N}_2\text{O}_5$ System at Night

REACTION	RATE CONSTANT @ 298 K (ppm min units)	REFERENCE
$\text{NO}_2 + \text{O}_3 \xrightarrow[8]{7} \text{NO}_3$	$k_7 = 0.05$	1
$\text{NO} + \text{NO}_3 \xrightarrow[44]{8} 2\text{NO}_2$	$k_8 = 29560$	1
$\text{NO}_2 + \text{NO}_3 \xrightarrow[45]{44} \text{N}_2\text{O}_5$	$k_{44} = 2510$	2
$\text{N}_2\text{O}_5 \xrightarrow[46]{45} \text{NO}_2 + \text{NO}_3$	$k_{45} = 2.9$	1,3
$\text{N}_2\text{O}_5 + \text{H}_2\text{O} \xrightarrow[53]{46} 2\text{HNO}_3$	$k_{46} = 1.9 \times 10^{-6}$	4
$\text{NO}_3 + \text{HCHO} \xrightarrow[54]{53} \text{HNO}_3 + \text{HO}_2 + \text{CO}$	$k_{53} = 0.86$	5
$\text{NO}_3 + \text{RCHO} \xrightarrow[56]{54} \text{RCO}_3 + \text{HNO}_3$	$k_{54} = 3.6$	5,6
$\text{NO}_3 + \text{OLE} \xrightarrow[57]{56} \text{RPN}^8$	$k_{56} = 12.4$	5,7,9
$\text{NO}_2 + \text{NO}_3 \longrightarrow \text{NO} + \text{NO}_2 + \text{O}_2$	$k_{57} = 0.59$	10
$\text{N}_2\text{O}_5 + \text{aerosol} \longrightarrow 2 \text{HNO}_3$	$k^*_{\text{N}_2\text{O}_5}$	11
$\text{NO}_3 + \text{aerosol} \longrightarrow \text{aerosol}$	$k^*_{\text{NO}_3}$	11

- 1 - Baulch et al. (1982)
- 2 - Tuazon et al. (1984)
- 3 - Malko and Troe (1982)
- 4 - Tuazon et al. (1983)
- 5 - Atkinson et al. (1984)
- 6 - The rate constant used for the NO_3 reaction with higher aldehydes is that measured for acetaldehyde.
- 7 - The value used for the rate constant of the NO_3 reaction with olefins is that measured for the NO_3 reaction with propene.
- 8 - The ultimate products of reaction 56 are reported to be nitroxyperoxyalkyl nitrates and dinitrates (Bandow et al., 1980).
- 9 - Bandow et al. (1980)
- 10 - Atkinson and Lloyd (1984)
- 11 - See text

higher than used in the present study, and the actual rate could still be smaller than used here. Measurement of that rate constant is plagued by rapid heterogeneous reactions with the surfaces of smog chambers used to study that reaction. Two approaches will be taken to estimate the magnitude of the effect that this uncertainty can have on the production of nitric acid. First, the chemical mechanism itself will be dissected to indicate the approximate functional dependence of overall nitric acid production on each of the key rate constants. Then the trajectory model will be used to conduct a study of the effect of perturbed rate constants on predicted HNO_3 formation routes.

The dynamics of the nighttime NO_3 - N_2O_5 system is described by the set of 11 reactions shown in Table 1 and can be studied in spite of the possible uncertainty in the rate constant for reaction 46. Excluding the aerosol reactions, the rate expressions for NO_3 and N_2O_5 using the system in Table 1 become:

$$\frac{d[\text{NO}_3]}{dt} = k_7[\text{NO}_2][\text{O}_3] - k_8[\text{NO}_3][\text{NO}] - k_{44}[\text{NO}_2][\text{NO}_3] + k_{45}[\text{N}_2\text{O}_5] - k_{\text{org}}[\text{ORG}][\text{NO}_3] - k_{57}[\text{NO}_2][\text{NO}_3] \quad (2)$$

and

$$\frac{d[\text{N}_2\text{O}_5]}{dt} = k_{44}[\text{NO}_2][\text{NO}_3] - k_{45}[\text{N}_2\text{O}_5] - k_{46}[\text{N}_2\text{O}_5][\text{H}_2\text{O}] \quad (3)$$

where

$$k_{\text{org}}[\text{ORG}] = k_{53}[\text{HCHO}] + k_{54}[\text{RCHO}] + k_{56}[\text{OLE}] \quad (4)$$

accounts for the reaction of the organics with NO_3 . Both NO_3 and N_2O_5

have short characteristic reaction times, and the pseudo-steady state approximation can be made:

$$[\text{NO}_3] = \frac{k_7[\text{O}_3][\text{NO}_2](k_{45}+k_{46}[\text{H}_2\text{O}])}{\{k_8[\text{NO}]+k_{\text{org}}[\text{ORG}]+k_{57}[\text{NO}_2]\}\{k_{45}+k_{46}[\text{H}_2\text{O}]\}+k_{46}k_{44}[\text{NO}_2][\text{H}_2\text{O}]} \quad (5)$$

and

$$[\text{N}_2\text{O}_5] = \frac{k_{44}k_7[\text{NO}_2]^2[\text{O}_3]}{\{k_8[\text{NO}]+k_{\text{org}}[\text{ORG}]+k_{57}[\text{NO}_2]\}\{k_{45}+k_{46}[\text{H}_2\text{O}]\}+k_{44}k_{46}[\text{NO}_2][\text{H}_2\text{O}]} \quad (6)$$

or

$$[\text{N}_2\text{O}_5] = \frac{k_{44}[\text{NO}_2]}{k_{45} + k_{46}[\text{H}_2\text{O}]} [\text{NO}_3] \quad (7)$$

Further simplification is possible in (5) by noting that

$$k_{45} \gg k_{46}[\text{H}_2\text{O}]:$$

$$[\text{NO}_3] = \frac{k_7k_{45}[\text{O}_3][\text{NO}_2]}{k_8k_{45}[\text{NO}]+k_{45}k_{\text{org}}[\text{ORG}]+k_{57}k_{45}[\text{NO}_2]+k_{46}k_{44}[\text{NO}_2][\text{H}_2\text{O}]} \quad (8)$$

The denominator in expression (8) is made up from the four sinks in the $\text{N}_2\text{O}_5 - \text{NO}_3$ system. The first term is due to NO_3 scavenging by NO , the second to the NO_3 reaction with organics, the third to the reaction with NO_2 to form NO , and the last corresponds to nitric acid production by N_2O_5 hydrolysis.

These steady state expressions can be used to perform an uncomplicated check on the NO_3 concentration values reported by Platt et al. (1980) at Claremont, California. Using the NO_2 (0.05 ppm) and

olefins plus aldehydes (0.04 ppm) values representative of nighttime conditions during Platt et al.'s (1980) experiments, given in Table 2, the magnitudes of the last three terms in the denominator of equation (8) are about 0.3, 0.09, and 5 min^{-2} , respectively. Compared to NO, the NO_2 and olefins plus aldehydes concentrations should be relatively constant with height. NO concentrations at ground level are needed if the first term in the denominator of (8) is to be evaluated. Platt et al. (1980) were unable to measure NO, and Tuazon et al. (1981) report NO concentrations at sunset below the detection limit of 1 ppb at Claremont, California. If 1 ppb is taken as an upper limit on the NO concentration at ground level, the first term in the denominator of (8) is of the order 86 min^{-2} , or much greater than the other terms combined. At that ground level NO concentration, the corresponding NO_3 concentration is 12 ppt. At the other extreme, if the ground level NO concentration is negligible, then the corresponding NO_3 concentration is 211 ppt. That range of NO_3 values brackets the peak NO_3 concentrations measured at ground level by Platt et al. (1980) at Claremont.

Equation (8) next can be used to examine the likely situation at night several hundred meters above the ground. Ozone scavenges the NO aloft, and the stability of the atmosphere at night does not allow surface NO emissions to diffuse upward rapidly. Under those conditions, the NO concentration several hundred meters above the ground should be very low (the trajectory model predicts less than 1×10^{-6} ppm aloft just after sunset). With NO levels very low, the

TABLE 2
Species Concentration Used in Analysis

SPECIES	CONCENTRATION (PPM)
NO (average)	$1 \times 10^{-4}{}^a$
NO ₂	0.05 ^b
O ₃	0.15 ^b
H ₂ O	$2 \times 10^4{}^b$
HCHO	0.020 ^c
RCHO	0.020 ^d
OLE	0.001 ^a
NO (ground level)	$1 \times 10^{-3}{}^c$
NO (above inversion)	$1 \times 10^{-6}{}^a$

^a Value taken from trajectory model calculations used in this study at 19:00 PST.

^b Value representative of those measured by Platt et al. (1980).

^c Value representative of those measured by Tuazon et al. (1981).

^d Concentration of higher aldehydes set equal to that of formaldehyde.

uncertainty in NO concentration present at ground level is removed, and NO₃ values aloft approaching the NO negligible case of 211 ppt should be present. These predictions derived quickly from a steady state analysis of an approximate nighttime chemical mechanism will be compared to the results of the full trajectory model shortly.

The expressions derived for NO₃ and N₂O₅ can be used to compute the nitric acid production rates at night and also to test the sensitivity of nitric acid production to the uncertainty in the N₂O₅ hydrolysis rate. Nitric acid is produced at night by N₂O₅ hydrolysis (reaction 46) and by two reactions between the organics and NO₃ (reactions 53, 54). Rates for these reactions are, respectively

$$\frac{d[\text{HNO}_3]}{dt} = \frac{2 k_{46} k_{44} k_7 [\text{H}_2\text{O}] [\text{O}_3] [\text{NO}_2]^2}{k_{46} k_{44} [\text{NO}_2] [\text{H}_2\text{O}] + k_{45} k_8 [\text{NO}] + k_{45} k_{\text{org}} [\text{ORG}] + k_{45} k_{57} [\text{NO}_2]} \quad (9)$$

and

$$\frac{d[\text{HNO}_3]}{dt} = \frac{k_{45} k_7 [\text{O}_3] [\text{NO}_2] (k_{53} [\text{HCHO}] + k_{54} [\text{RCHO}])}{k_{46} k_{44} [\text{NO}_2] [\text{H}_2\text{O}] + k_{45} k_8 [\text{NO}] + k_{45} k_{\text{org}} [\text{ORG}] + k_{45} k_{57} [\text{NO}_2]} \quad (10)$$

It is instructive to look at the magnitude of equations (9) and (10) in two regimes: if the NO is about 1 ppb and if the NO is negligible.

Using the species concentrations given in Table 2, with NO concentration at 1 ppb, and $k_{46} = 1.9 \times 10^{-6} \text{ ppm}^{-1} \text{ min}^{-1}$, the dominant route for nitric acid production is reaction 46, producing $4 \times 10^{-5} \text{ ppm}$

min^{-1} of HNO_3 (equation 9) compared to 1×10^{-6} ppm min^{-1} by the set of NO_3 -organics reactions (equation 10).

At high altitudes the NO concentration is very small, decreasing NO_3 scavenging and increasing HNO_3 production. If the NO concentration is negligible, then the nitric acid production rates by reaction 46 and by the organics- NO_3 reactions (reactions 53 and 54) are increased to 7×10^{-4} and 1.9×10^{-5} ppm min^{-1} respectively. Note that in the absence of NO, decreasing k_{46} has much less effect on HNO_3 production by N_2O_5 hydrolysis. This is because if $[\text{NO}] < 10^{-6}$ ppm and $k_{46}k_{44}[\text{NO}_2][\text{H}_2\text{O}] \gg k_{45}k_{\text{org}}[\text{ORG}]$, then (9) simplifies to

$$\frac{d[\text{HNO}_3]}{dt} = 2 k_7 [\text{O}_3][\text{NO}_2] \quad (11)$$

with no dependence on k_{46} .

An estimate of the importance of the N_2O_5 hydrolysis to the total rate of nitric acid production can be found by comparing the previous calculations to the rate of the NO_2 -OH radical reaction at noon. Assuming an NO_2 concentration of 0.100 ppm (Tuazon et al., 1981) and an OH radical level of 2×10^{-7} ppm (Chameides and Davis, 1982), daytime nitric acid production is about 3×10^{-4} ppm min^{-1} , less than the production of HNO_3 by reaction 46 after sunset at locations where the NO concentration is negligible (e.g. above the surface layer affected by fresh NO emissions).

Next the complete photochemical trajectory model was used to test the sensitivity of nitric acid production to variations in a number of key parameters. A comparison of the amount of nitric acid produced by the various reactions in six different cases is shown in Table 3. The base case reflects the calculations previously described in part 3 of this paper. Rate constants shown in Table 1 were used, and no scavenging of NO_3 and N_2O_5 by aerosols was assumed to take place. In this case, nighttime reactions (reactions 46, 53, and 54) account for 56% of the HNO_3 formed during the 24-hour trajectory, 41% of that by the homogeneous hydrolysis of N_2O_5 .

There is some possibility that the value of k_{46} given in Table 1 may be too high. A second set of calculations was executed with k_{46} decreased by an order of magnitude below the value in Table 1. In this case only 6% of the nitric acid is produced by reaction 46. However, reducing k_{46} increases the predicted NO_3 concentrations and thus increases the production of HNO_3 by the reactions involving organics. Still, 47% of the nitric acid is produced by nighttime reactions, and the total nitric acid produced is reduced by only 3% (see Table 3).

Morris and Niki (1973) placed an upper limit on the value of k_{46} equal to $1.5 \times 10^{-5} \text{ ppm}^{-1} \text{ min}^{-1}$. If this value is used, 44% of the nitric acid is produced by homogeneous hydrolysis of N_2O_5 and 36% by the OH-NO_2 daytime reaction. At the other extreme, if k_{46} is set equal to zero, the total nitric acid produced decreases by only 7%, and the nitrate radical reactions with organics now account for 44% of that

TABLE 3

Percent of Total Nitric Acid Produced by Each Reaction
Along a 24-hour Trajectory

REACTION STEP PRODUCING HNO ₃	BASE CASE	k ₄₆ DECREASED BY 10X	k ₄₆ of MORRIS & NIKI	k ₄₆ ⁼⁰	AEROSOL SCAVENGING		
					(α=0.001)	(α= 0.1)	(α=1.0)
NO ₂ + OH (18)	44%	53%	36%	56%	44%	37%	29%
N ₂ O ₅ + H ₂ O(g)(46)	24%	6%	44%	0%	22%	5%	tr*
NO ₃ + HCHO (53)	4%	7%	2%	7%	4%	1	tr
NO ₃ + RCHO (54)	28%	34%	18%	37%	28%	11%	4%
N ₂ O ₅ + AEROSOL					2%	46%	67%
Percent of base case nitric acid produced							
	100%	97%	117%	93%	101%	114%	124%

* tr = trace amount, less than 1%

produced. The final three columns of Table 3 indicate the possible effect that heterogeneous reactions could have on the production of nitric acid. These reactions will be discussed further in following paragraphs.

The results shown here indicate that the homogeneous hydrolysis of N_2O_5 probably is an important mechanism in the formation of nitric acid in the atmosphere. Reducing the rate constant used from that of Morris and Niki (1973) to that of Tuazon et al. (1983), a factor of eight decrease, lowered the amount of HNO_3 produced via reaction 46 by only 55%. Further reduction of k_{46} by an order of magnitude decreased total nitric acid produced at night by only 18%. In all cases the nitric acid produced at night is a significant fraction of the total. NO_3 - organic reactions also are shown to be an important source of nitric acid in this analysis. Perturbing k_{46} results in a redistribution of the amount of nitric acid produced by each reaction, but the total nitric formed is not as greatly affected (see bottom of Table 3).

5. Prediction of NO_3 Concentrations

As indicated earlier, two key species in explaining the production of HNO_3 are N_2O_5 and NO_3 . Unfortunately, there are no ground level measurements of N_2O_5 available and only one set of ambient measurements of NO_3 , NO_2 and O_3 (Platt et al., 1980). However, the rapid conversion of NO_3 to N_2O_5 , and subsequent rapid decomposition of N_2O_5 should cause NO_2 , NO_3 and N_2O_5 to reach equilibrium at night, such that

$$\frac{[\text{NO}_3][\text{NO}_2]}{[\text{N}_2\text{O}_5]} = K$$

where $K = 1.2 \times 10^{-3}$ ppm (Tuazon et al., 1984). Other reactions of NO_3 and N_2O_5 would perturb this equilibrium state only slightly because the timescales for the other competitive reactions are significantly longer than those that establish the equilibrium condition. Hence, an ability to correctly predict NO_3 concentrations at night would suggest that N_2O_5 concentrations also have been predicted correctly. A key test of nighttime nitric acid formation calculations at present thus involves comparison of observed and predicted NO_3 concentrations.

The trajectory model employed earlier can be used to estimate the NO_3 concentrations observed at Riverside on 12 September 1979 by Platt et al. (1980). The initial conditions used were the NO_2 (0.08 ppm), H_2O (23200 ppm), O_3 (0.23 ppm) and NO_3 (0.0 ppm) concentrations measured by Platt et al. (1980) at Riverside at 1800 Pacific Daylight Time (PDT). Emissions, again, were derived from a spatially resolved 1974 inventory of the area. Air mass motion at night on this occasion was small, and the nominal motion of the air parcel between 1800 and 2400 hours PDT would have been only 5.6 km. Since the emission inventory and the air parcel characteristics are defined over 5 km by 5 km grids, a horizontal transport distance of only 5.6 km implies that Platt et al.'s (1980) measurements at a fixed site in Riverside can be compared to a short Lagrangian trajectory calculation passing over that site. A comparison of the measured and predicted ground level NO_3

concentrations is shown in Figure 6. The measured peak was 288 ppt and the predicted peak was about 255 ppt, both profiles showing the dramatic rise in NO_3 just after sunset, and then a rapid decline. The predicted concentrations peak about one half hour before the measured concentrations, possibly due to dissociation rates of NO_2 and NO_3 after sunset that are greater than that modeled, or due to transport on a sub-grid scale. The latter is unlikely as the wind velocities during the experiment were not very great, and the measured ozone and nitrogen dioxide concentrations did not change markedly. O_3 and NO_2 predictions and measurements are shown in Figure 7. Predicted and observed ozone concentrations compare quite well. The NO_2 predictions are lower than observed, but the NO_2 trends over time track one another.

In order to account for the rapid decrease in ground level NO_3 concentrations observed after the peak at 1930 hours as shown in Figure 6, the O_3 concentration must decrease and the NO_3 concentration increase. Stockwell and Calvert (1983) used a box model, lacking vertical resolution and vertical diffusion, and achieved this result by greatly increasing NO emissions into their model. However, NO emissions in Los Angeles, in fact, are decreasing at that time of day. There are several key reasons why the trajectory model used here can reproduce the observed NO_3 peak without an NO emissions increase. Emissions into the vertically resolved trajectory model are treated as ground level sources. As night falls the atmosphere stabilizes, which decreases mixing, causing an increase in the ground level NO concentrations. However, the effect of this lowered mixing rate in the

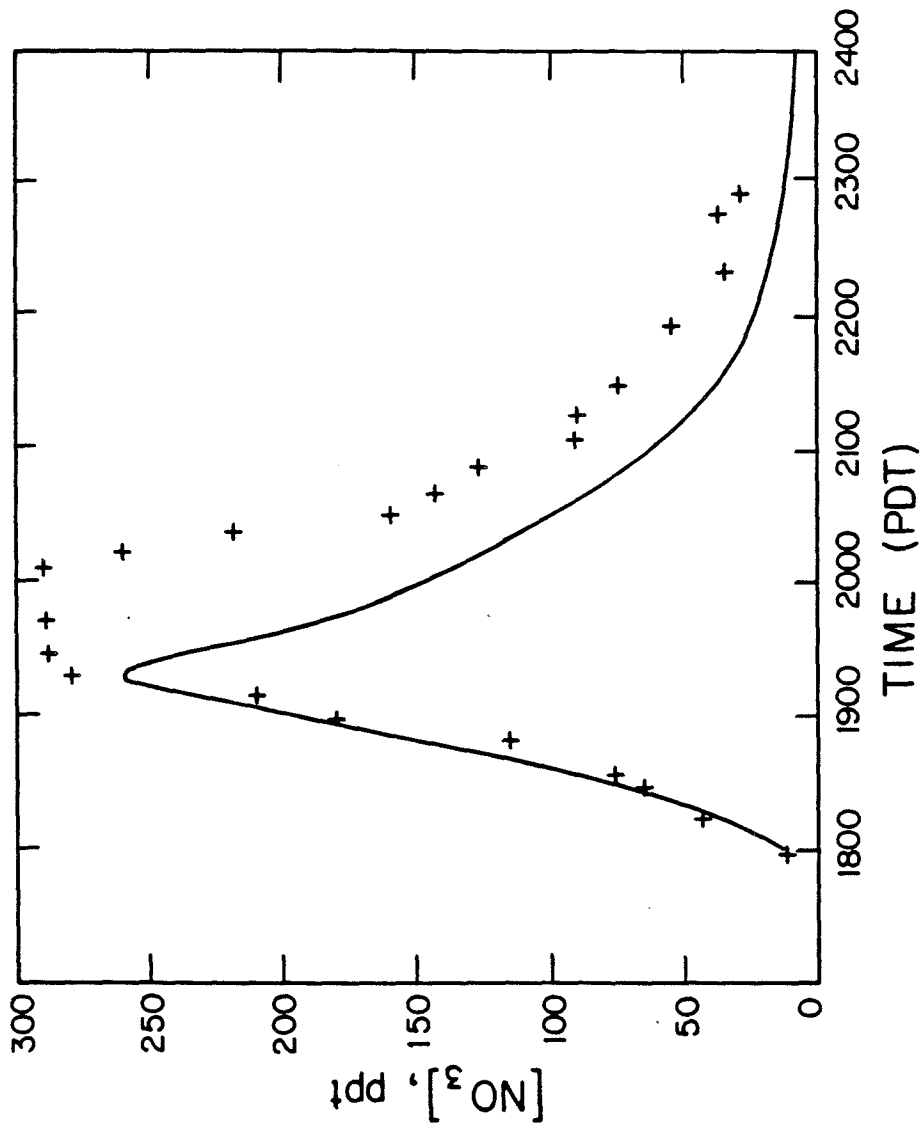


Figure 3.6

Predicted and measured NO_3 concentrations at Riverside, September 12, 1979.
(—) Predicted and (+) Measured (Platt et al. 1980)

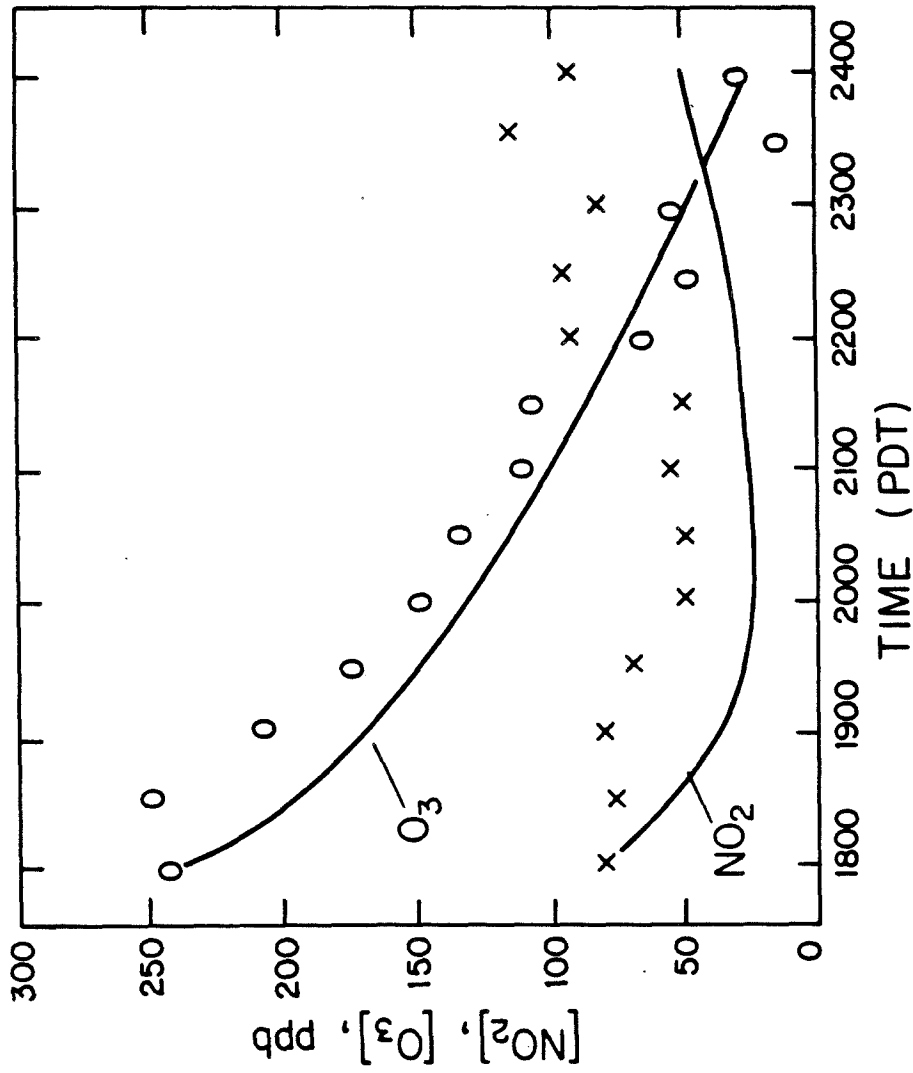


Figure 3.7

Predicted and measured O_3 and NO_2 concentrations at Riverside, September 12, 1979.
 (—) Predicted, (\bar{x}) Measured NO_2 (Platt et al. 1980)
 (o) Measured O_3 (Platt et al. 1980)

trajectory model is more widespread than its effect on increasing NO concentrations alone and is not equivalent to injecting more NO into a box model. The lowered mixing rate also affects the NO₂ and O₃ loss rate at the ground and slows the downward flux of O₃ from elevations above the ground level cell in the model. Emissions used in this study are derived from a spatially resolved emissions inventory for the Los Angeles basin, from which the emissions density in the Riverside area can be determined. In the trajectory model, deposition fluxes are computed based on the concentration in the bottom cell only. Use of ground level emissions and deposition, coupled with a stably stratified atmosphere at night, leads to a very pronounced NO₃ concentration profile with elevation in the atmosphere, as shown in Figure 8. Figure 8 also indicates the potential importance of nitric acid production aloft, where the NO₃ and N₂O₅ concentrations are predicted to be much greater than those observed at ground level.

The trajectory model can be used to elucidate the important processes affecting the NO₃ concentration at ground level over time. This will be done by systematically removing physical processes, such as mixing, deposition, chemical reaction and emissions of NO, from the trajectory model run that was initiated using the O₃ and NO₂ values that were measured by Platt et al. (1980) at 1800 PDT on 12 September 1979 at Riverside. The results of this analysis are shown in Figure 9. Removing NO emissions increases the NO₃ peak, to about 575 ppt, because NO is a very efficient NO₃ scavenger. Decreasing the N₂O₅ hydrolysis rate constant, k_{46} , by an order of magnitude, again increases the peak

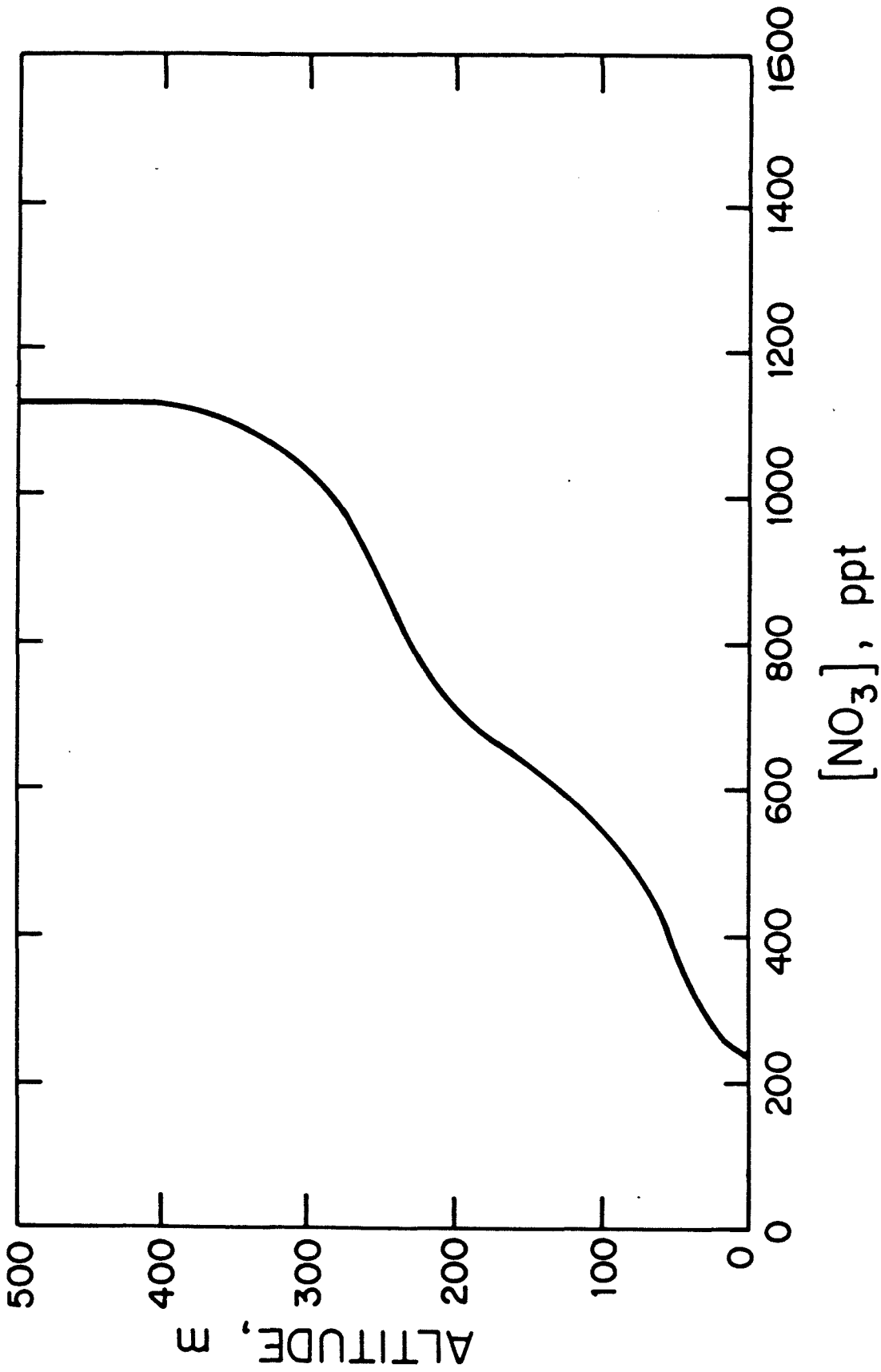


Figure 3.8
Predicted vertical NO₃ concentration profile at 1900 (PDT)
on September 12, 1979. Air parcel is located at Riverside.

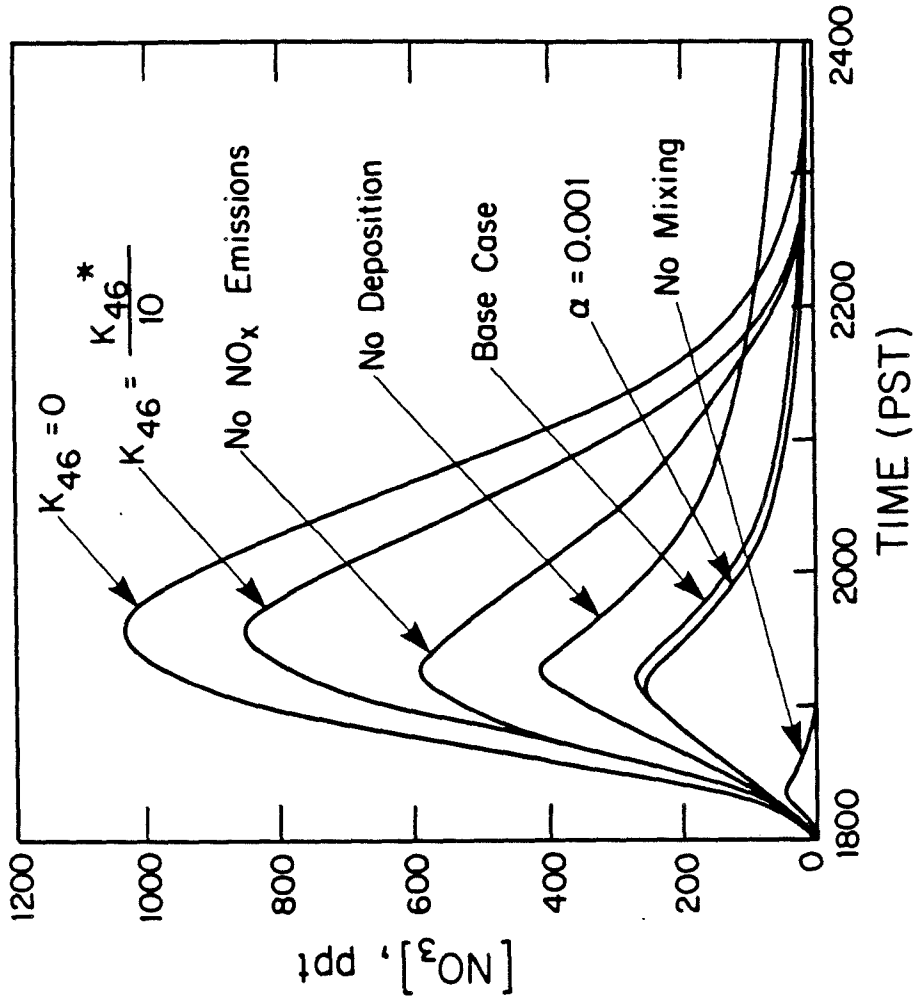


Figure 3.9

Predicted NO_3 concentrations at Riverside, September 12, 1979 for the base case and for several perturbations from the base case.

NO_3 concentration to about 830 ppt. Further decreasing k_{46} to zero only increases the NO_3 concentration peak to 1000 ppt. Reduction of the value of k_{46} in the two preceding cases causes a delay in the occurrence of the NO_3 peak because the removal of nitrogen oxides from the system is delayed. Deleting deposition of all species changes the NO_3 profile greatly, increasing the peak NO_3 concentration by about fifty percent relative to the base case.

Vertical mixing has a major effect on the NO_3 concentrations. Trapping the emissions in the bottom cell of the model almost removes the peak, whereas the base case calculation of the atmospheric mixing after sunset increases the peak NO_3 value and pushes the peak to a later time. Reduced vertical mixing in effect traps more NO emissions in the bottom cell of the model, giving an effect that is opposite to that discussed previously for the case where emissions are suppressed.

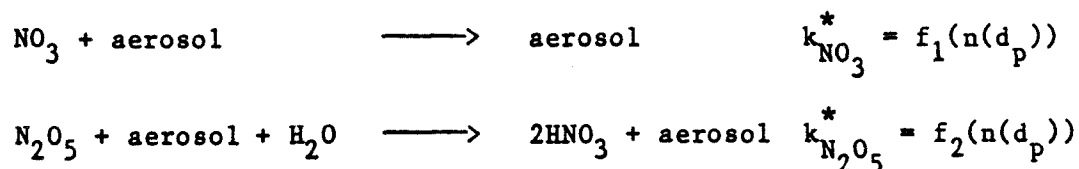
This brief analysis shows that chemistry alone cannot explain the behavior of NO_3 in the atmosphere. A complete analysis requires including the effects of transport, deposition and emissions. Given detailed data on emissions, meteorology, and O_3 and NO_2 concentrations, a similar analysis could be applied to the data of Noxon et al. (1980).

6. Aerosol-Radical Interactions

Both NO_3 and N_2O_5 possibly could be scavenged by surface reactions with aerosols (Chameides and Davis, 1982). Though the rates of these reactions are unknown, an upper bound can be found from

kinetic theory. The trajectory model can be used to assess the maximum effect of aerosol scavenging.

Possible products of the nitrate radical interaction with aerosols include aerosol nitrate, a sink in the system, or decomposition of the NO_3 into NO_2 and oxygen. N_2O_5 also might decompose into its precursors, react with the aerosol surface to form aerosol nitrate, or, if the N_2O_5 contacts water on the aerosol surface, it could undergo heterogeneous hydrolysis to produce nitric acid. In the following analysis, the aerosol surface reaction with NO_3 will be modeled as a sink for NO_3 , the products remaining in the aerosol phase; while N_2O_5 reaction with the aerosol will be assumed to produce nitric acid that could re-enter the gas phase. Thus, the two reactions added to the system are



where the two rate constants are calculated as functions of the aerosol size distribution function, $n(d_p)$, which determines the aerosol surface area as a function of particle diameter, d_p .

An upper bound for these rate constants can be derived from kinetic theory by calculating the collision rate of the gas molecules with the aerosol surface. Assuming that 100% of the collisions are effective in achieving reaction, these upper limit rate constants are given by (Dahneke, 1983)

$$k_i^* = \int_0^{\infty} 2 \pi D_i \left[\frac{1 + Kn}{\frac{2 Kn (1 + Kn)}{\alpha} + 1} \right] d_p n(d_p) d(d_p) \quad (12)$$

where D_i is the diffusion coefficient of species i , Kn is the Knudsen number based on aerosol size and the mean free path of gaseous species i , and α is the collision efficiency. An estimate of the heterogeneous reaction rate constants in the Los Angeles atmosphere can be found using the measured aerosol size distribution of Table 3 in Whitby et al. (1972). Upper bounds on these rate constants, using $\alpha=1$, are calculated to be

$$k_{NO_3}^* (\alpha=1) = 2.4 \text{ min}^{-1}$$

$$k_{N_2O_5}^* (\alpha=1) = 1.5 \text{ min}^{-1}$$

Collision efficiencies are both hard to measure and highly dependent on the aerosol surface characteristics. Baldwin and Golden (1979) measured the collision efficiency of N_2O_5 on a sulfuric acid surface to be greater than 3.8×10^{-5} . Chameides and Davis (1982) report measured efficiencies for OH radical-aerosol reactions from less than 10^{-4} to 0.25, the magnitude depending largely on the surface composition. In the present work, the assumed collision efficiency, α , for both N_2O_5 and NO_3 -surface reactions will be taken as 10^{-3} , which is between that measured for N_2O_5 on sulfuric acid and the OH interaction with $NaNO_3$ (Jech et al., 1982). The actual rate will vary as the aerosol surface characteristics and size distribution change.

The importance of aerosol scavenging is dependent on the time scales associated with the different sinks in the $\text{NO}_3\text{-N}_2\text{O}_5$ system. At night, given the species concentrations in Table 2, these sinks and their time scales (given as the NO_3 reaction rate per unit NO_3 concentration) are:

NO Scavenging	$0.03 < k_8[\text{NO}] < 30 \text{ min}^{-1}$
Organic Reactions	$k_{\text{org}}[\text{ORG}] \sim 0.10 \text{ min}^{-1}$
Aerosol Interaction	$k_{\text{NO}_3}^* (\alpha=0.001) \sim 0.004 \text{ min}^{-1}$

From these results, aerosol scavenging of NO_3 at night should be important only at very low NO concentrations or at collision efficiencies much higher than the $\alpha = 10^{-3}$ value assumed here. During daylight hours, the losses due to photolysis and NO scavenging are very much greater than the loss due to aerosols.

At night N_2O_5 -aerosol reactions can be examined by comparing the time scales for N_2O_5 loss:

Homogeneous Hydrolysis	$k_{46}[\text{H}_2\text{O}] < 0.04 \text{ min}^{-1}$
Aerosol Interaction	$k_{\text{N}_2\text{O}_5}^* (\alpha=0.001) \sim 0.003 \text{ min}^{-1}$

Considering the uncertainties, the time scales associated with the N_2O_5 sinks at night are close. The N_2O_5 homogeneous hydrolysis rate could easily be an order of magnitude lower and the aerosol interaction higher, the conclusion being that N_2O_5 -aerosol interactions are

possibly important at night, lowering the concentrations of both NO_3 and N_2O_5 in the atmosphere.

The trajectory model again can be used to explore the effect of aerosols on the oxides of nitrogen system and on the production of nitric acid by adding the last two reactions shown in Table 1. Again the 24-hour trajectory passing through Claremont was modeled, first with the collision efficiency equal to 0.001 and then with $\alpha = 0.1$ and 1.0. For $\alpha = 0.001$, little effect is seen on the nitric acid produced when compared to the base case as shown in Table 3. Likewise, with $\alpha = 0.001$ there is little effect on the NO_3 peak shown in Figure 9. If $\alpha = 0.1$ or 1.0, the NO_3 peak almost disappears, but a great deal of nitric acid is produced heterogeneously, indicating the importance of aerosol interactions at high collision efficiencies.

9. Conclusions

The photochemical trajectory model used by Russell et al. (1983) was applied to calculations along a 24-hour air parcel trajectory crossing the Los Angeles basin during a day that exhibits summertime high photochemical smog conditions. Ground level dry deposition calculations show that 58% of the nitrogen oxides inserted into the air parcel have deposited at the ground during that 24-hour period. Nitrogen oxides removal is dominated by HNO_3 (39%), PAN (33%), and NO_2 (24%). Much of the nitrogen left in the air column at the end of the 24-hour trajectory is predicted to be associated with NO_2 or PAN.

During the following day, this PAN can either continue to deposit or thermally decompose releasing NO_2 .

Significant nitric acid production takes place both at night and during the daytime. For the most probable case studied here (the base case of Table 3), about 56% of the nitric acid produced during a 24-hour urban trajectory traveling across the Los Angeles basin is generated at night by reactions involving NO_3 and N_2O_5 . Most of that HNO_3 production at night is due to the NO_3 reaction with higher aldehydes and hydrolysis of N_2O_5 . Both pseudo-steady state analysis of the nighttime chemical mechanism and trajectory model results indicate that nitric acid production is slightly sensitive to an order of magnitude decrease in the N_2O_5 homogeneous hydrolysis rate constant, except at high NO levels or if aerosol scavenging is relatively efficient ($\alpha \gg 0.001$).

Aerosol interactions with NO_3 should perturb the system only slightly except at very low NO concentrations, or if the aerosol collision efficiency is high. N_2O_5 interactions with aerosols are more important than NO_3 -aerosol reactions at the same collision efficiency, an effect magnified by any decrease in the N_2O_5 homogeneous hydrolysis rate constant. Heterogeneous reactions on aerosols may be important both in the formation of nitric acid, and as a sink for N_2O_5 .

An analysis of the possible effects of uncertainties in the N_2O_5 homogeneous hydrolysis rate constant shows that the effect of this uncertainty is much different near the ground than at several hundred

meters above the ground. Many of the perturbations used to estimate the effect of uncertainties within the trajectory model cause a redistribution of the mechanism by which nitric acid is formed but do not affect the total amount of nitric acid produced greatly during a 24-hour period (see the bottom of Table 3).

The nitrate radical, NO_3 , is a key species in the mechanism producing HNO_3 by N_2O_5 hydrolysis. The behavior of NO_3 predicted by the trajectory model used here compares well with field observations, and is consistent with known emission rates and atmospheric dynamics in the Los Angeles area. Results indicate that simultaneous calculation of dry deposition, emissions, chemistry, and vertical transport is needed to reproduce Platt et al.'s (1980) observations and that atmospheric measurements made at fixed ground level monitoring sites must be interpreted very carefully if one is to correctly capture the effect of transport processes on atmospheric chemical dynamics.

Acknowledgements: This work was supported, in part, by a grant from the Andrew W. Mellon Foundation and by gifts to the Environmental Quality Laboratory. The California Air Resources Board supported AGR and recent calculations under Agreement A2-150-32.

References

- Adeuyi, Y.G. and Carmichael, G.R. (1982) "A Theoretical Investigation of Gaseous Absorption by Water Droplets from SO_2 - HNO_3 - NH_3 - CO_2 -HCL Mixtures," Atmospheric Environment, 16, 719-729.
- Atkinson, R., Plum, C.N., Carter, W.P., Winer, A.M. and Pitts, J.N., Jr. (1984) "Rate Constants for the Gas Phase Reactions of NO_3 Radicals with a Series of Organics in Air at 298 ± 1 K," J. Phys. Chem., 88 1210-1215.
- Atkinson, R. and Lloyd, A. C. (1984) "Evaluation of Kinetic and Mechanistic Data for Modeling of Photochemical Smog," J. Phys. Chem. Ref. Data, 13 315-444.
- Baldwin, A.C. and Golden, D.M. (1979) "Heterogeneous Atmospheric Reactions: Sulfuric Acid Aerosols as Tropospheric Sinks," Science, 206, 562-563.
- Bandow, H., Okuda, M., Akimoto, H. (1980) "Mechanism of the Gas-Phase Reactions of C_3H_6 and NO_3 Radicals," J. Phys. Chem., 84, 3604-3608.
- Baulch, D.L., Cox, R.A., Crutzen, P.J., Hampson, R.F., Kerr, J.A., Troe, J. and Watson, R.T. (1982) "Evaluated Kinetic and Photochemical Data for Atmospheric Chemistry: Supplement 1," J. Phys. Chem. Ref. Data, 11, 327-496.
- Chameides, W.L. and Davis, D.D. (1982) "The Free Radical Chemistry of Cloud Droplets and its Impact on the Composition of Rain," J. Geophys. Res., 87, 4863-4877.
- Dahneke, B. (1983) "Simple Kinetic Theory of Brownian Diffusion in Vapors and Aerosols," in Theory of Dispersed Multiphase Flow. R. Meyer, Ed., Academic Press, New York.
- Falls, A.H. and Seinfeld, J.H. (1978) "Continued Development of a Kinetic Mechanism for Photochemical Smog," Env. Sci. Technol., 12, 1398-1406.
- Galloway, J.N. and Likens, G.E. (1981) "Acid Precipitation: The Importance of Nitric Acid," Atmospheric Environment, 15, 1081-1085.
- Graham, R.A. and Johnston, H.S. (1978) "The Photochemistry of NO_3 and the Kinetics of the N_2O_5 - O_3 System," J. Phys. Chem., 82, 254-268.

- Groblicki, P.J., Wolff, G.T. and Countess, R.J. (1981) "Visibility Reducing Species in the Denver "Brown Cloud", Part I. Relationships Between Extinction and Chemical Composition," Atmospheric Environment, 15, 2473-2484.
- Huebert, B.J. (1983) "Measurements of the Dry Deposition Flux of Nitric Acid Vapor to Grasslands and Forest," in Precipitation Scavenging, Dry Deposition, and Resuspension. Pruppacher, H.R., Semonin, R.G. and Slinn, W.G.N., coordinators, Elsevier, New York.
- Jech, D.D., Easley, P.G., and Krieger, B.B. (1982) "Kinetics of Reactions Between Free Radicals and Surfaces (Aerosols) Applicable to Atmospheric Chemistry," in Heterogeneous Atmospheric Chemistry, D.R. Schryer, Ed., American Geophysical Union, Washington, D.C. 107-121.
- Levine, S.Z. and Schwartz, S.E. (1982) "In-cloud and below-cloud scavenging of nitric acid vapor," Atmospheric Environment, 16, 1725-1734.
- Liljestrand, H.M. and Morgan, J.J. (1978) "Chemical Composition of Acid Precipitation in Pasadena, California," Env. Sci. Technol., 12 1271-1273.
- Liljestrand, H.M. (1980) "Atmospheric Transport of Acidity in Southern California by Wet and Dry Mechanisms" Ph.D. thesis, California Institute of Technology, Pasadena, California.
- Malko, M.W. and Troe, J. (1983) "Analysis of the Unimolecular Reaction $N_2O_5 + M \rightarrow NO_2 + NO_3 + M$," Int. J. Chem. Kinetics, 14, 399-416.
- McRae, G.J. (1981) "Mathematical Modeling of Photochemical Air Pollution," Ph.D. thesis, California Institute of Technology, Pasadena, California.
- McRae, G.J., Goodin, W.R. and Seinfeld, J.H. (1982) "Development of a Second Generation Mathematical Model for Urban Air Pollution: I Model Formulation," Atmospheric Environment, 16, 679-696.
- McRae, G.J. and Russell, A.G. (1984) "Dry Deposition of Nitrogen-Containing Species," in Deposition Both Wet and Dry, B.B. Hicks, Ed., Acid Precipitation Series-Vol 4, Butterworth, Boston, 153-193.
- Morris, E.D. and Niki, H. (1973) "Reaction of Dinitrogen Pentoxide with Water," J. Phys. Chem., 77, 1929-1932.
- Noxon, J.F., Norton, R.B. and Marovich, E. (1980) " NO_3 in the Troposphere," Geophys. Res. Lett., 7, 125-128.

- Platt, U., Perner, D., Winer, A.M., Harris, G.W. and Pitts, J.N. (1980) "Detection of NO_3 in the Polluted Troposphere by Differential Optical Absorption," Geophys. Res. Lett., 7, 89-92.
- Russell, A.G., McRae, G.J. and Cass, G.R. (1983) "Mathematical Modeling of the Formation and Transport of Ammonium Nitrate Aerosol," Atmospheric Environment, 17, 949-964.
- Russell, A.G. and Cass, G.R. (1984) "Acquisition of Regional Air Quality Model Validation Data for Nitrate, Sulfate, Ammonium Ion and Their Precursors," Atmospheric Environment, 18, 1815-1827.
- Russell, A.G., McRae, G.J. and Cass, G.R. (1984) "Acid Deposition of Photochemical Oxidation Products - A Study Using a Lagrangian Trajectory Model," from Air Pollution Modeling and Its Application III, C. DeWispelaere Ed., Plenum Publishing Corporation, New York.
- Stockwell, W.R. and Calvert, J.G. (1983) "The Mechanism of NO_3 and HONO Formation in the Nighttime Chemistry of the Urban Atmosphere," J. Geophys. Res., 88, 6673-6682.
- Tuazon, E.C., Winer, A.M. and Pitts, J.N., Jr. (1981) "Trace Pollutant Concentrations in a Multiday Smog Episode in the California South Coast Air Basin by Long Path Length Fourier Transform Infrared Spectroscopy," Env. Sci. Technol., 15, 1232-1237.
- Tuazon, E.C., Atkinson, R., Plum, C.N., Winer, A.M. and Pitts, J.N., Jr. (1983) "The Reaction of Gas Phase N_2O_5 with Water Vapor," Geophys. Res. Lett., 10, 953-956.
- Tuazon, E.C., Sanhueza, E., Atkinson, R., Carter, W.P.L., Winer, A.M. and Pitts, J.N., Jr. (1984) "Direct Determination of the Equilibrium Constant at 298K for the $\text{NO}_2 + \text{NO}_3 \rightleftharpoons \text{N}_2\text{O}_5$ Reactions," J. Phys. Chem., 88, 3095-3098.
- Waldman, J.M., Munger, J.W., Jacob, D.J., Flagan, R.C., Morgan, J.J. and Hoffmann, M.R. (1982) "Chemical Composition of Acid Fog," Science, 218, 677-680.
- Whitby, K.T., Husar, R.B. and Liu, B.Y.H. (1972) "The Aerosol Size Distribution of Los Angeles Smog," J. Colloid Interface Sci., 39, 177-204.
- White, W. H. and Roberts, P.T. (1977) "On the Nature and Origins of Visibility Reducing Species in the Los Angeles Basin," Atmospheric Environment, 11, 803-812.

CHAPTER 4

ACQUISITION OF REGIONAL AIR QUALITY MODEL

VALIDATION DATA FOR NITRATE, SULFATE, AMMONIUM

ION AND THEIR PRECURSORS

(Reprinted from Atmospheric Environment, 18, 1815-1827)

ACQUISITION OF REGIONAL AIR QUALITY MODEL VALIDATION DATA FOR NITRATE, SULFATE, AMMONIUM ION AND THEIR PRECURSORS

ARMISTEAD G. RUSSELL* and GLEN R. CASS†

*Mechanical Engineering Department and Environmental Quality Laboratory and †Environmental Engineering Science Department and Environmental Quality Laboratory, California Institute of Technology, Pasadena, CA 91125, U.S.A.

Abstract—An intensive field study was conducted throughout California's South Coast Air Basin to acquire air quality model validation data for use with aerosol nitrate formation models. Aerosol nitrate, sulfate, ammonium, other major ionic aerosol species, nitric acid gas and ammonia were measured concurrently at ten sites for forty-eight consecutive hours during the period 30–31 August 1982. Ozone, NO and NO_x were measured at all locations, and PAN was measured at Pasadena and Riverside, completing a nitrogen balance on the air masses studied.

The product of the measured nitric acid and ammonia concentrations ranged from less than 1 ppbv² to greater than 300 ppbv² during the experiment, providing a wide range of conditions over which comparisons can be drawn between chemical equilibrium calculations and experimental results. The ionic material in the aerosol phase was chemically more complex than is assumed by present theoretical models for the equilibrium between NH₃, HNO₃ and the aerosol phase, and included significant amounts of Na⁺, Ca²⁺, Mg²⁺, K⁺ and Cl⁻ in addition to NH₄⁺, SO₄²⁻ and NO₃⁻. Results of the experiment showed that aerosol nitrate levels in excess of 20 μg m⁻³ accumulated in near-coastal locations in the morning of 31 August, followed by subsequent transport across the air basin. Trajectory analysis showed that the afternoon aerosol nitrate peak observed inland at Rubidoux near Riverside was associated with the same air mass that contained the high morning nitrate levels near the coast, indicating that description of both transport and atmospheric chemical reactions is important in understanding regional nitrate dynamics.

1. INTRODUCTION

Ammonia and nitric acid vapor react to form ammonium nitrate aerosol. This is important because ammonium nitrate containing aerosols account for a significant fraction of local and regional visibility problems, particularly in Los Angeles and Denver (White and Roberts, 1977; Cass, 1979; Groblicki *et al.*, 1981). Nitric acid concentrations also are important because of their contribution to wet and dry acid deposition processes. Since NH₄NO₃ formation acts as an important sink for nitric acid, the formation of NH₄NO₃ must be understood if nitric acid levels are to be controlled in a deliberate fashion. Reliable air quality models are needed if emission control strategy development is to proceed. But before air quality models that compute aerosol nitrate and nitric acid concentrations are used for emission control strategy testing, the accuracy of their predictions must be evaluated.

An air quality model for NH₄NO₃ formation and transport recently has been developed (Russell *et al.*, 1983). The Caltech photochemical airshed model developed by McRae and Seinfeld (1983) is used to compute gaseous HNO₃ concentrations from reactive hydrocarbon and oxides of nitrogen emissions. An inventory of ammonia emissions is introduced into the model. Then NH₄NO₃ concentrations are computed at thermodynamic equilibrium between gaseous

HNO₃ and NH₃ using the approach outlined by Stelson and Seinfeld (1982a,b).

To date, this model has been tested in its trajectory form against the time series of gaseous ammonia, particulate ammonium ion and particulate nitrate ion concentration measurements at El Monte, California on a summer day during 1974. Although the model appears to perform well, the ability to confirm this conclusion is limited by the absence of field data on gaseous nitric acid during that event, and by the potential for artifact nitrate formation during sample collection by the measurement methods used in 1974. Better model validation data are needed.

Ideally, an air quality model validation data set for aerosol nitrate formation should provide measurements of all relevant gaseous species: NO, NO₂, HNO₃, NH₃, PAN (and O₃ if photochemical oxidant concentrations are to be checked as well). In addition, the concentration of the aerosol species NO₃⁻, SO₄²⁻, NH₄⁺ should be measured along with all other ionic species that are present in the aerosol. Temperature and relative humidity data are needed to compute the equilibrium dissociation constant that relates gaseous HNO₃ and NH₃ to the aerosol phase. Simultaneous measurements at a number of widely spaced monitoring sites are desirable if an Eulerian grid-based version of the aerosol nitrate formation model is to be tested. Two or more consecutive days of observation are required in Los Angeles if air is to be tracked from the

marine environment all of the way to the eastern end of the air basin near Riverside. Low artifact measurement methods are desired.

The purpose of this paper is to report on the acquisition of such an aerosol nitrate air quality model verification data set in southern California.

2. EXPERIMENTAL

A field experiment was conducted in the South Coast Air Basin (SCAB) that surrounds Los Angeles during the period 30–31 August 1982. Moderate levels of photochemical smog were encountered during the two days studied. Both days were warm with scattered clouds. Peak temperatures reached 35 and 37°C on 30 and 31 August, respectively at the eastern end of the Los Angeles basin. During the afternoons, onshore winds transported pollutants inland, with typical wind speeds of about 5 m s^{-1} . This combination of high temperatures and inland transport resulted in a peak 1-h average ozone concentration of 0.18 ppm on August 30, increasing to a 1-h average peak ozone level of 0.26 ppm in the Riverside area on 31 August.

Ten monitoring sites were established at the locations shown in Fig. 1. The sampling network operated for 48 consecutive hours from midnight at the start of the first day to midnight at the end of 31 August. Two-hour average and 4-h average measurements of $\text{HNO}_3(\text{g})$, $\text{NH}_3(\text{g})$, NO_3^- , NH_4^+ , SO_4^{2-} and other major ionic species were obtained at each site. All sites except Riverside were co-located with a South Coast Air Quality Management District (SCAQMD) or California Air Resources Board (CARB) continuous air monitoring station, and 1-h average data on NO , NO_2 , O_3 and SO_2 were obtained by cooperation with these agencies. Site descriptions are given by the U.S. Environmental Protection Agency (1973, 1978 *et seq.*). PAN was measured by electron capture gas chromatography, and NO and NO_2 were measured by chemiluminescence by researchers at the University of California at Riverside (UCR). PAN also was measured by the same principle at Caltech in Pasadena.

The aerosol, nitric acid and ammonia sampling apparatus for this experiment is shown schematically in Fig. 2. Aerosol nitrate and nitric acid concentrations were measured both by dual filter methods and by the denuder difference method. Gaseous ammonia was measured by a dual filter method using oxalic acid impregnated filters as a sink for NH_3 . Filter holders were of open-faced design so that any large particle nitrates would be collected. The sampling apparatus was surrounded by a bug screen and shaded by a sun shield to prevent nitrate volatilization through over-heating. Nine of the ten sampling sites shown in Fig. 1 were equipped as indicated in Fig. 2, while the 10th site at Riverside (UCR)

EXPERIMENTAL DESIGN

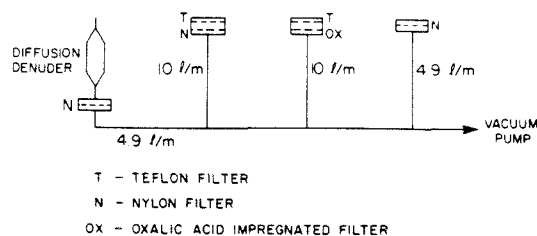


Fig. 2. Schematic of the sampling apparatus used at nine of the ten sites. The tenth station used only the two 10 l min^{-1} lines with dual filters.

consisted of only the two sampling lines that contained dual filter packs.

In the dual filter method for nitric acid determination, air was drawn at a rate of 10 l min^{-1} through a dual filter pack (Grosjean, 1983; Spicer *et al.*, 1982; Appel *et al.*, 1980). A Teflon prefilter (Membrana, Zefluor, 47 mm diameter, $1 \mu\text{m}$ pore size) first removed the aerosol phase constituents. Gaseous nitric acid that passed through the inert Teflon prefilter was collected as nitrate on a nylon after-filter (Ghia Corp., Nylasorb, 47 mm dia, $1 \mu\text{m}$ pore size). Filters, after exposure, were sealed immediately in petri dishes and chilled until analysis to minimize volatilization from the samples.

Water soluble material was extracted from these filters by mechanical shaking in distilled-deionized-distilled water for 1 h or more. Measured extraction efficiencies typically were above 97%. The extract was divided for subsequent chemical analysis. The aerosol material extracted from the Teflon prefilters was analyzed for nitrate, sulfate, chloride, potassium and sodium ions using Dionex Model 10 and Model 2120 ion chromatographs (Mueller *et al.*, 1978). Divalent cations (calcium and magnesium) were measured using a Varian Techtron model AA-6 atomic absorption spectrophotometer (Varian, 1975). Ammonium ion on the Teflon filters was determined by the phenol—hypochlorite method (Salorzano, 1967). Nitric acid concentrations were determined by extracting the nitrate ion collected on the nylon after-filters, with chemical analysis by ion chromatography as described above. Analytical uncertainties were assessed by analysis of reagent grade standards prepared in the range 0–5 ppm (wt/vol aqueous solution). Five replicate analyses of each of three standard solutions that span the concentration range of interest for each species were used to estimate the uncertainty associated with the laboratory procedures. The relative uncertainty associated with these measurements is shown in the first data column of Table I. A contribution due to the

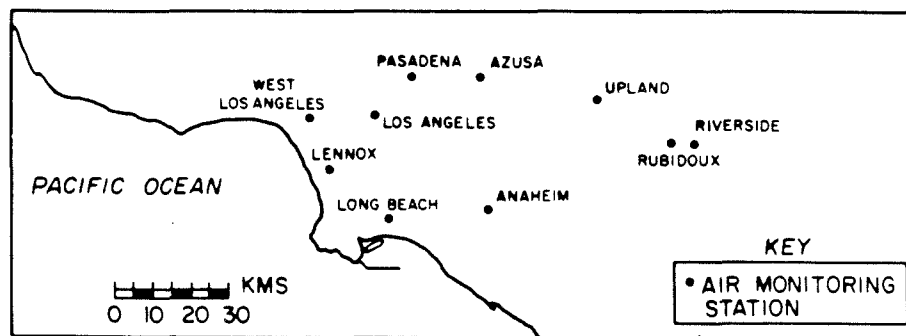


Fig. 1. Locations of nitrate monitoring sites in the South Coast Air Basin.

Table 1. Measurement uncertainties

Species	Uncertainty due to chemical analysis procedure* (%)	Uncertainty due to filter blank† ($\mu\text{g m}^{-3}$)
NO_3^-	15	1.0
SO_4^{2-}	15	1.6
Cl^-	22	0.6
NH_4^+	20	0.2
Ca^{2+}	18	1.4
Na^+	15	0.8
K^+	18	1.1
Mg^{2+}	18	0.5
HNO_3	15	0.8
NH_3	20	0.3

* One standard error, as % of nominally measured value.

† One standard error, stated in equivalent atmospheric concentration.

variability of the filter blanks was added to this analytical error. More than twenty blank filters of each type were taken into the field but not exposed. The average blank values from these filters were subtracted from the measured filter loadings. The contribution to the uncertainty in these measurements due to the variability of the filter blank also is shown in Table 1. This uncertainty in the filter blank governs the lowest quantifiable pollutant concentrations during this experiment. A complete listing of the data from this experiment and their associated uncertainties has been compiled (Russell and Cass, 1983).

The dual filter method for measuring aerosol nitrate and nitric acid has the advantage of simplicity, low cost, sensitivity and ability to produce both particulate and gaseous nitrate concentration data from the same air stream. Results from the nitric acid measurement method intercomparison (Spicer *et al.*, 1982) conducted in the SCAB showed that the dual filter measurements were highly correlated with the median value obtained by all competitive nitric acid measurement methods. One of the two groups of investigators that used a Teflon-nylon filter pair during the intercomparison study obtained results suggesting a small positive proportional bias, while a second group obtained results that suggest no significant bias when measuring nitric acid. Dual filter methods are susceptible to both positive and negative errors. Volatilization of ammonium nitrate would decrease measured nitrate aerosol (Appel *et al.*, 1980). Nitric acid may also react with collected aerosol increasing the measured nitrate aerosol (Appel *et al.*, 1980; Spicer and Schumacher, 1979).

The second method used for nitric acid determination during the present experiment was based on the diffusion denuder design described by Forrest *et al.* (1982), except that 10 sodium carbonate coated tubes 30 cm in length were contained within each denuder housing. At a total air flow rate of 4.9 l min^{-1} , laminar flow was achieved inside the denuder tubes at a nominal Reynolds number of 175 based on tube diameter. Air flowing through the denuder was stripped of nitric acid by reaction with the tube walls. Particulate nitrate (PN) penetrated the denuder and was collected on the nylon after-filter. A separate parallel sample line operating at 4.9 l min^{-1} contained a single nylon filter used to collect total inorganic nitrate (i.e. nitric acid plus aerosol nitrate). Nitric acid concentrations by the denuder difference method were obtained by subtracting the particulate nitrate concentration from the total inorganic nitrate concentration. Nitrate ion levels on these nylon filters were determined by water extraction and ion chromatography, with filter blank subtraction as described previously.

Nitrate measurements obtained by denuder also are susceptible to interferences. Large particle nitrate may be lost in the denuder by impaction. Laboratory experiments performed on the denuders used in this experiment show losses of about 30% for particles larger than $4 \mu\text{m}$ in diameter (Strand, 1983). Because of this measurable bias in the denuder system, nitric acid concentrations presented in this paper will be based on the dual filter method.

Gaseous ammonia concentrations were determined from the dual filter pack shown in Fig. 2 that contained an oxalic acid impregnated back-up filter. The aerosol phase containing ammonium ion first was removed by a Teflon prefilter (Membrana, Zefluor, 47 mm dia, $1.0 \mu\text{m}$ pore size). Ammonia gas remaining in the air stream was collected by reaction with an oxalic acid impregnated glass fiber filter (Gelman Type AE, 47 mm diameter) (Yoong, 1981; Appel *et al.*, 1980; Cadle *et al.*, 1980). After collection, filters were sealed and chilled as described previously. Ammonia concentrations were determined from the ammonium ion collected on the oxalic acid impregnated filters by a modified version of the phenol-hypochlorite method (Salorzano, 1967). The excess oxalate and acid on the glass fiber filters interfered significantly with the method of Salorzano (1967), so the method was modified, adding a phosphate buffer (Harwood and Kuhn, 1970) and additional hydroxide. The modified method is described by Russell (1983) and was found to give reproducible results with a correlation coefficient of $r = 0.99$. Standard deviations for recovery of NH_4^+ standards containing 1 and 0.5 ppm (N by wt) were 2.5 and 3.5%, respectively.

The calculated equilibrium dissociation constant for the $\text{HNO}_3\text{-NH}_3\text{-NH}_4\text{NO}_3$ system is highly dependent on ambient temperature and relative humidity. Temperature measurements to accompany each ambient sample were obtained from nearby weather monitoring stations, where possible, or from temperature measurements that were taken at the air monitoring site by the station operators using mercury thermometers. Instantaneous temperatures were taken each hour. Relative humidities were computed from measured dew point saturation temperatures that are monitored at a number of locations in the SCAB. Dew point temperatures were interpolated to the location of each monitoring site by the method of Goodin *et al.* (1979).

3. RESULTS

Based on previous descriptions of aerosol nitrate concentrations in the Los Angeles area (Appel *et al.*, 1978), high aerosol nitrate concentrations were expected in the Riverside area in the late afternoon due to production of nitric acid in the plume downwind of metropolitan Los Angeles. High aerosol nitrate levels (above $25 \mu\text{g m}^{-3}$) were observed at Rubidoux as expected, as is seen in Fig. 3(a). However, unexpectedly high nitrate levels also were observed at near-coastal sites like Lennox and Long Beach in the morning of 31 August, as seen in Fig. 3(c).

Hourly averaged data on surface wind speed and direction at 39 monitoring sites in Southern California were acquired from governmental agencies for the period 30–31 August 1982. A mass-consistent wind field defined over a $5 \text{ km} \times 5 \text{ km}$ grid system that covers the geographic area shown in Fig. 1 was developed for each hour by the method of Goodin *et al.* (1979). Air parcel trajectories were integrated over these gridded wind fields using 10 min time steps. Trajectory analysis shows that the peak nitrate concen-

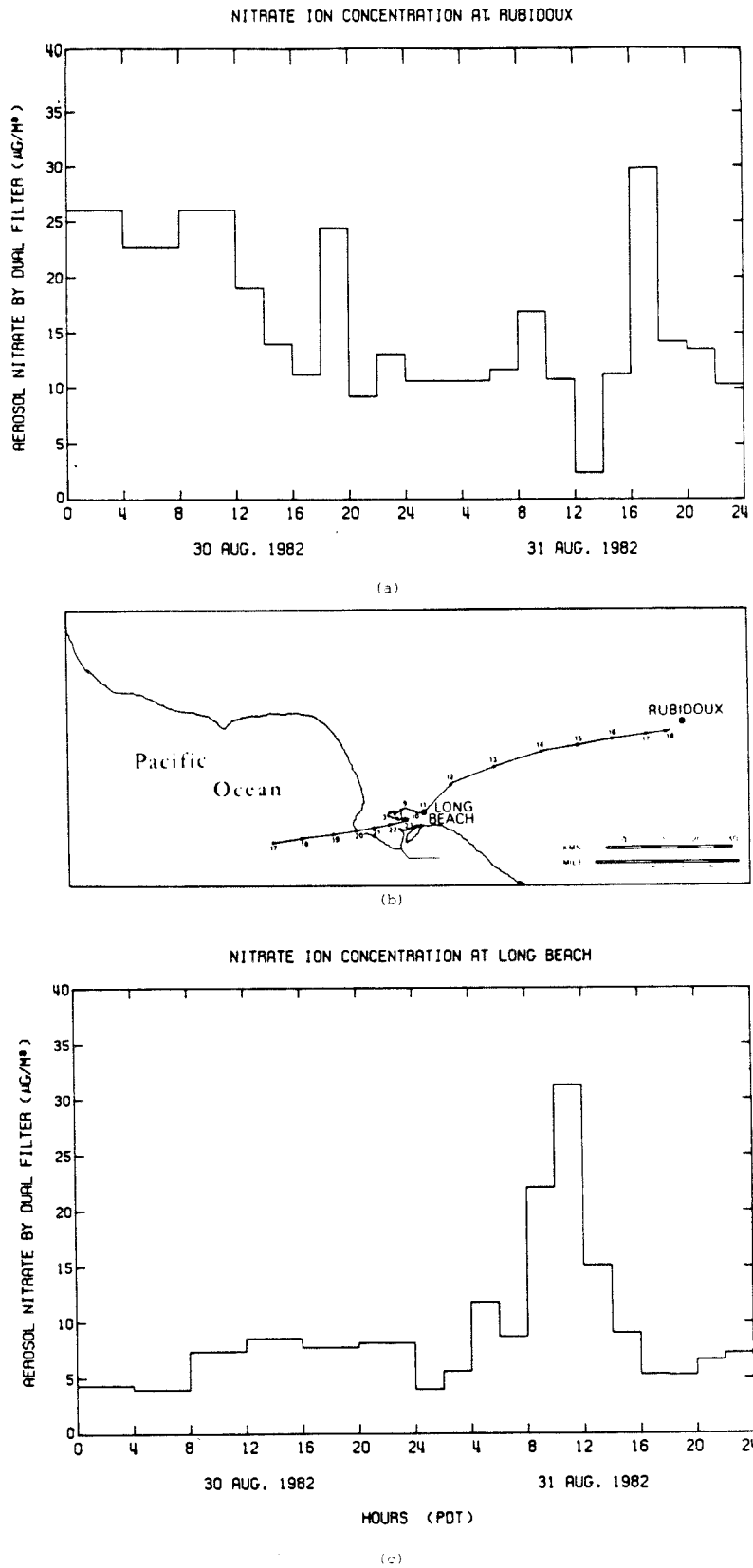


Fig. 3. (a) Nitrate concentration observed at Rubidoux, 30-31 August 1982. (b) Trajectory of the air mass passing over the long Beach area at 1100 on 31 August and over the Rubidoux area at 1800 on 31 August 1982. (c) Nitrate concentrations at Long Beach, 30-31 August 1982.

tration at Rubidoux on the afternoon of 31 August is related to the coastal peak observed at Long Beach earlier that morning. A forward trajectory drawn from the nitrate peak in the Long Beach area at 1100 hours on the morning of 31 August passes within 3.5 km of Rubidoux between 1700 and 1800 hours in the late afternoon at the time of the nitrate peak in the eastern portion of the air basin [see Fig. 3(b)]. A backward trajectory drawn from Long Beach at 1100 hours on 31 August shows that that air mass first crossed the coastline during the sea breeze portion of the late afternoon of 30 August. At night, wind speeds dropped to less than 0.5 m s^{-1} with variable wind direction. The air mass stagnated overnight in Long Beach, an area of

high NO_x emissions (see Fig. 6 in Russell *et al.*, 1983). The high nitrate concentration observed at Long Beach in the morning of 31 August resulted from progressive aerosol accumulation within a largely stagnant and stable air mass. This nitrate-rich air parcel then was advected inland on the next day's sea breeze. It appears that transport may play as important a role as chemical reaction in accumulating high nitrate levels.

A balance on the ionic material in the samples taken at Long Beach is shown in Fig. 4. The major constituents are NH_4^+ , NO_3^- and SO_4^{2-} , but Na^+ and Ca^{2+} often account for about one third of the cations present, suggesting sea salt and soil dust contributions

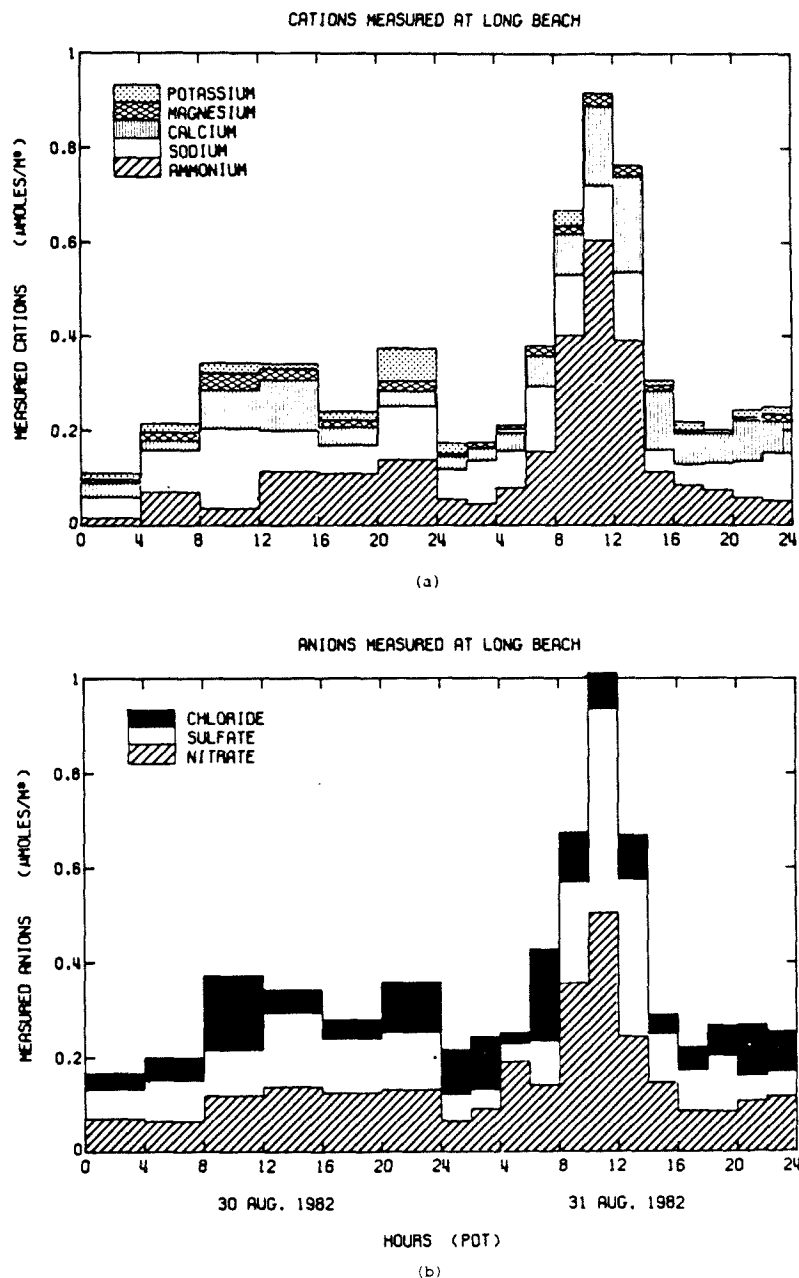


Fig. 4. Ionic species concentration at Long Beach. (a) Cations. (b) Anions.

to the aerosol samples. Na^+ usually is present in excess of Cl^- , suggesting that reaction with strong acids like H_2SO_4 or HNO_3 has displaced some of the chloride from the sea salt portion of the aerosol (Martens *et al.*, 1973; Duce, 1969; Robbins *et al.*, 1959; Hitchcock *et al.*, 1980). The ion balance is good in spite of the fact that CO_3^{2-} , OH^- and H^+ concentrations were not measured. Previous studies in the SCAB show the presence of very low carbonate carbon levels in the aerosol (Mueller *et al.*, 1972). Large amounts of hydrogen ion would not be expected because of the great excess of ammonia present during this experiment.

The composition of the aerosol observed inland at Riverside is shown in Fig. 5. The largest contributors to the ionic material are NH_4^+ and NO_3^- , but noticeable amounts of K^+ , Mg^{2+} , Ca^{2+} , Na^+ and Cl^- also are found. Note that Cl^- arrives with the aerosol between 1600 and 1800 hours on 31 August near the time of arrival of the trajectory from Long Beach discussed previously. The important point to note from these ion balances is that the ionic material in the actual aerosol is much more complex than the mixed sulfate, nitrate and ammonium salts that can be described by present theoretical models for the equilibrium between NH_3 , HNO_3 and the aerosol phase.

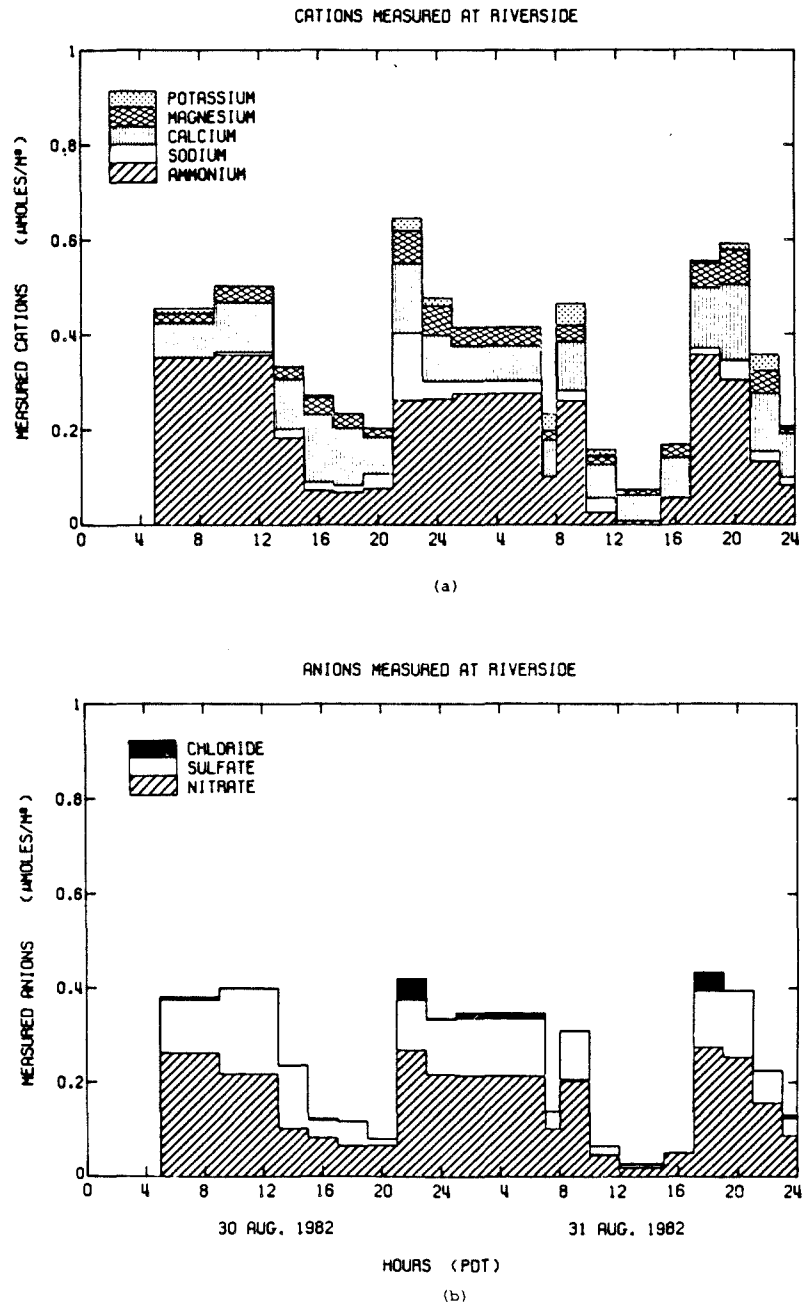


Fig. 5. Ionic species concentration at Riverside. (a) Cations. (b) Anions.

Gas phase HNO_3 concentrations are compared to aerosol NO_3^- at the polluted near-coastal sites at Long Beach and Lennox in Fig. 6. Nearly all of the inorganic nitrate is in the aerosol phase. In contrast, Fig. 7 shows that ammonia is partitioned about equally between $\text{NH}_3(\text{g})$ and aerosol NH_4^+ at Long Beach, while at Lennox ammonia gas concentrations often were quite elevated, suggesting an NH_3 source upwind of Lennox (possibly at a nearby refinery or at the nearby Hyperion sewage treatment plant).

Inland from the coast, gaseous nitric acid concentrations begin to increase in the late morning and early afternoon, due possibly to photochemical production

of HNO_3 or to volatilization of NH_4NO_3 . This can be seen in Fig. 8 at Anaheim (which is located between Long Beach and Riverside). By the time that the air parcel defined at Long Beach at 1100 hours on 31 August reaches Rubidoux between 1600 and 1800 hours, a tremendous increase in NH_3 in the air parcel has occurred [Fig. 9(b)], and most of the inorganic nitrate again is found in the aerosol phase [Fig. 9(a)]. This increase in NH_3 is consistent with estimates of the spatial distribution of NH_3 sources in the Los Angeles area given by Cass *et al.* (1982) and Russell *et al.* (1983), which shows that the largest source of NH_3 in the Los Angeles area arises from a large group of dairies and

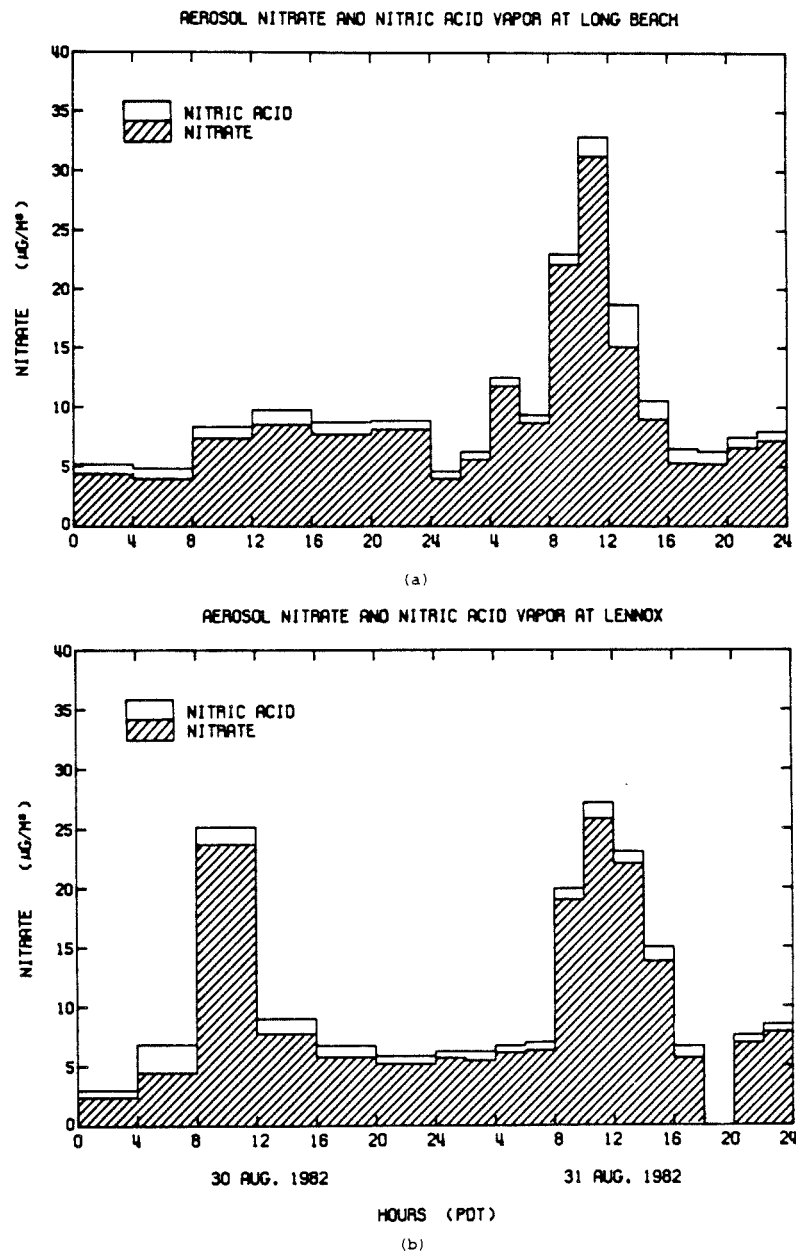


Fig. 6. Particulate nitrate and gaseous nitric acid concentrations ($\mu\text{g m}^{-3}$ as NO_3^-). (a) Long Beach. (b) Lennox.

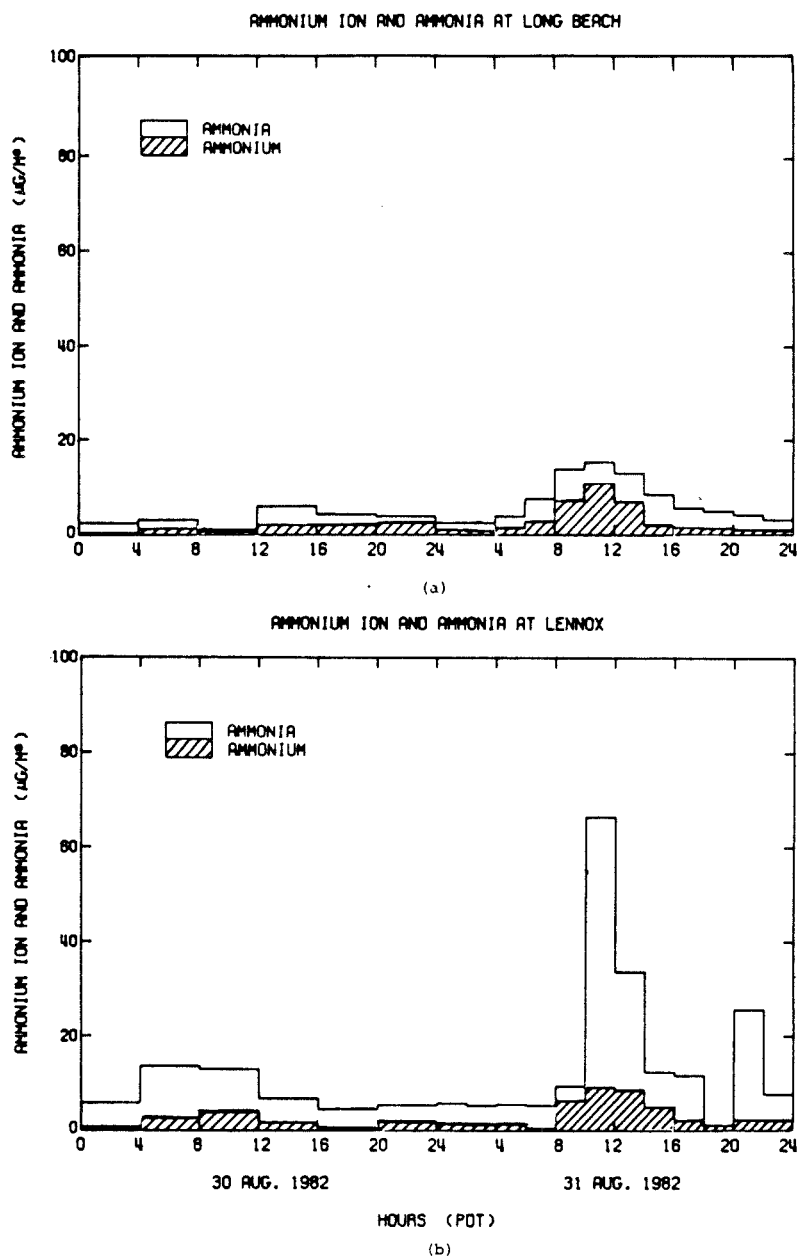


Fig. 7. Particulate ammonium and gaseous ammonia concentrations ($\mu\text{g m}^{-3}$ as NH_4^+).
(a) Long Beach. (b) Lennox.

animal husbandry operations in the Chino area just to the west of Riverside and Rubidoux.

The product of the measured concentrations of ammonia and nitric acid vapor is a key parameter that can be compared to the predictions of theoretical models for the ammonia and nitric acid concentrations expected at thermodynamic equilibrium with the aerosol phase. Nitric acid and ammonia concentration measurements were used to calculate their concentration product (CP) at each monitoring site. As seen in Fig. 10, the measured CP at Rubidoux varies from less than 20 to over 300 ppbv^2 , and measured CP's at some monitoring sites were observed below 1 ppbv^2 . A very

wide range of NH_3 and HNO_3 concentration product data thus have been acquired for use in verifying theoretical calculations. The hypothesis that aerosol nitrates were in equilibrium with gas phase nitric acid and ammonia during this experiment has been tested by Hildemann *et al.* (1984).

At two locations, Riverside and Pasadena, the major gaseous and aerosol species that evolve from NO_x emissions were measured. Fig. 11 shows that most of the pollutant oxides of nitrogen at these two sites were present as NO and NO_2 throughout this experiment. Only a small fractional conversion of NO emissions to HNO_3 and NH_4NO_3 is needed to explain the nitrate

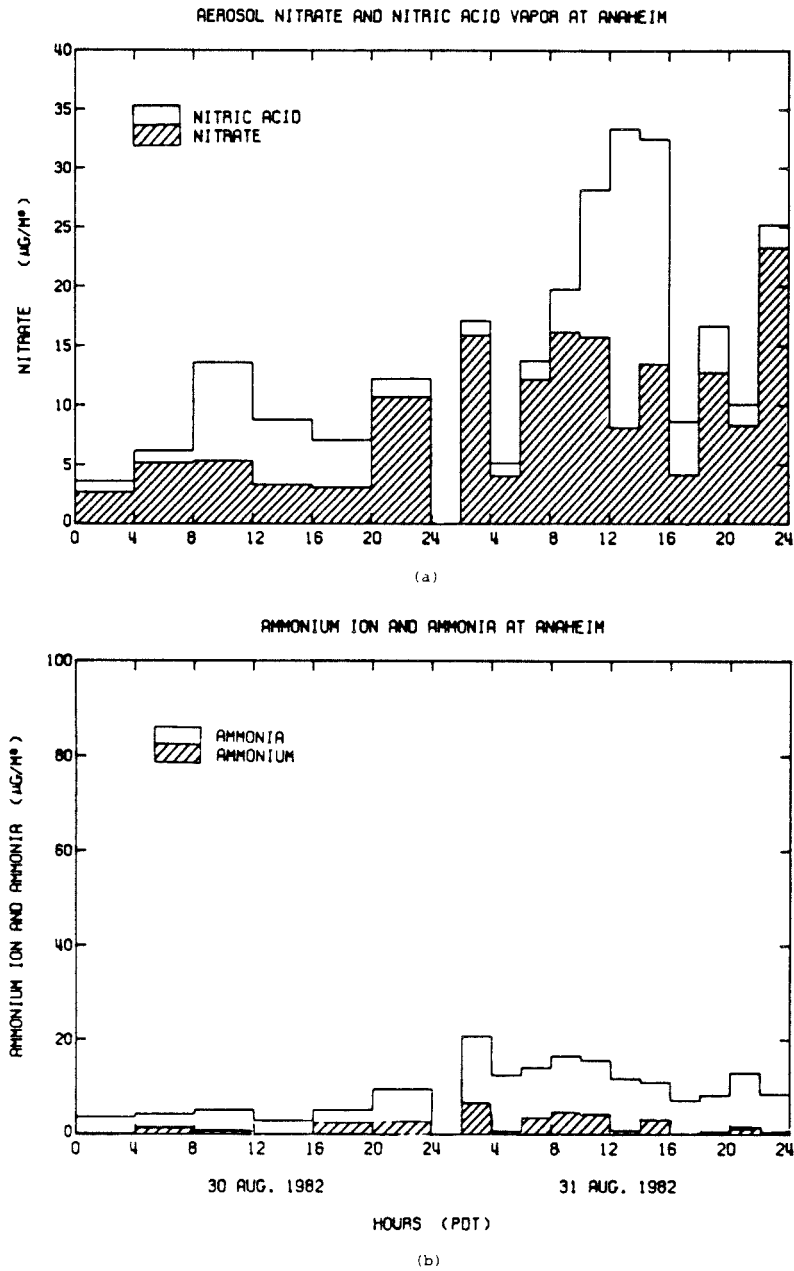


Fig. 8. (a) Particulate nitrate and gaseous nitric acid concentrations at Anaheim ($\mu\text{g m}^{-3}$ as NO_3^-). (b) Particulate ammonium and gaseous ammonia concentrations at Anaheim ($\mu\text{g m}^{-3}$ as NH_4^+).

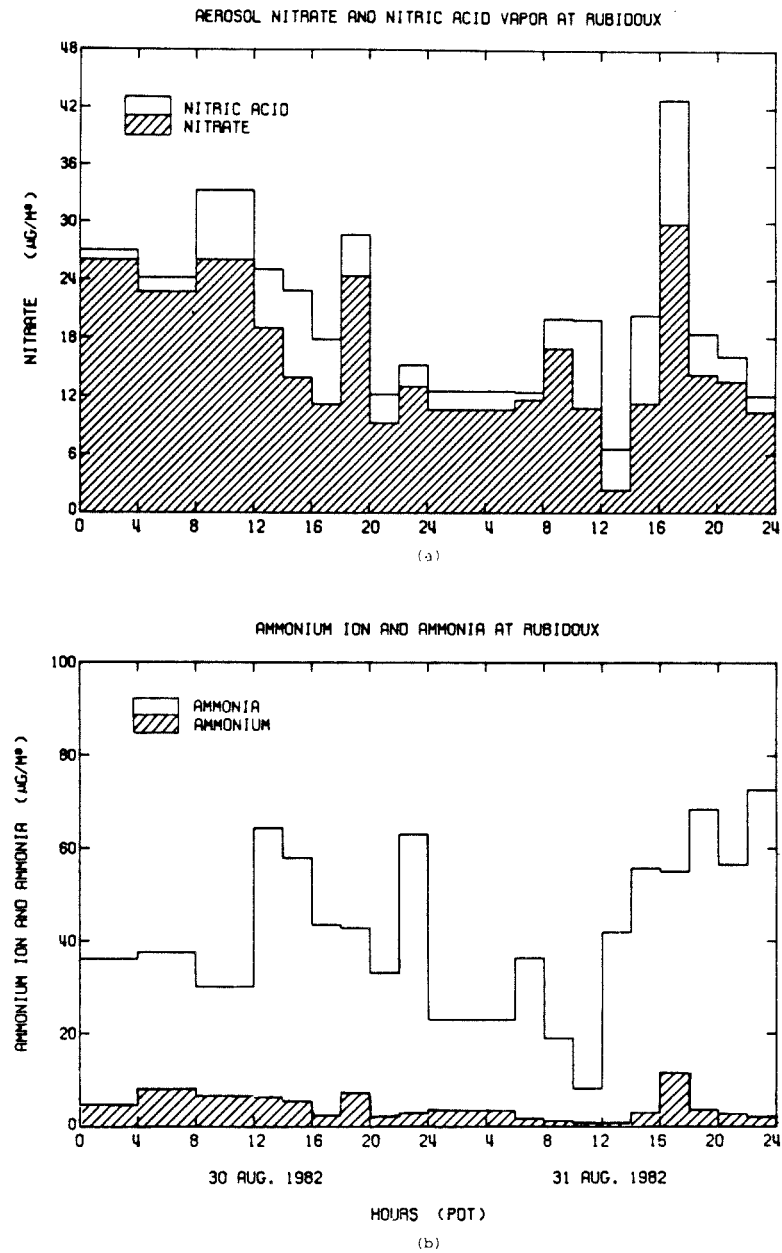


Fig. 9. (a) Particulate nitrate and gaseous nitric acid at Rubidoux ($\mu\text{g m}^{-3}$ as NO_3^-).
 (b) Particulate ammonium and gaseous ammonia concentrations at Rubidoux ($\mu\text{g m}^{-3}$ as NH_4^+).

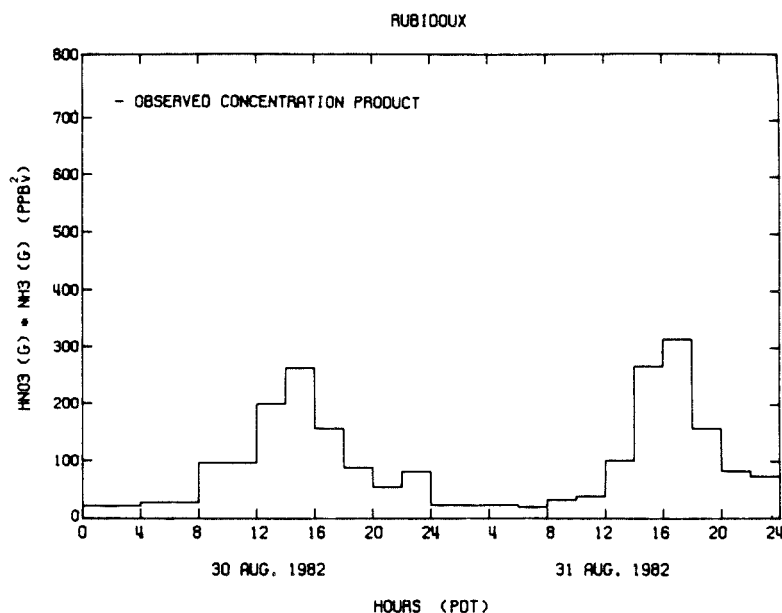


Fig. 10. Partial pressure concentration product of ammonia and nitric acid at Rubidoux.

concentrations observed. The fractional conversion of NO and NO_2 to nitrate species during this experiment is lower than observed during some other field measurement programs (Grosjean, 1983; Spicer, 1982) but this is consistent with the lower level of photochemical activity experienced during this 2-day experiment. On the days sampled, peak 1-h average O_3 concentrations exceeded 0.20 ppm at only a few monitoring sites, with the basin-wide 1-h O_3 peak within the region shown in Fig. 1 amounting to 0.26 ppm. In contrast, the O_3 concentration on the 1974 day modeled previously by Russell *et al.* (1983) exceeded 0.40 ppm with a correspondingly higher conversion of NO_x to HNO_3 and PAN.

4. CONCLUSIONS

Results from the field experiment show that the ionic material in the aerosol phase throughout the South Coast Air Basin is chemically complex. At most times, the bulk of the ionic aerosol is composed of nitrate, sulfate and ammonium ion. However there are significant amounts of Na^+ , Ca^{2+} , Mg^{2+} , K^+ , Cl^- and possibly CO_3^{2-} , OH^- or H^+ ions also present. The coastal nitrate-containing aerosol has a significant sea salt derived fraction, probably from the displacement of chloride by reaction with nitric acid. These multi-component aerosols are more complex than can be handled by present mathematical models for the equilibrium between HNO_3 , NH_3 and a mixed sulfate, nitrate and ammonium containing aerosol.

Trajectory analysis has been used to judge the importance of transport in determining aerosol nitrate concentrations. Large amounts of nitrate were shown to accumulate in an air mass that stagnated near the coast at night. Later, this nitrate laden air mass was transported inland by the sea breeze. The time of the nitrate peak inland near Riverside coincided with the time that that nitrate laden air mass reached that area. This indicates that a description of transport characteristics as well as atmospheric chemistry is important in understanding the dynamics that govern the high nitrate levels observed in the eastern portion of the Los Angeles basin.

A nitrogen balance constructed at two locations in the Los Angeles basin shows that conversion of only a small fraction of the NO_x emissions to HNO_3 and NH_4NO_3 is sufficient to explain the aerosol nitrate and nitric acid observed. The two days studied here were both considered to have moderate smog (fairly typical of a summer day), and a correspondingly lower oxidation of NO_x to HNO_3 and PAN than would occur during an extreme air pollution episode in Los Angeles.

The data set derived from this experiment can be used in verification tests of aerosol nitrate formation models, and will challenge the predictive capability of current air quality models. The days sampled during this experiment exhibited both interesting transport patterns and evidence of chemical transformations that can be used to test both the transport and gas-to-particle conversion descriptions built into regional scale air quality models.

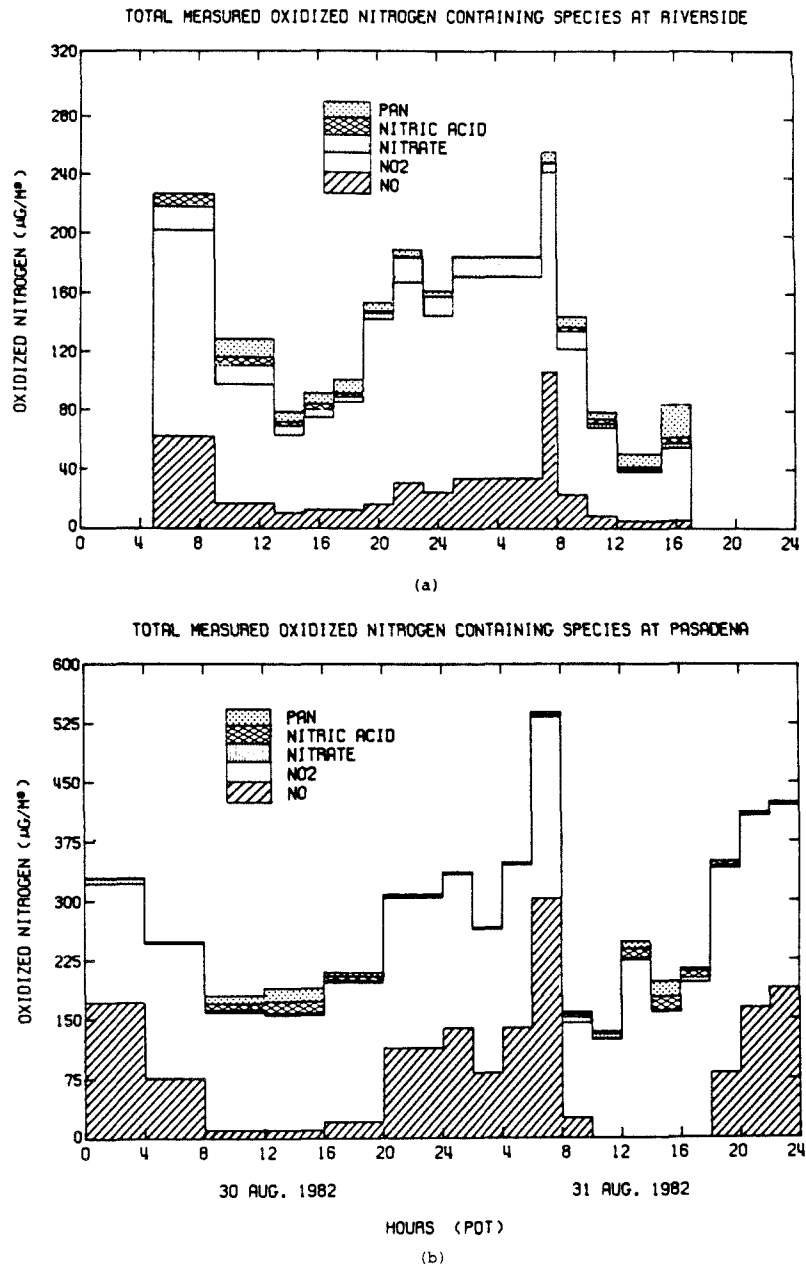


Fig. 11. Measured NO , NO_2 , HNO_3 , PAN and nitrate (in $\mu\text{g m}^{-3}$ stated as equivalent NO_3^-). (a) Pasadena. (b) Rubidoux.

Acknowledgements—This study was supported by the California Air Resources Board under Agreement No. A2-150-32 and by gifts to the Environmental Quality Laboratory. The South Coast Air Quality Management District and the California Air Resources Board cooperated by allowing access to their air monitoring sites, and provided meteorological and gaseous pollutant data. Special thanks also goes to Dennis Fitz and the Statewide Air Pollution Research Center at the University of California at Riverside whose services were greatly appreciated. We would also like to thank the Caltech students and staff who helped to operate each of the pollutant sampling sites.

REFERENCES

- Appel B. R., Kothny E. L., Hoffer E. M., Hidy G. M. and Wesolowski J. J. (1978) Sulfate and nitrate data from the California Aerosol Characterization Experiment (ACHEX). *Envir. Sci. Technol.* **12**, 418-425.
- Appel B. R., Wall S. M., Tokiwa Y. and Haik M. (1980) Simultaneous nitric acid, particulate nitrate and acidity measurements in ambient air. *Atmospheric Environment* **14**, 549-554.
- Cadle S. H., Countess R. J. and Kelly N. A. (1980) Nitric acid and ammonia concentrations in urban and rural locations.

- Atmospheric Environment* **16**, 2501–2506.
- Cass G. R. (1979) On the relationship between sulfate air quality and visibility with examples in Los Angeles. *Atmospheric Environment* **13**, 1069–1084.
- Cass G. R., Gharib S., Peterson M. and Tilden J. W. (1982) The origin of ammonia emissions to the atmosphere in an urban area. Open File Report 82-6, Environmental Quality Laboratory, California Institute of Technology, Pasadena, CA.
- Duce R. A. (1969) On the source of gaseous chlorine in the marine atmosphere. *J. geophys. Res.* **70**, 1775–1779.
- Forrest J., Spandau D. J., Tanner R. L. and Newman L. (1982) Determination of atmospheric nitrate and nitric acid employing a diffusion denuder with a filter pack. *Atmospheric Environment* **16**, 1473–1485.
- Goodin W. R., McRae G. J. and Seinfeld J. H. (1979) A comparison of interpolation methods for sparse data: application to wind and concentration fields. *J. appl. Met.* **18**, 761–771.
- Groblicki P. J., Wolff G. T. and Countess R. J. (1981) Visibility-reducing species in the Denver "Brown Cloud"—I. Relationships between extinction and chemical composition. *Atmospheric Environment* **15**, 2473–2484.
- Grosjean D. (1983) Distribution of atmospheric nitrogenous pollutants at a Los Angeles area receptor site. *Envir. Sci. Technol.* **17**, 13–19.
- Harwood J. E. and Kuhn A. L. (1970) A colorimetric method for ammonia in natural waters. *Water Res.* **4**, 805–811.
- Hildemann L. M., Russell A. G. and Cass G. R. (1984) Ammonia and nitric acid concentrations in equilibrium with atmospheric aerosols: experiment vs theory. *Atmospheric Environment* **18**, 1737–1750.
- Hitchcock D. R., Spiller L. L., and Wilson W. E. (1980) Sulfuric acid aerosols and HCl release in coastal atmospheres: evidence of rapid transformation of sulphuric acid particulates. *Atmospheric Environment* **14**, 165–182.
- Martens C. S., Wesolowski J. J., Harriss R. C. and Kaifer R. (1973) Chlorine Loss from Puerto Rican and San Francisco Bay Area Marine Aerosols. *J. geophys. Res.* **78**, 8778–8792.
- McRae G. J. and Seinfeld J. H. (1983) Development of a second generation mathematical model for urban air pollution—II. Performance evaluation. *Atmospheric Environment* **17**, 501–523.
- Mueller P. K., Mendoza B. V., Collins J. C. and Wilgus E. S. (1978) Application of ion chromatography to the analysis of anions extracted from airborne particulate matter. In *Ion Chromatographic Analysis of Environmental Pollutants* (edited by Sawicki E., Mulik J. D. and Wittgenstein E.). Ann Arbor Science, Ann Arbor, MI.
- Mueller P. K., Mosley R. W. and Pierce L. B. (1972) Chemical composition of Pasadena aerosol by particle size and time of day. *J. Colloid Interface Sci.* **39**, 235–239.
- Robbins R. C., Cadle R. D. and Eckhardt D. L. (1959) The conversion of sodium chloride to hydrogen chloride in the atmosphere. *J. Met.* **16**, 53–56.
- Russell A. G. (1983) Analysis of oxalic acid impregnated filters for ammonia determination. Open File Report 83-1, Environmental Quality Laboratory, California Institute of Technology, Pasadena, CA.
- Russell A. G. and Cass G. R. (1983) Nitric acid, ammonia and atmospheric particulate matter concentrations in the South Coast Air Basin, 30–31 August 1982. Open File Report 83-3, Environmental Quality Laboratory, California Institute of Technology, Pasadena, CA.
- Russell A. G., McRae G. J. and Cass G. R. (1983) Mathematical modeling of the formation and transport of ammonium nitrate aerosol. *Atmospheric Environment* **17**, 949–964.
- Salorzano L. (1967) Determination of ammonia in natural waters by the phenolhypochlorite method. *Limnol Oceanogr.* **14**, 799–801.
- Spicer C. W. (1982) The distribution of oxidized nitrogen in urban air. *Sci. Tot. Envir.* **24**, 183–192.
- Spicer C. W., Howes J. E., Bishop T. A., Arnold L. H. and Stevens R. K. (1982) Nitric acid measurement methods: an intercomparison. *Atmospheric Environment* **16**, 1407–1500.
- Spicer C. W. and Schumacher P. M. (1979) Particulate nitrate: laboratory and field studies of major sampling interferences. *Atmospheric Environment* **13**, 543–552.
- Stelson A. W. and Seinfeld J. H. (1982a) Relative humidity and temperature dependence of the ammonium nitrate dissociation constant. *Atmospheric Environment* **16**, 983–992.
- Stelson A. W. and Seinfeld J. H. (1982b) Relative humidity and pH dependence of the vapor pressure of ammonium nitrate–nitric acid solutions at 25°C. *Atmospheric Environment* **16**, 993–1000.
- Strand S. R. (1983) Aerosol losses in diffusion denuders. Laboratory report, California Institute of Technology, Pasadena, CA.
- U.S. Environmental Protection Agency (1973) Directory of Air Quality Monitoring Sites—1972. Document EPA-450/2-73-006, U.S. Environmental Protection Agency, Research Triangle Park, NC.
- U.S. Environmental Protection Agency (1978) Directory of Air Quality Monitoring Sites Active in 1977. Document EPA-450/2-78-048, U.S. Environmental Protection Agency, Research Triangle Park, NC.
- Varian (1975) Instruction Manual for Model AA-6 Atomic Absorption Spectrophotometer. Varian Techtron, Melbourne, Australia.
- White W. H. and Roberts P. T. (1977) On the nature and origins of visibility reducing species in the Los Angeles Basin. *Atmospheric Environment* **11**, 803–812.
- Yoong M. (1981) Measurement of ambient ammonia concentrations in southern California. Rockwell International, Newbury Park, CA. Final Report to the California Air Resources Board under Contract No. A7-188-30. To be available from NTIS.

CHAPTER 5

AMMONIA AND NITRIC ACID CONCENTRATIONS IN

EQUILIBRIUM WITH ATMOSPHERIC AEROSOLS:

EXPERIMENT VS THEORY

(Reprinted from Atmospheric Environment, 18, 1737-1750)

AMMONIA AND NITRIC ACID CONCENTRATIONS IN EQUILIBRIUM WITH ATMOSPHERIC AEROSOLS: EXPERIMENT VS THEORY

LYNN M. HILDEMANN,* ARMISTEAD G. RUSSELL† and GLEN R. CASS*

*Environmental Engineering Science Department and Environmental Quality Laboratory and †Mechanical Engineering Department and Environmental Quality Laboratory, California Institute of Technology, Pasadena, CA 91125, U.S.A.

Abstract—The equilibrium between gaseous ammonia, nitric acid, and aerosol nitrate is discussed on the basis of a recent field experiment in southern California. Comparison is drawn between theoretical equilibrium calculations and simultaneous measurements of nitric acid, ammonia, ammonium ion, nitrate ion, sulfate ion, other ionic species, temperature and dewpoint. Particulate and gaseous pollutant concentrations at some inland sampling sites are readily explained if the aerosol is assumed to exist as an external mixture with all particulate nitrate and ammonium available to form pure NH_4NO_3 . At other monitoring sites, especially near the coast, aerosol nitrate is found in the presence of NH_3 and HNO_3 concentrations that thermodynamic calculations show are too low to produce pure NH_4NO_3 . This can be explained when the amount of aerosol nitrate that can be derived from reaction of nitric acid with sea salt and soil dust is taken into account. A calculation approach that accounts for the presence of mixed sulfate and nitrate salts improves the agreement between predicted and observed pollutant concentrations in the majority of cases studied. Uncertainties in these calculations arise from a number of sources including the thermodynamic quantities, and the effect of these uncertainties on the comparison between theory and experiment is discussed.

INTRODUCTION

Theoretical calculations for the formation of atmospheric aerosol nitrate based on thermodynamic equilibrium between ammonia, nitric acid and aerosol constituents have been presented recently by several research groups (Stelson *et al.*, 1979; Stelson and Seinfeld, 1982 a,b,c; Tang, 1976, 1980; Saxena and Peterson, 1981; Saxena *et al.*, 1983; Bassett and Seinfeld, 1983). These chemical equilibrium calculations when embedded within a photochemical airshed model show promise of being able to predict the aerosol nitrate concentrations that will result from regional emissions of sulfurous, nitrogenous and hydrocarbon (HC) gaseous precursors (Russell *et al.*, 1983).

Very few complete sets of atmospheric measurements exist, however, against which these chemical equilibrium calculations have been tested. Stelson *et al.* (1979) and Doyle *et al.* (1979) have shown that measurements of gaseous nitric acid and ammonia often are consistent with the upper limit on those concentrations predicted if the gases were in equilibrium with pure solid NH_4NO_3 . In those studies, the aerosol phase was not characterized completely, and little insight is gained into the cause of those cases where the atmospheric concentration products of NH_3 and HNO_3 fall below the equilibrium dissociation constant for pure NH_4NO_3 . The hypothesis that NH_3 , HNO_3 , and NH_4NO_3 are in equilibrium also has been pursued in cool humid atmospheres (Harrison and Pio, 1983) and at the low concentrations present in rural atmospheres (Cadle *et al.*, 1982). Very little work has been published to date that examines

the agreement between equilibrium-based calculation schemes and field observations in cases where the ionic components in the aerosol are treated as being more complex than pure NH_4NO_3 . A step in this direction is provided by Tanner (1982), who compared the thermodynamics of aqueous mixed sulfate-nitrate solutions and solid ammonium nitrate to field experiments under conditions present on Long Island, New York.

In the present paper, the role of atmospheric nitric acid and ammonia in the formation of nitrate-containing aerosols is discussed on the basis of field experiments conducted in southern California. Comparison is drawn between theoretical equilibrium calculations and an extensive collection of simultaneous observations on HNO_3 , NH_3 , NH_4^+ , NO_3^- , SO_4^{2-} , other ionic species, temperature and dewpoint. Calculations for the chemical equilibrium within multi-component aerosols are contrasted to the results obtained if a pure NH_3 , HNO_3 , NH_4NO_3 system had been present. The case where non-volatile nitrates are present due to reaction between nitric acid and either sea salt or soil dust is considered. The effect of uncertainties in the thermochemical data required for these equilibrium calculations is discussed, as well as the implications that these uncertainties hold for verification studies of regional airshed models for aerosol nitrate formation.

EXPERIMENTAL

The measurements used in this comparison were taken on 30-31 August 1982, as part of a project designed to acquire an air quality model validation data set for use in testing models for aerosol nitrate formation and transport. Gaseous nitric

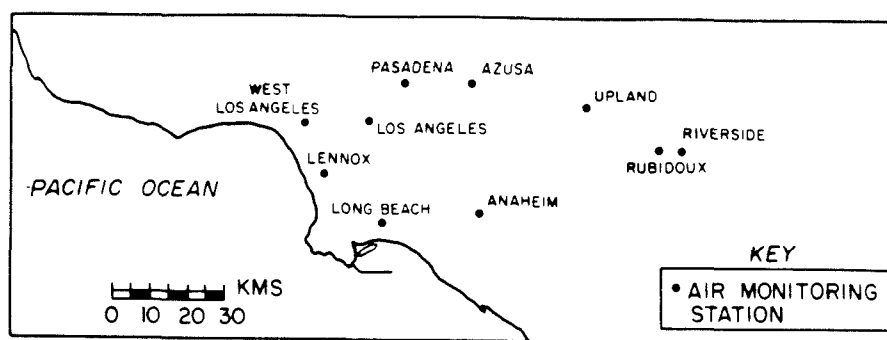


Fig. 1. Air monitoring sites in the South Coast Air Basin that surrounds Los Angeles.

acid and ammonia, and aerosol sulfate, nitrate, ammonium and other major ionic species were monitored at 10 locations in southern California (Fig. 1) over a 48-h period. The details of the experiment are described by Russell and Cass (1984), and only will be summarized here.

Gaseous nitric acid and ammonia and the major ionic aerosol species were measured over 2-h and 4-h intervals using filter-based techniques. Nitric acid measurements used in this study were obtained by the dual filter method, using a Teflon prefilter (Membrana Zefluor, 47 mm dia, 1 μ m pore size) for aerosol removal, followed by a nylon filter (Ghia Nylasorb, 47 mm dia, 1 μ m pore size) which quantitatively collects nitric acid as nitrate (Spicer and Schumacher, 1979; Appel *et al.*, 1980; Spicer *et al.*, 1982). Ammonia was collected as ammonium using an oxalic acid impregnated glass fiber filter (Gelman AE) preceded by a separate Teflon prefilter that removed aerosol NH_4^+ (Yoong, 1981; Appel *et al.*, 1980; Cadle *et al.*, 1982). Aerosol phase constituents were measured from material collected on the two Teflon prefilters. Ion chromatography was used to determine SO_4^{2-} , NO_3^- , Cl^- , Na^+ and K^+ concentrations. Divalent cations, Ca^{2+} and Mg^{2+} , were analyzed using atomic absorption spectroscopy (Varian Techtron Model AA6). Ammonium ion concentrations were measured by the phenol hypochlorite method (Salorzano, 1967; Harwood and Kuhn, 1970; Russell, 1983).

EQUILIBRIUM CALCULATIONS

Several alternative methods were used to calculate the partial pressures of ammonia and nitric acid vapor which in theory should be found in equilibrium with the aerosol phase. When the aerosol phase was assumed to consist of pure ammonium nitrate (s or aq) or an aqueous NH_4^+ , NO_3^- , SO_4^{2-} mixture, the calculations were based on the studies by Stelson and Seinfeld (1982a,c). Calculations involving dry, internally mixed NH_4^+ , NO_3^- , SO_4^{2-} aerosols can be viewed, from two perspectives. If the solid phase is assumed to exist as a solid solution, then calculations can be performed by the method of Saxena *et al.* (1983). If the solid phase exists as a heterogeneous mixture of various crystalline phases, then the vapor pressures could be as high as over solid NH_4NO_3 (Stelson and Seinfeld, 1982c). Each of these approaches is based on fundamental thermodynamic concepts, and provides a method for calculating the equilibrium partial pressure product of NH_3 and HNO_3 which should be found in the presence of a specified level of gaseous and aerosol constituents. The algorithm outlined by Russell *et al.*

(1983) was used to check the apportionment of measured total nitrate ($\text{HNO}_3(\text{g})$ plus NO_3^-) and total ammonia ($\text{NH}_3(\text{g})$ + NH_4^+) between the gaseous and aerosol phases.

Because it is important to an understanding of the data analysis which follows, the mechanics of the aerosol equilibrium model calculations will be described here in some detail, illustrated for the case of pure NH_4NO_3 formation. First, the equilibrium dissociation constant, K , for pure ammonium nitrate is calculated from the ambient temperature, (T), and relative humidity, (r.h.) (Stelson and Seinfeld, 1982a). Then the total nitrate, $[\text{TN}]$, and total ammonia, $[\text{TA}]$, available to form ammonium nitrate is calculated as

$$[\text{TN}] = [\text{HNO}_3(\text{g})]_m + [\text{NO}_3^-]_m \quad (1)$$

$$[\text{TA}] = [\text{NH}_3(\text{g})]_m + [\text{NH}_4^+]_m \quad (2)$$

where $[\text{HNO}_3(\text{g})]_m$ is the measured gaseous nitric acid concentration, $[\text{NH}_3(\text{g})]_m$ is the measured gaseous ammonia concentration, and $[\text{NO}_3^-]_m$ and $[\text{NH}_4^+]_m$ are the measured aerosol nitrate and ammonium concentrations, respectively, available or free to form NH_4NO_3 . Then the equilibrium constraint

$$[\text{NH}_3(\text{g})][\text{HNO}_3(\text{g})] \leq K$$

is imposed. If $[\text{TN}][\text{TA}] \leq K$, no ammonium nitrate is predicted to be present because there is not enough total nitrate and total ammonia to support aerosol NH_4NO_3 formation. If $[\text{TN}][\text{TA}] > K$ then aerosol ammonium nitrate is predicted to form from the gas phase precursors such that the product $[\text{NH}_3(\text{g})]_c [\text{HNO}_3(\text{g})]_c = K$. The subscript c indicates a theoretically computed pollutant concentration that may differ from measured values. Conservation of TA and TN gives the final expression for the ammonium nitrate formed as

$$[\text{NH}_4\text{NO}_3]_c = \frac{1}{2} \{ [\text{TA}] + [\text{TN}] - \{ ([\text{TA}] + [\text{TN}]^2 - 4([\text{TA}][\text{TN}] - K))^{1/2} \} \} \quad (3)$$

and the gas phase concentrations

$$[\text{NH}_3(\text{g})]_c = [\text{TA}] - [\text{NH}_4\text{NO}_3]_c \quad (4)$$

and

$$[\text{HNO}_3(\text{g})]_c = [\text{TN}] - [\text{NH}_4\text{NO}_3]_c \quad (5)$$

Thus the inputs to the model calculation are TA, TN, T

and r.h., and the outputs are the calculated aerosol and gas phase concentrations, and the dissociation constant, K . K and the calculated concentrations are very sensitive to T , and also to r.h. if the r.h. is high (Fig. 2).

Addition of ammonium sulfate to solutions containing aqueous ammonium nitrate would lower the vapor pressure product $[\text{NH}_3][\text{HNO}_3]$ in equilibrium with the aerosol phase (Fig. 2). In Fig. 2, Y is the ionic strength fraction of ammonium nitrate and is calculated as

$$Y = \frac{[\text{NH}_4\text{NO}_3]}{[\text{NH}_4\text{NO}_3] + 3[(\text{NH}_4)_2\text{SO}_4]} \quad (6)$$

Note that the concentration product of nitric acid times ammonia in equilibrium with a mixed sulfate/nitrate solution having a value of $Y = 0.5$ is about half as high as that in equilibrium with a pure ammonium nitrate solution. The temperature dependence of the partial pressure product for the aqueous mixed salt case should be similar to that of the pure salt. In the case of a dry internally mixed ammonium nitrate and sulfate solid solution, the vapor pressure product is given as

$$[\text{NH}_3][\text{HNO}_3] = zK, \quad (7)$$

where z is the mole fraction NH_4NO_3 in the aerosol phase and K is the dissociation constant for ammonium nitrate (Saxena *et al.*, 1983). If the dry mixed salt is viewed as a combination of the stable NH_4^+ , NO_3^- , SO_4^{2-} salts, such as NH_4NO_3 and $3(\text{NH}_4\text{NO}_3) \cdot (\text{NH}_4)_2\text{SO}_4$, then the concentration

product $[\text{NH}_3][\text{HNO}_3]$ at equilibrium with the solid phase could be as high as K calculated for pure NH_4NO_3 (Stelson and Seinfeld, 1982c).

UNCERTAINTY ANALYSIS

Uncertainties arise in this analysis from a number of sources and are important when comparing the theoretically computed pollutant concentrations to the field experimental results. For those cases where the gas phase is assumed to be in equilibrium with pure ammonium nitrate, a formal error analysis was conducted.

An estimate was provided for the standard error of each of the measured parameters required in the calculation: NH_3 , NH_4^+ , HNO_3 , NO_3^- , T and r.h. Uncertainties associated with the Gibbs free energies involved in calculations by the method of Stelson and Seinfeld (1982a) were taken from Parker *et al.* (1976).

The global sensitivity of the calculation scheme to uncertainties in the input variables is very non-linear, and analytical methods for calculating the standard error associated with the model outputs are difficult to execute. Instead, a stochastic simulation approach was used to propagate the error estimates for the measured quantities and Gibbs free energies through the equilibrium calculations. For each time interval at all air sampling sites, the modified Box-Mueller method (Jansson, 1966) was used to generate 200 random, normally distributed, perturbed values for the model input parameters, each set having a mean equal to the nominally measured parameter value and a standard deviation associated with the uncertainty in that value. Then 200 alternative values for K were calculated and 200 estimates of the partition of TN and TA between the gaseous and aerosol phase were generated using the perturbed data sets. In the figures that follow, error bounds shown represent one standard error about the nominally measured or computed value based on the error propagation study just described. In most cases, uncertainty in the ambient temperatures is the principal contributor to uncertainty in the computed value of the equilibrium dissociation constant, K .

Additional potential contributors to uncertainty in this analysis can be noted, but were not quantified. No attempt was made to include the contribution from uncertainties in thermodynamic properties other than the Gibbs free energies. The additional uncertainty due to the other thermodynamic properties involved in the calculations, such as the molal heat content, osmotic coefficient, ionic activity and specific heats, should be small. The equilibrium between nitric acid, ammonia, water vapor and the aerosol is assumed to prevail at a single instant in time, but calculations were actually based on concentrations and temperatures averaged over 2-h and 4-h intervals. It can be shown that if the ambient nitric acid and ammonia concentrations are positively correlated, then the product of the averaged concentrations is less than the averaged concentration

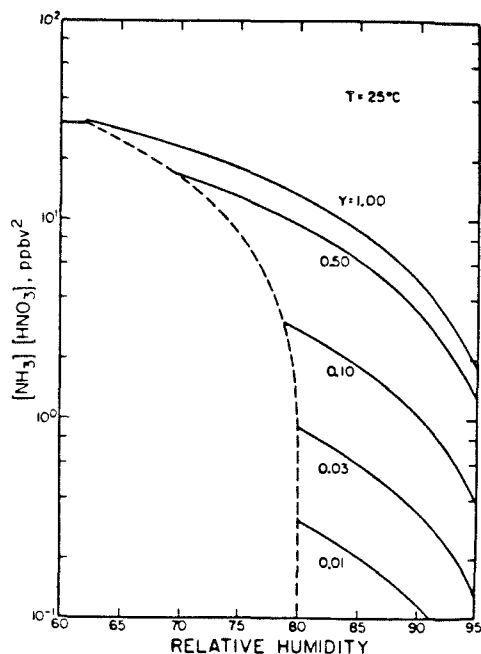


Fig. 2. Partial pressure product of ammonia and nitric acid in equilibrium with a sulfate, nitrate and ammonium containing aerosol as a function of relative humidity and ammonium nitrate ionic strength fraction at 25°C (from Stelson and Seinfeld, 1982c).

product,

$$\overline{P_{\text{HNO}_3}} \overline{P_{\text{NH}_3}} < \overline{P_{\text{HNO}_3 P_{\text{NH}_3}}} \quad (8)$$

for any finite time period. Since the extent of this bias is unknown, it was not included in the error analysis. The duration of the sampling interval may also affect the extent of artifact nitrate formation (Appel *et al.*, 1980; Spicer and Schumacher, 1979). It will be seen in the figures that follow that generally better agreement is obtained between theory and experiment when the shorter-term (2-h) samples are used rather than the longer-term (4-h) samples.

CASES EXAMINED

Models for ionic aerosol formation in equilibrium with gas phase precursors have been developed only for a limited range of aerosol chemical compositions. The most advanced treatments at present are for concentrated mixed salt solutions containing different combinations of nitrate, sulfate, ammonium, hydrogen and magnesium ions (Saxena *et al.*, 1983; Tang, 1980; Bassett and Seinfeld, 1983). The actual aerosol is much more complex than is assumed by current theoretical models. Results from the present experiment show that the ionic portion of the bulk aerosol contains all of the above, plus sodium, potassium, calcium and chloride ions (see Figs 4 and 5 of Russell and Cass, 1984). From the experimental data, it is impossible to tell how the individual aerosol particles are speciated. In other words, it is not known what fraction of the nitrate or ammonium, if any, is present as ammonium nitrate, and whether the ammonium nitrate is associated with ammonium sulfate (for example) within individual aerosol particles. As a result, three hypothetical distributions of aerosol constituents between particles will be discussed which span the likely range of aerosol composition: a purely external mixture, a purely internal mixture, and a size-segregated internal mixture.

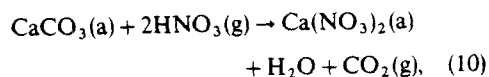
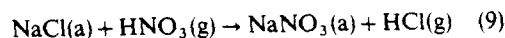
In an external mixture, each particle is composed of a single salt (possibly aqueous) such as pure NH_4NO_3 , $(\text{NH}_4)_2\text{SO}_4$ or NaCl , and the bulk aerosol composition (as seen in Figs 4 and 5 of Russell and Cass, 1984) is achieved by dispersing a variety of particles with different chemical compositions in the same air mass. At the other extreme, an internal mixture is achieved if each particle has the same chemical composition as the bulk aerosol, and hence consists of a complex mixture of many different anions and cations.

An interesting and intermediate case is that of a size-segregated internal mixture. In this case, the aerosol will be assumed to exist in two size classes, coarse (particle diameter, d_p , $> 2.5 \mu\text{m}$) and fine ($d_p \leq 2.5 \mu\text{m}$). Coarse aerosols usually are generated mechanically. Sea spray and soil dust aerosols would be prime examples. Gas-particle reactions may take place on the surface of coarse particles, altering the original composition of the aerosol, but the particle

size would not decrease significantly. Ionic species concentrated in the large particle fraction would include chiefly, Ca^{2+} , Mg^{2+} , K^+ , Na^+ and Cl^- , plus enough large particle NO_3^- to achieve a charge balance (obtained by reaction of nitric acid with sea salt or soil dust). The fine particle fraction will be assumed to have been formed by gas to particle conversion processes, and would contain all of the ammonium, all of the sulfate and that portion of the nitrate not attributed to the coarse particle mode. This framework for the size-segregated internal mixture hypothesis is consistent with observations that sulfate and ammonium are found chiefly in the small particle size ranges; Na^+ , Ca^{2+} and Cl^- are found in large particles, while NO_3^- is found in significant amounts in both the coarse and fine fractions (Appel *et al.*, 1978; Kadowaki, 1977).

EXTERNAL MIXTURE

In the case of an external mixture, pure salt particles, such as NH_4NO_3 , NaCl , or $(\text{NH}_4)_2\text{SO}_4$, are assumed to be present, and the gas phase concentrations of NH_3 and HNO_3 are governed by equilibrium with NH_4NO_3 . The key remaining question centers on the possibility that other nitrate containing aerosol species less volatile than NH_4NO_3 are present in separate particles (e.g. NaNO_3), and hence some of the aerosol nitrate is not available to interact with the precursor gases. Field experimental measurements do not give an absolute answer to this question, but two extreme possible cases can be studied. In the first case, all of the ammonia, nitric acid, and aerosol ammonium and nitrate are assumed to be available to form NH_4NO_3 . This provides an upper limit on the amount of pure NH_4NO_3 that can be formed. A second case provides the lower limit on the predicted pure ammonium nitrate concentration by assuming that the NO_3^- ion is bound preferentially as a relatively non-volatile salt of Ca^{2+} , Mg^{2+} , K^+ or Na^+ . A number of displacement reactions would bind nitrate in this manner, such as



where (a) indicates the aerosol phase. NaNO_3 has been identified in field measurements in the Los Angeles area (Mamane and Poeschel, 1980). In this study the term FREE NITRATE will be used to identify the fraction of the aerosol nitrate in excess of that which could be bound with the alkali metals or alkaline earths, given mathematically for this experiment as

$$[\text{FREE NITRATE}] = [\text{NO}_3^-] - \{2[\text{Ca}^{2+}] + 2[\text{Mg}^{2+}] + [\text{K}^+] + [\text{Na}^+] - [\text{Cl}^-]\} \quad (11)$$

where the brackets [] indicate the measured ionic aerosol concentration in $\mu\text{moles m}^{-3}$. The FREE NITRATE concentration was constrained to be

greater than or equal to zero. In constructing (11) it was assumed that the chloride ion present is found as sodium chloride. The HCl produced by reaction (9) might, in some cases, react with NH_3 to form NH_4Cl , and thus alternative forms of (11) could be hypothesized.

The choice between the two types of external mixtures just described has no effect on the calculated equilibrium dissociation constant of ammonium nitrate, as K is solely a function of T and r.h., but it does affect the calculated gas and aerosol phase pollutant concentrations. If pure ammonium nitrate is present and is at equilibrium with the gas phase, then the equilibrium dissociation constant should be equal to the observed partial pressure product of NH_3 times HNO_3 to within experimental and calculation uncertainties. If the FREE NITRATE concentration is zero, then ammonium nitrate may not be present, and the calculated dissociation constant has no bearing on the partial pressure of ammonia and nitric acid gas, except that it should act as an upper bound on the measured concentration product, CP .

Given the external mixture hypotheses, the theoretically predicted partition of measured total nitrate and total ammonia between the aerosol and gas phases was computed at each monitoring site shown in Fig. 1 over each sampling interval during the period 30–31 August 1982. Results at three locations in the basin will be discussed in detail: a near coastal site, Long Beach, a mid-basin site, Anaheim, and a far inland site, Rubidoux. Data on aerosol speciation at these sites are

presented elsewhere (Russell and Cass, 1984). The Long Beach sampling station, which is located about 6 km from the Pacific Ocean, experienced lower temperatures (down to 18°C) and higher relative humidities (1-h average above 90%) than the inland sites. This led to a minimum 2-h average calculated NH_4NO_3 dissociation constant of less than $0.75 (\text{ppbv})^2$. Rubidoux, located about 60 km inland, was typically hotter and dryer, with peak temperatures above 38°C , and a correspondingly high calculated dissociation constant that exceeded $650 (\text{ppbv})^2$ over one 2-h sampling interval. Comparison between theory and experiment thus will be discussed for dissociation constants varying over about three orders of magnitude.

The calculated NH_4NO_3 dissociation constant, K , and the product of the measured $\text{HNO}_3(\text{g})$ and $\text{NH}_3(\text{g})$ concentrations at Anaheim are shown in Fig. 3. One standard error about each calculated value of K is given by the vertical bars, while the standard error of the measured concentration product is indicated by the dashed horizontal lines. Agreement between the theoretical calculations and measurements generally is good, especially for the second day when shorter sampling intervals were used. Recall that the calculated dissociation constant should serve as an upper bound on the concentration product, CP .

In the first of the two external mixture cases considered, all of the aerosol nitrate is assumed to be present as ammonium nitrate. Given the time history of the computed dissociation constant, the measured

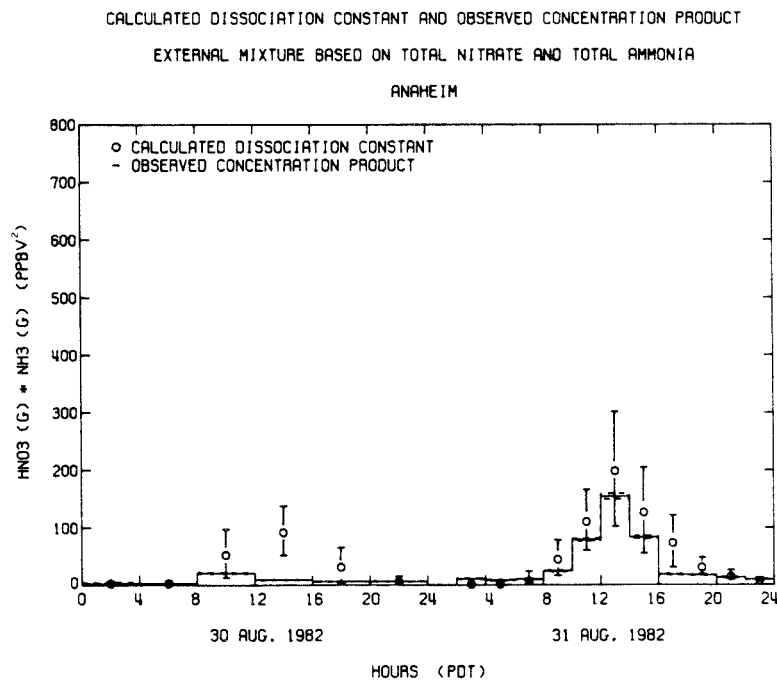


Fig. 3. Observed $[\text{HNO}_3][\text{NH}_3]$ concentration product and calculated dissociation constant of pure NH_4NO_3 at Anaheim, CA. No data between 0000 and 0200 on 31 August.

total inorganic nitrate and total ammonia concentrations at Anaheim were apportioned between the gaseous and the aerosol phase in accordance with the equilibrium calculations. As seen in Figs 4(a) and (b), the measured gas phase concentrations are somewhat below those predicted, but still are in good agreement given the results of the uncertainty analysis. The calculated and measured aerosol concentrations likewise are in good agreement at Anaheim [Figs 4(c) and (d)]. Note that at a number of times (e.g. between 0800 and 1200 hours on 30 August) no ammonium nitrate was predicted to be present. In this case there was not enough total ammonia and total nitrate to support the formation of pure ammonium nitrate at the prevailing ambient conditions.

Moving further inland to Rubidoux, the agreement between the calculated K and measured CP still is good, with the measured CP , again, usually at or below the theoretical value for K during the midday (Fig. 5). At night the measured concentration product often lies slightly above K , but there is very little nitric acid vapor present and thus the nitric acid measurement is prone

to larger than usual relative error. Rubidoux is downwind of a large collection of dairy farms, and experiences very high ammonia and ammonium ion concentrations [as seen in Figs 6(b) and (d)]. Agreement between measured and predicted NH_3 concentrations is quite good at all times. The remaining predicted pollutant concentrations match observations at most times, with the largest exceptions occurring between 1000 and 1200 hours and between 1400 and 1600 hours on 31 August (see Fig. 6).

At the near-coastal sites, like Long Beach and Lennox, the agreement between calculated dissociation constants and measured concentration products is very poor during the daytime (Fig. 7). The measured product of the concentrations of nitric acid vapor and ammonia falls significantly below that expected if the gas phase material were in equilibrium with pure NH_4NO_3 . In Fig. 8, it can be seen that the lower than expected concentration product measured in the atmosphere is due mainly to lower nitric acid concentrations than would be expected if aerosol ammonium and nitrate ion concentrations were governed solely by the

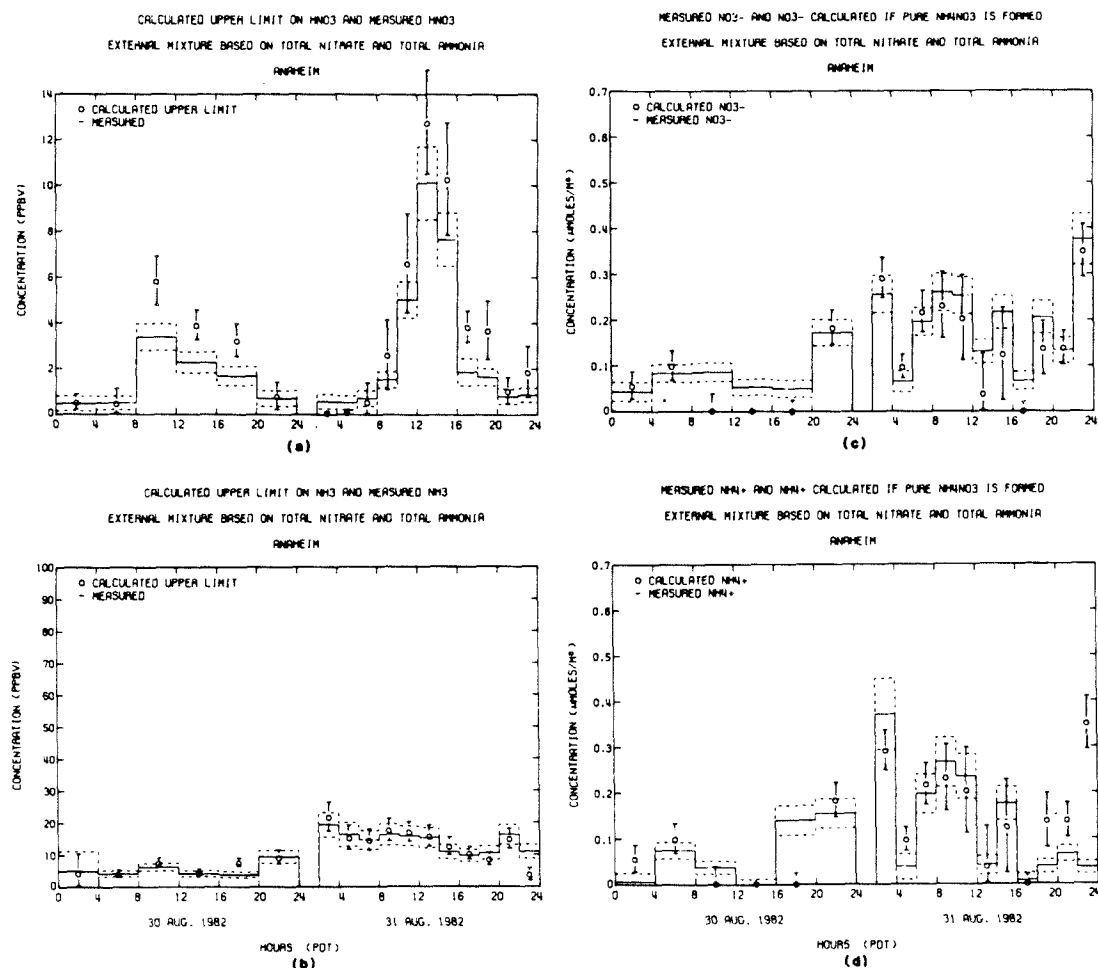


Fig. 4. Observed and calculated pollutant concentrations at Anaheim—external mixture with all aerosol nitrate available to form NH_4NO_3 . No data between 0000 and 0200 on 31 August. (a) HNO_3 , (b) NH_3 , (c) NO_3^- , (d) NH_4^+ .

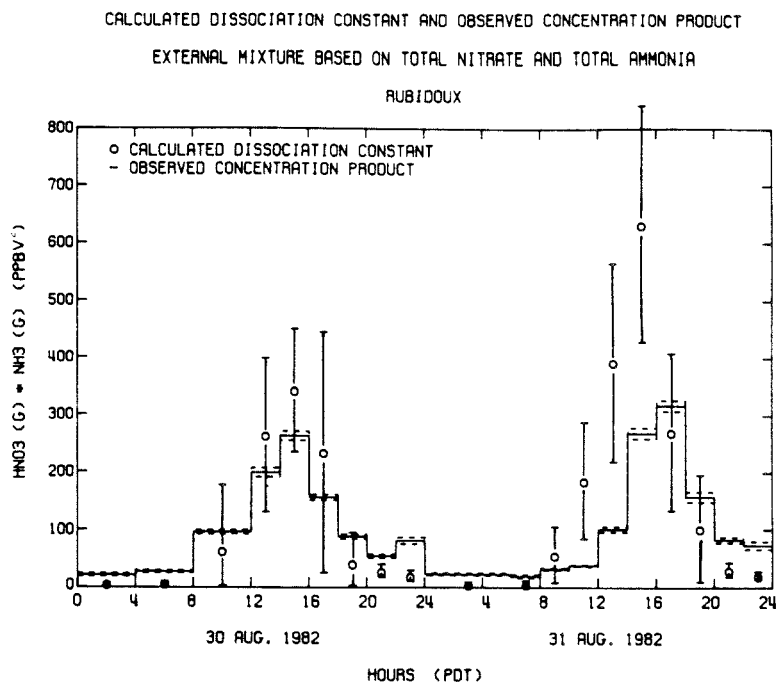


Fig. 5. Observed $[\text{HNO}_3][\text{NH}_3]$ concentration product and calculated dissociation constant of pure NH_4NO_3 at Rubidoux, CA.

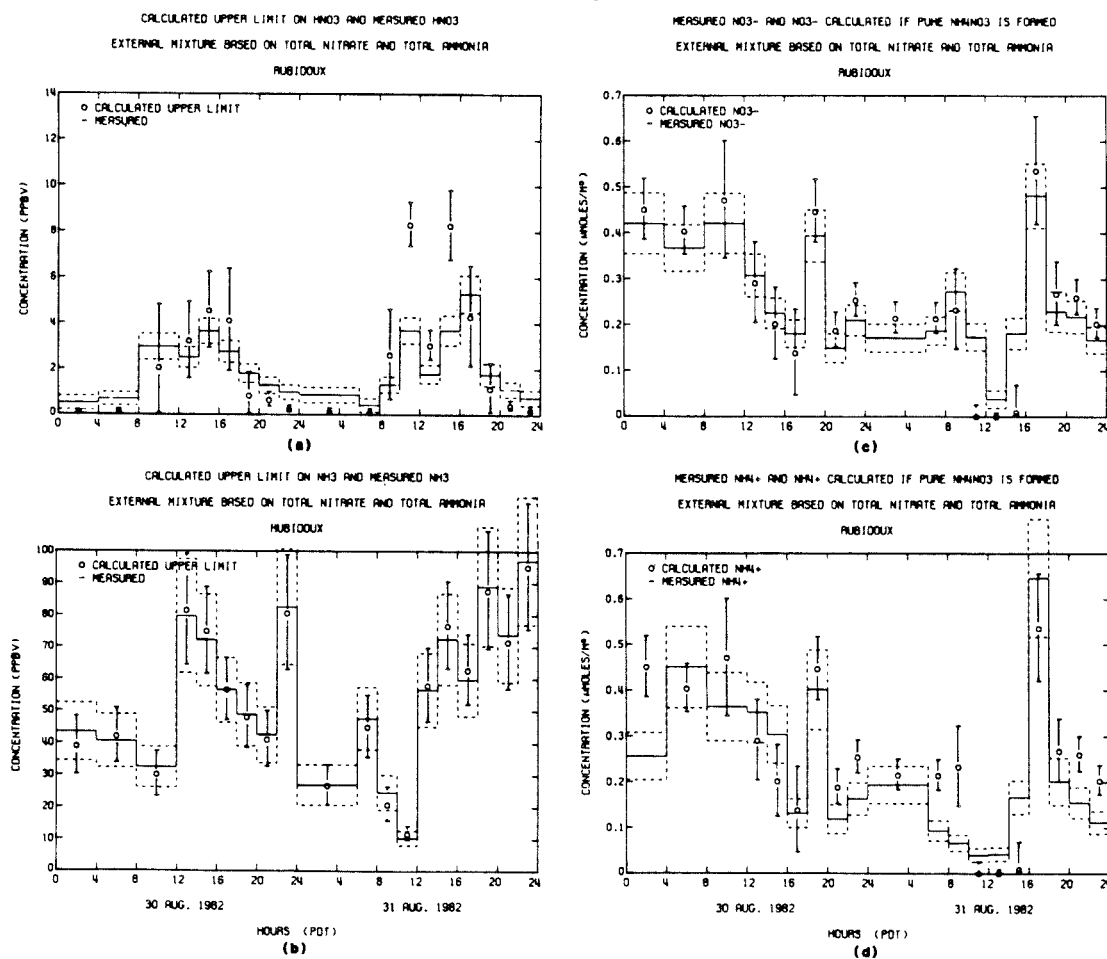


Fig. 6. Observed and calculated pollutant concentrations at Rubidoux—external mixture with all aerosol nitrate available to form NH_4NO_3 . (a) HNO_3 , (b) NH_3 , (c) NO_3^- , (d) NH_4^+ .

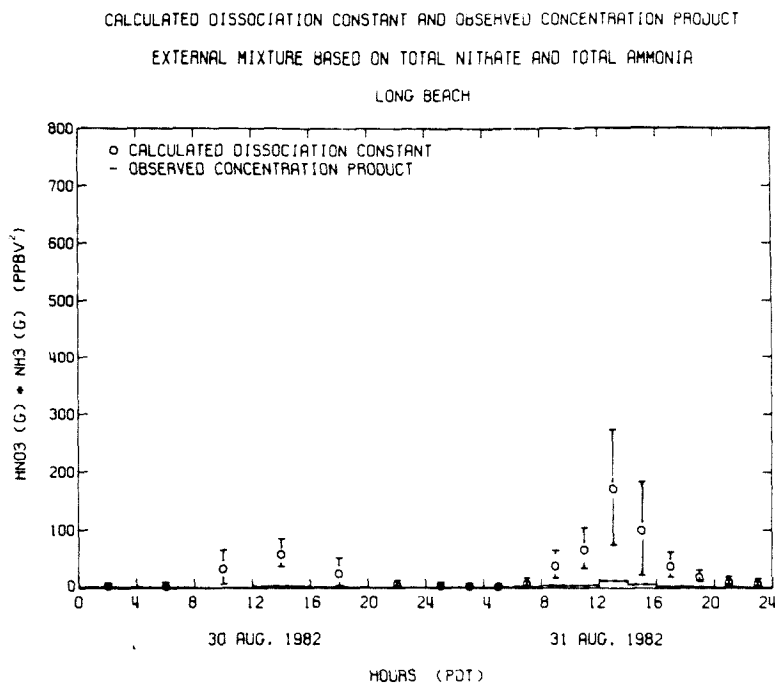


Fig. 7. Observed $[\text{HNO}_3][\text{NH}_3]$ concentration product and calculated dissociation constant of pure NH_4NO_3 at Long Beach, CA.

equilibrium between HNO_3 , NH_3 and NH_4NO_3 . At a number of times in the afternoon of both days sampled, the total nitrate and total ammonia concentrations fall below the level needed to form any ammonium nitrate aerosol, as seen in Figs 8(c) and (d). Nevertheless, measurable nitrate and ammonium ion concentrations were observed in the aerosol phase during both afternoons (Fig. 8). The likely explanation is that pure ammonium nitrate is not present, but that other nitrate and ammonium containing species are formed. In this case, the second external mixture hypothesis will be examined to determine whether part (if not all) of the nitrate could be bound as a relatively non-volatile salt.

The amount of nitrate ion present at each monitoring site in excess of that that could be bound with Na^+ , Ca^{2+} , Mg^{2+} and K^+ was determined. This excess NO_3^- ion, called FREE NITRATE, is defined in (11). The HNO_3 , NH_3 , NH_4NO_3 equilibrium calculations then were repeated assuming that only the FREE NITRATE plus an equal amount of ammonium ion was available to equilibrate with the gas phase. Results obtained under this hypothesis at Long Beach are shown in Fig. 9. In 15 of the 18 sampling periods, no NH_4NO_3 formation would be predicted and indeed no FREE NITRATE was present. At a sixteenth sampling interval NH_4NO_3 is predicted to be present, and the predicted NO_3^- level matches the observed FREE NITRATE almost exactly. Two of the 18 observations still show that FREE NITRATE was present at times when the $[\text{NH}_3][\text{HNO}_3]$ concentration product was too low to form pure NH_4NO_3 .

Results at the remaining monitoring sites are similar to those at Long Beach. The great majority of the occasions where nitrate aerosol is observed at NH_3 and HNO_3 concentrations too low to form pure NH_4NO_3 occur when the aerosol composition is consistent with the presence of nitrate species other than ammonium nitrate. This is illustrated in Fig. 10. Figures 10(a) and (b) show the NH_3 and HNO_3 concentrations predicted at all stations under the first external mixture hypothesis (that all aerosol nitrate is speciated as NH_4NO_3). A large number of the theoretically calculated HNO_3 concentrations exceed the field observations in that case, indicating that more inorganic nitrate should have been found in the gas phase. When the second external mixture hypothesis is imposed (e.g. some nitrate speciated as NaNO_3 , $\text{Ca}(\text{NO}_3)_2$ and other non-volatile salts) then the number of outlying data points is reduced to about 10% of the 180 total observations, as shown in Fig. 10(d). Agreement between observed and predicted NH_3 gaseous concentrations is fairly good at all times under both external mixture hypotheses, as seen in Figs 10(a) and (c). This is because gaseous NH_3 is present in such excess that transfer of NH_4^+ ion from the aerosol into the gas phase will not change gaseous NH_3 levels greatly.

INTERNAL MIXTURE

The aerosol observed at each sampling site could be idealized as a pure internal mixture. In this case each aerosol particle would contain a variety of anions and

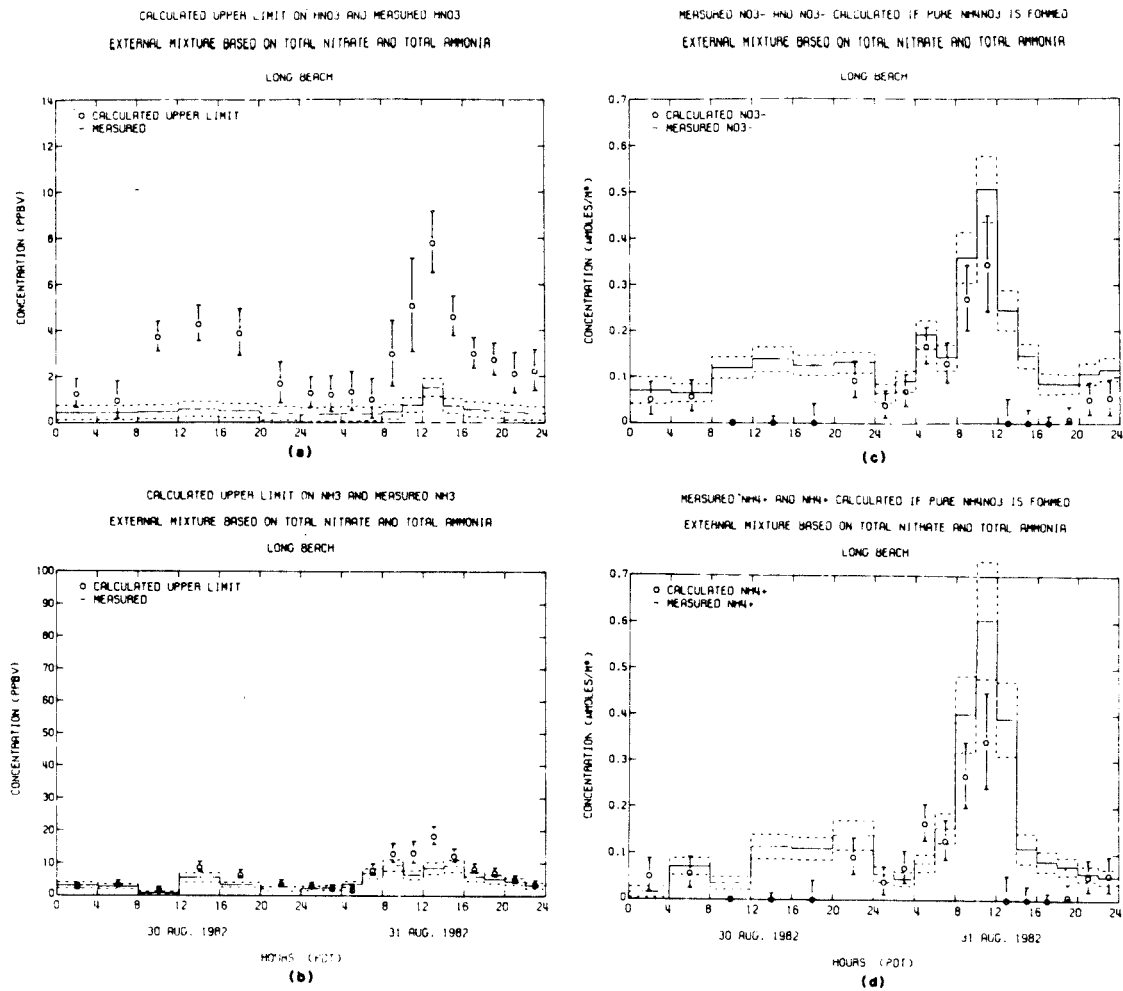


Fig. 8. Observed and calculated pollutant concentrations at Long Beach—external mixture with all aerosol nitrate available to form NH_4NO_3 . (a) HNO_3 , (b) NH_3 , (c) NO_3^- , (d) NH_4^+ .

cations in direct proportion to their ionic abundance in the bulk filter sample. For the conditions observed during this experiment, such an internally mixed aerosol would be much more complex than the mixed sulfate, nitrate and ammonium containing aerosols that can be handled by present theoretical models that describe the equilibrium between aerosol and gas phase constituents. If a complete set of thermodynamic data for the species possible in a highly concentrated mixed NH_4^+ , Na^+ , Ca^{2+} , Mg^{2+} , K^+ , NO_3^- , SO_4^{2-} , Cl^- system existed, which it does not, then a general purpose Gibbs free energy minimization technique could provide predictions. Such a technique has been used successfully for the sulfate/nitrate/ammonium system (Bassett and Seinfeld, 1983). Data from the present study can be used to test the predictions of such a complete model once the thermodynamic data for the full system become available. Lacking the thermodynamic data at present, no attempt will be made to model a purely internal mixture at this time.

SIZE-SEGREGATED INTERNAL MIXTURE

Chemically resolved size distribution measurements show that most of the atmospheric aerosol sulfate and ammonium, and much of the nitrate, is found in a fine particle accumulation mode ($d_p \leq 2.5 \mu\text{m}$), reflecting that they are formed by a gas to particle conversion process. Sea salt, soil dust and other mechanically generated aerosols typically are found in a coarse particle mode ($d_p > 2.5 \mu\text{m}$). Any nitrate aerosol formed by reaction of nitric acid with sea salt or soil dust likewise would be concentrated in the coarse particle mode. To capture these characteristics of the atmospheric aerosol, a size-segregated internal mixture hypothesis was tested. The aerosol was assumed to exist in two size fractions for computational purposes. The large particle fraction was taken to be composed of the sea salt and soil dust derived material (all Na^+ , Ca^{2+} , Mg^{2+} , K^+ , Cl^- and enough NO_3^- to achieve a charge balance) and the fine particle fraction was

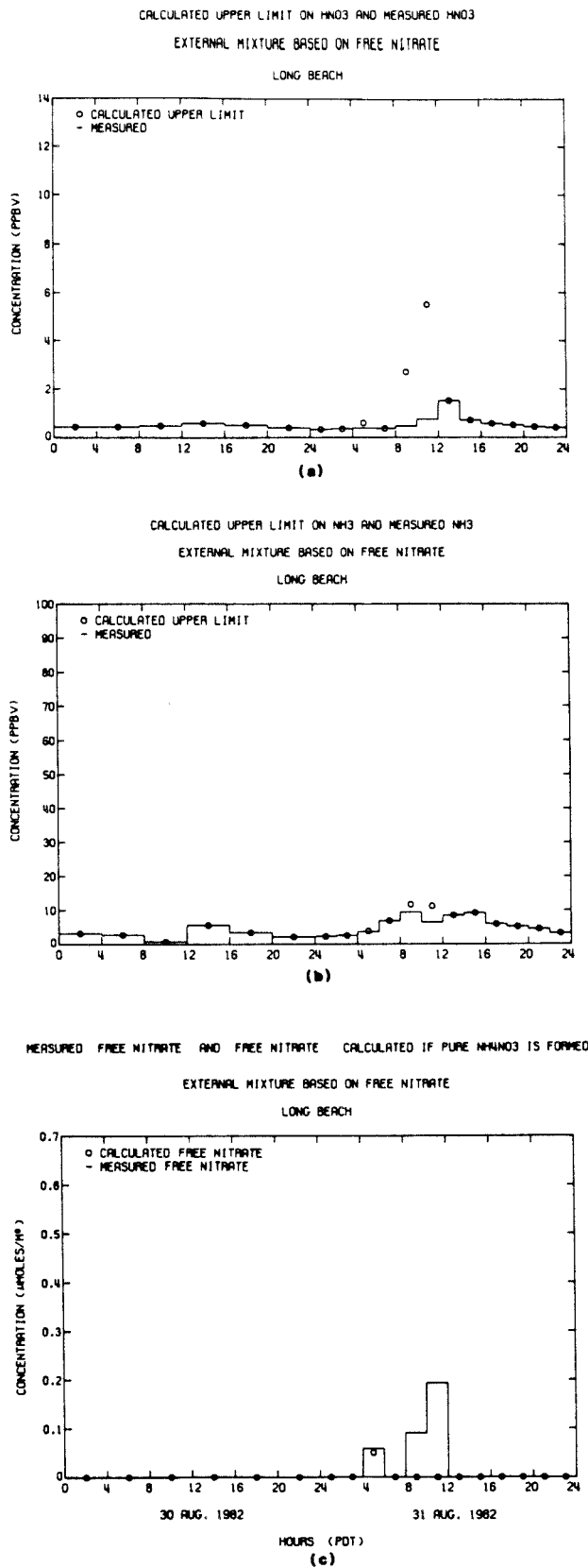


Fig. 9. Observed and calculated pollutant concentrations at Long Beach—external mixture with only the FREE NITRATE available to form NH₄NO₃. (a) HNO₃, (b) NH₃, (c) FREE NITRATE.

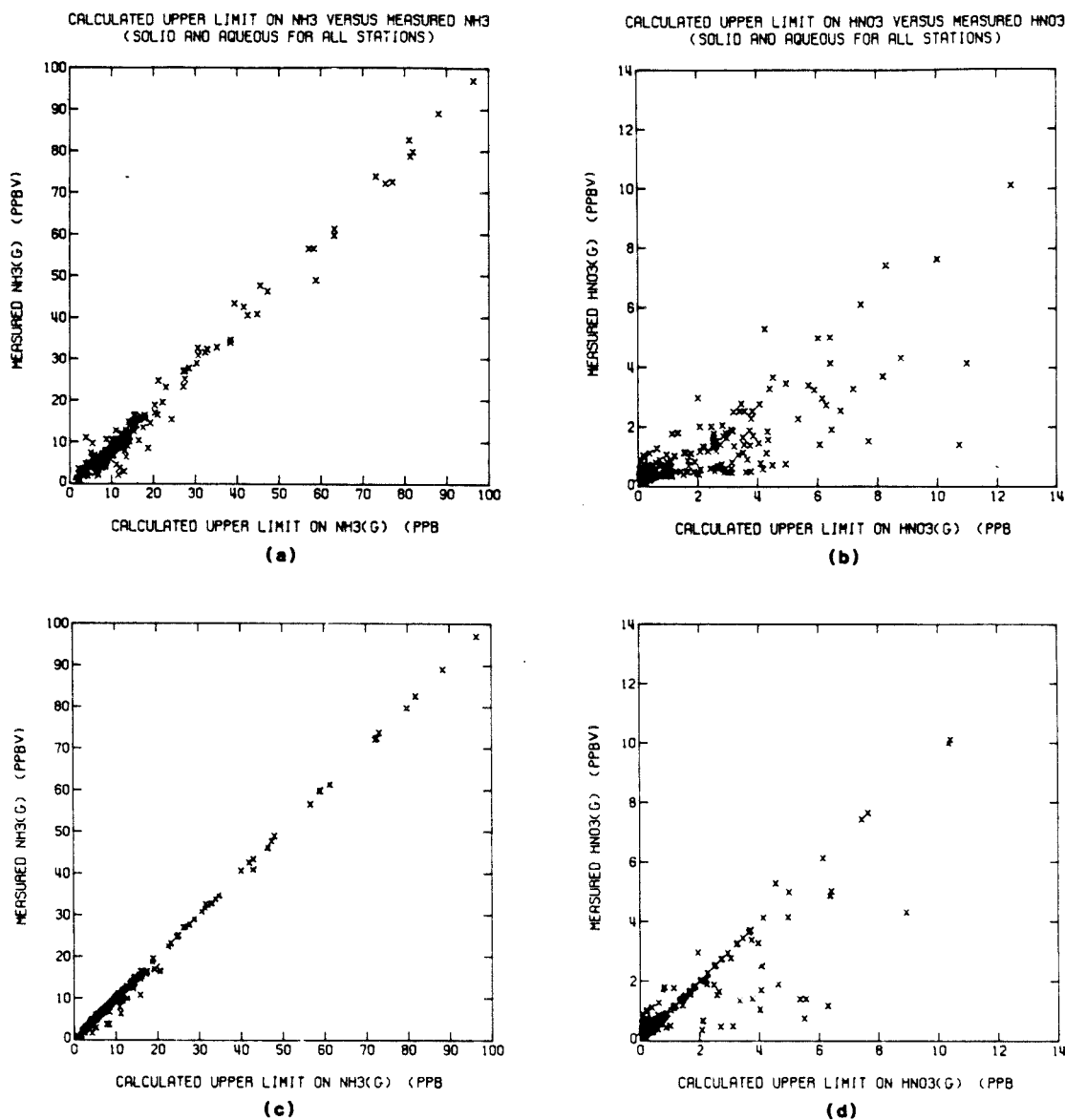


Fig. 10. Comparison of observed and calculated gas phase concentrations at all monitoring stations under two alternative external mixture hypotheses (180 observations). Case (1), all aerosol nitrate available to form NH_4NO_3 . Case (2), only the FREE NITRATE available to form NH_4NO_3 . (a) Ammonia (Case 1), (b) Nitric Acid (Case 1), (c) Ammonia (Case 2), (d) Nitric Acid (Case 2).

assumed to contain the sulfate, ammonium and FREE NITRATE in the form of an internally mixed aerosol. Again, the resulting aerosol may be aqueous or solid, for which the calculation methods of Stelson and Seinfeld (1982a, c) and Saxena *et al.* (1983) will be used, as described previously. Both Fig. 2 and Equation (7) indicate that addition of ammonium sulfate to the internal mixture lowers the resulting vapor pressures in equilibrium with the aerosol phase below the levels observed when pure NH_4NO_3 is present. Thus the size segregated internal mixture hypothesis acts in the direction needed to account for the few cases in Fig. 10(d) where HNO_3 concentrations are found to be

lower than would be expected in equilibrium with NH_4NO_3 alone.

A difficulty arises when considering the size-segregated internal mixture case if no FREE NITRATE is present. If no ammonium nitrate is mixed with the sulfate, the predicted CP goes to zero. At any time when this occurs in the presence of a significant concentration product of ammonia and nitric acid, it will be assumed that the size-segregated internal mixture idealization for the distribution of nitrates between fine and coarse particles is inappropriate. There must have been some nitrate aerosol not bound in a non-volatile form even though ion balance considerations

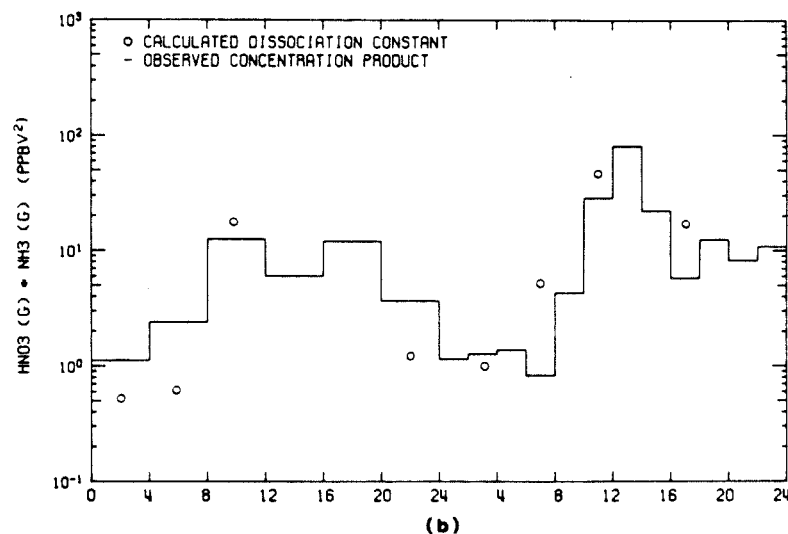
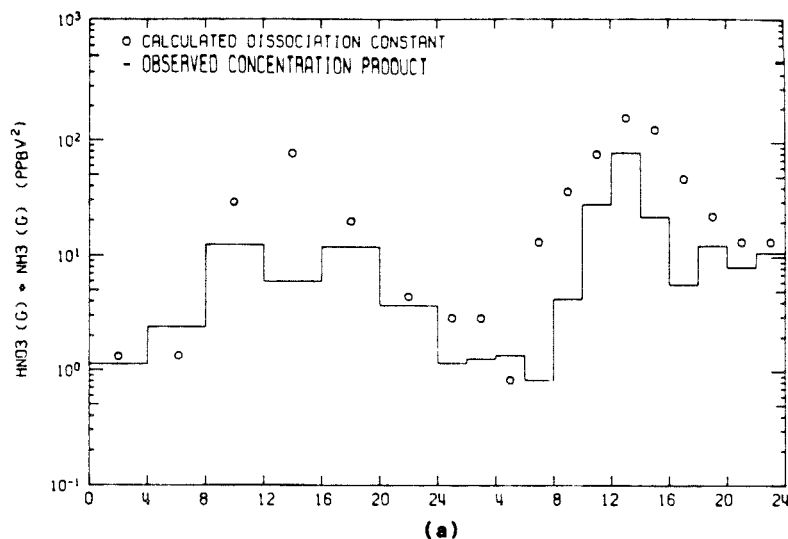


Fig. 11. Observed and calculated $[\text{HNO}_3][\text{NH}_3]$ concentration product at Upland—comparison of external mixture and size-segregated internal mixture hypotheses. (a) External mixture, (b) Size-segregated internal mixture.

show that all nitrates might have been speciated as non-volatile coarse particle material. No theoretical calculations will be attempted in those cases where the underlying assumption about particle composition is untenable.

The concentration product of HNO_3 and NH_3 calculated for the size-segregated internal mixture case is compared to ambient measurements at Upland in Fig. 11 and Long Beach in Table 1. Concentration products that would be predicted for the case of equilibrium with pure NH_4NO_3 also are shown. At Upland, the aerosol is predicted to be aqueous from 0000 to 0800 and from 2000 to 2400 on 30 August and

between 0000 and 0800 on 31 August. The remainder of the time, the aerosol was predicted to be in the solid phase. Results shown in Fig. 11(b), when the aerosol is solid, are those obtained by the method of Saxena *et al.* (1983). Alternatively, if the solid mixed salt consists of a heterogeneous mix of solid phases, such as NH_4NO_3 and $3\text{NH}_4\text{NO}_3 \cdot (\text{NH}_4)_2\text{SO}_4$, then the CP could be as high as for NH_4NO_3 shown in Fig. 11(a). At Upland the observed and computed concentration products shown in Fig. 11(b) are in better agreement with the size segregated internal mixture case than with the pure external mixture hypothesis in five of the cases, particularly those cases with the higher concentration products.

Table 1. Comparison of measurements at Long Beach to predictions given by the pure external mixture hypothesis based on FREE NITRATE (Case 1) and by the size-segregated internal mixture hypothesis (Case 2)

Time*	Phase [†]	CP (ppbv ²)			HNO ₃ (ppbv)			NH ₃ (ppbv)			FREE NITRATE (μg m ⁻³)		
		Case 1†	Case 2	Meas.	Case 1	Case 2	Meas.	Case 1	Case 2	Meas.	Case 1	Case 2	Meas.
4-6	aqueous(aq)	2.6	1.4	1.2	0.6	0.3	0.3	4.3	4.1	4.0	2.6	3.4	3.5
8-10	solid(s)	39.0	9.6	4.5	2.7	1.0	0.5	11.7	9.9	9.5	0.0	4.4	5.9
10-12	solid(s)	69.0	16.0	4.9	5.4	2.1	0.8	11.1	7.7	6.4	0.0	8.4	12.0

* At all other times Case 1, Case 2 and measurements match exactly because no FREE NITRATE is present. All times shown are on 31 August 1983.

[†] When solid, Case 2 is computed by the method of Saxena *et al.* (1983). For solid particles containing a mixture of solid phases, such as NH₄NO₃ and 3NH₄NO₃·(NH₄)₂SO₄, CP could be as high as for pure NH₄NO₃ in the Case 1 column.

† Values shown are for equilibrium dissociation constant, *K*, for NH₄NO₃. This can exceed concentration product of [NH₃][HNO₃] if no FREE NITRATE is predicted to be present.

In the three cases where improvement is not noted, the absolute value of the discrepancy is only 1 or 2 (ppbv)². At Long Beach, the size-segregated internal mixture hypothesis brings the aqueous phase observation into almost complete agreement between computed and observed concentration products.

CONCLUSIONS

In theory, the equilibrium dissociation constant for NH₄NO₃ should place an upper limit on the product of the NH₃ and HNO₃ concentrations in the atmosphere. In most cases the [NH₃][HNO₃] concentration product measured during this experiment indeed is found to be less than or equal to the calculated dissociation constant of pure NH₄NO₃ at the prevailing conditions. At inland sites like Anaheim and Rubidoux, the assumption that NH₃ and HNO₃ are in equilibrium with pure NH₄NO₃ yields agreement between predicted and measured gas and aerosol phase pollutant concentrations that is qualitatively and, in most cases, quantitatively quite good. At other sites, particularly near the coast, the measured CP and HNO₃ concentrations fall well below those predicted if pure ammonium nitrate is present. A majority of those measurements can be explained by the hypothesis that some nitrate is bound in large particles by the reaction of nitric acid with sea salt or soil dust. If the aerosol is assumed to exist as a size-segregated internal mixture with nitrates distributed on the basis of ion balance considerations between non-volatile coarse particle material and fine particles containing NH₄⁺, SO₄²⁻ and NO₃⁻, then further improvement is obtained between observed and predicted [NH₃][HNO₃] concentration products.

The results of this study hold important implications for the construction and use of mathematical models for the formation and transport of nitrate-containing aerosols. First, in the vast majority of cases, measured pollutant concentrations are consistent with computations based on equilibrium between the gas phase and aerosol phase species, to within our present ability to supply the necessary data for the calculations. Given a model like that of Russell *et al.* (1983) which can compute HNO₃ and NH₃ concentrations from emissions plus gas phase kinetics, in principle it is possible to predict the amount of aerosol nitrate formed. The simplest treatment, that of pure NH₄NO₃ formation, will work well at some monitoring sites, but it is not universally applicable. A knowledge of the speciation of the co-existing non-nitrate ionic material in the aerosol phase is needed if accurate aerosol nitrate concentration predictions are to be made. A formidable problem is faced if that co-existing aerosol concentration and composition also must be computed from emissions data.

Acknowledgements—This work was supported by the California Air Resources Board under Agreement No. A2-

150-32, and by gifts to the Environmental Quality Laboratory.

REFERENCES

- Appel B. R., Kothny E. L., Hoffer E. M., Hidy G. M. and Wesolowski J. J. (1978) Sulfate and nitrate data from the California Aerosol Characterization Experiment (ACHEX). *Envir. Sci. Technol.* **12**, 418-425.
- Appel B. R., Wall S. M., Tokiwa Y. and Haik M. (1980). Simultaneous nitric acid, particulate nitrate and acidity measurements in ambient air. *Atmospheric Environment* **14**, 549-554.
- Bassett M. and Seinfeld J. H. (1983) Atmospheric equilibrium model of sulfate and nitrate aerosols. *Atmospheric Environment* **17**, 2237-2252.
- Cadle S. H., Countess R. J. and Kelly N. A. (1982) Nitric acid and ammonia concentrations in urban and rural locations. *Atmospheric Environment* **16**, 2501-2506.
- Doyle G. J., Tuazon E. C., Graham R. A., Mischke T. M., Winer A. M. and Pitts J. N., Jr. (1979) Simultaneous concentrations of ammonia and nitric acid in a polluted atmosphere and their equilibrium relationship to particulate ammonium nitrate. *Envir. Sci. Technol.* **13**, 1416-1419.
- Harrison R. M. and Pio C. A. (1983) An investigation of the atmospheric HNO_3 - NH_3 - NH_4NO_3 equilibrium relationship in a cool, humid climate. *Tellus* **35B**, 155-159.
- Harwood J. E. and Kuhn A. L. (1970) A colorimetric method for ammonia in natural waters. *Water Res.* **4**, 805-811.
- Jansson B. (1966) *Random Number Generator*, p. 177. Almqvist and Wiksell, Stockholm.
- Kadowaki S. (1977) Size distribution and chemical composition of atmospheric particulate in the Nagoya area. *Atmospheric Environment* **11**, 671-675.
- Mamane Y. and Pueschel R. F. (1980) A method for the detection of individual nitrate particles. *Atmospheric Environment* **14**, 629-639.
- Parker V. B., Wagman D. D. and Garvin D. (1976) Selected thermochemical data compatible with the CODATA recommendations. NBSIR 75-968.
- Russell A. G. and Cass G. R. (1984) Acquisition of regional air quality model validation data for nitrate, sulfate, ammonium ion and their precursors. *Atmospheric Environment* **18**, 1815-1827.
- Russell A. G. (1983) Analysis of oxalic acid impregnated filters for ammonia determination. Open File Report 83-1; Environmental Quality Laboratory, California Institute of Technology, Pasadena, CA.
- Russell A. G., McRae G. J. and Cass G. R. (1983) Mathematical modeling of the formation and transport of ammonium nitrate aerosol. *Atmospheric Environment* **17**, 949-964.
- Salorzano L. (1967) Determination of ammonia in natural waters by the phenol hypochlorite method. *Limnol. Oceanogr.* **14**, 799-801.
- Saxena P. and Peterson T. W. (1981) Thermodynamics of multicomponent electrolytic aerosols. *J. Colloid. Interface Sci.* **79**, 496-510.
- Saxena P., Seigneur S. and Peterson T. W. (1983) Modeling of multiphase atmospheric aerosols. *Atmospheric Environment* **17**, 1315-1329.
- Spicer C. W., Howes J. E., Bishop T. A., Arnold L. H. and Stevens R. K. (1982) Nitric acid measurement methods: an intercomparison. *Atmospheric Environment* **16**, 1407-1500.
- Spicer C. W. and Schumacher P. M. (1979) Particulate nitrate: laboratory and field studies of major sampling interferences. *Atmospheric Environment* **13**, 543-552.
- Stelson A. W. and Seinfeld J. H. (1982a) Relative humidity and temperature dependence of the ammonium nitrate dissociation constant. *Atmospheric Environment* **16**, 983-992.
- Stelson A. W. and Seinfeld J. H. (1982b) Relative humidity and pH dependence of the vapor pressure of ammonium nitrate-nitric acid solutions at 25°C. *Atmospheric Environment* **16**, 993-1000.
- Stelson A. W. and Seinfeld J. H. (1982c) Thermodynamic prediction of the water activity, NH_4NO_3 dissociation constant, density and refractive index for the NH_4NO_3 - $(\text{NH}_4)_2\text{SO}_4$ - H_2O system at 25°C. *Atmospheric Environment* **16**, 2507-2514.
- Stelson A. W., Friedlander S. K. and Seinfeld J. H. (1979) A note on the equilibrium relationship between ammonia and nitric acid and particulate ammonium nitrate. *Atmospheric Environment* **13**, 369-371.
- Tang I. N. (1976) Phase transformation and growth of mixed salts. *J. Aerosol Sci.* **7**, 361-371.
- Tang I. N. (1980) On the equilibrium partial pressures of nitric acid and ammonia in the atmosphere. *Atmospheric Environment* **14**, 819-828.
- Tanner R. L. (1982) An ambient experimental study of phase equilibrium in the atmospheric system: aerosol H^+ , NH_4^+ , SO_4^{2-} , NO_3^- , $\text{NH}_3(\text{g})$, $\text{HNO}_3(\text{g})$. *Atmospheric Environment* **16**, 2935-2942.
- Yoong M. (1981) Measurement of ambient ammonia concentrations in southern California. Rockwell International, Newbury Park, California, Final Report to the California Air Resources Board under Contract No. A7-188-30. Available from NTIS.

CHAPTER 6

VERIFICATION OF A PHOTOCHEMICAL MODEL TO PREDICT AEROSOL
NITRATE AND NITRIC ACID CONCENTRATIONS, AND ITS USE FOR
CONTROL MEASURE EVALUATION6.1 Introduction

Anthropogenic emissions of NO_x and reactive organic gases (ROG) are the recognized precursors for a number of pollutants found in the atmosphere including ozone (O_3), nitrogen dioxide (NO_2), nitric acid (HNO_3), and aerosol nitrate (AN). Emission control measures are being taken to reduce the formation of O_3 and NO_2 in geographic areas burdened by excessive concentrations. These control programs are quite expensive, and an extended debate still surrounds the question of determining the most effective strategies to reduce O_3 and NO_2 concentrations (Pitts et al. 1983; Chock et al. 1981, 1983; Glasson 1981, 1983). A key problem faced when selecting between alternative control programs is that the decisions made will also affect the concentrations of a number of currently unregulated but potentially damaging co-pollutants, in particular HNO_3 and aerosol nitrate.

Nitric acid results in deposition of strong acids at the earth's surface by both dry and wet processes, including the acidification of fog, rain, and snow (Galloway and Likens, 1981; Liljestr and and Morgan, 1978; Russell et al. 1985; Waldman et al. 1982). Nitric acid also can be a factor in the formation of mutagens and suspected carcinogens in the atmosphere (Grosjean et al. 1983).

HNO_3 can react with ammonia (NH_3) and pre-existing particulate matter in the atmosphere to produce fine, nitrate-containing, particles. These fine aerosol nitrates are very effective at scattering visible solar radiation and thus contribute to visibility reduction. Studies conducted in Denver, for example, found that 12% of the fine particle mass was present as nitrate, accounting for about 17% of the light extinction (Groblicki et al., 1981). At Rubidoux, downwind of Los Angeles, California, nitrate comprises about 21% of the total particulate mass, responsible for 40% of the decreased visibility (White and Roberts, 1977). Thus an understanding of how to control HNO_3 and aerosol nitrate concentrations is an important feature of any air pollution abatement plan directed at the control of acid deposition, fine particulate matter reduction, or visibility improvement.

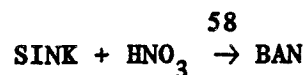
The purpose of the present study is to develop and test engineering methods for predicting the effect of ROG, NO_x , and NH_3 control programs on atmospheric HNO_3 , O_3 and aerosol nitrate concentrations. A photochemical trajectory model that predicts O_3 , NO_2 , total inorganic nitrate (TN), aerosol nitrate (AN), HNO_3 , NH_3 , and PAN concentrations from emissions data will be tested for its ability to reproduce field experimental data. Following this evaluation, the air quality model will be used to determine what effect reducing the emissions of ROG, NO_x , and NH_3 has on O_3 , PAN, HNO_3 , NH_3 and AN concentrations. Example calculations will be presented for Rubidoux, near Riverside, CA, which experiences some of

the most serious nitrate-induced fine particulate loading and visibility problems in the United States.

6.2 Model Description

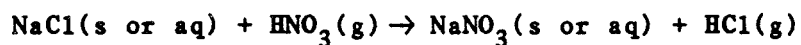
Results presented in this paper were obtained using a Lagrangian trajectory formulation of the atmospheric diffusion equation that describes atmospheric chemical reactions, turbulent vertical diffusion, horizontal advective transport, and ground-level pollutant deposition. Within the chemical mechanism the concentration of ammonium nitrate aerosol is computed to be at thermodynamic equilibrium with ammonia and nitric acid vapor, and where noted, the heterogeneous formation of nitrate aerosol from the reaction of nitric acid with preexisting aerosol is treated. Except for the following specific details, a complete description of the gas phase model appears elsewhere (Russell et al., 1983, 1985), and it will not be described further here.

Reaction 58, describing the interaction between preexisting aerosol and nitric acid, has been added to the previously described version of this model in order to simulate the stripping of atmospheric nitric acid by certain aerosols, such as sea salt,



where SINK is that portion of the aerosol material available to react with nitric acid and BAN is irreversibly Bound Aerosol Nitrate. This

is a generalized reaction that includes a variety of specific chemical reactions, such as the displacement reaction



which is thermodynamically favorable, and is suggested by the excess of Na^+ ions in comparison to the chloride ions in many atmospheric aerosol samples (Russell and Cass, 1984; Duce, 1969; Martens et al., 1973). Unlike the reaction forming ammonium nitrate, this reaction, as modeled, is irreversible. The aerosol available to strip nitric acid, thus, is depleted as the reaction proceeds, just as the NaCl would be depleted. The rate constant for this reaction is derived from kinetic theory for the bombardment of the aerosol surface by nitric acid vapor. Aerosol surface area per unit mass is computed from the size distribution of Larson et al. (1984), which was obtained on a moderately smoggy August day in California's South Coast Air Basin (SoCAB). Collision efficiencies for the reactions between gases and atmospheric aerosol surfaces vary with aerosol surface characteristics and composition, and are not known for all the relevant combinations of reactive gases and aerosols. Baldwin and Golden (1979) measured a value of 2.4×10^{-4} as the lower bound on the collision efficiency of HNO_3 with a sulfuric acid surface. With this in mind, a collision efficiency of 0.001 was assumed for the reaction of nitric acid vapor with the SINK aerosol surface.

In this study, the height of the air column modeled is 1000 m, divided into ten cells with vertical dimensions of 30, 50, 70, five

100, 150 and 200 m. The emissions inventory, meteorological fields and terrain characteristics are developed on a grid system containing 5 km by 5 km cells, so the horizontal dimensions of the air parcels studied are set to the same size as a single grid cell.

A number of assumptions are involved in the derivation of a trajectory model of this type, notably that the effects of horizontal diffusion, vertical wind shear and vertical advection are small. Implications of these assumptions are discussed by Liu and Seinfeld (1975). In addition to the effects of these physical processes, which are excluded from all trajectory models, deviation of predictions from observations can occur due to uncertainties in the input data. Uncertainties in the emissions arise from possible errors in the emission inventory and small uncertainties in the actual path followed by the air parcel. Emissions, winds, temperatures, surface roughness and humidity are not homogeneous within each of the 5 km by 5 km grid cells for which those fields are developed, though this sub-grid scale inhomogeneity should affect the results little. Concentration measurements are made at only a limited number of locations and upper level concentrations are not measured routinely. Uncertainty can arise from extrapolating ground level measurements in order to set initial conditions aloft. In the present study, the effect of the uncertainty arising from initial conditions has been minimized by using long trajectories that start in relatively clean air over the ocean upwind of the Los Angeles urban area.

6.3 Model Evaluation Data Base

6.3.1 Pollutant Concentrations

Model evaluation tests will be conducted using a number of air parcel trajectories that cross the SoCAB (Fig 6.1) on 30-31 August, 1982. During this two-day period an experiment was conducted to acquire a set of data for use in verifying this type of photochemical air quality model (Russell and Cass, 1984). That set of experimental data includes aerosol nitrate, sulfate, ammonium and other ionic species, as well as gas-phase ammonia, nitric acid and PAN concentrations. Data at sites shown in Figure 6.1 will be used in this analysis. Gas-phase concentrations of total hydrocarbons, CO, NO, NO_x, and O₃ for this time period were obtained from South Coast Air Quality Management District (SCAQMD) and California Air Resources Board (CARB) monitoring stations. PAN concentrations were measured at the University of California, Riverside (UCR) and at Caltech in Pasadena, CA. O₃, NO_x and NO concentrations reported by the SCAQMD and the CARB are averaged over one hour periods, and are reported to the nearest 10 ppb.

6.3.2 Hourly Meteorological Data

Wind fields for the two-day period of interest were obtained using measured wind velocities at 39 sites in the SoCAB. These wind data were interpolated over the 80 by 30 grid of 25 km² cells superimposed over the air basin using the method detailed in Goodin et al. (1979). Hourly averaged temperature and relative humidity fields

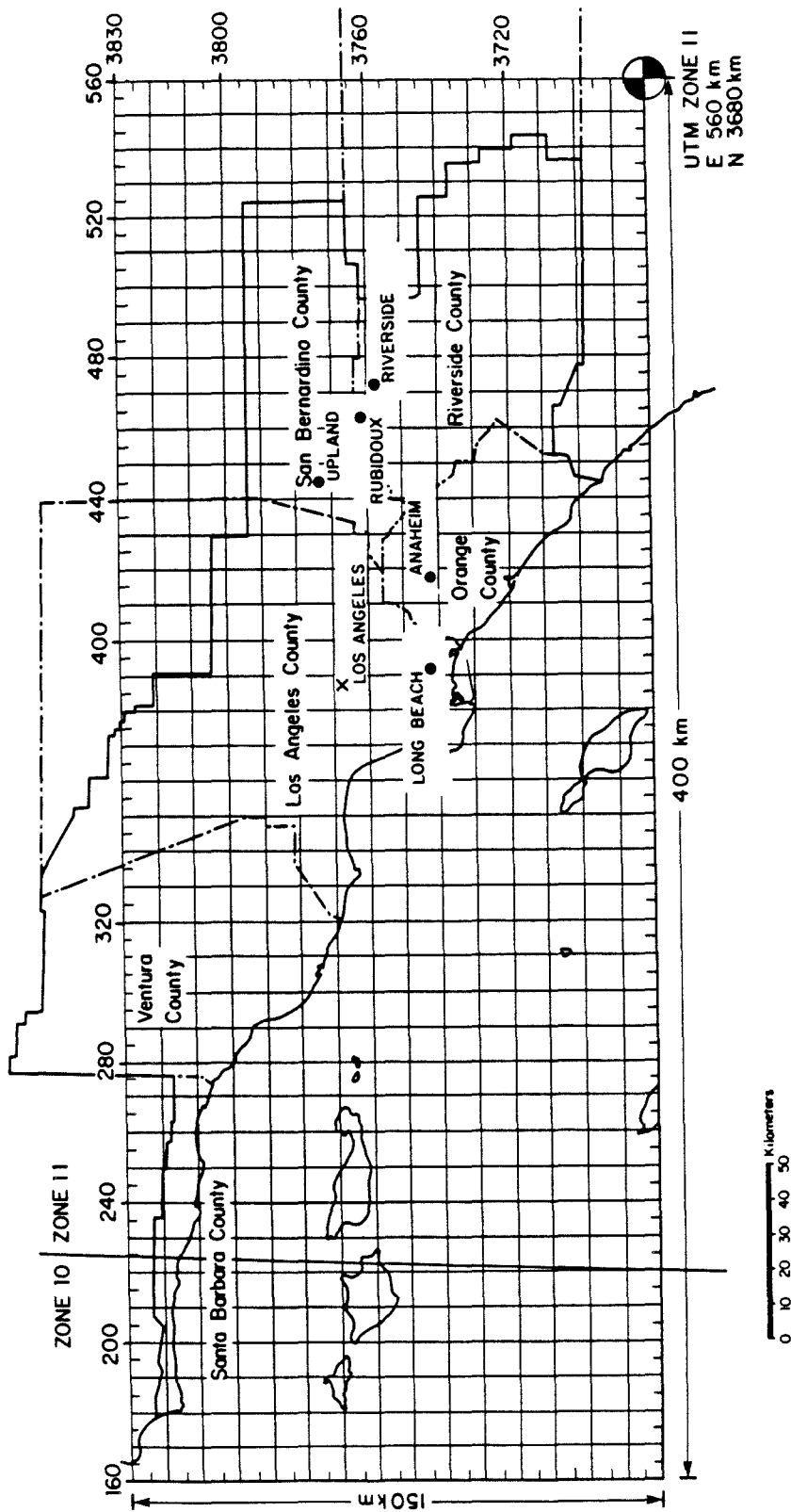


FIGURE 6.1

Gridded map of California's South Coast Air Basin (SoCAB) used for constructing concentration fields, meteorological fields, and emissions inventories. Symbols (·) indicate the locations of aerosol measurement stations used in this work. The solid line marks the boundary of the SoCAB.

were obtained by interpolation between the 29 and 18 measurement locations, respectively. Hourly averaged mixing depth fields were obtained from the measured vertical atmospheric temperature profiles available at 8 locations. Solar radiation levels measured at downtown Los Angeles, Pasadena and Upland were used to set the photolysis rate constants within the chemical mechanism.

6.3.3 Emissions

NO_x , total hydrocarbon (THC) and CO emissions into the air parcels modeled are calculated from a 1982 forecast emission inventory for the SoCAB provided by the CARB (Ranzierrri, 1983, 1984). The inventory details the emissions, by species, from over 2600 source categories distributed spatially and temporally over the basin. Hourly emission rates are given for over 200 organic species, NO, NO_2 , and CO for each of the 5 km X 5 km grid cells throughout the SoCAB. A summary of the daily totals of the emissions from mobile and stationary sources is given in Table 6.1. The spatial distributions of the THC, NO_x and CO emissions are shown in Figure 6.2. Emission rates given for the individual organic gas species are lumped into the six organic classes compatible with the model used in this study.

The ammonia emissions inventory for 1982 used in this study was developed by updating the 1974 emissions inventory previously described by Cass et al. (1982). Total ammonia emissions, by source category, are shown in Table 6.2, and spatially in Figure 6.2. Variables that affect ammonia emissions from animal waste decomposition have been investigated by Muck and Steenhuis (1982) and

TABLE 6.1

1982 Estimated Emissions
in the South Coast Air Basin

<u>Source Type</u>	THC kg/day	NO _x kg/day	CO kg/day
Stationary Sources			
Fuel Combustion			
External Combustion Boilers			
Utilities	6678.0	97716.6	8184.0
Industrial	2994.6	41017.0	7119.9
Commercial and Institutional	116.8	3577.6	26.4
Internal Combustion Engines			
Utilities	4467.7	8387.1	2999.3
Industrial	25127.7	58149.8	19212.0
Petroleum Refining and Production	2839.1	35291.8	1105.0
Other Manufacturing	3075.0	39488.5	181310.9
Residential, Agricultural, and Other	16929.0	53296.7	127061.4
Subtotal Fuel Combustion	62227.9	336925.1	347018.9
Waste Burning and Incineration	85.8	378.6	314.4
Landfill	777887.8	0.0	0.0
Solvent Use			
Surface Coating	195379.2	1938.4	362.5
Other	161841.0	152.2	26.4
Petroleum Processes, Storage, and Transfer	99857.9	11310.5	13600.0
Industrial Processes	26140.9	2640.9	18074.3
Miscellaneous	440015.1	3799.3	118576.4
Subtotal Stationary Sources	1763435.6	357145.0	497972.9
Motor Vehicle Emissions			
On-Road Vehicles	581375.2	662526.1	5001918.5
Off-Road Vehicles	26769.0	67112.8	172631.4
Railroads	3844.8	15343.0	5798.4
Ships	22155.2	15972.6	88599.6
Aircraft	18154.0	16243.2	84513.6
Subtotal Motor Vehicle Emissions	652298.2	777197.7	5353461.5
TOTAL	2415733.8	1134342.7	5851434.4

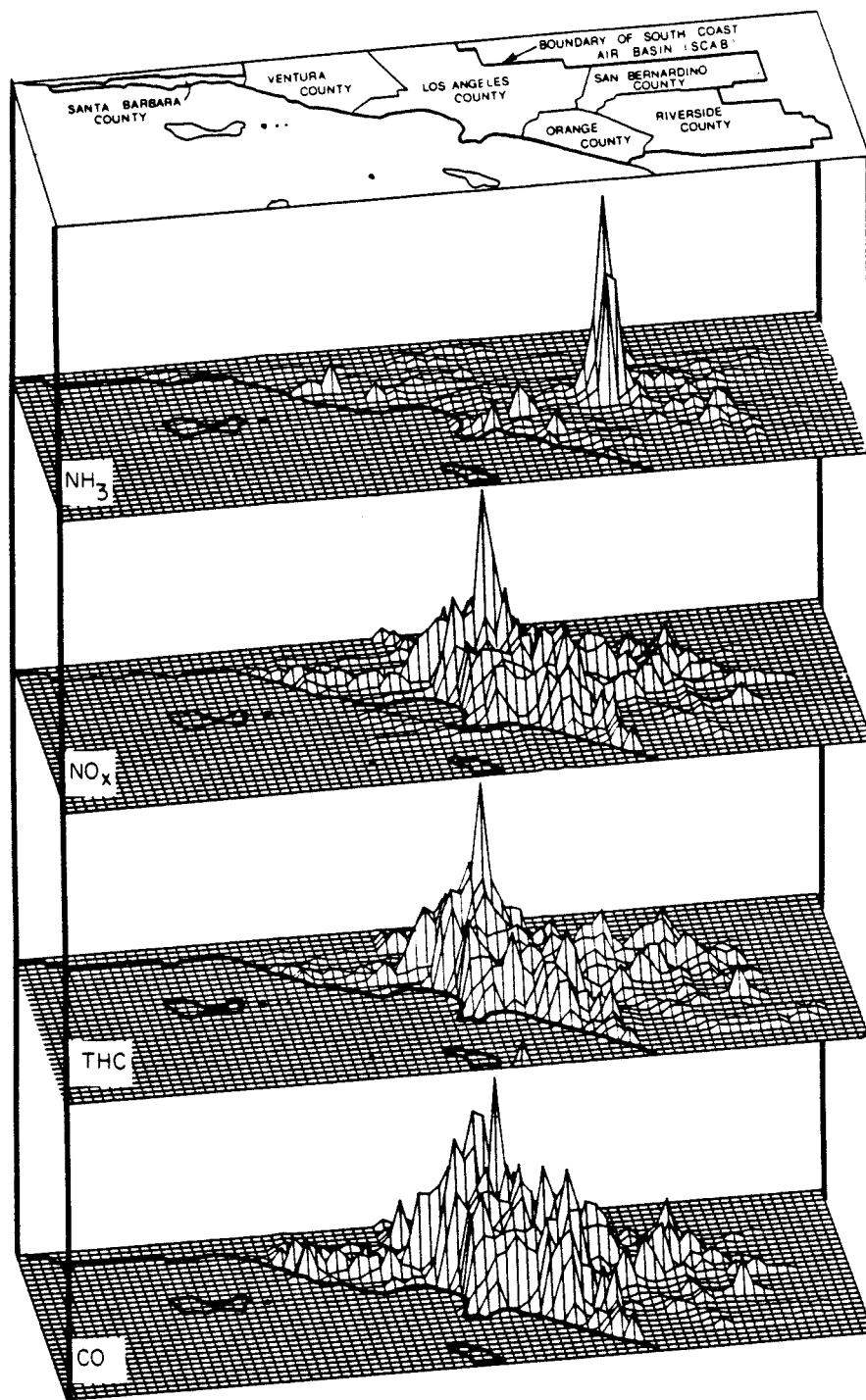


FIGURE 6.2

Spatial distribution of the 1982 estimated daily emissions of NH_3 , NO_x , THC, and CO in the South Coast Air Basin.

TABLE 6.2

Summary of Ammonia Emissions by Source Category
in the South Coast Air Basin

1982

SOURCE CATEGORY	TOTAL EMISSIONS (kg/day)	
Stationary Fuel Combustion		
Electric Utility		
Natural Gas	1180.0	
Residual Oil	380.0	
Digester Gas	0.9	
Refinery Fuel Burning		
Natural Gas	118.0	
Residual Oil	15.0	
Refinery Gas	390.0	
Industrial Fuel Burning		
Natural Gas	470.0	
Liquified Petroleum gas (LPG)	8.0	
Residual Oil	22.0	
Distillate Oil	123.0	
Digester Gas	26.0	
Coke Oven Gas	15.0	
Residential/Commercial Fuel Burning		
Natural Gas	207.0	
Liquid Propane Gas (LPG)	4.0	
Residual Oil	85.0	
Distillate Oil	79.0	
Coal	23.0	
Subtotals	3145.9	(1.91%)
Mobile Source Fuel Combustion		
Automobiles		
Catalyst Autos and Light Trucks	2350.0	
Non-catalyst Autos and Light Trucks	485.0	
Diesel Autos and Light Trucks	3.5	
Catalyst Medium Vehicles	230.0	
Non-catalyst Medium and Heavy Trucks	140.0	
Diesel Trucks	23.0	
LPG for Carburetion	7.1	
Civilian Aircraft		
Jet	6.9	
Piston	2.1	
Shipping		
Residual Oil Boilers	68.0	
Diesel Ships	1.6	
Railroad--Diesel Oil	3.5	
Military		
Gasoline	4.9	
Diesel	2.3	
Jet Fuel	2.3	
Residual Oil	0.8	
Off-Highway Vehicles	6.5	
Subtotals	3337.5	(2.03%)
Industrial Point Sources	2450.0	(1.49%)
Sewage Treatment Plants	14,614.0	(8.88%)
Soil Surface	23,790.0	(14.5%)
Fertilizer		
Farm Crop	2010.0	
Orchards	1630.0	
Handling	420.0	
Non-farm	4810.0	
Subtotals	8870.0	(5.39%)
Livestock		
Cattle		
Dairy	29,840.0	
Feedlot	7210.0	
Range	13,590.0	
Horses	16,220.0	
Sheep	860.0	
Hogs	260.0	
Chickens	16,450.0	
Turkeys	490.0	
Subtotals	84,920.0	(51.6%)
Domestic		
Dogs	11,590.0	
Cats	3530.0	
Human Respiration	46.0	
Human Perspiration	7650.0	
Household Ammonia Use	570.0	
Subtotals	23,386.0	(14.2%)
*** Total ***	164,512.4	(100.0%)

Steenhuis et al. (1982). Based on their work, the ammonia release rate from animal waste decomposition is assumed to depend on temperature and wind velocity, such that:

$$E_i \propto 2.36 \left(\frac{T_i - 273}{10} \right) V_i^{0.8} A \quad (1)$$

and

$$A = \sum_{i=1}^{24} E_i \quad (2)$$

where E_i is the hourly emission rate in the grid cell at hour i from animal waste decomposition, A is the daily average emission rate of NH_3 from animal waste in the grid cell, T_i is the absolute temperature in $^{\circ}\text{K}$ and V_i is the wind velocity in m s^{-1} at hour i . A minimum wind velocity of 0.1 m s^{-1} is assumed.

6.3.4 Initial Conditions

Surface level initial conditions for trajectories ending at Rubidoux and Upland were based on the concentration fields constructed by spatially interpolating the measured concentrations. Those concentration fields start with the Pacific Ocean background values (in ppb: O_3 , 40; NO_2 , 10; NO , 10; CO , 100; HNO_3 , 1; NH_3 , 1; THC, 1000) at the western edge of the grid and rise to match the on-land data at the near coastal monitoring sites established during the field experiment. Initial upper level pollutant concentrations over the ocean were set to (in ppb): O_3 , 40; NO , 0.0; NO_2 , 1.0; CO , 500; HNO_3 , 1.0; NH_3 , 1.0; and THC, 500. Initial NH_4NO_3 concentrations over the

ocean were set to $3.25 \mu\text{g m}^{-3}$. Trajectories ending at Upland and the trajectory extending from Long Beach to Rubidoux start over land where measurements are taken. Ground level initial conditions for those trajectories are based on measured concentrations at the start of the trajectories, while upper level initial conditions are based on pollutant concentrations observed before the mixing depth descended the previous afternoon.

Atmospheric total hydrocarbon measurements available from the SCAQMD are reported on a ppm C, or ppm carbon atoms, basis and are not speciated into the many different organic gases actually present. The initial conditions for each of the six hydrocarbon classes employed by the trajectory model are found by splitting the measured THC values into the six classes using the set of splitting factors given in Table 6.3. These factors were derived from the measurements taken by Grosjean and Fung (1984) of the speciated hydrocarbon composition of Los Angeles air, averaged over a number of sampling periods.

6.3.5 Integration of Air Parcel Trajectories

Forward and backward air parcel trajectories were calculated from the interpolated wind fields using ten-minute time steps.

6.4 Model Evaluation for 30-31 August 1982

The ability to accurately predict O_3 and NO_2 concentrations usually is the most stringent test used to evaluate a gas-phase photochemical model. In this study, the ability to calculate total

TABLE 6.3

Splitting Factors for Converting Total Measured Hydrocarbons (ppmC)
into Hydrocarbon Classes for Use as Initial Conditions

Class	Factor
HCHO	0.0037
RCHO	0.0033
OLE	0.0042
ALK	0.0675
ARO	0.0177
C2H4	0.0061

For example, the initial HCHO concentration = 0.0037 X THC measured
in ppmC.

inorganic nitrate (TN), HNO_3 , NH_3 , aerosol-phase nitrate and PAN will be tested in addition to O_3 and NO_2 .

Progress towards model verification for a few of these co-pollutants was reported by Russell et al. (1983), when an earlier version of this model was tested using nitrate ion, ammonium ion, and ammonia gas concentration data for a short period on 28 June 1974 (Russell et al., 1983). Model verification data used during that study were limited in that they were available at only one site, for a few sampling periods, and contained data for only three of the pollutants of interest, aerosol NO_3^- , NH_4^+ , and gas-phase ammonia. Because the aerosol nitrate samples were collected on glass fiber filters, questions of artifact nitrate formation cloud the assessment of data quality. In this section a much more extensive model evaluation effort is carried out for the two-day period of 30-31 August 1982.

Three sets of trajectories are studied in this evaluation: a forward trajectory starting at Long Beach and ending near Rubidoux, a set of trajectories ending at Rubidoux throughout 31 August 1982, and a second set of trajectories terminating at the Upland measurement site. Upland and Rubidoux both are in the eastern, downwind portion of the SoCAB. Rubidoux historically experiences the highest aerosol nitrate concentrations in the basin, and during the 1982 experiment had the highest measured total inorganic nitrate concentrations. The Rubidoux-Riverside area also had the highest measured ozone concentrations during the 30-31 August, 1982 study period

(230-260 ppb). Upland experienced elevated total nitrate concentrations and often has some of the highest reported ozone concentrations in the SoCAB. Both of these locations are downwind of the Los Angeles metropolitan area and are affected by the reaction products formed in the atmosphere downwind of a major city. As such, these trajectories serve as ideal candidates for model verification tests and can best be used to show the effect of emission control strategies on pollutant concentrations, especially ozone and oxidized nitrogen compounds.

6.4.1 Long Beach Forward Trajectory

During a previous examination of the data from the 1982 field experiment (Russell and Cass, 1984), an air parcel trajectory was identified that started in the morning at the Long Beach sampling site at the time of the aerosol nitrate peak at that location, passed just north of the Anaheim measurement station in the afternoon, and in the evening terminated close to the Rubidoux site at the time of the aerosol nitrate peak in the Riverside area. This single trajectory provides an ideal opportunity for use in part of the model evaluation effort because the contents of the air parcel are well defined at several locations along its path. Likewise the initial conditions are established using measured pollutant concentrations, minimizing the uncertainty added from interpolating data.

Two distinct calculation schemes were tested against data taken along the Long Beach to Rubidoux trajectory just discussed. In the first calculation, Case 1, aerosol nitrate was assumed to be

formed only by the reaction between NH_3 and HNO_3 . In the second test, Case 2, aerosol nitrate formation proceeded by the reaction of HNO_3 with NH_3 , and by the irreversible reaction of HNO_3 with preexisting aerosol (reaction 58, described previously). Use of reaction 58 requires that emissions along the trajectory be specified for the aerosol materials that react readily with HNO_3 . The emission rate of SINK aerosol available to react was set at a constant rate, such that the total unreacted SINK aerosol plus BAN at the end of the trajectory is approximately equal to the sum of the sodium, calcium, potassium, and magnesium concentrations measured when the trajectory reached Rubidoux. Actual emission rates of these species as a function of location are unknown.

The presence of the added SINK aerosol acts to increase the predicted aerosol nitrate and total inorganic nitrate concentrations. Total inorganic nitrate is increased because some of the nitric acid, which otherwise would undergo rapid removal by dry deposition, instead is bound as aerosol nitrate, which deposits out more slowly. The magnitude of this effect is a complex function of the ammonia concentrations, nitric acid concentrations, and aerosol SINK emission rate. If there is a large amount of NH_3 in the air parcel, most of the nitric acid will have reacted to form NH_4NO_3 , suppressing the HNO_3 concentration and greatly slowing the formation of irreversibly bound non- NH_4NO_3 nitrate aerosol (BAN).

Results of the Long Beach to Rubidoux forward trajectory calculations are shown in Table 6.4, along with the measured pollutant

TABLE 6.4

Predicted and measured concentrations along the trajectory beginning at Long Beach, California, at 1100 (PDT) 31 August 1982

Pollutant	1400 PDT			1800 PDT		
	Measured Concentration	Case 1 Predicted NH_4NO_3 Only	Case 2 Predicted Reaction 58 Included	Measured at Rubidoux	Case 1 Predicted NH_4NO_3 Only	Case 2 Predicted Reaction 58 Included
O_3 (ppb)	173 ³	174	174	130	152	152
NO_2 (ppb)	70 ³	51 ¹	52 ¹	50	35 ¹	38 ¹
HNO_3 (ppb)	10.1-7.72	10.0	8.2	5.3-1.8 ²	2.0	2.5
AN ($\mu\text{g m}^{-3}\text{NO}_3^-$)	7.6-13.4 ²	11.6	19.9	29.7-14.4 ²	14.1	22.7
TN ($\mu\text{g m}^{-3}\text{NO}_3^-$)	33.0-32.8 ²	36.8	40.6	43.1-18.9 ²	22.4	29.0
NH_3 (ppb)	15.3-10.9 ²	10.8	13.2	59.8-89.0 ²	27.3	36.4
PAN (ppb)	*	*	*	*	20.1	20.1
NH_4NO_3 ($\mu\text{g m}^{-3}\text{NO}_3^-$)		11.6	6.1		14.1	11.3
BAW ⁴ ($\mu\text{g m}^{-3}\text{NO}_3^-$)			13.9			11.3

NOTES:

- (1) Predicted NO_2 concentrations are the sum of predicted NO_2 , HNO_3 , AM, and PAN. The instruments used to measure NO_2 possess a quantitative interference due to co-pollutant species (Winer et al., 1974)
- (2) Both at Anaheim and at Rubidoux, the trajectory passed nearby between two sampling periods. Both the measured concentrations from 1200 to 1400 and 1400 to 1600 are shown, respectively, at Anaheim. Likewise at Rubidoux the measured concentrations for 1600 to 1800 and 1800 to 2000 are given. The UCR site sampling interval was from 1700 to 1900. Predicted ozone values are one-hour averages, as are the measured concentrations.
- (3) Ozone and NO_2 concentrations are averaged values from the nearest three stations. Other concentrations are as measured at Anaheim.
- (4) Bound Aerosol Nitrate
- (*) PAN measured only at UCR.

concentrations, at 1400 and 1800 PDT, 31 August 1982. The trajectory passed nearest to Anaheim at 1400 PDT, and the measured HNO_3 , NH_3 , aerosol nitrate, and total nitrate are from that station. Measured O_3 and NO_2 values at 1400 are available from a number of monitoring sites in the area and the O_3 and NO_2 values shown are an average of the three stations nearest to the air parcel's position at that time.

At 1800 PDT, the trajectory path calculation showed that the air parcel was 3 km southwest of the Rubidoux sampling site and about 8 km west of the Riverside (UCR) site. Measured pollutant concentrations from both of these sites are included. The O_3 concentration at Riverside was measured at a SCAQMD site at Riverside City College. PAN was measured at the UCR site.

Looking first at the results from the trajectory originating in Long Beach at 1100 PDT, as it passes near Anaheim at 1400, the ozone prediction very nearly equals the observed average, well within the uncertainty in the observed concentrations which are reported to the nearest 10 ppb. The predicted NO_2 is slightly lower than the observed. The observed nitric acid is very close to that predicted regardless of whether or not an aerosol sink for nitric acid is included in the calculation. In both cases, the predicted nitric acid is between the values measured for the sampling periods straddling 1400 PDT, when the trajectory is closest to Anaheim. The aerosol nitrate predicted for Case 1 is between the measured concentrations, while the amount predicted in Case 2 is slightly greater than the

observed values. In both cases the predicted ammonia matches the two measured values to within the measurement uncertainties.

Farther downwind near Rubidoux at 1800 PDT a similar comparison can be performed. Ozone, predicted to be 152 ppb, is equal within the reporting uncertainty of 10 ppb to that measured in Riverside and is slightly greater than that measured at Rubidoux. Again the NO_2 predictions are slightly below the measured values. In this case, the trajectory arrival at Rubidoux again straddles two measurement periods for HNO_3 , NO_3^- , and NH_3 , while at the UCR site the 1800 arrival falls within a single sampling interval. In all cases, except for ammonia gas, the concentrations measured at UCR lie between the range of values observed at Rubidoux. In both Cases 1 and 2, the predicted concentrations of HNO_3 , AN, and TN fall within the range of the observations at Rubidoux and Riverside. The predicted NH_3 concentration resulting from the Case 2 calculation also lies within the measured range. While the NH_3 concentration prediction for Case 1 may appear slightly lower than that at UCR, the circa 5 ppb NH_3 deficit is still within the experimental uncertainty of the lowest measured NH_3 concentration at that time.

PAN also was measured at the UCR site, and as seen in Table 6.4, the model closely predicts the observed PAN concentration, which peaked at that time. Note that organic nitrate comprises a substantial fraction of the total oxidized nitrogen at 1800 PDT in the Riverside area. From the results shown in Table 6.4, it is concluded

that the trajectory model is capable of predicting the downwind concentrations of the secondary pollutants of interest in the Riverside area at the time of arrival of the peak nitrate concentrations, given measured initial conditions at Long Beach.

6.4.2 Trajectories Ending at Rubidoux

The Long Beach to Rubidoux trajectory calculation just discussed provides an almost ideal example of a model verification test in which both the ground level initial conditions and final composition of the air parcel are known experimentally for a large number of uncommonly measured air pollutants. While this test adds to confidence in the model's capability, it is unrealistic to expect that high quality data on initial conditions always will be available for arbitrarily selected trajectories. Likewise, the upper level pollutant concentrations needed to initialize the model are seldom, if ever, known. Upper level initial conditions must be estimated from ground level measurements, while pollutants stored aloft may have been affected by chemical processes not evident at the ground. This is especially true in the early morning because of the markedly decreased vertical mixing overnight that traps fresh emissions near the ground and isolates portions of the upper air column from nighttime emissions and from deposition. In this case the ground level portion of the air mass may be heavily burdened by NO and NO₂, while in the upper levels of the atmosphere nighttime chemical reactions can convert almost all of the NO and NO₂ to HNO₃ (Russell et al. 1985). Atmospheric stratification at night also could affect the concentrations of the

more reactive organic gases. If this situation is not taken into account initial conditions based on ground level observations could be specified that are inconsistent with actual pollutant concentrations several hundred meters above the ground.

An alternative method for initializing trajectories was examined. Air parcels arriving at Rubidoux throughout the day of 31 August were followed backward to midnight at the end of 29 August. In that case all the trajectories begin over the ocean upwind of the city and end between 24 and 47 hours later at the Rubidoux monitoring site. Use of the longer, two-day trajectories has three major advantages. First, starting more than 24 hours before the arrival of the trajectory allows sufficient time for most of the reactive pollutants present due to initial conditions to be depleted from the system by both ground level deposition and by chemical reactions to form products less crucial to the formation of photochemical oxidants. Secondly, starting the air parcel at a relatively clean background location over the ocean minimizes the effect of initial conditions and the uncertainty in the outcome arising from their specification. Thus, predicted concentrations at the end of the trajectory are primarily a function of the emissions along the trajectory, not initial conditions, and the mass of each species in the air parcel at the start of 31 August is consistent with the known emissions, meteorology and chemistry of 30 August. Finally, this procedure enhances the usefulness of subsequent control strategy calculations because predicted concentrations are dominated by emissions along the

trajectory that can be attributed to particular air pollution sources rather than being heavily influenced by initial conditions (e.g. at Long Beach) that are not readily assigned to their source. This is a more demanding test of a model and the associated emissions inventory than is the case when using shorter trajectories in which initial conditions play a major, if not dominating, role.

In an effort to determine the importance of the uncertainties in these initial conditions, a test was performed in which the initial concentrations established over the ocean were first doubled and then cut in half for the trajectory arriving at Rubidoux at 1600 PDT. This trajectory displayed the greatest predicted nitrate loading and second highest ozone concentration among the trajectories terminating at Rubidoux. The predicted total inorganic nitrate concentrations at Rubidoux at 1600 PDT for the base case, for the case with the initial conditions doubled and for the case with initial concentrations cut in half were 18.2, 15.5, and 20.6 ppb, respectively. The ozone concentrations averaged over the last hour of travel along that trajectory were 185, 195, and 176 ppb, respectively. This test shows that initial conditions play a very small role in determining predicted pollutant concentrations for the multi-day trajectories studied here. On the other hand, if the emissions are set to zero along this same trajectory, the total inorganic nitrate predicted at Rubidoux falls to only 1.6 ppb, and ozone falls to 38 ppb. Thus, the predicted pollutant levels are almost solely a function of emissions

within the urban area when a reasonable set of initial conditions starting over the ocean is used.

Next the air quality model's ability to reproduce the time history of pollutant concentrations at Rubidoux given trajectories that originate over the ocean was examined. Again the model was evaluated in two modes: with and without the addition of aerosol that can irreversibly react with nitric acid to form aerosol nitrate.

Plots of the pollutant concentrations predicted at Rubidoux for 31 August without the emission of SINK aerosol along the trajectories are compared to measured values in Figures 6.3 through 6.8. Ozone and NO_2 concentrations averaged over the last hour of travel are shown in Figures 6.3 and 6.4. Trajectories arriving at Rubidoux on the hour were used to estimate two hour average concentrations when needed for comparison to measured values (two hour average weighted 1/4 start hour, 1/2 midpoint, 1/4 end hour). Predicted two hour average total inorganic nitrate concentrations are shown, with the measured values, in Figure 6.5, nitric acid in Figure 6.6, aerosol nitrate in Figure 6.7 and NH_3 in Figure 6.8.

A plot of the predicted and observed concentrations of O_3 and NO_2 throughout 31 August at Rubidoux shows that the model predictions are in good agreement with the measured species concentrations. Figure 6.5 shows the comparison of averaged predicted and observed TN. The model predicts the trends and, approximately, the two-hour averaged concentrations. The peak predicted TN, $38 \mu\text{g m}^{-3}$ (as NO_3^-), is only slightly less than the peak measured, $43 \mu\text{g m}^{-3}$, which is

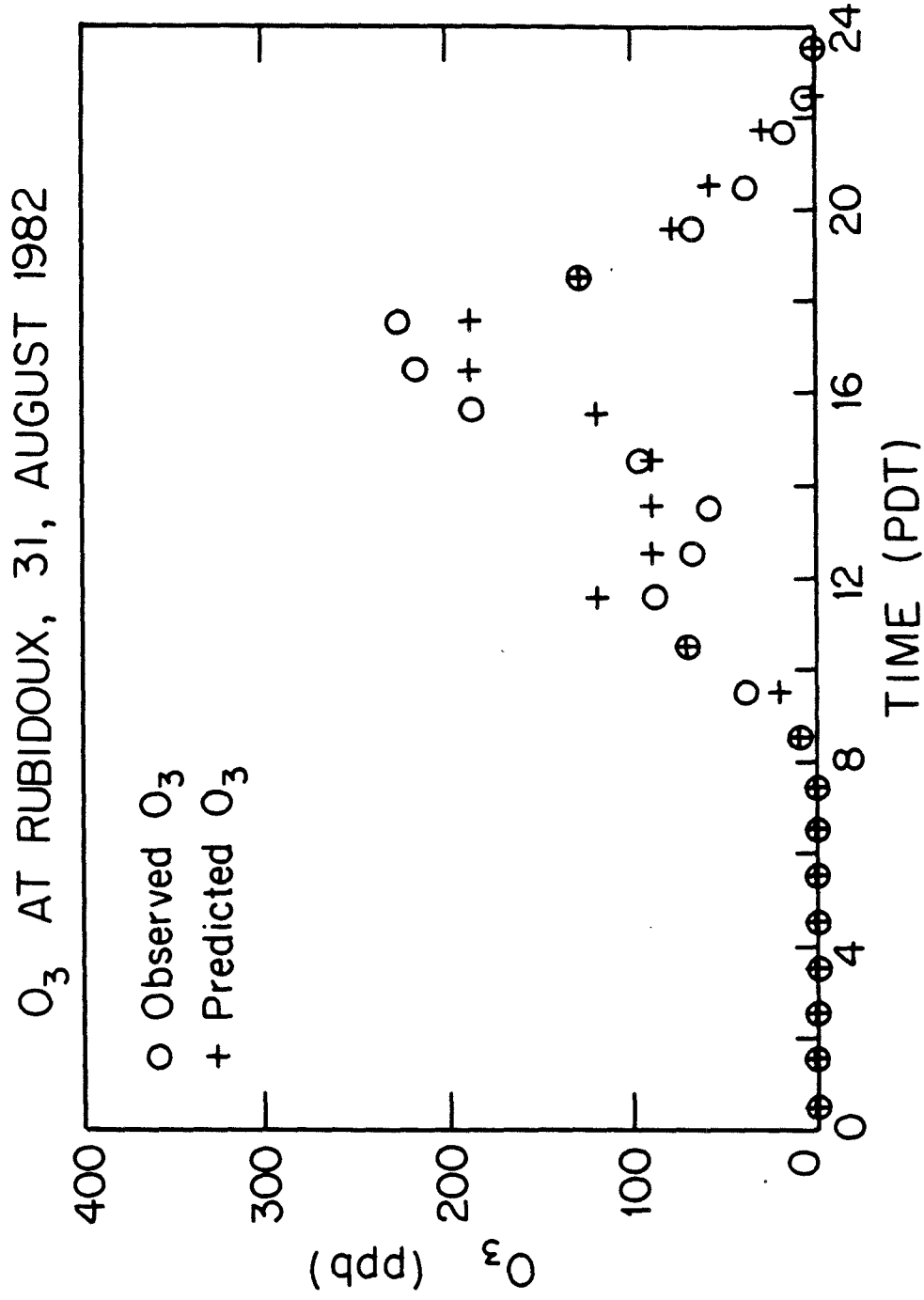


FIGURE 6.3

Observed and predicted O₃ at Rubidoux, CA, 31 August 1982.

NO₂ AT RUBIDOUX, 31, AUGUST 1982

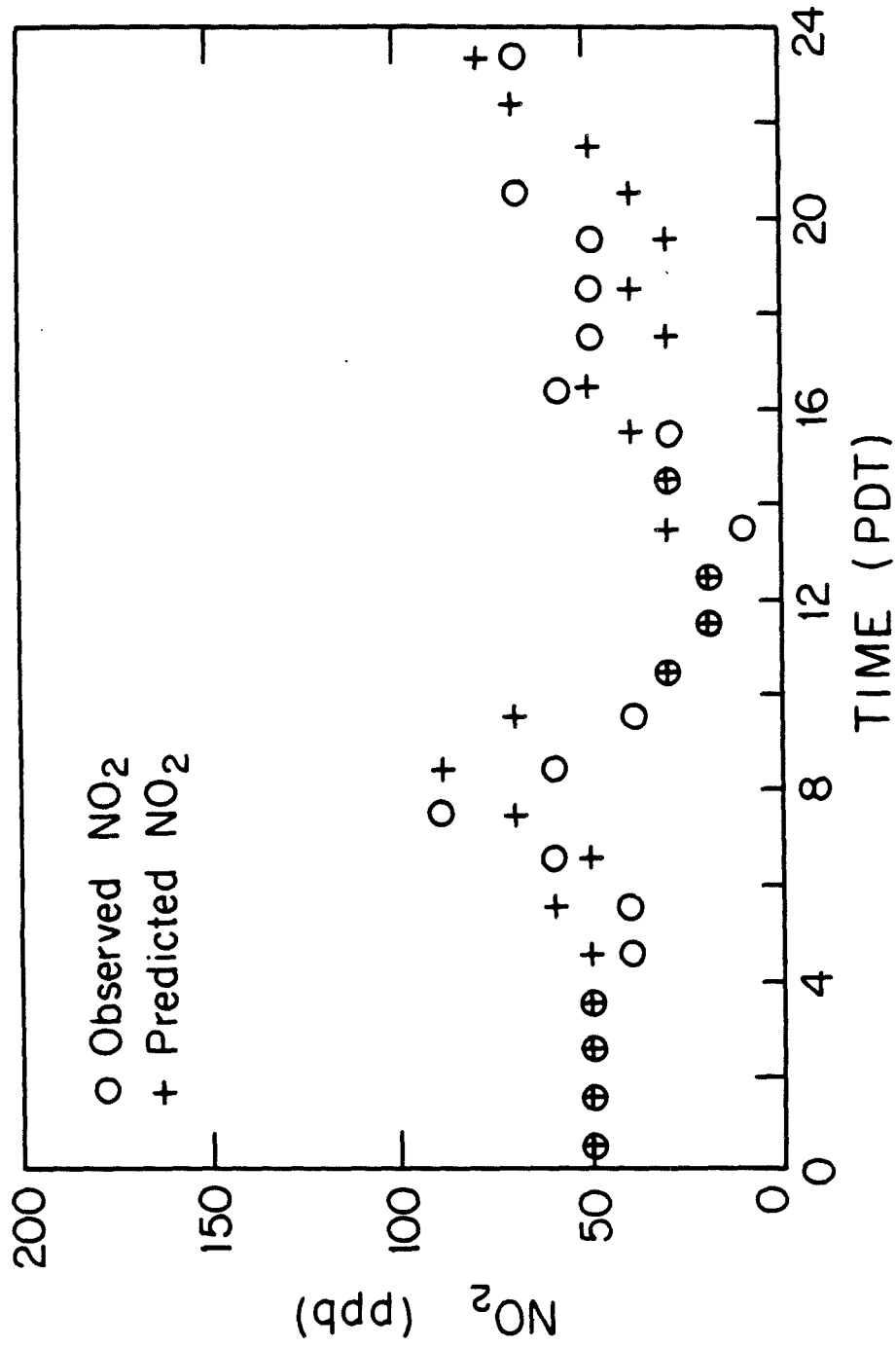


FIGURE 6.4

Observed and predicted NO₂ at Rubidoux, CA, 31 August 1982.

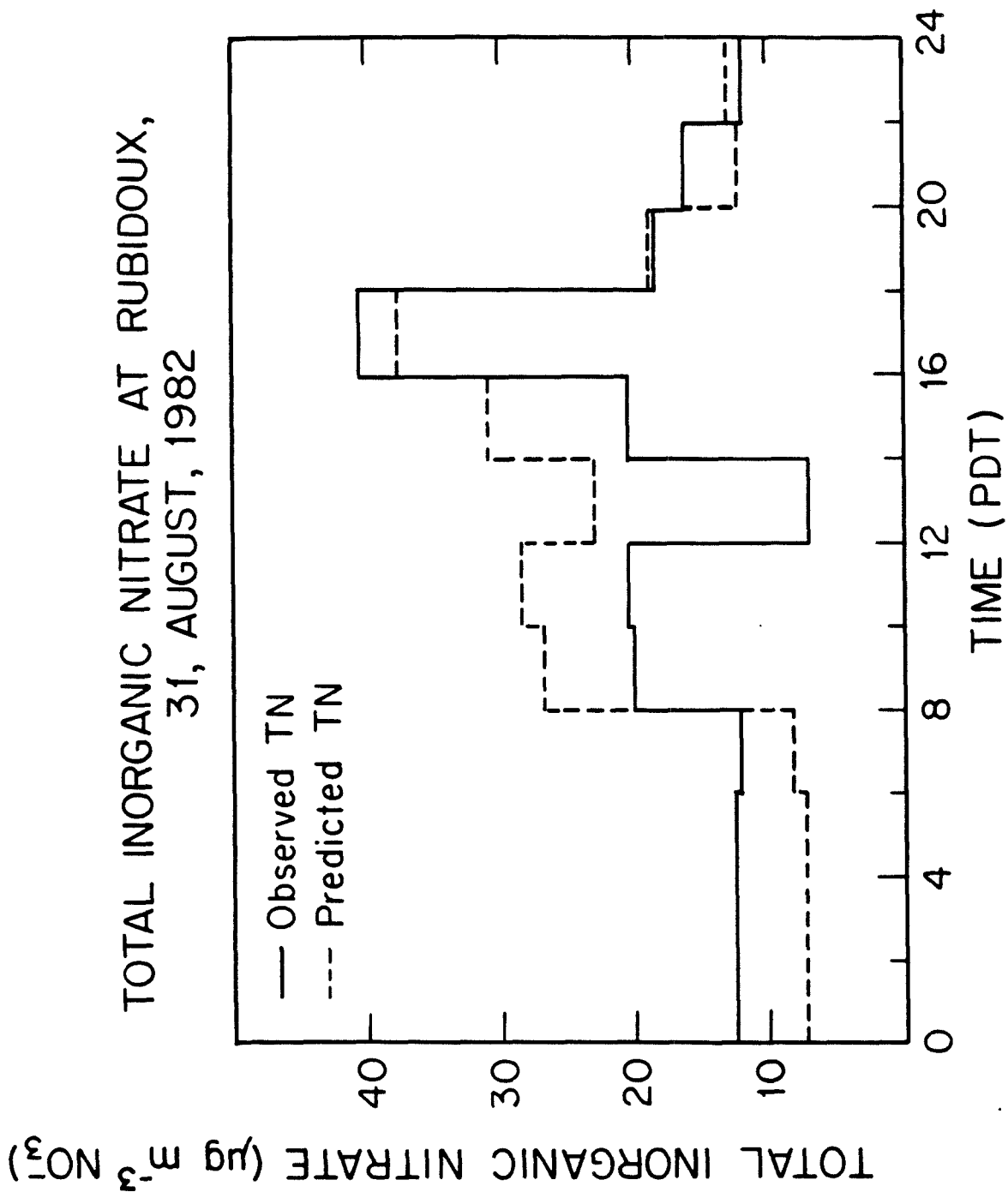


FIGURE 6.5

Observed and predicted Total Nitrate (TN = AN + HNO₃) at Rubidoux, CA, 31 August 1982.

NITRIC ACID GAS AT RUBIDOUX,
31, AUGUST, 1982

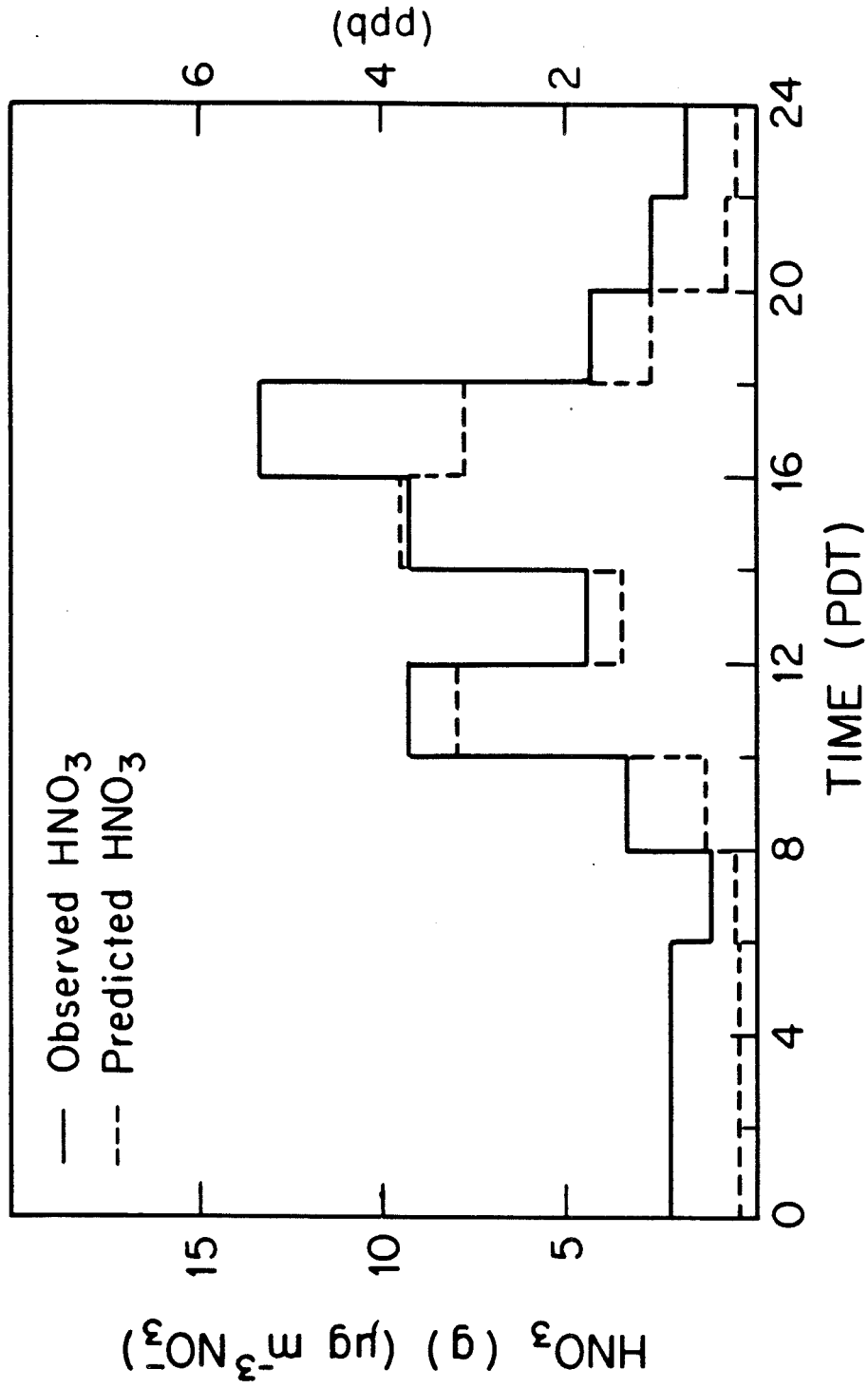


FIGURE 6.6

Observed and predicted HNO_3 (g) at Rubidoux, CA, 31 August 1982.

AEROSOL NITRATE AT RUBIDOUX 31, AUGUST 1982

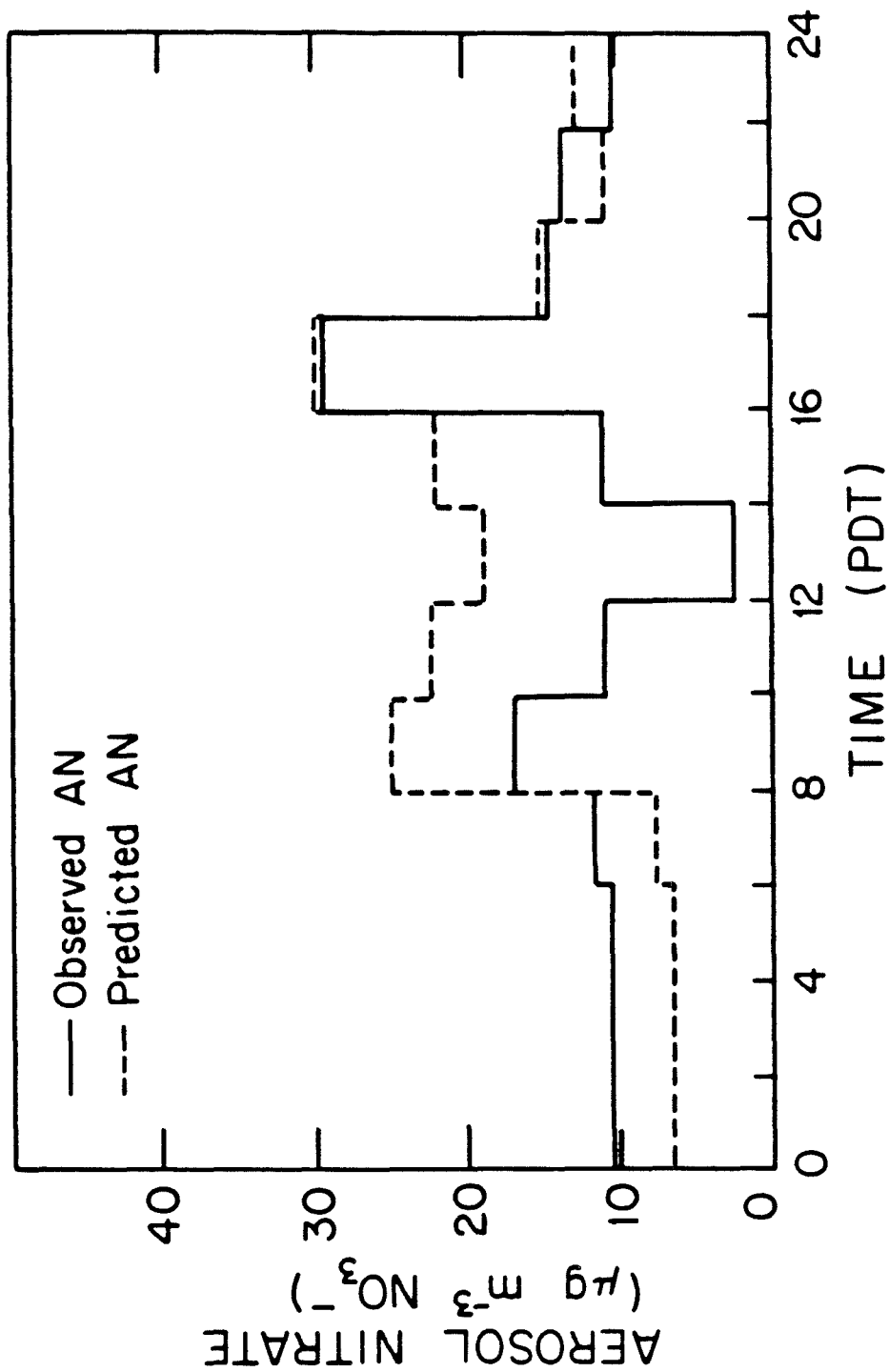


FIGURE 6.7
Observed and predicted NO_3^- at Rubidoux, CA, 31 August 1982.

AMMONIA GAS AT RUBIDOUX,
31, AUGUST, 1982

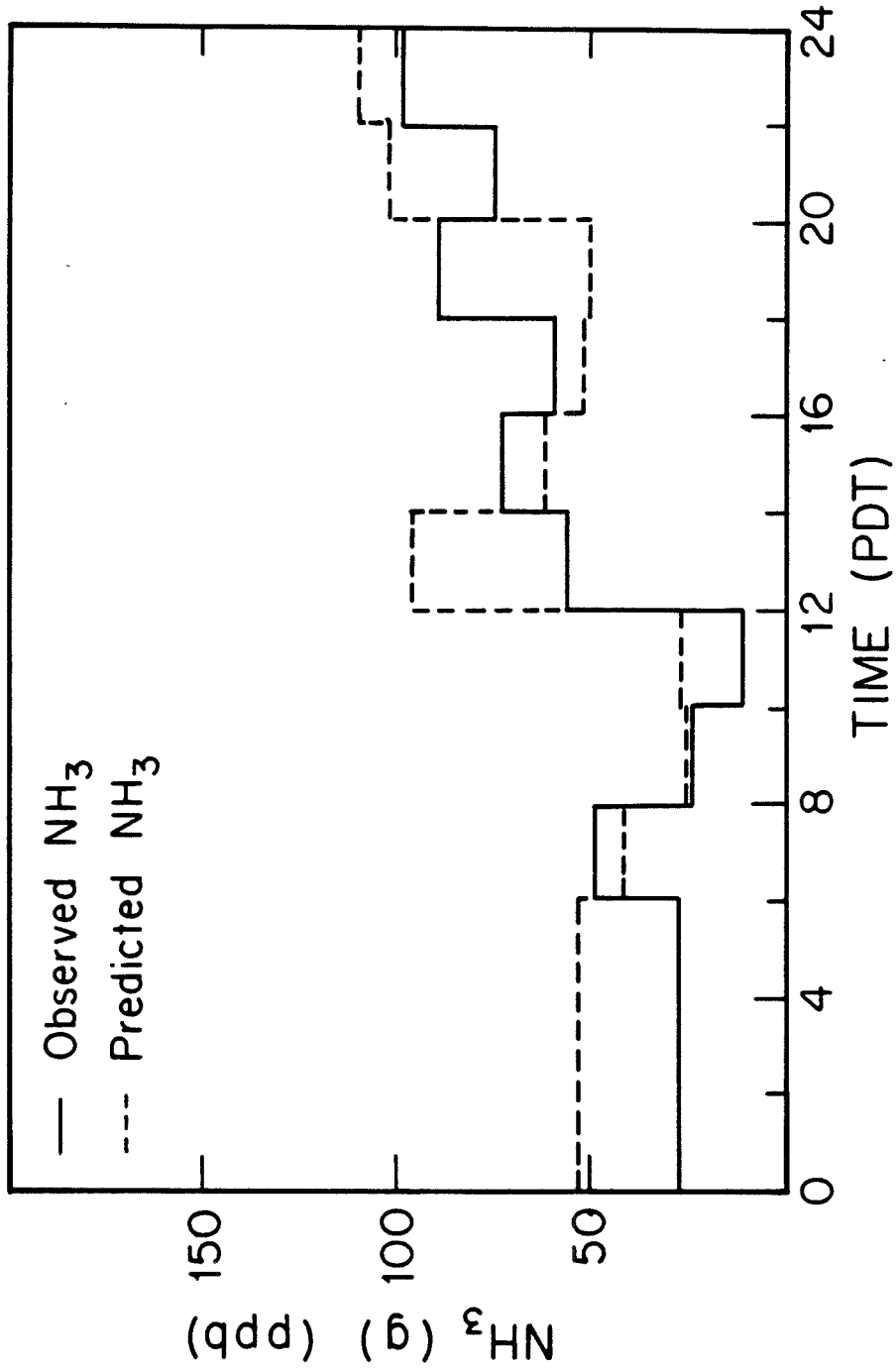


FIGURE 6.8

Observed and predicted NH₃ at Rubidoux, CA, 31 August 1982.

considered close given measurement and model input uncertainties. The predicted 24-hour average TN is $19 \mu\text{g m}^{-3}$, whereas the measured average is $18 \mu\text{g m}^{-3}$, showing very good agreement.

Having shown that the predicted and measured TN agree well, the question of apportioning the nitrate between the gas and aerosol phases arises. The apportionment of nitrate between the aerosol and gas phases is sensitive to the temperature, humidity, and NH_3 concentration (Russell et al., 1983), and to the presence of other aerosol constituents (Hildemann et al., 1984). In the first case studied here, pure NH_4NO_3 is assumed to be the only aerosol nitrate species formed. Most of the inorganic nitrate is predicted to be found in the aerosol phase, not the gas phase, and the measurements confirm that prediction (Fig. 6.6). The measured and predicted 24-hour averaged aerosol nitrate concentrations were 13 and $16 \mu\text{g m}^{-3}$, respectively (Fig. 6.7). Measured gas phase nitric acid levels in this case exceed observed values throughout the day (Fig. 6.6), but the absolute magnitude of this discrepancy is very small. The measured 24-hour averaged HNO_3 was 1.9 ppb compared to the predicted 1.1 ppb. Measurement uncertainties on the nitric acid values are approximately 0.4 ppb (one standard error).

A plot comparing the ammonia concentrations, Figure 6.8, indicates that throughout much of the day the predictions agree well with the measurements. This is remarkably good agreement considering that the ammonia emission inventory and model used here represent the first test of a procedure for calculating atmospheric ammonia levels.

In the trajectories terminating at Rubidoux, most of the ammonia emissions are due to livestock operations, which determine the very tall spike in the NH_3 emission inventory (Fig. 6.2) located immediately upwind of Rubidoux. The major peak in the NH_3 emission inventory is so sharp that a slight perturbation in the calculated path of an air parcel can create a noticeable difference in the predicted NH_3 concentrations. Also, knowledge of the diurnal emission pattern for livestock waste decomposition and the exact spatial distribution of the animals during the August, 1982 experiment could be improved. As a result, NH_3 concentrations cannot be predicted with the same precision as other pollutant concentrations, even though the source of the NH_3 emissions has been identified with reasonable certainty.

In the early morning when the inversion base is very low, ammonia is trapped in the lower cells of the model. An over prediction of ammonia occurs at this time. A slight change either in the diurnal profile for ammonia release from livestock waste decomposition or in the trajectory path would greatly change the concentration of NH_3 at Rubidoux during this period. The 24-hour average NH_3 measured was 51 ppb, compared to the predicted 61 ppb. This overprediction of NH_3 levels could explain part of the reason why the predicted HNO_3 is slightly lower than that measured (Fig 6.6): excess NH_3 would react with HNO_3 to increase predicted aerosol phase NH_4NO_3 , while reducing predicted HNO_3 .

A second explanation can be offered for measured ambient HNO_3 levels that are below those predicted by a model that considers only the equilibrium between NH_3 , HNO_3 , and NH_4NO_3 . Additional species (e.g. sulfates) coexisting with nitrate in the aerosol phase could lower the vapor pressure of nitric acid over the particle, thus increasing the aerosol nitrate formation and decreasing the amount of HNO_3 . This effect is discussed in a previous examination of the verification data being used here (Hildemann et al., 1984).

In view of the sensitivity of the model's nitrate predictions to ammonia concentration and temperature and of the uncertainty in the ammonia emissions from the large sources just upwind of Rubidoux, a second set of calculations was performed in which total inorganic nitrate concentrations predicted by the model were apportioned between gas phase HNO_3 and aerosol NH_4NO_3 using the ambient ammonia concentrations and temperatures measured at Rubidoux. The temperatures at Rubidoux used in the previous modeling calculations were obtained from filtered, interpolated temperature field values calculated for the center of each grid cell and need not equal the measured temperatures at Rubidoux, exactly. Using the measured ambient temperature and ammonia concentration to partition the nitrate at the trajectory endpoint improved the model predictions from those shown in Figure 6.7 to those shown in Figure 6.9. Thus, given the ability to more precisely predict the ammonia concentrations and using actual measured temperatures the model can accurately partition the

AEROSOL NITRATE AT RUBIDOUX
31, AUGUST 1982

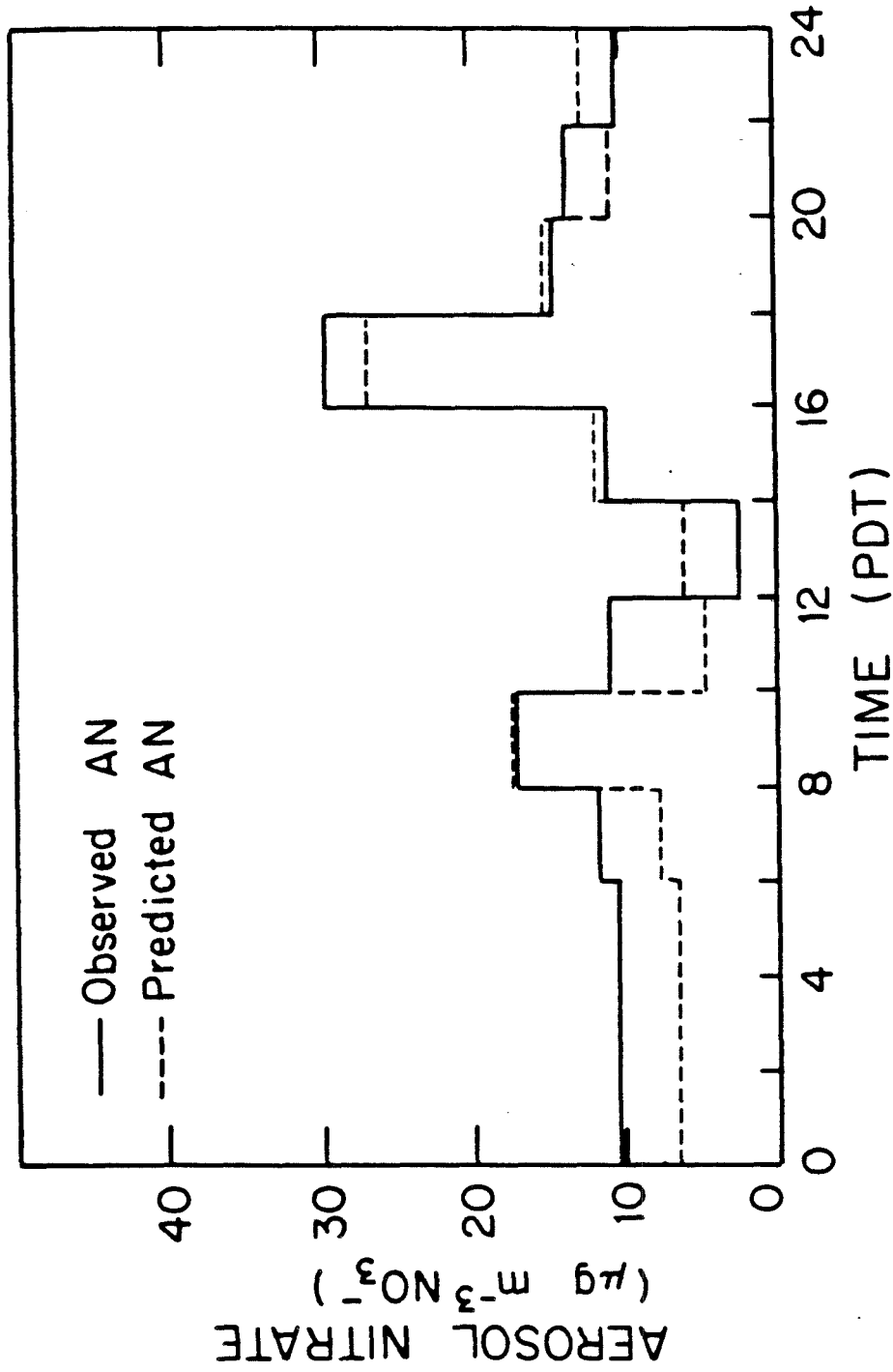


Figure 6.9

Observed and predicted NO_3 at Rubidoux, CA, 31 August 1982 when the partition of computed TN between $\text{HNO}_3(\text{g})$ and aerosol nitrate is based on ambient temperatures and ammonia concentrations measured at the Rubidoux monitoring site.

inorganic nitrate at Rubidoux between the vapor and aerosol phases. This calculation also decreases the predicted 24-hour average aerosol nitrate from $16 \mu\text{g m}^{-3}$ to $12 \mu\text{g m}^{-3}$, bracketing the measured value of $13 \mu\text{g m}^{-3}$.

Next the emissions of SINK aerosol were added along each trajectory at a constant rate needed to approximately match the total non-ammonium cationic material seen to arrive at Rubidoux. The entire set of multi-day trajectory calculations beginning over the ocean was repeated with HNO_3 allowed to react with SINK aerosol by reaction 58. This change in assumptions tends to increase the aerosol nitrate and total nitrate concentrations predicted, though in this case the effect is small. As seen in Figure 6.10, the 24-hour average AN increases to $18.4 \mu\text{g m}^{-3}$, of which 84% is ammonium nitrate and the remaining 16% is bound aerosol nitrate (BAN). The HNO_3 concentrations predicted remain virtually unchanged because of the large ammonia concentrations.

An interesting model result is obtained when the aerosol sink for HNO_3 is included in the calculation. The model predicts the co-existence of ammonium nitrate, bound aerosol nitrate, HNO_3 , NH_3 and unreacted aerosol SINK. Consumption of aerosol SINK is kinetically limited. Given more time, or if the collision efficiency for HNO_3 on SINK aerosol is much higher than $\alpha = 0.001$, then the aerosol has the capacity to strip a large fraction, if not all, of the nitric acid from the atmosphere.

CALCULATED NITRATE AT RUBIDOUX
 31, AUGUST, 1982
 IF SINK AEROSOL EMISSIONS ARE INCLUDED

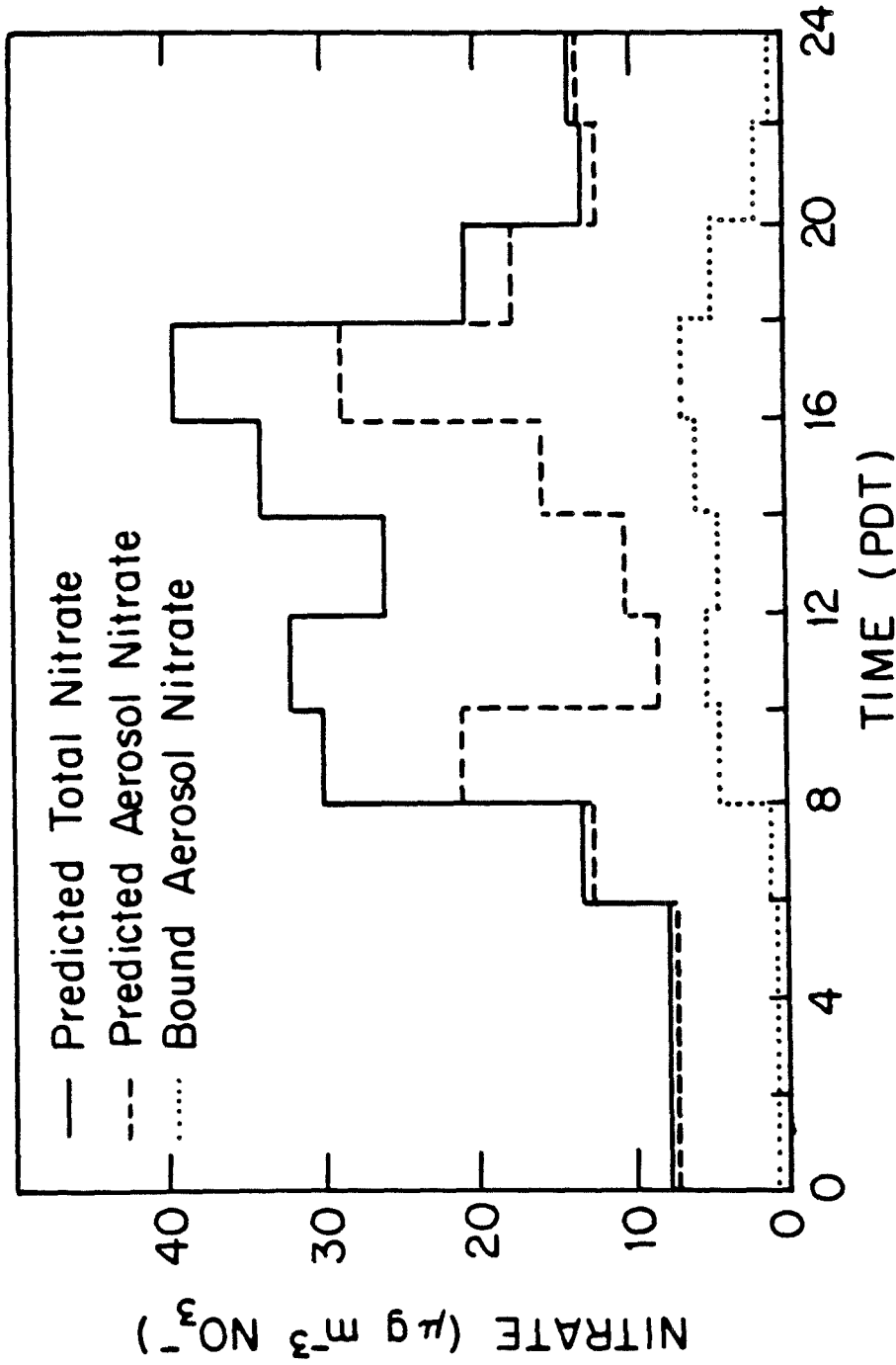


FIGURE 6.10

Predicted Total Nitrate (TN = HNO₃(g) + NH₄NO₃ + BAN), Aerosol Nitrate (AN = NH₄NO₃ + BAN) and aerosol nitrate formed by reaction 58 (BAN, see text) at Rubidoux, CA, 31 August 1982.

6.4.3 Trajectories Ending at Upland

A similar analysis was carried out for air parcels reaching Upland on 31 August. Trajectories were initiated at midnight on 30 August, and the only case examined was that of pure NH_4NO_3 formation. Predicted and measured ozone, total nitrate, aerosol nitrate and total NH_3 are shown in Figures 6.11 through 6.14.

Predicted and observed ozone concentrations at Upland also agree very well. However, the model predicts more TN to be present during the middle of the day than was observed. The reason for the discrepancy is not clear. In the trajectories ending at Rubidoux, PAN was a major product of NO_2 oxidation. Results from the trajectories ending at Upland show PAN concentrations averaging about 3 ppb less than in the Rubidoux trajectories. Transfer of oxidized nitrogen from PAN to HNO_3 could account for the predicted inorganic nitrate at Upland being higher than that measured. The predicted AN and that measured match well throughout much of the day (Fig. 6.13). In the afternoon there is measurable nitrate aerosol though the model predicts that no pure NH_4NO_3 would form. As seen in the Rubidoux trajectories (Fig 6.10), the small amount of measured AN at Upland in the afternoon could easily be accounted for by the reaction of HNO_3 with SINK aerosol to form bound aerosol nitrate.

OZONE AT UPLAND 31, AUGUST 1982

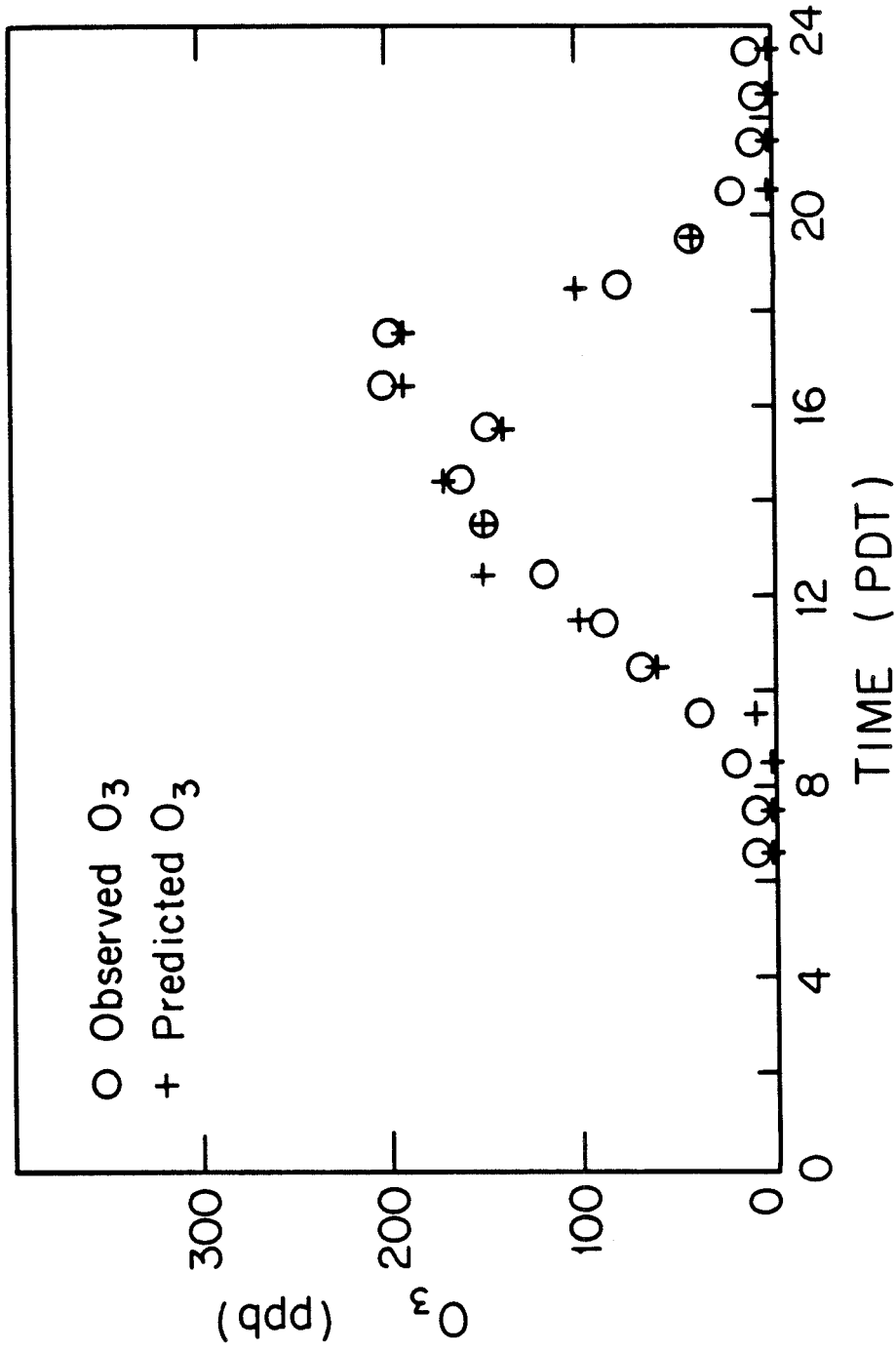


FIGURE 6.11

Observed and predicted O₃ at Upland, CA, 31 August 1984.

TOTAL INORGANIC NITRATE AT UPLAND
31, AUGUST 1982

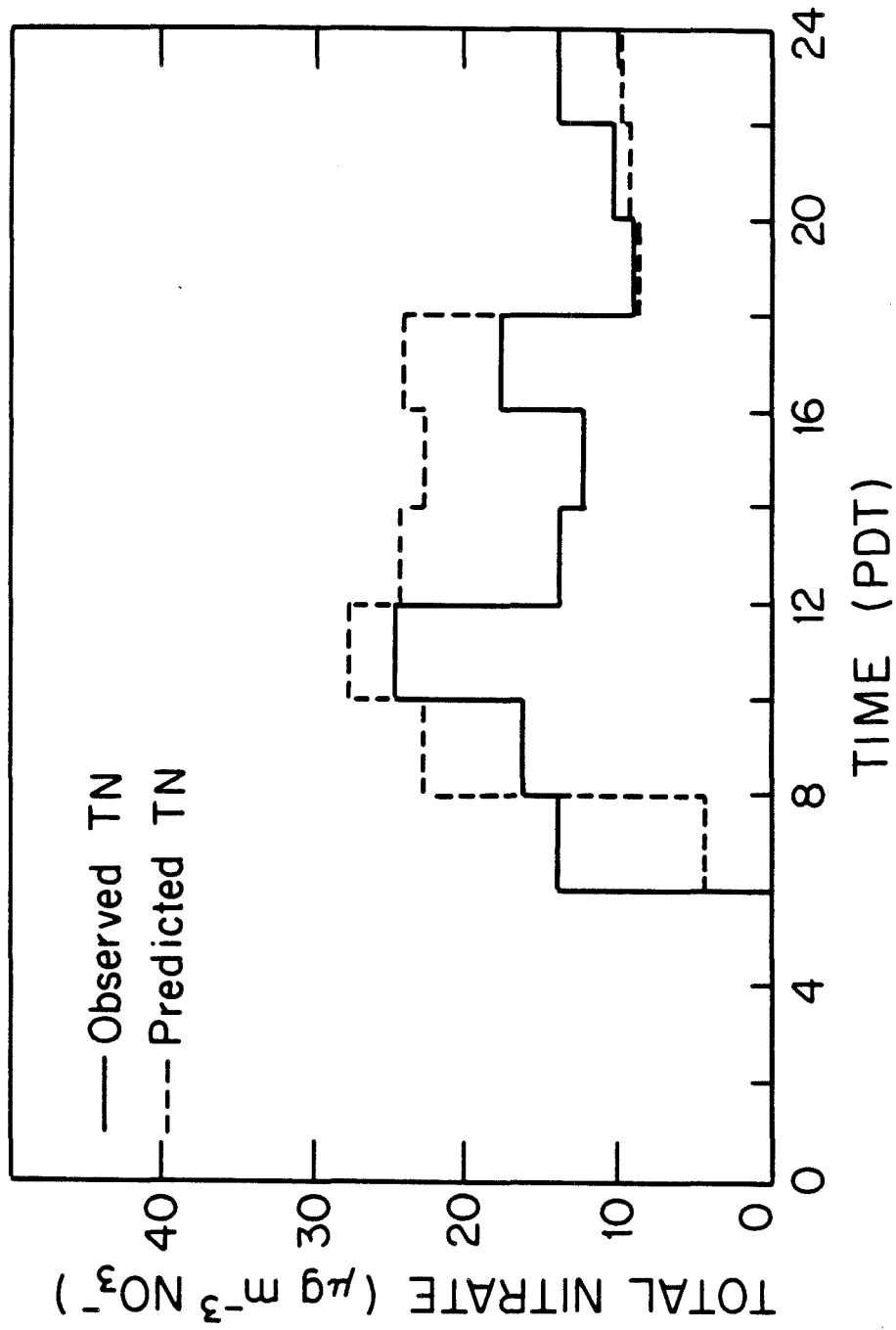


FIGURE 6.12

Observed and predicted Total Nitrate at Upland, CA, 31 August 1982.

AEROSOL NITRATE AT UPLAND
31, AUGUST 1982

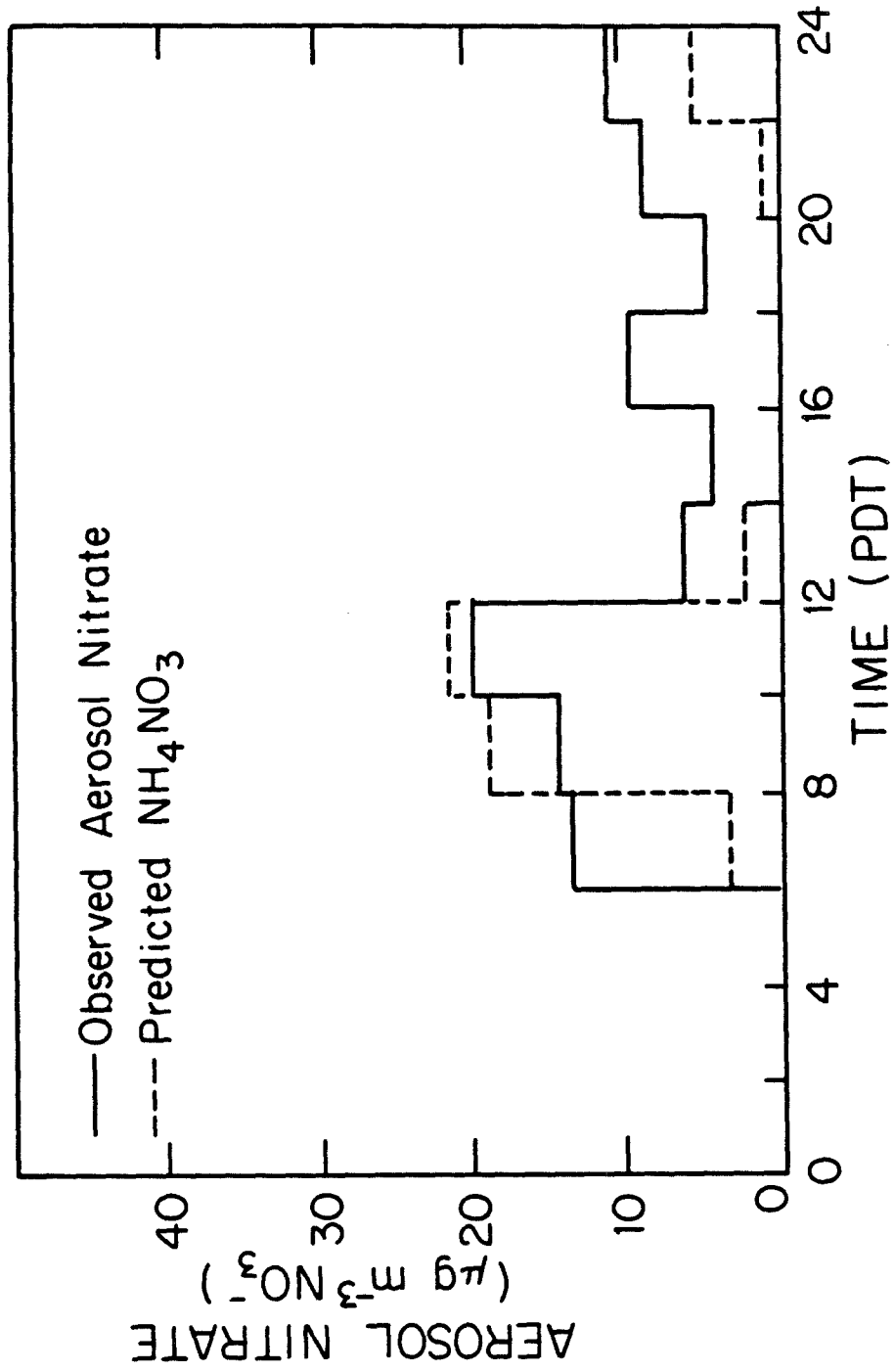


FIGURE 6.13

Observed and predicted aerosol nitrate at Upland, CA, 31 August 1982.

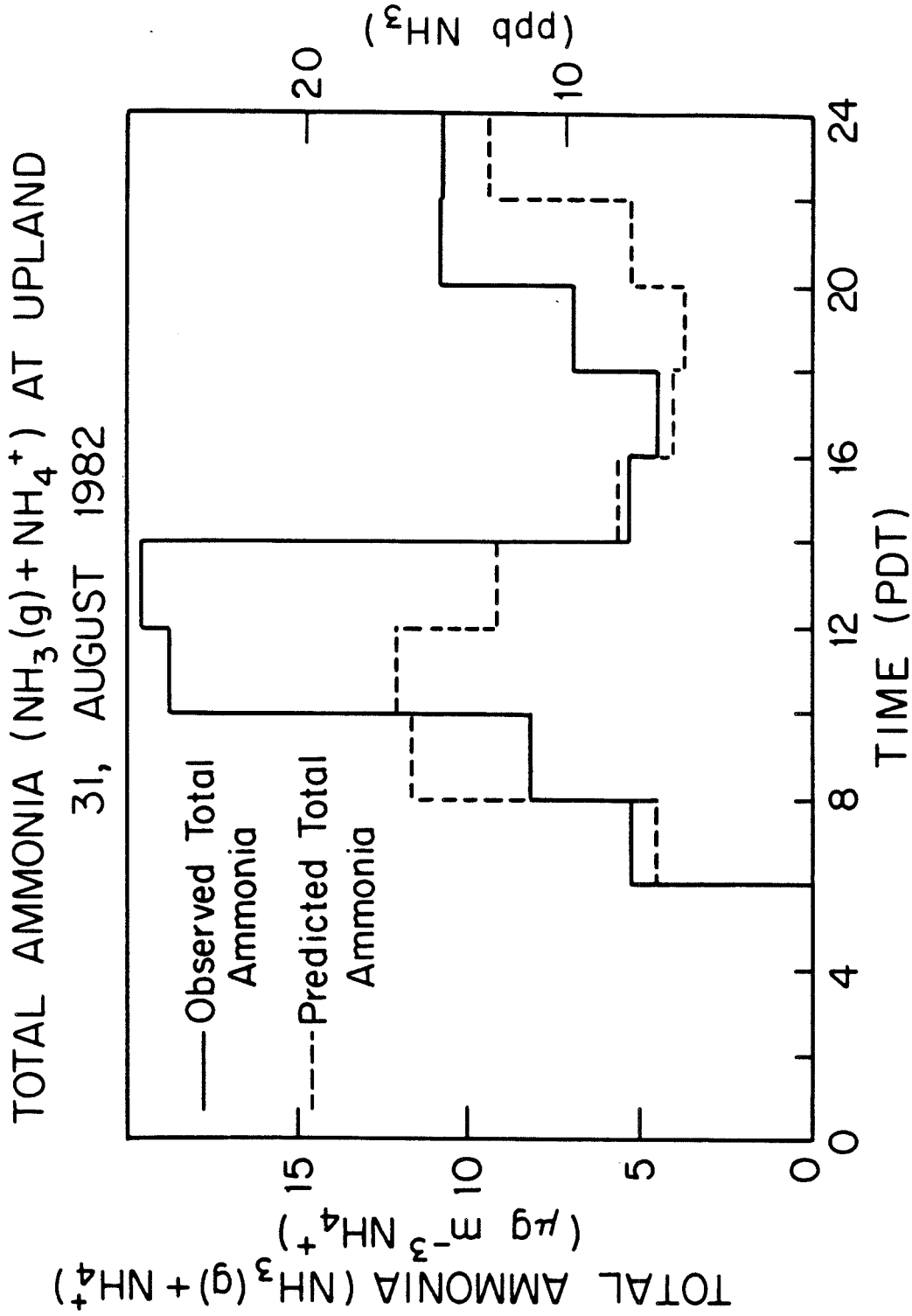


FIGURE 6.14

Observed and predicted Total Ammonia at Upland, CA, 31 August 1982.

A scatter diagram of predicted O_3 against that observed at both Upland and Rubidoux shows that the data points are grouped closely about the 1:1 line (Fig. 6.15). Ordinary least squares regression of O_3 predictions vs. observations yields the relationship:

$$[O_3]_{\text{pred}} = 0.93 [O_3]_{\text{obs}} + 4 \quad (3)$$

with O_3 values expressed in ppb. The correlation coefficient is 0.96, indicating a very good fit.

In this study, sets of results from the shorter (single day) and longer (multi-day) trajectories have been used to evaluate the model's performance. In both cases the model has performed well. Some uncertainty in the air parcel path is added to the analysis when trajectory paths are calculated over multi-day periods, especially if the trajectories are continued during the night when wind speeds are low and variable. However, this is the only way to decrease the uncertainties that would otherwise arise from misspecifying initial conditions and to accurately show the effects that changing pollutant emissions have on the resulting concentrations. If initial conditions dominate or greatly affect the predicted concentrations, a change in emissions within the model may have little effect on model predictions, or in some cases could produce predictions that move in a direction opposite to reality. A good example of the latter case could arise if initial conditions placed an excessive amount of NO_x in the air parcel as it starts in the morning. In this case increasing NO_x emissions further could decrease the peak O_3 concentration, while if the correct initial NO_x concentrations were used, then the

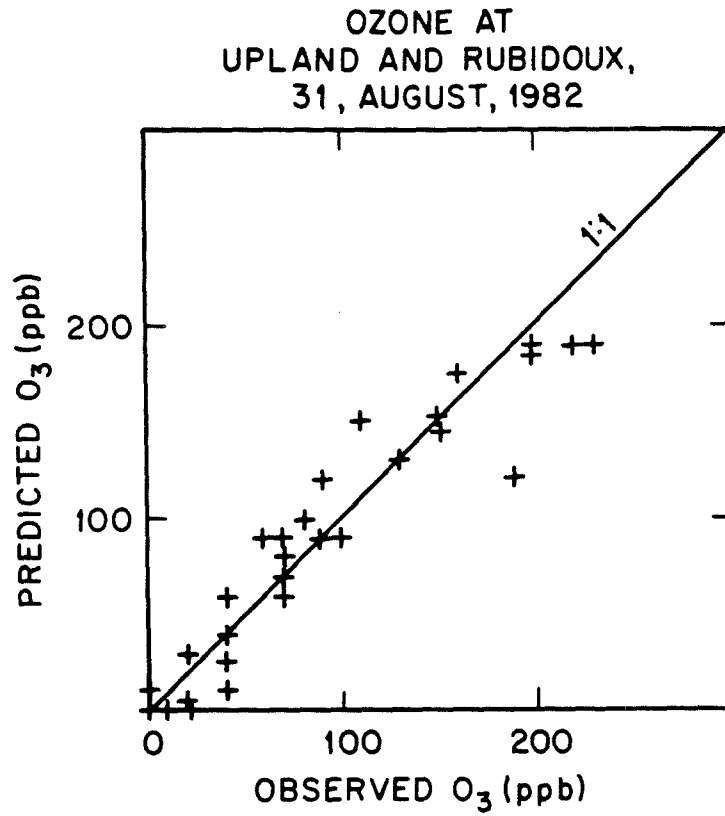


FIGURE 6.15

Predicted O₃ plotted against observed O₃ for both Rubidoux and Upland, CA, 31 August 1982.

atmosphere would be sufficiently starved for NO_x that further NO_x emissions would increase predicted O_3 levels.

The use of multi-day trajectories could suffer from the effects of vertical wind shear at night. On this particular occasion it appears that these effects were small. Upper level wind data were collected at a number of sites. At Point Mugu where the early morning winds were measured at 0419 PDT, the winds varied little in direction (less than 10°) with height. Upper level velocities also were low, less than 2.5 m s^{-1} , to well above the height of the modeling region. In the eastern portion of the basin, the early morning measurement taken at 300 PDT showed that the difference between the ground level velocity and the velocities up to 188 m was less than 1 m s^{-1} with direction varying no more than 25 degrees. That 188 m elevation is greater than the depth of the early morning mixed layer within which the pollutants emitted at ground level are trapped. Given the low wind speeds and small variation in direction with elevation on this day, the upper levels of the air parcel should move approximately with the air parcel path computed from surface wind data.

The above discussion, along with the successful model evaluation results, argues that the multi-day trajectories can, and should be, used for testing the effects of emission control measures.

6.5 Evaluation of Control Strategies for HNO₃ and Aerosol Nitrate Abatement

A primary use of the air quality model is to study the effect of proposed emission control strategies in advance of their adoption and, in turn, to help guide researchers and public agencies toward an optimal control strategy. In this section, the effects of a number of simple candidate control strategies are simulated and the results are discussed. The focus of this study is primarily directed towards developing strategies that will reduce aerosol nitrate and nitric acid concentrations in the atmosphere, however these control measures may also inhibit or promote the formation of other photochemical pollutants, notably O₃, PAN and NO₂. Thus, when discussing the results of the following tests, the effect of possible strategies on pollutants other than HNO₃ and AN will be detailed.

Choice of the first set of control measures examined was motivated by the 1982 Air Quality Management Plan (AQMP) for the SoCAB (SCAQMD and Southern California Association of Governments, 1982). The AQMP outlines control measures that will be used to decrease oxides of nitrogen emissions by about 23% and ROG by about 34% between the years 1979 and 1987, or about a 20% and 30% decrease, respectively, below the 1982 estimated emissions inventory used in the present study. For the purpose of this study, these reductions will be applied homogeneously over the air basin and will be applied equally to emissions of each of the lumped organic species. In a more detailed analysis, the original emissions inventory could be modified

to reflect the specific reductions in each source category. This would result in a less spatially homogeneous reduction and could change the relative chemical composition of the organic emissions.

Long-term air quality data taken throughout the SoCAB during 1982 (Gray et al. 1985) show that Rubidoux is the monitoring site most heavily affected by high AN levels. Therefore, the set of trajectories beginning over the ocean and ending at Rubidoux throughout 31 August were chosen for emission control measure evaluation. On this day, the Rubidoux-Riverside area had the highest O_3 reported in the basin and, as expected, had the highest total nitrate concentrations.

Table 6.5 shows the effects on the inorganic nitrate species of different combinations of emission reductions applied to the multi-day trajectories ending at Rubidoux. Pollutant emissions into these trajectories as they actually occurred on 31 August 1982 will be referred to as the base case emissions, and the observed ammonia concentration and temperature at Rubidoux are used to apportion total inorganic nitrate between HNO_3 and aerosol nitrate. Results in Table 6.5 are for the case without the addition of SINK aerosol to react with HNO_3 . The effect of including the addition of SINK via reaction 58 on various control measures will be discussed later. Predicted maximum two-hour average AN, 24-hour average AN, 24-hour average TN, and maximum two-hour HNO_3 are given in each case for comparison.

A 20% decrease in the NO_x emissions alone relative to the base case decreases the predicted maximum AN 40%, and the 24-hour average

TABLE 6.5

Predicted inorganic nitrate concentrations at Rubidoux,
California, resulting from decreases in emissions

	Aerosol Nitrate Maximum Two-Hour Average ($\mu\text{g m}^{-3}$)					THC Emissions Reduced 30%	
	Base Case THC					THC Emissions Reduced 30%	
	NO _x 0%	Emissions Reduction				NO _x 0%	Emissions Reduction 20%
	20%	40%	60%	80%			
Base Case NH ₃ Emissions	27.0	16.3	11.7	8.3	3.4	31.2	19.5
Reduced NH ₃ Emissions	7.2	6.4	-	-	-	7.0	6.3

	Aerosol Nitrate 24-hour Average ($\mu\text{g m}^{-3}$)					THC Emissions Reduced 30%	
	Base Case THC					THC Emissions Reduced 30%	
	NO _x 0%	Emissions Reduction				NO _x 0%	Emissions Reduction 20%
	20%	40%	60%	80%			
Base Case NH ₃ Emissions	11.5	8.4	4.8	2.7	1.1	13.3	9.0
Reduced NH ₃ Emissions	2.8	1.8	-	-	-	2.8	1.8

	Total Nitrate 24-hour Average ($\mu\text{g m}^{-3}$)					THC Emissions Reduced 30%	
	Base Case THC					THC Emissions Reduced 30%	
	NO _x 0%	Emissions Reduction				NO _x 0%	Emissions Reduction 20%
	20%	40%	60%	80%			
Base Case NH ₃ Emissions	18.6	15.4	10.3	6.8	4.0	21.2	15.9
Reduced NH ₃ Emissions	16.1	13.1	-	-	-	16.9	13.1

	Nitric Acid Maximum Two-Hour Average (ppb)					THC Emissions Reduced 30%	
	Base Case THC					THC Emissions Reduced 30%	
	NO _x 0%	Emissions Reduction				NO _x 0%	Emissions Reduction 20%
	20%	40%	60%	80%			
Base Case NH ₃ Emissions	9.6	7.9	5.9	4.1	2.6	10.1	8.0
Reduced NH ₃ Emissions	16.9	13.2	-	-	-	18.8	14.2

AN value decreases 27%. TN decreases about 18%, or by about the same percentage as the decrease in NO_x emissions. Less change is noted in the predicted nitric acid. This occurs because HNO_3 concentrations are largely governed by the NH_4NO_3 equilibrium dissociation constant and the ambient NH_3 concentrations. The excess of ammonia tends to allow only a small amount of nitric acid in the gas phase while the rest of the inorganic nitrate is transferred into the aerosol phase. Elsewhere in the air basin, NH_3 levels are much lower and a change in TN would be reflected more readily in a change in HNO_3 levels.

Decreasing the organic gas emissions results in an increase in AN, TN, and HNO_3 . At first glance this is a slightly discouraging result. Careful examination shows that this increase in inorganic nitrate is due primarily to the oxidized nitrogen being displaced from PAN into inorganic nitrate species. The peak total inorganic plus organic nitrate concentration remains essentially unchanged when organic gas emissions are reduced. PAN is known to be a plant toxicant and eye irritant. Under some circumstances this trade-off between organic and inorganic nitrate species formation might be deliberately manipulated in order to achieve a desired balance between TN and PAN. Decreasing organic gas emissions also may decrease the formation of other potentially harmful organic and nitrated organic compounds not studied here.

Reducing the NO_x and organic emissions has a beneficial effect on reducing the O_3 levels (Table 6.6). Note that a 20% decrease in NO_x emissions from the base case decreases the maximum O_3 at Rubidoux

TABLE 6.6

Predicted Peak One-Hour Ozone Concentrations (ppb)
 at Rubidoux, California,
 as a Function of Emission Reductions

	NO _x Emission Reduction				
	0%	20%	40%	60%	80%
% THC Reduction					
0%*	190	170	144	117	80
30%	181	166	-	-	-

* 0% = base case

more than a 30% decrease in organic emissions for the particular event examined here. This finding differs from the results of some previous studies. Possible reasons for these differences are discussed later.

Just before arriving at Rubidoux, the trajectories pass over a number of farming and animal husbandry operations, resulting in the high observed ammonia concentrations. One possible control strategy for reducing the aerosol nitrate concentrations could be predicated on relocating these large NH_3 sources. The same result may be achieved indirectly as urban sprawl pushes farming operations further away from the center of the SoCAB. To simulate this possibility, ammonia emissions from farm-oriented operations (due to livestock waste and fertilizer used for agricultural purposes) were removed from the inventory. The same sets of trajectory calculations used in the previous control measure evaluation study were repeated except that the ammonia emissions were reduced. These results are given in Table 6.5. The 24-hour average ammonia concentration at Rubidoux decreased from the base case value of 51.0 ppb down to 4.3 ppb when farm-related activities were eliminated. Decreasing the ammonia has a tremendous effect on the ammonium nitrate and nitric acid predictions. With farm related NH_3 emissions removed, only $2.8 \mu\text{g m}^{-3}$ of nitrate is found in the aerosol phase, compared to $13.3 \mu\text{g m}^{-3}$ of nitric acid gas, a reversal of the base case. Reducing ammonia to control aerosol nitrate formation results in an increase in HNO_3 and the problems associated with HNO_3 . Thus, the advantages and disadvantages of this avenue of control must be weighed before any action is taken.

If SINK aerosol is present that can react with nitric acid to produce aerosol nitrate, reducing the ammonia emissions does not lead to as large a decrease in aerosol nitrate as was predicted above for the case of a pure NH_3 , HNO_3 and NH_4NO_3 system. Increased nitric acid concentrations that result from NH_3 removal lead to more bound aerosol nitrate being formed due to reaction 58. As shown in Table 6.7, the 24-hour average aerosol nitrate drops from $13.8 \mu\text{g m}^{-3}$ with the base-case level of ammonia emissions to $8.3 \mu\text{g m}^{-3}$ for the reduced ammonia case—not so drastic a reduction as when no SINK is included in the calculations.

Further reduction of NO_x emissions beyond the 20% anticipated by the AQMP was examined. TN concentrations were seen to decline in almost direct proportion to changes in NO_x emissions. Reducing NO_x emissions by 20, 40, 60, and 80% resulted in decrease in TN of 18, 45, 64, and 78%, respectively at Rubidoux. A similar, almost linear dependence, between HNO_3 formation and NO_x input was found by Spicer (1983) in smog chamber experiments. In this study, AN decreased at a slightly greater rate than TN: 27, 58, 78, and 90% for the four levels of decreased NO_x emissions defined above. Maximum O_3 concentrations predicted at Rubidoux also declined as NO_x emissions were decreased. During the present study, a 60% reduction in NO_x emissions would have been sufficient to meet the federal ozone standard along the trajectories ending at Rubidoux.

In some previous modeling studies investigators found that, contrary to the findings presented here, lowering NO_x emissions

TABLE 6.7

Predicted Pollutant Concentrations
at Rubidoux, California
when Emissions of SINK aerosol are Included

	AN Max 2-Hr Avg ($\mu\text{g m}^{-3}$)	AN 24-Hr Avg ($\mu\text{g m}^{-3}$)	TN 24-Hr Avg ($\mu\text{g m}^{-3}$)	HNO ₃ (g) Max 2 Hr (ppb)
Base Case, No SINK	27.0	11.5	18.6	9.6
Base Case, SINK Included	29.4	13.8	21.4	9.3
SINK Included, NH ₃ Emissions Reduced	14.4	8.3	18.9	12.7

increased O_3 concentrations. There are obvious reasons that could account for the different findings, and some more subtle reasons, too.

First it is well known that depending on the hydrocarbon to NO_x ratio in an air parcel, NO_x control can either increase or decrease O_3 concentrations. A different mix of organic gas and NO_x emissions, resulting from different trajectory paths and that emission inventories for different years have been used, could account for part of the difference in the O_3 response to NO_x emission changes. Along the same lines, some investigators have examined the effect of a further decrease in NO_x emissions only after a large decrease in ROG emissions from mobile sources was imposed. This resulted in a larger reduction in total ROG emissions than studied here, and also a different organic gas emission composition. Also, there are inherent differences in the models used. More subtle causes for the differences in the outcomes of the calculations may well lie in the way that the trajectories are initialized. If shorter trajectories are used, as has been customary in previous studies, the choice of initial conditions could play a very large role in determining the results. Application of emission controls will affect those initial conditions but a great deal of uncertainty surrounds the question of estimating the effect of emission controls on initial conditions for short trajectories that start over land within the air basin. If in previous modeling studies the concentrations of NO and NO_2 in the upper levels of a model at the start of the trajectory were based on

ground level observations in the morning, then those NO and NO₂ levels may have been estimated to be much higher than reasonably could be expected. Nighttime reactions between NO₂ and O₃ would convert almost all the NO₂ present aloft at night to HNO₃ by sunrise the next morning (Russell et al., 1985). Many organic gases, however, can persist aloft at night because little or no photolysis takes place and OH radical concentrations are greatly reduced at night. As the mixing depth increases the next day, the air entrained downward from aloft is comparatively lean in NO and NO₂, and, as a result, fresh NO_x emissions are required to promote the formation of O₃.

This study concludes that reducing NO_x emissions will result in lower AN, HNO₃, PAN, and NO₂ concentrations. Lowering NO_x and ROG emissions may also decrease the formation of other nitrogenous organic compounds, certain of which are mutagenic and carcinogenic (Ohgaki et al., 1982). For the case considered here, NO_x control, independently or combined with ROG control, also assisted in controlling ozone at Rubidoux.

6.6 Conclusions

The predictions of a trajectory model describing the photochemical dynamics of ozone, NO_2 , HNO_3 , PAN, and aerosol nitrate were compared to field measurements. Predicted O_3 and NO_2 concentrations closely followed the measured concentrations. Predicted total inorganic nitrate concentrations at Rubidoux were very close to those measured at that site, often matching observations to within experimental error. The ability to closely account for the origin of measured O_3 , NO_2 , and TN concentrations is one of the most severe tests of a gas-phase photochemical model. Model predictions of the apportionment of TN between the aerosol and gas phases compare satisfactorily to the observations through much of the day, although on the average the model underpredicts the HNO_3 concentrations by a fraction of a ppb. This could be due to a number of reasons. Among the more likely reasons are: inaccuracies in the interpolated temperature fields, and uncertainties in the ammonia emissions inventory. When the observed ambient ammonia concentrations and temperature are used to apportion the total inorganic nitrate between the gas and aerosol phases, the AN predictions match observations very well. In spite of the uncertainties, the predicted NH_3 levels are close to the observed values, averaging slightly greater than observed, indicating that the inventory does not differ greatly from the actual emissions.

Control strategy tests indicate that reductions in NO_x emissions would result in nearly proportional reductions in total inorganic nitrate formation and slightly greater than proportional reductions in aerosol nitrate. For the cases studied, ozone concentrations also declined as the NO_x emissions were reduced. Decreasing ROG emissions also lowered O_3 concentrations and decreased organic nitrate (PAN) concentrations, though at the expense of increasing inorganic nitrate formation.

Nitrate aerosol formation at Rubidoux would be greatly decreased if ammonia emissions from farm-related operations were suppressed. However a corresponding increase in nitric acid concentrations would be expected to accompany this approach to aerosol nitrate control. Combined emission control strategies can be formulated that include a combination of controls on organic gases, NO_x , and NH_3 emissions that will achieve a greater control of aerosol nitrate and HNO_3 levels than a strategy predicated on control of only a single precursor species.

6.7 References

- Baldwin, A.C. and Golden, D.M. (1979) "Heterogeneous Atmospheric Reactions: Sulfuric Acid Aerosols as Tropospheric Sinks," Science, 206, 562-563.
- Cass, G.R., Gharib, S., Peterson, M. and Tilden, J.W. (1982) "The Origin of Ammonia Emissions to the Atmosphere in an Urban Area," Open File Report 82-6, Environmental Quality Laboratory, California Institute of Technology, Pasadena, CA.
- Chock D.P., Dunker, A.M., Kumar, S. and Sloane, C.S. (1981) "Effect of NO_x Emission Rates on Smog Formation in the California South Coast Air Basin," Envir. Sci. Technol., 15, 933-939.
- Chock D.P., Dunker, A.M., Kumar, S. and Sloane, C.S. (1983) Reply to "Comment on "Effect of Nitrogen Oxide Emissions in Metropolitan Regions", "Effect of NO_x Emission Rates on Smog Formation in the California South Coast Air Basin", and "Effect of Hydrocarbon and NO_x on Photochemical Smog Formation Under Simulated Transport Conditions", " Envir. Sci. Technol., 17, 58-62.
- Duce, R.A. (1969) "On the Source of Gaseous Chlorine in the Marine Atmosphere," J. Geophys. Res., 70, 1775-1779.
- Galloway, J.N. and Likens, G.E. (1981) "Acid Precipitation: The Importance of Nitric Acid," Atmospheric Environment, 15, 1081-1085.
- Glasson, W.A. (1981) "Effect of Hydrocarbons and NO_x on Photochemical Smog Formation Under Simulated Transport Conditions," J. Air Pollut. Control Assoc. 31 1169-1172.
- Glasson, W.A. (1983) Reply to "Comment on "Effect of Nitrogen Oxide Emissions in Metropolitan Regions", "Effect of NO_x Emission Rates on Smog Formation in the California South Coast Air Basin", and "Effect of Hydrocarbon and NO_x on Photochemical Smog Formation Under Simulated Transport Conditions", " Envir. Sci. Technol., 17, 62-63.
- Goodin, W.R., McRae, G.J., and Seinfeld, J.H. (1979) "A Comparison of Interpolation Methods for Sparse Data: Application to Wind and Concentration Fields," J. Appl. Met., 18, 761-771.
- Gray, H.A., Cass, G.R., Huntzicker, J.J. Heyerdahl, E.K. and Rau, J.A. (1985) "Characteristics of Atmospheric Organic and Elemental Carbon Particles in Los Angeles," Envir. Sci. Technol., (submitted).

- Groblicki, P.J., Wolff, G.T. and Countess, R.J. (1981) "Visibility Reducing Species in the Denver "Brown Cloud", Part I. Relationships Between Extinction and Chemical Composition," Atmospheric Environment, 15, 2473-2484.
- Grosjean, D. and Fung, K. (1984) "Hydrocarbons and Carbonyls in Los Angeles Air," J. Air Pollut. Control Assoc., 34, 537-543.
- Grosjean, D., Fung, K. and Harrison, J. (1983) "Interactions of Polycyclic Aromatic Hydrocarbons With Atmospheric Pollutants," Envir. Sci. Technol., 17, 673-679.
- Hildemann, L.M., Russell, A.G., and Cass, G.R. (1984) "Ammonia and Nitric Acid Concentrations in Equilibrium with Atmospheric Aerosols: Experiment vs. Theory," Atmos. Environ., 18, 1737-1750.
- Larson, S.M., Cass, G.R., Hussey, K.J., and Luce, F. (1984) "Visibility Model Verification by Image Processing Techniques," Report to the California Air Resources Board.
- Liljestrand, H.M. and Morgan, J.J. (1978) "Chemical Composition of Acid Precipitation in Pasadena, California," Envir. Sci. Technol., 12, 1271-1273.
- Lin, M-K. and Seinfeld, J.H. (1975) "On the Validity of Grid and Trajectory Models of Urban Air Pollution," Atmos. Environ., 9, 555-574.
- Martens, C.S. Wesolowski, J.J. Harriss, R.C. and Kaifer, R. (1973) Chlorine Loss from Puerto Rican and San Francisco Bay Area Marine Aerosols," J. Geophys. Res., 78, 8778-8792.
- Muck, R.E. and Steenhuis, T.S. (1982) "Nitrogen Losses From Manure Storages" Agricultural Wastes, 4, 41-54.
- Ohgaki, H., Matsukura, N., Morino, K., Kawachi, T., Sugimura, T., Morita, K., Tokima, H. and Hirota, T. (1982) "Carcinogenicity in Rats of the Mutagenic Compounds 1-Nitropyrene and 3-nitrofluoranthene" Cancer Letters, 15, 1-7.
- Pitts, J.N., Winer, A.M., Atkinson, R. and Carter, W.P.L. (1983) "Comment on "Effect of Nitrogen Oxide Emissions in Metropolitan Regions", "Effect of NO_x Emission Rates on Smog Formation in the California South Coast Air Basin", and "Effect of Hydrocarbon and NO_x on Photochemical Smog Formation Under Simulated Transport Conditions", " Envir. Sci. Technol., 17, 54-57.
- Ranzierrri, A. (1983) Private Communication, Tape AR3288, "1982-SCAB Point and Area Source Emissions."

- Ranzi, A. (1984) Private Communication, Tape AR3292, "1982-SCAB Motor Vehicle Traffic Emissions."
- Russell, A.G. and Cass, G.R. (1984) "Acquisition of Regional Air Quality Model Validation Data for Nitrate, Sulfate, Ammonium Ion and Their Precursors," Atmospheric Environment, 18, 1815-1827.
- Russell, A.G., McRae, G.J. and Cass, G.R. (1983) "Mathematical Modeling of the Formation and Transport of Ammonium Nitrate Aerosol," Atmospheric Environment, 17, 949-964.
- Russell, A.G., McRae, G.J. and Cass, G.R. (1985) "The Dynamics of Nitric Acid Production and the Fate of Nitrogen Oxides," Atmospheric Environment (in press).
- South Coast Air Quality Management District and Southern California Association of Governments (1982) Final Air Quality Management Plan, 1982 Revision.
- Spicer, C.W. (1983) "Smog Chamber Studies of NO Transformation Rates and Nitrate/Precursor Relationships," Envir. Sci. and Technol., 17, 112-120.
- Steenhuis, T.S., Bubbenzer, G.D., and Converse, J.C. (1982) "Ammonia Volatilization of Winter Spread Manure," in Transactions of the American Society of Agricultural Engineers, 22, 152-161.
- Waldman, J.M., Munger, J.W., Jacob, D.J., Flagan, R.C., Morgan, J.J. and Hoffmann, M.R. (1982) "Chemical Composition of Acid Fog," Science, 218, 677-680.
- White, W. H. and Roberts, P.T. (1977) "On the Nature and Origins of Visibility Reducing Species in the Los Angeles Basin," Atmospheric Environment, 11, 803-812.
- Winer, A. M., Peters, J.W., Smith, J.P. and Pitts, J.N. (1974) "Response of Commercial Chemiluminescent NO-NO₂ Analyzers to Other Nitrogen Containing Compounds," Envir. Sci. Technol., 8, 1118-1121.

CHAPTER 7

FUTURE RESEARCH

7.1 Introduction

Research, by its nature, often raises new questions in addition to answering those questions originally addressed. Among the areas requiring future research that were identified during the execution of this work, five general areas stand out: aerosol formation, atmospheric chemistry, deposition of atmospheric pollutants and aerosols, development of advanced air quality models and applications of air quality models to the design of air pollutant control programs. Each of these topics will be reviewed in this chapter, with specific recommendations given for further research.

7.2 Aerosol Formation

The present work was concerned with understanding the formation and dynamics of atmospheric aerosol nitrates, which were studied using both field experimental and mathematical modeling techniques. Observations and predictions were stated in simple terms based on the concentration of nitrate aerosol. A number of aspects of the formation of nitrate aerosol, and of the nitrate air quality problem, remain to be fully understood. In particular, how can one predict the size distribution of the atmospheric nitrate aerosol that is produced? This question of size distribution prediction is critical to an understanding of how to control the visibility problems

that result from high nitrate loadings, because the fine particle fraction of the aerosol burden contributes more to visibility impairment than does the coarse particle fraction. In order to undertake an analysis of these size distribution issues, one must understand whether or not HNO_3 and NH_3 react to form very small particles of ammonium nitrate that then would coagulate to form fine particles in the accumulation mode (around $1 \mu\text{m}$), or if the products of the HNO_3 - NH_3 reaction are incorporated directly onto preexisting aerosol material. One must further examine if the composition of the ambient aerosol greatly affects the formation paths of nitrate aerosol.

As discussed in Chapters 3 and 6 of the present work, gas phase species like N_2O_5 , NO_3 , and HNO_3 continuously bombard the surface of aerosols at a rate predictable from kinetic theory. However, the fraction of these collisions that result in heterogeneous chemical reaction have not been studied extensively, in particular it is not known how surface characteristics or aerosol composition affect the heterogeneous reaction rate. As shown, if the collision efficiencies, α , are high, then the presence of aerosol could greatly affect the gas phase concentrations of these species and greatly enhance the production of nitrate aerosol, even in the absence of NH_3 . The collision efficiency and reaction products for the reactions of HNO_3 , N_2O_5 , and NO_3 with a variety of candidate aerosols (e.g., NaCl , CaCO_3 , $(\text{NH}_4)_2\text{SO}_4$, etc.) should be determined experimentally. These results would advance the predictive capability of gas and aerosol

phase photochemical air quality models. They also will have a profound effect on the ability to account for the size distribution of the aerosol nitrates since much of the alkaline particle surface area resides in the large particle sizes.

In Chapter 4 it was shown that the chemical composition of the water soluble portion of the atmospheric aerosol is quite complex, containing not only NH_4^+ , NO_3^- , and SO_4^{--} , but also Cl^- , Mg^{++} , K^+ , Na^+ , and Ca^{++} . In Chapter 5 it was shown that the presence of these additional materials can perturb the equilibrium between $\text{HNO}_3(\text{g})$, $\text{NH}_3(\text{g})$, and the aerosol phase, thus affecting the amount of aerosol nitrate formed. At present, air quality models that exist describe the equilibrium composition of a gas and aerosol phase system comprised of nitrate, sulfate, and ammonium compounds. One research project envisioned would extend the knowledge of the thermodynamics of mixed salt aerosols, resulting in more complete models of the equilibrium between atmospheric gases and aerosols. First, basic thermodynamic data sufficient to define phase diagrams for realistic mixed salt aerosols are required. A second project could entail obtaining experimental data on the actual composition and surface structure of single solid aerosol particles and microdroplets which are needed to define and test models constructed to describe the equilibrium between NH_3 , HNO_3 , and a complex aerosol system. Experimental data on particle composition likewise could be acquired and then used to test the hypothesis that HNO_3 and NH_3 are in equilibrium with the aerosols.

In this study, photochemical production of the precursor gas and gas-to-particle conversion were studied for nitrate aerosol. A model was developed that predicted the rate of formation of nitric acid gas, followed by equilibration with the aerosol phase. There may well be other relevant classes of particulate formation problems that could be modeled by an analogous approach, in particular, the photochemical production of low vapor pressure organic gases that then condense to form organic aerosols. Again, the same questions could be raised concerning whether the low vapor pressure organic gases nucleate homogeneously or if they condense on preexisting aerosols. Prediction of organic aerosol size distributions is important not only for visibility studies but also because of the health implications of breathing fine particulate organic compounds.

7.3 Atmospheric Chemistry

As discussed in Chapter 3 a number of critical reaction rates required for use in the air quality model remain uncertain. In particular, the rate constant for the homogeneous hydrolysis of dinitrogen pentoxide (N_2O_5), reaction 46 in Chapter 3, is one of the more important factors needed to determine the formation rate of HNO_3 and the ultimate fate of NO_x emissions. Depending on the magnitude of that constant, a tremendous amount of nitric acid can be formed by this path. The reactions of N_2O_5 with other atmospheric constituents remains largely unexplored. Experimental work on the kinetics of N_2O_5 should be pursued.

Atmospheric radical chemistry is just beginning to be investigated for a number of key species. The present model uses a description of NO_3 radical chemistry that was unknown until just recently. Again the rates of these reactions, their products, and other radical reactions should be examined further. Chapter 3 suggests that one class of these reactions, radical reactions with aerosols, could be a very significant determinant of atmospheric gas concentrations. Other reactions to be studied would include those that take place primarily at night in the upper atmosphere.

A number of field experimental programs are suggested by this work. Chapter 3 dealt with theoretically modeling the atmospheric chemistry and transport of a number of constituents for which little or no atmospheric concentration data exist, such as HNO_3 , NO_3 , and N_2O_5 . In response to the need for better data, an extensive field experiment was conducted to better define the $\text{HNO}_3(\text{g})$ and $\text{NH}_3(\text{g})$ concentrations. However, few measurements of NO_3 radical concentrations have been made, and no ground-level concentrations of N_2O_5 are available. Experiments should be conducted that will better define the concentrations of these trace species. Those experiments would provide a data set for use in a more complete evaluation of air quality models. A more detailed knowledge of an essential set of atmospheric chemical reactions would result.

Most experimental programs have been limited to obtaining ground level measurements of pollutants, though in Chapter 3 it was shown that a large quantity of the atmospheric nitric acid can be

produced above the ground level in the air quality model, depleting the reactive nitrogen oxides. As discussed in Chapter 5, misspecification of the concentrations of the upper level pollutants can seriously affect the results of control strategy evaluation studies. However, very little data are available to accurately specify the day or nighttime concentrations of such pollutants as HNO_3 , NO_2 , and NO_3 in the upper levels of the boundary layer. Though the modeling study indicated that high concentrations of NO_3 should be present at night several hundred meters above the ground, there are no data with which to test this finding. A program to study the upper level pollutant concentrations would be very useful to elucidate atmospheric chemical reactions that play a significant role in the formation of photochemical pollutants, and for use in further model development and verification.

A largely unexplored area of atmospheric chemistry is the production, reactions and fate of $\text{HCl}(\text{g})$, a strong acid. As shown in Chapter 4, $\text{HCl}(\text{g})$ could be displaced from sea salt aerosol by reaction with HNO_3 . Measurements of $\text{HCl}(\text{g})$ and Cl^- concentrations could be examined to determine the extent to which sea salt acts as a sink for nitric acid, and how important the deposition and reactions of HCl could be to the environment. $\text{HCl}(\text{g})$ also may perturb the equilibrium between HNO_3 , NH_3 and the aerosol phase.

7.4 Deposition of Atmospheric Pollutants

Ground level deposition is the ultimate fate of a large fraction of the gaseous pollutants, and almost all of the aerosol, yet

many of the details of this deposition process are largely undetermined. In Chapter 3 it was shown that a significant fraction of the NO_x emissions can be removed at the earth's surface by dry deposition during the the first 24 hours after pollutant release. Little data exist to verify this finding in detail. The deposition rates of both aerosols and gases should be studied to better understand the deposition process and to evaluate the present model.

7.5 Application

The results of this study are immediately applicable to the development of emission control strategies that will reduce the formation of atmospheric nitric acid and aerosol nitrate. But before this can be done, additional information is needed. First, an understanding of available emission control techniques and their costs is needed. The nitric acid/aerosol nitrate system involves a number of unusual pollutants, such as NH_3 . Little or no thought has been devoted to the questions that surround NH_3 control to date. This is a particularly important deficiency that requires immediate attention because the most advanced NO_x control techniques (e.g. selective catalytic reduction) proposed for future use involve NH_3 injection and subsequent NH_3 release to the atmosphere. This trade-off between NO_x and NH_3 emissions must be evaluated quickly before additional NH_3 emitting sources are introduced into urban air basins. A second topic that requires research centers on the definition of appropriate goals for air quality control programs. Synergisms between pollutants must be acknowledged. A good example is that without NH_3 , no NH_4NO_3 will

be formed. However, starving the atmosphere for NH_3 will increase the nitric acid burden in the atmosphere. Thus, acceptable or desired levels of all pollutants should be prescribed.

7.6 Development and Evaluation of Advanced Air Quality Models

As additional knowledge is gained of the physical processes that determine gaseous pollutant concentrations in the atmosphere, these advances should be incorporated into the model presented here. Chapters 2, 3 and 6 showed that incorporation of some of the most recent findings in atmospheric chemistry made it possible to determine the concentrations of a number of trace, yet very significant, atmospheric components. For aerosol phase pollutants, the model could be expanded to include a description of the thermodynamics of a mixed sulfate-nitrate aerosol, and for the formation of organic aerosol.

An Eulerian, grid based, photochemical air quality model that predicts nitric acid and aerosol nitrate formation simultaneously at all sites in an airshed can be developed as a direct extension of the trajectory model approach used here. This type of model can be used to investigate the basinwide dynamics of pollutants, not just those along a given set of trajectories. More importantly, it shows the basinwide effect of proposed emission control strategies.

7.7 Meteorology

A number of improvements in governmental routine meteorological observations would be beneficial to the type of research undertaken in this project. Atmospheric air quality modeling

studies would greatly benefit from more frequent, more widespread, and more accurate, measurements of the mixing depths, turbulent diffusivities, temperature, humidity and solar insolation, for example.

7.8 Conclusion

A number of areas for future research have been presented. They include experimental and theoretical studies of both a basic and applied research nature. The list is only a partial one, and other areas also may be apparent to the reader. Basic research will produce refinements to the model, while its immediate application to analysis of emission control programs promises to be beneficial and instructive.

CHAPTER 8

SUMMARY AND CONCLUSIONS

This work has investigated the important factors that determine the dynamics of nitric acid and aerosol nitrate in the atmosphere. Both theoretical modeling studies and experimental methods were employed. Initially, a mathematical model was developed to describe the formation and transport of photochemically produced gases and ammonium nitrate aerosol. Using basic equations of atmospheric transport, deposition, and gas phase chemical kinetics, the model mechanistically calculates ammonia and nitric concentrations from emissions. Ammonium nitrate aerosol concentrations then are computed at thermodynamic equilibrium with gas phase NH_3 and HNO_3 . As such, this model represents the first attempt to predict the concentration of secondary aerosol nitrate from gaseous emission data using a fundamental description of the transport, chemical reactions and thermodynamics leading to aerosol formation. A sensitivity study on the model indicated that aerosol nitrate concentrations are highly dependant on the temperature. The model was tested against a limited set of daytime atmospheric NH_3 , NO_3^- and NH_4^+ data available at El Monte, CA, from experiments conducted in 1974, and adequately predicted the observed concentrations.

Next the existing description of daytime oxides of nitrogen chemistry was extended to cover nighttime conditions. By adding a description of the nighttime chemistry of two trace oxides of

nitrogen, NO_3 and N_2O_5 , it was found that, contrary to prevailing opinion, a significant amount of nitric acid can be formed at night. Model evaluation indicated that this expanded description of atmospheric chemistry, transport, and emissions was necessary, and sufficient, to reproduce observed atmospheric NO_3 concentration measurements. Other studies that have not included a complete description of transport processes or emissions have been unable to reproduce the NO_3 concentration profile without using ad hoc methods.

Homogeneous hydrolysis of N_2O_5 could be responsible for a large fraction of the nitrate produced in the atmosphere. However the rate constant for this reaction is very difficult to measure accurately so a sensitivity test was conducted to determine the effect of this uncertainty on atmospheric nitric acid production. Though the predicted nitric acid produced by the hydrolysis of N_2O_5 will decrease as the rate constant for that reaction is decreased, competing nighttime reactions involving NO_3 will produce more nitric acid and the overall effect on nighttime nitric acid formation is small. A theoretical investigation into the possible role that aerosols can play in determining gaseous pollutant concentrations and the formation of nitrate aerosol showed that a significant fraction of nitrate in the atmosphere is formed heterogeneously if the collision efficiency for the N_2O_5 bombardment on existing aerosol surfaces is high. At more moderate collision efficiencies, a less than 0.001, heterogeneous reactions are less important and gas phase reactions dominate the chemistry of the formation of inorganic nitrate species like HNO_3 .

Verification of the accuracy of air quality model predictions

was impeded by a lack of data on the concentrations of pollutants important to the dynamics of nitric acid and nitrate aerosol. To alleviate this problem, a field program was designed and executed to measure the concentrations of $\text{HNO}_3(\text{g})$, $\text{NH}_3(\text{g})$, NO_3^- , NH_4^+ , $\text{SO}_4^{=}$, and other aerosol species. PAN, NO, NO_2 , and O_3 , also were measured during the experiment completing a nitrogen balance on the air masses studied.

Measurements indicated that the atmospheric aerosol could be more complex than is assumed by present models, consisting not only of NH_4^+ , NO_3^- and $\text{SO}_4^{=}$, but also significant amounts of Na^+ , Cl^- , K^+ , Mg^{++} and Ca^{++} . A number of hypotheses were tested to determine whether or not a mathematical model based on an equilibrium between NH_3 , HNO_3 and the aerosol phase could account for the observed nitrate. Most of the data were consistent with the assumption that some pure NH_4NO_3 aerosol coexisted as an external mixture with other aerosol particles. Further improvement is obtained if a mixed $\text{NH}_4^+-\text{NO}_3^--\text{SO}_4^{=}$ aerosol is assumed. An important finding was that nitrate aerosol can build up overnight near the coast in the absence of large NH_3 concentrations. This aerosol production can be explained as being formed by the reaction of HNO_3 with sea salt or soil dust-like aerosol. The nitrate aerosol then is transported inland the following day.

An evaluation of the photochemical, gas and aerosol phase, air quality model showed that the model predictions compare favorably with the O_3 , NO_2 , total nitrate, NH_3 , and nitric acid concentrations

observed during the experiment. The model then was used to test the effects of emission control programs suggested by recent public agency documents. Model results indicate that NO_x emissions control will decrease aerosol nitrate, $\text{HNO}_3(\text{g})$, NO_2 and PAN. For the particular trajectories studied, NO_x control also would have reduced the peak O_3 levels. Control of NH_3 emissions would decrease the formation of nitrate aerosol at the expense of increasing the HNO_3 concentrations. Organic gas emissions control could be used to abate O_3 and PAN formation. Model results show that a mixed strategy, controlling both NO_x and organic gas emissions simultaneously, would have decreased the O_3 concentrations more than either control measure used independently for the trajectories studied here.